# ARS JOURNAL

## RUSSIAN SUPPLEMENT

Igor Jurkevich, Editor

Concerning the Analogy Between Combustion in a Detonation Wave and in a Rocket Engine . . . . . Yu. N. Denisov, Ya. K. Trashin and K. I. Shchelkin 834

Location of Frontal Wave in Asymmetrical Flow of Gas at High Supersonic Speed Over a Pointed Body . . . . . A. L. Gonor 841

Calculation of the Stability of a Nonlinear Control System in the Presence of Vibration Noise . . . . . A. G. Bogdanov 843

Study of an Optimal Control System in Presence of Random Perturbations . . . . . V. M. Kuntsevich 846

Problem of Nearly Self-Similar Unsteady Motion . . . . . T. G. Koldobskaya 853

Determination of the Preliminary Orbits of Artificial Satellites From Observations With Time Approximately Known . . . . . Yu. V. Batrakov 859

Method for Improving Orbits of Artificial Satellites of the Earth Using Observations With Approximate Values of Time . . . . . D. K. Kulikov and Yu. V. Batrakov 865

Dependence of the Internal Energy of Air on the Pressure and Density at High Temperatures . . . . . S. S. Kvashnina 875

Technical Comment . . . . . 876

DIGEST OF TRANSLATED RUSSIAN LITERATURE . . . . . 877

*Published Under National Science Foundation Grant-in-Aid*

# Concerning the Analogy Between Combustion in a Detonation Wave and in a Rocket Engine

YU. N. DENISOV
YA. K. TRASHIN
K. I. SHCHELKIN

**An aerothermodynamic analysis of the overall combustion process in a rocket engine shows that the deflagration branch of the Hugoniot curve can be considered as the geometric locus of points, each of which corresponds uniquely to a definite rate of heat evaluation (called herein "forcing" of the combustion mode) in the jet engine chamber. It is shown that this process is unstable in a high output chamber, and a criterion of the instability is derived. The combustion instability at a definite degree of "forcing" leads to resonant high frequency pressure oscillations in the chamber. The instability of the combustion front in a detonation wave, where high frequency pulsations have been experimentally observed, is characterized by the same criterion. It has been experimentally established that the oblique shocks play a decisive role in the mechanism of the high frequency oscillations in the case of pulsating and spinning detonations, and that in this case there is no plane wave front. It is suggested that the pulsation mechanism in detonation is analogous to the vibration mechanism in the combustion in jet engine chambers.**

THE MODERN jet engine is a complex unit, in which the principal role is played by the combustion chamber, from which emerges a gaseous jet made up of the fuel combustion products. However, leaving aside structural details, the combustion chamber of a jet engine (Fig. 1a) can be considered as a cylindrical tube, into one end of which fuel is fed through injector $i$ together with the oxidizer; the two form in region 1 a mixture that serves as the initial substance (propellant). After the initial propellant 1 is chemically converted in the combustion zone 2, gaseous products 3 are formed, the specific volumes of which exceed considerably the volume of the initial propellant. The escape of these gaseous products from the chamber is throttled and accelerated by means of exit nozzle $l$, which shapes the moving reactive jet.

In order to perfect a jet engine chamber, it is necessary to know the conditions and the mechanism of combustion of the fuel in the chambers. The available data show that the detailed chemical-physical process of combustion in a heat evolving chamber is rather complicated. One can consider, however, a simpler overall picture of the combustion process in the jet engine chamber. For this purpose the combustion process, and the entire combustion chamber, are analyzed (1, 2)[1] in a one-dimensional system of coordinates, the $z$ axis of which is aligned with the axis of the chamber.

Regardless of the actual size and complexity of the physical and chemical structure of the combustion zone 2, the latter can be represented as a strong discontinuity. Passage of substance through this discontinuity from the initial state 1 into the final state 3 is accompanied by liberation of energy $Q$. The initial state of the substance is characterized by the following initial parameters: Pressure $p_1$, density $\rho_1$, temperature $T_1$ and stream velocity $u_1$; the corresponding final parameters are $p_3$, $\rho_3$, $T_3$ and $u_3$, respectively.

Translated from *Izvestiia Akademii Nauk SSSR, Otdelenie Tekhnicheskikh Nauk, Energetika i Avtomatika* (Bull. USSR Acad. Sci., Div. Tech. Sci., Power and Automation), no. 6, 1959, pp. 79–89. Translated by J. George Adashko.

[1] Numbers in parentheses indicate References at end of paper.

An aerothermodynamic analysis of such a discontinuity is made possible by the well-known Hugoniot equation, derived from consideration of the conservation of mass, momentum and energy

$$\frac{p_3}{p_1} = \frac{\kappa - (\rho_1/\rho_3) + [2Q/(p_1/\rho_1)]}{\kappa(\rho_1/\rho_3) - 1} \qquad \left(\kappa = \frac{\gamma + 1}{\gamma - 1}\right) \qquad [1]$$

where $\gamma$ is the ratio of the specific heats $c_p/c_V$.

It is assumed here that in zone 1 the initial substance (liquid or even solid) is converted by evaporation into an ideal gas, which in passing through the discontinuity 2 retains a constant specific heat. All kinds of friction, heat transfer and similar losses are neglected.

The physical meaning of different sections of the Hugoniot curve, shown in Fig. 2 in $(p, V)$ coordinates (where $V = 1/\rho$ is the specific volume), becomes clear upon analysis of the equation of this curve simultaneously with the equation of the Michelson line, which results from the laws of conservation of mass and momentum

$$u_1 = \sqrt{\frac{(p_3/p_1) - 1}{1 - (V_3/V_1)}}\, p_1/\rho_1 \qquad [2]$$

It is seen from this equation that the section $JK$ of the Hugoniot curve has no physical meaning, since it corresponds to imaginary values of the velocity of discontinuity propagation, i.e., propellant feed rate $u_1$.

The upper branch of the curve $JF$ is an aggregate of states with high discontinuity-propagation velocities, i.e., it corresponds to a detonation wave with a given liberated energy $Q$. According to the Jouguet principle, the rate of propagation of the detonation front relative to the gas moving behind the wave equals the velocity of sound $a$ in the detonation products. The branch $JF$ contains therefore only one point $G$, which describes the state of the gas in a detonation wave of velocity $D$.

The points above $G$ pertain to an overcompressed detona-

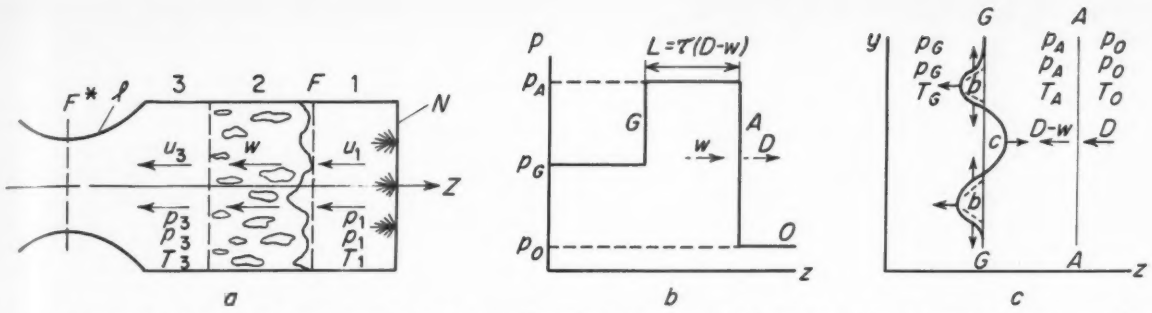


Fig. 1 a—Diagram of jet engine combustion chamber; b—Pressure diagram of a schematized plane detonation wave; c—schematized representation of disturbance in ignition zone

tion wave, observed, for example, when a detonation passes from a wide tube to a narrow one (3).

The points lying on the curve $JG$ correspond to an undercompressed wave, which, for a fixed liberated energy, cannot be realized by means of ignition in a shock wave (4).

The lower deflagration branch of the curve $KM$ corresponds to the propagation of rarefaction waves, accompanied by combustion.[2] This branch is divided by the tangent $BC$ into sections of weak ($KL$) and strong ($LM$) deflagrations. The points lying on the section $LM$ do not correspond to real combustion modes, since their realization would require (analogous to the section $JG$) larger energies than are liberated during the course of the reaction.

Experimental estimates of the velocities of a flame zone in tubular chambers, relative to the particles of the combustible mixture (2), which have shown that there exist combustion velocities exceeding the normal flame velocities by several tens of times, lead to the conclusion (1 and 2) that the entire weak-deflagration branch ($KL$) is physically real. The point $L$ corresponds to a fully developed deflagration with an overall velocity of discontinuity propagation $u_1 = u_L$, when the velocity of the flow of the reaction products equals the local velocity of sound (thermal choking limit). The combustion mode in which the same amount of mixture is burned in zone 2 as in a plane laminar flame front of normal combustion, having an area equal to the area of the tranverse cross section $F$ of the chamber, corresponds to a discontinuity propagation velocity $u_1 = u_n$.

The bundle of Michelson lines (see Fig. 2) included in the interval $u_n - u_L$ gives a set of possible input velocities $u_1$ each of which is determined by a given heat evolution rate of the jet engine in operation. The higher the input velocity $u_1$ and consequently the combustion velocity, the greater the pressure drop $\Delta p$ along the length of the combustion zone.

The connection between the Mach number of the input flow, $M_1 = u_1/a_1$, with the Mach number of flow away from the discontinuity, $M_3 = u_3/a_3$, is given by the following equation, obtained from the law of conservation of mass

$$M_3 = M_1 \sqrt{\rho_1 p_1 / \rho_3 p_3} \qquad [3]$$

If the combustion rate in the jet engine chamber is "forced" by varying the degree of throttling of the gas escaping into the atmosphere from the region 3 [by shaping in various ways the subsonic portion of the Laval nozzle (1)], then the dependence of the constriction of the nozzle $F/F^*$ on $M_3$ is of the form

$$\frac{F}{F^*} = \frac{1}{M_3}\left[\frac{2 + (\gamma - 1)M_3^2}{\gamma + 1}\right]^{(\gamma+1)/[2(\gamma-1)]} \qquad [4]$$

The two last equations show clearly the connection between the velocity of discontinuity propagation (or input flow

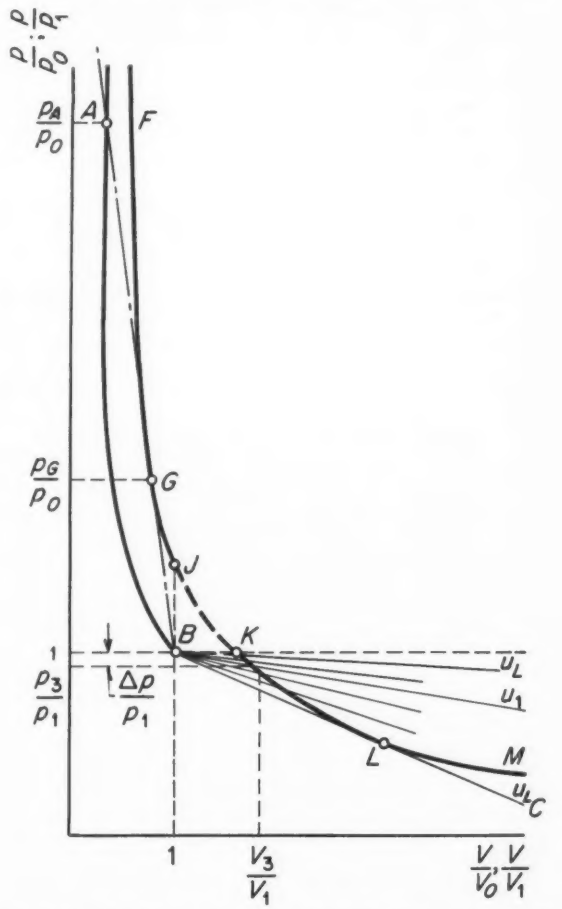


Fig. 2 Hugoniot adiabat. For sake of clarity, both branches of adiabat, $EJ$ and $KM$ are normalized to an equal effective amount of liberated energy $Q$, independent of initial pressure of reacting mixture

[2] We note that, depending on the boundary conditions, the propagation of a flame along a tube is accompanied also by a compression wave in the initial mixture (2, 5 and 6). The steady boundary conditions of the jet engine chamber stabilize the stationary combustion mode at a compression of constant magnitude $p_1$ and a drop $\Delta p = p_1 - p_3$, without production of a compression wave.

velocity) with the constriction of the nozzle at a constant heat delivery $Q$, chamber cross section $F$ and gas parameters $p_1$, $\rho_1$ and $T_1$ in region 1.

The points of the deflagration branch $KL$ describe the states of the reaction products, corresponding to the combustion rates of an entire set of combustion chambers, each of which differs from the other only in the value of the critical cross section $F^*$ of the outlet nozzle.

The lower a point is located on the curve $KL$, the more developed is the deflagration and the less constriction is necessary to bring the velocity of escape of the reaction products to sonic in the critical section of the nozzle. In a fully developed deflagration ($M_3 = 1$) constriction is unnecessary and then a semithermal nozzle is realized with maximum "forcing" of the combustion mode.

Consideration of the deflagration branch of the Hugoniot curve as the geometric locus of points, each of which corresponds uniquely to a definite degree of "forcing" of the combustion mode in the jet engine chamber, allows us, without going into the specific ignition mechanism, to obtain an approximate comparative estimate of the principal parameters of the engine and of the degrees of "forcing" of the combustion modes in the chambers.

On the other hand, if we consider a specific ignition mechanism, then many indirect considerations of the possibility of heating the combustible mixture by stirring it with the reaction product (liquid jet engines), or by adiabatic compression (ramjet engines with $M > 3$), give grounds for assuming that in combustion, in high pressure high output chambers, the predominating mechanism is successive self-ignition. (This does not exclude, naturally, the simultaneous existence the mechanisms of wrinkled flame and microdiffusion turbulent combustion in these chambers.)

The foregoing considerations give ground for assuming that a certain analogy exists between combustion in high output jet engine chambers and in a detonation wave. This analogy consists of the following:

Firstly, both in a high pressure chamber and in a detonation wave it is assumed that the same ignition mechanism predominates—successive self-ignition of a compressed and heated combustible mixture.

Secondly, the ultimate states of the chemical reaction products of both processes is described by thermogasdynamic equations of one and the same type, and the state of the detonation combustion products is close in order of pressure (several times ten atmospheres) and temperature (about 3000 K) to the state of the combustion products in region 3 of a high output jet engine chamber.

Thirdly, the thermodynamically possible stationary combustion modes are determined in both processes by the input rate of the combustible mixture into the combustion zone, and by the possibility of igniting the mixture at the same rate.

Furthermore, the equivalent combustion velocities of the combustible mixture in a jet engine chamber ($u_0$) and in a detonation wave ($D$), reduced to identical initial conditions ($p_0$, $\rho_0$) satisfy the equation $D/u_0 = \psi$, where $\psi$ is a coefficient that depends on the pressure in the jet engine chamber and on the degree of "forcing" of the combustion mode in it. For highly "forced" combustion chambers of high pressure jet engines, $\psi$ is found to be close to unity.

In addition, both detonation and combustion in high output chambers display experimentally observed fluctuations (7–12) in the parameters of the chemical reaction products ($p_3$, $\rho_3$, $T_3$ and $u_3$). Both processes are characterized by high frequency oscillations, which evidence instability in the combustion zone.

Taking into account the exceeding difficulty of experimental and theoretical investigations of the instability of the mechanism of combustion in high output chambers, it is advisable to analyze (13) one of these processes—detonation. A study of one process is essential for knowledge of the other, starting from the analogy between the two.

An analysis of the stability of the combustion in a detonation wave, represented as a combination of a plane shock wave and an ignition zone, shows that the application of a small perturbation on the combustion zone results in an increase in this perturbation. This conclusion can be drawn from the following analysis.

In view of the exponential dependence of the rate of chemical reaction on the temperature, it is assumed that after the lapse of the induction period $\tau$ the gas mixture reacts instantaneously. This corresponds to the form of the wave (plotted in coordinates $p$, $z$) shown in Fig. 1b. The distance $\lambda$ between the forward shock front of the wave $A$ and the front $G$, where the chemical reaction occurs instantaneously, equals the product of the induction time $\tau$ by the gas velocity in the wave relative to its front ($D - w$).

Fig. 1c shows a section through such a wave, which we consider, for the sake of simplicity, not in a cylindrical but in a two-dimensional system of coordinates $y$, $z$. The coordinate system moves with the wave in the direction of the $z$ axis and is connected to both fronts $AA$ and $GG$. Then, on the right, unburned gas enters into the front $AA$ with a velocity $D$; the combustion products leave on the left, out of the discontinuity $GG$, at the local velocity of sound (thermal choking).

A disturbance that appears on the left of the discontinuity $GG$ cannot propagate towards the gas contained between $GG$ and $AA$, since the local velocity of sound with which such disturbances propagate equals the velocity of escape of the combustion product from $GG$. There is nothing, however, to prevent the propagation of these disturbances along the $y$ axis.

In the shock-compressed region $AA$-$GG$, the local velocity of sound is higher than the velocity ($D - w$) of the nonreacting gas, and therefore the disturbances produced to the right of $GG$ propagate in the region $AA$-$GG$ along both the $y$ and the $z$ axes, both with and against the gas stream.

A small perturbation that is quite possible under real conditions is $bcb$—a small bending of the front $GG$, resulting, for example, from a change in the ignition delay $\tau$, and this can propagate, for the reasons indicated in the foregoing, without opposition in directions perpendicular to the tube axis $z$, as indicated by the vertical arrows in Fig. 1c. In this case the unburned gas, after being first compressed to a pressure $p_A$, will expand in the zones $b$, i.e., the pressure discontinuity produced will attempt to break up in the direction of the $y$ axis, and to assume the value of the pressure $P_G$ of the surrounding burned gas. Consequently, rarefaction waves, the fronts of which are shown by the dotted lines, will travel inside the indicated zones. Such an expansion leads to an adiabatic cooling of the unburned gas in the zones $b$ and an associated lengthening of the ignition delay period $\tau$.

In the region to the right of zone $c$, the unburned gas, after being compressed to a pressure $p_A$, will be compressed even further, for when the disturbances $b$ break up in the direction of the $y$ axis, the already burned gas is additionally compressed in zone $c$. This additional compression of the combustion products violates the Jouguet principle, the wave becomes overcompressed in the region $c$, and a compression wave will travel through the unburned gas toward the forward front $AA$ of the detonation wave; this compression wave will lead to an even further adiabatic heating of the unburned gas and to a resultant reduction in the ignition delay time $\tau$. In the limit, the unburned gas in the zones $b$ may become cooled to a temperature $T = T_A(p_G/p_A)^{(\gamma - 1)/\gamma}$ and the unburned gas to the right of zone $c$ will correspondingly become heated.

The change in temperature of the unburned gas in the perturbation zone $bcb$ will lead to an increase in the perturbation. This increase in perturbation will be limited only by the limiting increase or decrease in temperature of the unburned mixture in the perturbation zone and by the corresponding change in the induction period $\tau$. Taking into account the exponential dependence of the ignition delay period on the

temperature, we must conclude that the perturbation will increase exceedingly rapidly—the detonation wave structure will become inhomogeneous.

It is logical to consider only inhomogeneities that are commensurate in size with the width $\lambda$ of the *AA-GG* combination, since small-scale inhomogeneities can be neglected compared with $\lambda$, while inhomogeneities that are considerably greater than $\lambda$ will obviously no longer be inhomogeneities, but will represent a detonation wave that is curved as a whole. For inhomogeneities commensurate with $\lambda$, a natural scale for the time of the processes in the detonation wave is the ignition induction period $\tau$.

We can therefore formulate the following condition for the instability of the detonation zone with respect to perturbations.

If the disturbance on the combustion front increases the delay in ignition by a time approximately equal to or greater than the induction period $\tau$, then the arbitrary initial curving of the front will increase and the plane front becomes unstable.

If the increase in the ignition delay is small compared with the induction period $\tau$, then the detonation front is stable. On the basis of this analysis, the condition for instability can be written

$$(d\tau/dT)\Delta T \gtrsim \tau \qquad [5]$$

where

$\Delta T$ = change in gas temperature in disturbance region
$d\tau/dT$ = change in ignition delay corresponding to temperature change

The dependence of the ignition delay on the temperature $T$ and on the reaction activation energy $E$ is given by

$$\tau = ke^{E/RT} \qquad [6]$$

where

$R$ = gas constant
$k$ = pre-exponential factor

If the pre-exponential factor is independent of the temperature and the pressure, the result is a criterion for the instability of a plane ignition zone in the detonation wave

$$\frac{E}{RT_A}\left(1 - \frac{T}{T_A}\right) \gtrsim 1 \qquad [7]$$

or, replacing the temperature ratio by a pressure ratio

$$\frac{E}{RT_A}\left[1 - \left(\frac{p_G}{p_A}\right)^{(\gamma - 1)/\gamma}\right] \gtrsim 1 \qquad [8]$$

The foregoing criteria for many known detonating gas mixtures shows that instability should occur in practically all cases.

The results of such an instability are high frequency oscillations, the symptoms of which were observed experimentally by Campbell and Woodhead (8) for the first time in 1926, and were subsequently observed by many other scientists, who have investigated the detonation of different gas mixtures in tubes. If the propagation of a detonation wave is photographed on a film moving in a direction perpendicular to the axis of the tube, the picture will show the development of this process with time. Photographs of the detonation of certain gas mixtures have a front that moves along a wavy line and their combustion products have a band-like structure (Fig. 3), indicating that the zone of maximum light emission propagates along a spiral path.[3] Such a detonation process was therefore called "spin detonation" unlike the "normal" detonation, whose front moves in a straight line and which shows no band-like afterglow (Fig. 4).

Further experimental and theoretical investigations (7,

[3] In Figs. 3, 4 and 5 the horizontal direction is that of the $z$ axis, and the vertical is the time axis $t$.

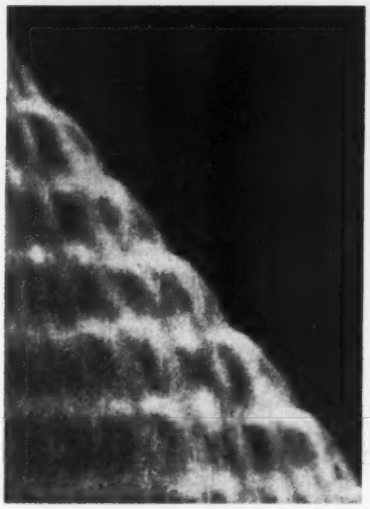

**Fig. 3 Photograph of spin detonation**

**Fig. 4 Photograph of so-called "normal" detonation. The photograph was obtained with low resolution apparatus**

**Fig. 5 Photograph of "normal" detonation, obtained with apparatus of higher resolution. Mixture $2H_2 + O_2$, $p_0 = 760$ mm Hg, $d = 15$ mm, magnification ($G$) 3 × natural size along $z$ axis, scale along time axis—0.2 $\mu$sec/mm**

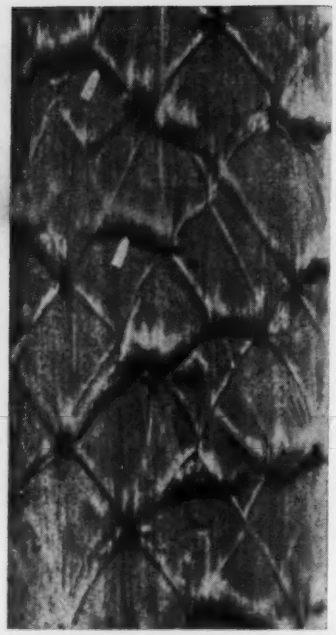

**Fig. 6 Track prints of a pulsating detonation. Mixture $2H_2 + O_2$, $p_0$ = 300 mm Hg, $d$ = 16 mm, $G$ (magnification) = 5. Direction of propagation of the detonation wave is upwards. The arrows indicate the tracks of the periodic flashes**

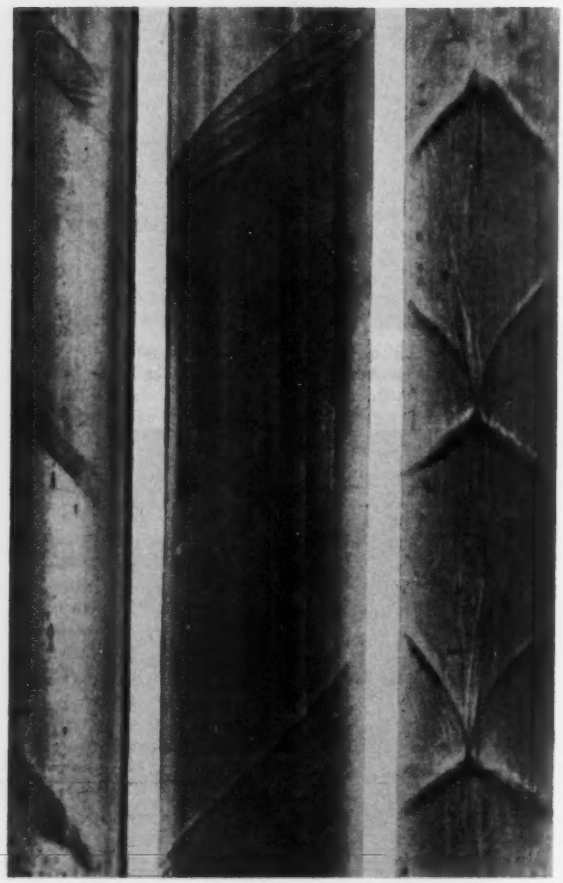

a b c

**Fig. 7 Track prints of detonation of a mixture $2H_2 + O_2$. a, b—spin: $P_0$ = 50 mm Hg; $d$ = 16 mm; $G$ (magnification) for a = 1.3, for b = 2.25. c—pulsating with $n$ = 2: $p_0$ = 130 mm Hg, $d$ = 11 mm, $G$ = 2.5**

14–16) have shown that in spin detonation the forward front of the detonation wave, which occupies a portion of the transverse section of the tube, experiences a kink and becomes an overcompressed oblique detonation wave. It was remarked (17) that spin detonation is generally observed in a detonable mixture that operates near the limit of its detonating ability.

High resolution photography has made it possible recently (12) to show that photographs of complex structure are produced not only by spin-detonation waves, but also by so-called normal-detonation waves, the structure of which is schematically shown in Fig. 1b. One such photograph, obtained with high resolution apparatus, is shown in Fig. 5 and displays periodic inhomogeneities in the front of the detonation wave. To study the nature and mechanism of these inhomogeneities, it was found particularly effective to use a very simple method, that of passing the detonation wave through a glass tube, sufficiently strong to remain unbroken after the explosion and covered inside by a thin layer of lampblack. Tracks are produced on the sooty surface by the inhomogeneities in the detonation front-oblique compression shocks (Fig. 6). Such track prints indicate the places where collisions occur between the oblique shocks. The spacing and the number of shocks near the surface of the tube are calculated from these tracks.

An analysis of the experimental data obtained by such a "track" method and by high resolution photographic scanning, has made it possible to deduce the existence of two types of detonation waves: Spin and pulsation. The corresponding track prints are shown in Figs. 7a and b, and Figs. 6 and 7c, respectively. Spin detonations (Figs. 3, 7a and b) include detonation processes with a single oblique detonation wave, occupying only a portion of the area of the wave front over the section of the tube. The shape of the front remains unchanged in a system of coordinates that moves together with the wave front in rotation and in translation.

The oblique wave, as can be seen clearly from Figs. 7a and b, has in turn a fine structure, evidencing periodic inhomogeneities of the type of oblique shocks, i.e., the instability of the plane structure of the ignition zone and pulsations in the parameters of this overcompressed oblique detonation wave.

In the case of pulsating detonations (Figs. 5, 6 and 7c), the shape of the front changes periodically in a coordinate system that moves together with the front of the wave in translation: The peaks of the front are replaced by valleys, and vice versa. Such a change in the shape of the front of a pulsating detonation is the consequence of periodic collisions between the oblique shocks and the associated pulsations of pressure at the point of collision.

The breakup of the structure of the detonation wave with increasing initial mixture pressure is accompanied by an increase in the velocity of the propagation of the detonation $D$ (Fig. 8a). Corresponding to this change in the velocity $D$ is an increase in the computed theoretical average temperature in the wave $T_A$, leading to a reduction in the delay in ignition $\tau$ and consequently in the width of the ignition zone, $\lambda = \tau(D - w)$ (see Figs. 1b and 8a). As the ratio of the width of the ignition zone $\lambda$ to the tube diameter $d$ is decreased, different modes are realized, from spin to pulsating detonation, with ever increasing values of the number of pulsations $n$ (Fig. 8b) or their frequencies $\nu$, owing to the increase in their temperature $T_A$ as a result of the increase in the initial pressure $p_0$ of the combustible mixture. Fig. 8c shows the graph of such a dependence of the frequency of pulsations in the detonation front $\nu$ and of the number of pulsations over the periphery of the tube $n$ on the initial pressure of a hydrogen-oxygen stoichiometric mixture at a constant tube diameter.

It is thus experimentally confirmed that the instability of a complex with a plane ignition front leads to localization of the chemical reaction in individual sections of the forward front $AA$ of the detonation wave, and to oblique shocks and places of collision between these oblique shocks, where the tempera-

ture and density are higher than in a plane wave. Furthermore, any section of the tube within the zone *A-G* of the schematized detonation complex (see Fig. 1b), contains both unburned gas and ignition products.

It is possible, however, independently of this, to draw behind the real detonation wave a control plane *G-G*, back of which chemical equilibrium exists—the tube is filled either by combustion products containing no unreacted gas, or else it contains reaction products and unreacted matter in a constant ratio.

In a real jet engine combustion chamber the combustion process is also inhomogeneous and, as already noted, there are grounds for assuming that the predominating mechanism of ignition is successive self-ignition of the heated and mixed fuel components. In this case the reaction time (the ignition-delay period) is determined by the same expression as for the detonation wave

$$\tau' = ke^{E/RT}$$

In the jet engine chamber (see Fig. 1a) the role of the control plane *G-G* is played by the boundary between the combustion zone 2 and region 3, while the role of the zone *AA-GG* is played by region 2. Consequently, the initial data that yield the criterion for the instability of combustion in a jet engine chamber are analogous to the initial data used to derive the criterion of instability of combustion in detonation, and it is therefore possible to apply to the high output chamber all the discussions and derivation regarding instability of a plane ignition front, which were used in the case of detonation.

The criterion of combustion instability in a jet engine chamber is written in the form

$$\frac{E}{RT_1}\left[1 - \left(\frac{p_1 - \Delta p}{p_1}\right)^{(\gamma-1)/\gamma}\right] > 1 \qquad [9]$$

where $\Delta p$ is the pressure drop along the chamber due to combustion (Fig. 2).

In jet engine chambers $u_1 \ll a_1$ always, and consequently $\Delta p$ is small compared with $p_1$. Expanding $[(p_1 - \Delta p)/p_1]^{(\gamma-1)/\gamma}$ in powers of $\Delta p/p_1$, and discarding terms of second degree and higher, the instability criterion in a jet engine chamber becomes

$$\frac{\gamma - 1}{\gamma}\frac{E}{RT_1}\frac{\Delta p}{p_1} \gtrsim 1 \qquad [10]$$

Starting with the equation for the Michelson line [2], the Hugoniot curve [1], and again neglecting the square of the quantity $\Delta p_1/p_1$ and the product $(\Delta p/p_1)M_1^2$, we obtain $\Delta p/p_1 = \gamma(\gamma - 1)M_1^2(Q/a_1^2)$. We can now write the criterion [10] in the form

$$(\gamma - 1)^2\frac{EM_1^2}{RT_1}\frac{Q}{a_1^2} \gtrsim 1 \qquad [10a]$$

At sufficiently large $\gamma$, $E$, $\Delta p$, $M_1$ and $Q$ and sufficiently small $T_1$ and $p_1$, the left halves of Equations [10 and 10a] can reach an order of unity. Then the stability of the combustion front will be disturbed, and pulsations of the combustion front will take place in the chamber. Owing to the negligibly small drift of the disturbance in the jet engine chamber ($w \ll a_2$), the dimension of each pulsation in a direction perpendicular to the $z$ axis of the chamber will be on the order of two widths of the combustion zone 2, and therefore a total of

$$n' = \left(\frac{d}{2\lambda}\right)^2 = \left(\frac{d}{2\tau w}\right)^2 \qquad [11]$$

pulsations of the flame front will fit within the cross section area of the jet engine chamber.

The time of development of each disturbance is

$$t_d = \frac{\lambda}{a_2} = \frac{\tau w}{a_2}$$

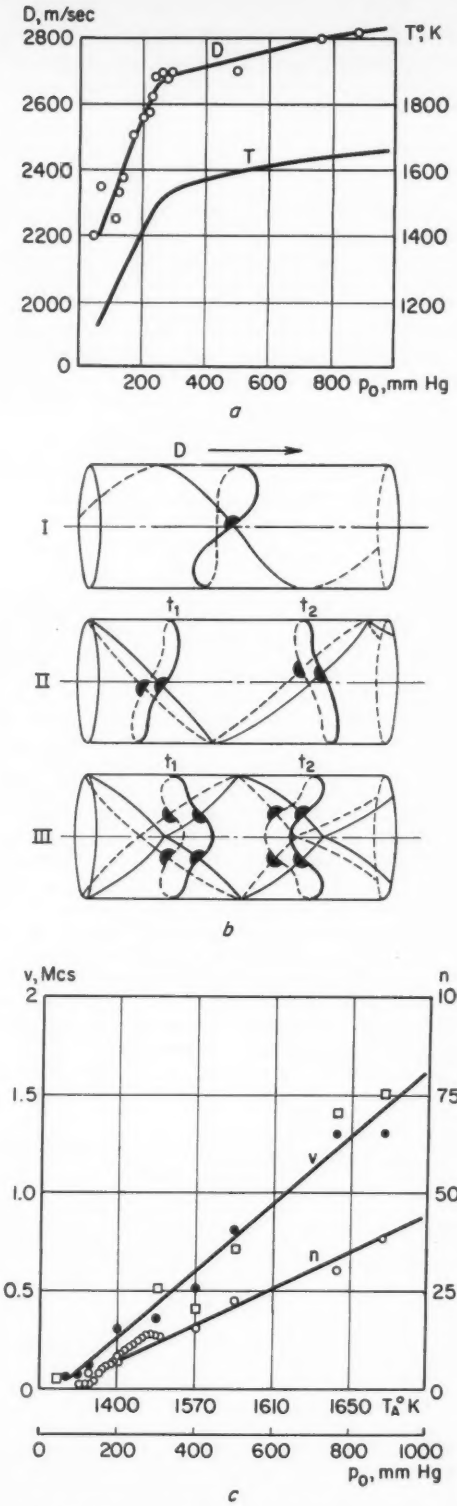


**Fig. 8 Dependence of parameters of detonation wave on initial pressure of reacting mixture (mixture $2H_2 + O_2$, $d = 16$ mm). a—detonation speed $D$ and average temperature $T_A$ in the rate calculated from this velocity. b—shapes of leading front of detonation waves at instants of time $t_1$ and $t_2$: I—spin; II—pulsating with $n = 1$ pulsation along contour of tube cross section; III—pulsating with $n = 2$. c—frequency and number of pulsations $n$; the experimental points shown by squares have been obtained by photographic scanning method, while the others have been obtained by using track method**

The recovery of the disturbed front proceeds at the same rate with which the region 2 is filled with unburned gas. Then the time of liquidation of the disturbance equals the period of induction of ignition

$$t_r \approx \frac{\lambda}{w} = \frac{\tau w}{w} = \tau$$

The total pulsation period consists of the time of development of the disturbance and the time of recovery of the disturbed front. However, for the pulsations in the chamber, where $w \ll a_2$, one can neglect the time of the development of the disturbance $t_d = \tau w/a_2$ compared with $\tau$, and then the period of the oscillations in the chamber is determined only by the time $t_r \approx \tau$. It is seen from Equation [11] that when the region 2 has a width $\lambda$ equal to half the diameter of the chamber, we get $n' = 1$. In this case the fundamental frequency of the oscillations is $\nu_0 = 1/\tau$.

When $n' = 2, 3, 4, \ldots$, i.e., the width of the region 2 is considerably less than half the diameter of the chamber, the frequency of oscillation is

$$\nu_n = \nu_0 n' = \frac{1}{\tau}\left(\frac{d}{2\lambda}\right)^2 \qquad [12]$$

If, at a definite degree of forcing of the combustion in a jet engine chamber, the oscillations enter into resonance with the natural oscillations of the gas in the chamber, a strong increase in the oscillation amplitude is possible.

The resonance mechanism is caused by the fact that when the pressure waves, whose intensity is on the order of $\Delta p$, pass through the combustion zone, they accelerate the combustion, acquire some of the combustion energy, and therefore increase in amplitude. An approximate estimate shows that at resonance the pressure in the compression wave may become twice as large as the initial pressure $p_1$ in the chamber.

It is established furthermore by aerothermodynamic computations (1) that the increase in the rate of ignition causes a considerable increase in pressure in the jet engine chamber, owing to the production of shock waves. Thus, if the rate of ignition is doubled, a compression wave is produced in the chamber with the pressure of four times greater than $p_1$.

The high frequency oscillation in the case of combustion in high output chambers and in detonations has not yet been sufficiently investigated, either experimentally or theoretically, but the foregoing analogy of the two processes enables us to advance the hypothesis that the pulsations in these processes may have a similar nature and a similar mechanism.

If the mechanism of wrinkled flame front turbulent combustion predominates in the chamber, then the instability criterion [9] cannot be employed. But even in this case the thermodynamic analogy between combustion in such a chamber and combustion in a detonation wave is retained.

## References


1 Troshin, Ya. K., "Lower Branch of the Hugoniot Curve as an Aggregate of Points Describing Combustion Modes in Jet-Engine Chambers," *Izvestiia Akad. Nauk SSSR, OTN, Energetika i Avtomatika* (Bull. USSR Acad. Sci., Div. Tech. Sci., Power and Automation), no. 2, 1959.

2 Troshin, Ya. K., "The Generalized Hugoniot Adiabatic Curve," "Seventh Symposium on Combustion," London, 1959, pp. 789–798.

3 Ayvazov, B. V. and Zel'dovich, Ya. B., "Production of an Overcompressed Detonation Wave in a Narrowing Tube," *J. Exptl. Theoret. Phys. (USSR)*, vol. 17, 1947, p. 889.

4 Zel'dovich, Ya. B., "Teoriya Goreniya i Detonatsii Gazov" (Theory of Combustion and Detonation of Gases), USSR Acad. Sci. Press, 1944.

5 Zel'dovich, Ya. B., "Remark on the Article by A. S. Sokolik 'On the Mechanism of Pre-Detonation Acceleration of a Flame,'" *J. Exptl. Theoret. Phys. (USSR)*, vol. 21, 1951, p. 1172.

6 Troshin, Ya. K., "Gasdynamic Analysis of Nonstationary Processes of Propagation of Flames in Tubes," *Izvestiia Akad. Nauk SSSR, OTN* (Bull. Acad. Sci. USSR, Div. Tech. Sci.), no. 1, 1956.

7 Shchelkin, K. I., "Bystroe Gorenie i Spinovaya Detonatsiya Gazov" (Rapid Combustion and Spin Detonation of Gases), Voyenizdat, 1949.

8 Campbell, C. and Woodhead, D. W., "The Ignition of Gases by an Explosion-Wave. Carbon Monoxide and Hydrogen Mixtures," *J. Chem. Soc.*, vol. 129, 1926, p. 3010.

9 Crocco, L. and Cheng, S. I., "Theory of Combustion Instability in Liquid Rocket Engines" (Russian translation), Foreign Literature Press, Moscow, 1958. (Originally published in English by Pergamon Press, New York, 1956.)

10 Smith, R. and Sprenger, D., "Combustion Instability in Solid Propellant Rockets," "Fourth Symposium on Combustion, 1953," Baltimore, 1953, pp. 893–906.

11 Ross, C. C. and Datner, P. P., "Combustion Instability in Liquid Propellant Rocket Motors—A Survey, Selected Combustion Problems," London, 1954.

12 Denisov, Yu. N. and Troshin, Ya. K., "Pulsating and Spin Detonation of Gas Mixtures in Tubes," Doklady Akad. Nauk SSSR (Trans. Acad. Sci. USSR), vol. 125, 1959, p. 110. English translation published by American Institute of Physics, Inc., New York.

13 Shchelkin, K. I., "Two Cases of Unstable Combustion," *J. Exptl. Theoret. Phys. (USSR)*, vol. 36, no. 2, 1959, p. 600. English translation published by American Institute of Physics, Inc., New York.

14 Shchelkin, K. I., "On the Theory of Detonation Spin," Doklady Akad. Nauk SSSR (Trans. Acad. Sci. USSR), vol. 47, 1945, p. 501.

15 Zel'dovich, Ya. B., "On the Theory of Detonation Spin," Doklady Akad. Nauk SSSR (Trans. Acad. Sci. USSR), vol. 52, no. 2, 1946.

16 Zel'dovich, Ya. B. and Kompaneets, A. S., "Teoriya Detonatsii" (Theory of Detonation), Moscow, 1955.

17 Troshin, Ya. K. and Shchelkin, K. I., "On Spin and Limits of Gas Detonation," *Izvestiia Akad. Nauk SSSR, OTN* (Bull. Acad. Sci. USSR, Div. Tech. Sci.), no. 8, 1957.


*—Original received June 13, 1959*

# Location of Frontal Wave in Asymmetrical Flow of Gas at High Supersonic Speed Over a Pointed Body

A. L. GONOR

IN VARIOUS gasdynamic problems it is necessary to know the form of the frontal shock wave produced in flow over a pointed body at an angle of attack.

If the body is a round cone, the form of the wave can be readily determined from the analytical equations given in (1).[1] In engineering practice one is particularly interested in the behavior of the shock angles in the plane of symmetry of the stream (in the shadow and in the windward sides) as functions of the angle of attack, the angle of the cone and the Mach number of the incoming stream. The corresponding formula (1) for these angles, after passing to the limit, has the form

$$\theta_{\pm}^{*} = \theta_0 + \frac{\gamma - 1}{\gamma + 1}\frac{\tan(\theta_0 \pm \alpha)}{t^2}[(1 + t)\ln(1 + t) - t] \times \left[1 + \frac{2}{(\gamma - 1)M^2 \sin^2(\theta_0 \pm \alpha)}\right]$$

$$t = \frac{\pm \sin \alpha}{\sin \theta_0 \cos(\theta_0 \pm \alpha)}$$

where

$\theta_0$ = half the cone vertex angle
$\alpha$ = angle of attack
$\gamma = 1.4$ = adiabatic exponent

The upper sign in the equation corresponds to a meridional plane located on the windward side, and the lower one to a meridional plane located on the shadow side. The shock angle $\theta_{\pm}^{*}$ is measured from the axis of the cone. Results of the calculation with this formula are given in Figs. 1 and 2, which show curves of the shock angles in the symmetry plane, as functions of the angle of attack, for different cone angles at $M = 4$ and $\infty$. The solid lines represent the angles on the windward side, and the dotted ones the angles on the shadow side. These curves disclose an interesting variation in the position of the wave with increasing Mach number. Specifically, while at $M = 4$ the shock angle on the shadow side is greater than on the windward side in all cases (with the exception of the cone with $\theta_0 = 40$ deg) the situation is re-

Translated from *Izvestiia Akademii Nauk SSSR, Otdelenie Tekhnicheskikh Nauk, Mekhanika i Mashinostroenie* (Bull. USSR Acad. Sci., Div. Tech. Sci., Mechanics and Machine Building), no. 5, 1959, pp. 117–118. Translated by J. George Adashko.

[1] Numbers in parentheses indicate References at end of paper.

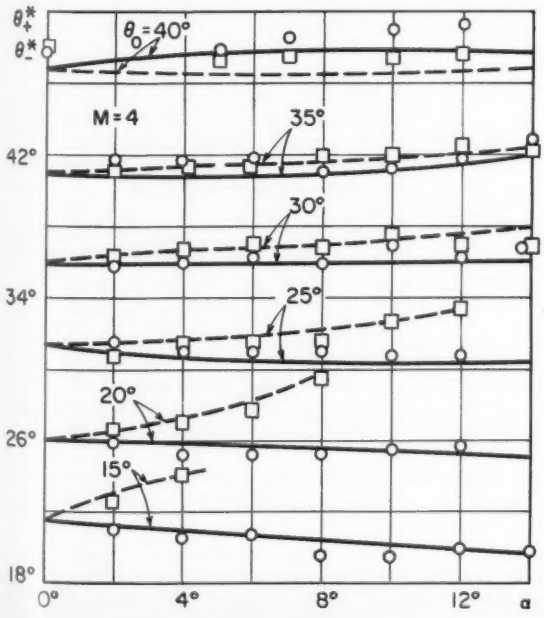


Fig. 1

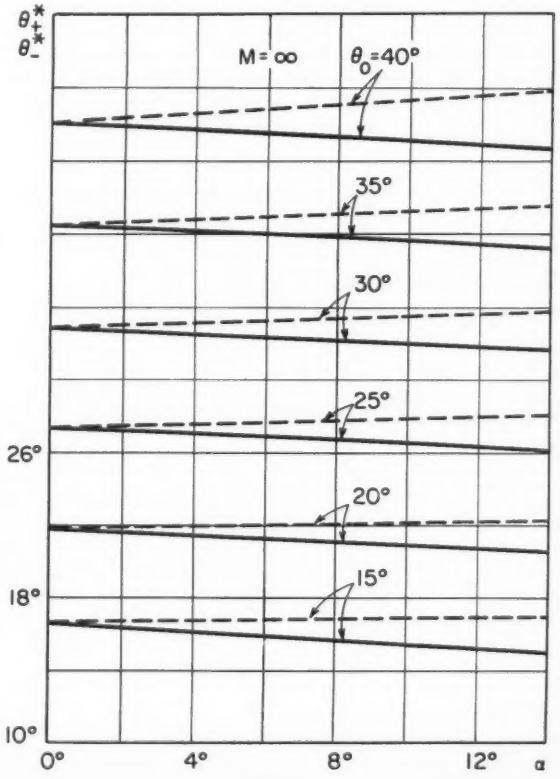


Fig. 2

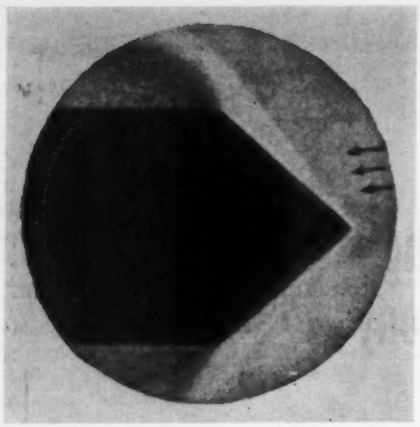

**Fig. 3**

versed at $M = \infty$. This means that for each cone there exists a Mach number at which the shock again becomes almost round, and then flattens towards the body more strongly on the shadow side. As follows from Fig. 1, the thicker the cone, the faster this occurs at a specified Mach number, and at a cone with angle $\theta_0 = 40$ deg this change in the placement of the wave occurs at $M < 4$. In two-dimensional flow a similar conclusion follows directly from an analysis of flow over a wedge. As to the asymmetry of flow over the cone, an analysis of Stone's numerical solution (2) as $M \to \infty$ also leads to a similar result, although the use of this solution for $M \gg 1$ is doubtful.

The published papers do not mention this singularity; to the contrary, the prevailing opinion is that the wave on the shadow side always departs farther away from the body than on the windward side. To verify this conclusion, considering that the increase in the Mach number is equivalent to a changeover to a thicker cone, an experiment was performed, in which flow of air was investigated over six models of cones with half-angles $\theta_0 = 15$, 20, 25, 30, 35 and 40 deg at $M = 4$. A Toepler instrument was used to obtain shadow photographs of the shocks in the symmetry plane of the stream. The shock angles were measured by three methods:

1 The negative was projected on a screen and the contour of the shock wave and of the body was traced and then measured with a protractor.

2 The angles were measured directly on the magnified photographs.

3 The angles were measured through a microscope.

The last method was found to be impractical, since a large spread was obtained of the data obtained when reducing one and the same experiment. The first two methods gave nearly equal results, although the overall accuracy of the measurement remained within 20 min. The results of processing of the pictures are shown in Fig. 1. Here the circles show the values of the angle in the windward side, and the squares those in the shadow side. The experimental points, as can be seen, are located near the corresponding theoretical curves, and the corresponding average curves differ somewhat from the theoretical ones. From the experimental data it follows that as the cone angle increases the shock actually tends to equalize the angles in diametrically opposite planes, and then to assume a smaller angle in the shadow side. Thus, while the angle in the windward side is considerably less than in the shadow side on a cone with angle $\theta_0 = 50$ deg in the presence of an angle of attack, this difference vanishes as the cone angle is increased and at $\theta_0 = 40$ deg the experimental values for the angle are much lower on the shadow side than on the windward side. Fig. 3 shows a shadow photograph of the flow over a cone with angle $\theta_0 = 40$ deg at $\alpha = 12$ deg and $M = 4$. It is seen directly from the photograph that the angle in the shadow side is considerably less than in the windward side.

## References


1 Gonor, A. L., "Flow Over a Cone at an Angle of Attack With Large Supersonic Velocities," *Izvestiia Akad. Nauk SSSR, OTN* (Bull. Acad. Sci. USSR, Div. Tech. Sci.), no. 7, 1958.

2 Stone, A. H., "On Supersonic Flow Past a Slightly Yawing Cone," *J. Math. and Phys.*, vol. XXVII, no. 1, April 1948, pp. 67–81, and vol. XXX, no. 4, Jan. 1952. (Russian translation, collection "Gas Dynamics," Foreign Literature Press, 1950.)



*—Original received May 7, 1959*


---

## Reviewer's Comment

It is noteworthy that Gonor's theoretical curves in Figs. 1 and 2 agree well at zero angle of attack with the shock angle data given in NACA Tech. Rep. 1135, except for cones with half-angles of 30, 35 and 40 deg and at Mach 4 (Fig. 1); these are approximately 1 to 2 deg lower than the NACA cone data. However, this discrepancy does not appear in Fig. 2, the $M = \infty$ case.

This reviewer would be interested in seeing Gonor's original paper (his reference 1) translated or abstracted.


—H. P. Liepman
Space Technology Laboratories, Inc.

# Calculation of the Stability of a Nonlinear Control System in the Presence of Vibration Noise

A. G. BOGDANOV

IN THIS article we calculate the permissible noise amplitude for an airplane-autopilot control system, and make recommendations on the choice of certain autopilot parameters from the point of view of reducing the influence of noise.

The noise may be caused by elastic vibrations of the airplane fuselage, electric fluctuations in the control system circuits, local vibrations, etc.

We assume that the vibration noise obeys a sinusoidal law

$$f_2(t) = B \sin \Omega t \qquad [1]$$

with an amplitude $B$ and a frequency $\Omega$ that is considerably higher than the possible range of frequencies of the useful signal in the system. This means that the vibration component of the signal is in practice blocked by the linear elements located past the nonlinear one, and consequently, the control system is an open-loop one as far as noise goes. In other words, the system is a low-pass filter. The overwhelming majority of airplane control systems have this property.

A more general case, when the signal due to noise may be closed by the feedback loop, and the noise itself may be a random function of time, has been considered in detail in (1 and 2).[1]

If the control system is subject to noise, the input of the nonlinear element will have two components

$$x = x^\circ(t) + A \sin (\Omega t + \varphi) \qquad [2]$$

where $x^\circ(t)$ is a slowly variable component (the useful signal), and $A \sin (\Omega t + \varphi)$ is the noise component.

The amplitude $A$ and the phase $\varphi$ of this component are determined by the transfer function of the linear part of the system $W_l'$ from the noise input point to the input to the nonlinear element (Fig. 1), by means of the formula

$$A = B|W_l'| \qquad \varphi = \arg W_l' \qquad [3]$$

A Fourier expansion of the output of the nonlinear element will have the form

$$y = F^\circ(x) + \text{harmonic components} \qquad [4]$$

where $F^\circ(x)$ is the useful signal, which is defined as the d-c component of the Fourier series. (One can neglect small variations of this component over the vibration period $T_n = 2\pi/\Omega$.)

The harmonic components may be disregarded, since they are suppressed in the linear elements following the nonlinearity. It follows from Equations [2 and 4] that $F^\circ$ is a function of two variables, $A$ and $x^\circ$. Usually $F^\circ(x^\circ)$ (at fixed $A$) is a smooth function, even if the initial nonlinearity is jumplike, and can be linearized for small variation of the useful signal. Then the equation of the nonlinear element in terms of the useful signal becomes

$$F^\circ(x) = K_n x^\circ \qquad [5]$$

where $K_n$ is the gain of the useful signal in the nonlinear element.

The quantity $K_n$ depends on $A$ and is determined (1) by the formula

$$K_n = \left(\frac{\partial F^\circ(x^\circ, A)}{\partial x^\circ}\right)_{x^\circ = 0} \qquad [6]$$

It is found that for most typical nonlinear elements, $K_n$ has the simple analytic expression (see Appendix).

Thus, if the amplitude of the noise component at the input of the nonlinear element is known, then the nonlinear element can be linearized with regard to the useful signal, with a gain $K_n$. Then the nonlinear element will be seen by the useful signal as a linear element of gain $K_n$. The control system can now be investigated by any method of linear theory.

Assume that we have the following automatic control system (Fig. 1):

The airplane equation (longitudinal motion) (3, Fig. 1) is

$$(p^3 + a_1p^2 + a_2p + a_3)\vartheta = K_0(T_0p + 1)\delta \qquad [7]$$

(Here and henceforth, $p \equiv d/dt$.)

The equation of the sensing element (1, Fig. 1) is

$$x_1 = (K_1 + K_2p)[\vartheta + f_1(t) + f_2(t)] \qquad [8]$$

The feedback equation (4, Fig. 1), is

$$x_f = K_f\delta \qquad [9]$$

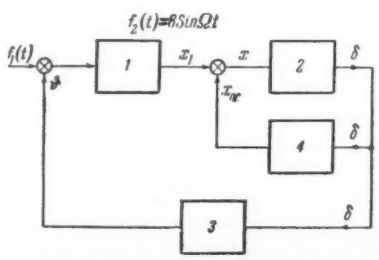


Fig. 1 Translation: $x_{oc} = x_f$

Translated from *Izvestiia Akademii Nauk SSSR, Otdelenie Tekhnicheskikh Nauk, Energetika i Avtomatika* (Bull. USSR Acad. Sci., Div. Tech. Sci., Power and Automation), no. 1, 1960, pp. 165–168. Translated by J. George Adashko.

[1] Numbers in parentheses indicate References at end of paper.

The equations of the steering motor (2, Fig. 1) and amplifier are also assumed given.

On the basis of the physical processes that take place in these blocks, they can be considered as the series connection of a nonlinear element and an inertial-type integrating element (Fig. 2).

Let the noise frequency be known, say $\Omega = 100$ sec$^{-1}$, and let $T = 0.08$ sec. Then, after passing through the steering motor and the amplifier, the fundamental harmonic of the noise will be attenuated and its amplitude will become

$$|W(j\Omega)| = \frac{1}{\Omega\sqrt{T^2\Omega^2 + 1}} \approx \frac{1}{T\Omega^2} = \frac{1}{800} \qquad [10]$$

of the amplitude at the output of the nonlinear element. In practice, therefore, there will be only one noise component at the input of the nonlinear element, and the assumptions made at the beginning of the article are satisfied.

Then the equation of the steering machine and the amplifier, with respect to the useful signal, becomes

$$(T_p + 1)p\delta = K_n x \qquad x = x_1 - x_f \qquad [11]$$

Considering Equations [7–9] and [11], we can represent the system as consisting of two blocks (Fig. 3), the airplane and the autopilot.

In Fig. 3, $K_a = 1/K_f$ is the autopilot gain, while $T_1 = T/K_nK_f$ and $T_2 = 1/K_nK_f$ are the time constants of the autopilot.

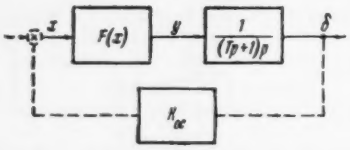


**Fig. 2 Translation:** $K_{oc} = k_f$

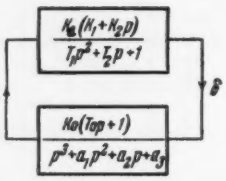


**Fig. 3**

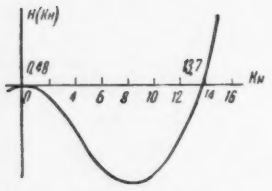


**Fig. 4 Translation:** $K_H = K_n$

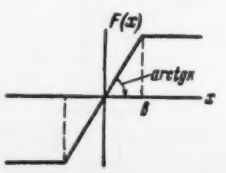


**Fig. 5 Translations:** $B = b$; $\text{arctg} = \tan^{-1}x$

Thus, the time constants of the autopilot depend essentially on the nonlinear gain, meaning that the noise affects the dynamics of the system and may lead under certain conditions to a loss of stability. The characteristic equation of the system becomes

$$A_0p^5 + A_1p^4 + A_2p^3 + A_3p^2 + A_4p + A_5 = 0 \qquad [12]$$

In accordance with the Hurwitz criterion for the stability of a fifth-order system, it is necessary and sufficient that the following inequalities be satisfied

$$A_0 > 0 \quad A_1 > 0 \quad A_2 > 0 \quad A_3 > 0 \quad A_4 > 0$$
$$A_5 > 0 \quad (A_1A_2 - A_0A_3) > 0$$
$$(A_1A_2 - A_0A_3)(A_3A_4 - A_2A_5) - (A_1A_4 - A_0A_5)^2 > 0 \qquad [13]$$

After inserting the values of the parameters and making certain simplifications, the last inequality becomes

$$H(K_n) = K_n^3 - 14.2K_n^2 + 6.51K_n > 0 \qquad [14]$$

A plot of Equation [14] is shown in Fig. 4.

In the interval $0 \leq K_n < 0.48$ condition [14] is satisfied, but the second condition of [13] is not satisfied.

When $K_n > 13.7$, all three Hurwitz conditions are satisfied. Consequently, the system is stable only if

$$K_n > 13.7 \qquad [15]$$

If the nonlinear element has a saturation-type characteristic (Fig. 5), then $K_n$, as a function of the noise amplitude at the input of the nonlinear element $A$, is given by the following formula (see Appendix)

$$K_n = \frac{2K}{\pi} \arcsin \frac{b}{A} \qquad [16]$$

From [16], taking [15] into account, we can readily obtain the maximum permissible amplitude $A_{max}$ of the maximum noise component at the input of the nonlinear element

$$A_{max} = \frac{b}{\sin(\pi K_{n\,min}/2K)} \qquad [17]$$

where $K_{n\,min} = 13.7$.

If, for example, $K = 80$ and $b = 0.5$, then $A_{max} = 1.87$, and the noise amplitude $B_{max}$ will be

$$B_{max} = \frac{A_{max}}{\sqrt{K_1^2 + K_2^2\Omega^2}} \approx \frac{A_{max}}{K_2\Omega} \qquad [18]$$

When

$$A_{max} = 1.87 \quad \Omega = 100 \quad K_1 = 0.9 \quad K_2 = 0.4 \qquad [19]$$

we have

$$B_{max} = 0.047$$

The amplitude of the velocity of the vibrations, corresponding to the resultant value $B_{max}'$, can also be readily determined from [18]

$$B_{max}' \cong \frac{A_{max}}{K_2} = \frac{1.87}{0.4} = 4.7 \qquad [20]$$

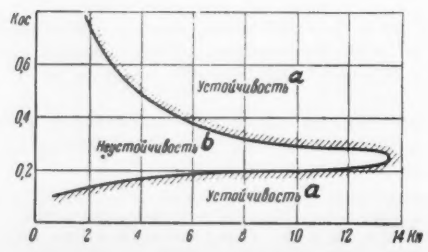


**Fig. 6 Translations:** [a] **stability;** [b] **instability;** $K_{oc} = K_f$; $K_H = K_n$

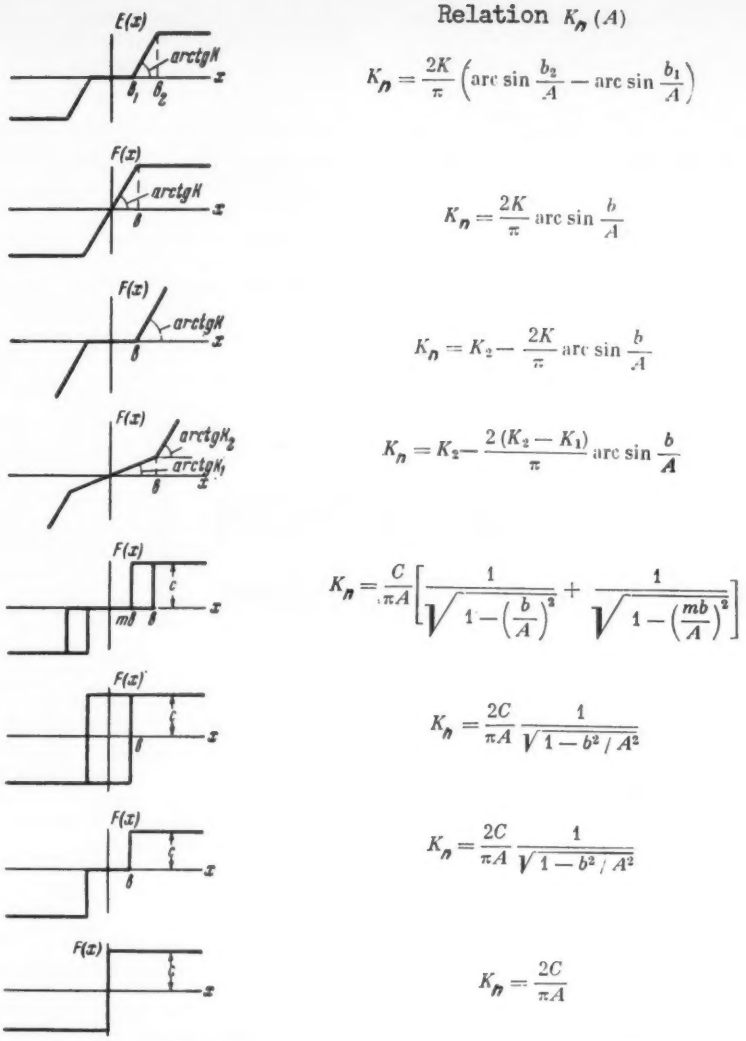


**Fig. 7 Translations: arctg = $\tan^{-1}x$. Note: All formulas valid for $A > b + |x^\circ|$**

Thus, it is enough to apply to the input of the autopilot a vibration noise $B_{max}' = 4.7$ deg/sec in order for the control system to become unstable.

In this example it was found that $B_{max}'$ was independent of the vibration frequency. This is explained by the fact that the component of the noise frequency vibration amplitude at the input of the nonlinear element is determined principally by the derivative of the vibration noise.

The effect of vibration in the system can be reduced by a rational choice of the autopilot parameters. For example, from an examination of the curve of Fig. 6, which shows the stability boundary of the system in the plane of the parameters $K_n$ and $K_f$, it is seen that the most unfavorable feedback coefficients, from the point of view of the effect of noise, are $K_f = 0.2$ to 0.3.

If $K_f$ is chosen on the basis of other conditions (for example, from the condition of insuring specified accuracy or speed of response), it is possible to vary other parameters of the autopilot, for example, $K$, $b$ or $K_2$. If these parameters also fail to give the required stability margin, the structure of the autopilot must be modified.

## Appendix

Useful signal gains in the presence of vibration noise for certain nonlinear elements are shown in Fig. 7.

## References

1 Popov, E. P., "Effect of Vibration Noise on the Stability and Dynamic Quality of Nonlinear Automatic Systems," *Izvestiia Acad. Nauk SSSR, Otd. Tekh. Nauk, Energetika i Avtomatika* (Bull. USSR Acad. Sci., Div. Tech. Sci., Power and Automation), no. 4, 1959.

2 Popov, E. P., "Estimating the Quality of Nonlinear Automatic Systems Subject to Random Noise," *Avtomatika i Telemekhanika* (Automation and Remote Control), no. 10, 1959.

—Submitted December 12, 1959

## Reviewer's Comment

The article represents an interesting, specific investigation of the stabilizing effects of sinusoidal noise in a nonlinear control system of reasonably high degree. The work illustrates an application of the effect pointed out by Tsien in his book "Engineering Cybernetics." Application of the Routh criterion to Equation [12] would normally yield one addi-

tional condition not listed in Equation [13]; whether this condition is implicit in the constraints of [13] or, if not, whether the condition affects the conclusions on the allowable ranges of parameters is not obvious to the reviewer without unwarranted, routine algebraic toil. Regardless of this aspect, the paper emphasizes the importance of a concept frequently overlooked in American literature—a concept which Y. T. Li has illustrated is also useful in the logical design of a class of adaptive systems (in his paper presented at the 1960 IFAC Congress).

—JOHN G. TRUXAL
Department of Electrical Engineering
Polytechnic Institute of Brooklyn

---

# Study of an Optimal Control System in Presence of Random Perturbations

V. M. KUNTSEVICH

**This paper considers an extremal control system employing a synchronous detector[1] and operating in presence of random perturbations. The influence of random factors on the behavior of an extremal system has been considered in various forms in (1,2,5,6).[2] However, papers (2–6) do not carry out the statistical study of the entire closed system as a whole. The paper by A. A. Fel'dbaum (7) considers closed-loop extremal systems of the on-off type, using an idealized impulsive element under the influence of a random interference. However, the study is devoted only to static operating modes, leaving problems of system dynamics out of consideration.**

## 1 Investigation of Interference Immunity of an Optimal Open-Loop System

CONSIDER an optimal control system with a synchronous detector, with a block diagram as shown in Fig. 1. It is known that the operation of this system is based on the fact that when the input of the controlled object contains a modulating signal, the phase of the alternating component at the output is reversed whenever the position of the system is shifted relative to its extremal point. The controlled object is represented in the form of a linear element, which takes into account the inertia of the object, connected in series with a nonlinear inertialess element, which contains the optimalized quantity (8). To simplify the derivations, the origin is made coincident with the optimum point.

The equation of the optimal characteristic, with allowance for the perturbations that change the position of the optimum point, will be written in the form

$$\varphi = -\alpha_3(x + \lambda_1)^2 + \lambda \qquad [1.1]$$

When $\lambda_1$ changes, the optimum point shifts in the $\varphi,x$ plane (where $\varphi$ is the criterion for optimization, and $x$ is the control signal at the input of the nonlinear element) only along the $x$ axis, and when $\lambda$ changes, the optimum point shifts only along the $\varphi$ axis (Fig. 2).

It is the task of the optimal system to follow up the optimum point, i.e., to compensate the effect of the perturbation $\lambda_1$, which shifts the working point relative to the optimum; the system should not respond to a change in the perturbation $\lambda$, since in this case the optimization criterion changes only in absolute value. But, as will be shown in the following, the perturbation $\lambda$ does act as a noise in an optimal system with a detector, and interferes with an accurate determination of the position of the working point relative to the optimum point.

The equation of the linear part of the object will be written in the form

$$L_1(p)x = \mu \qquad [1.2]$$

$$\mu = \mu_r + \mu_m \qquad [1.3]$$

where

$\mu_r$ = regulating signal of the regulator
$\mu_m$ = modulating signal, assumed to be equal to

$$\mu_m = a_m' \sin(\omega_m t + \theta) \qquad [1.4]$$

Solving Equations [1.1, 1.2 and 1.3] simultaneously and assuming that $\theta = \tan^{-1} V^*(\omega_m)/V(\omega_m)$, where $V(\omega_m)$ and $V^*(\omega_m)$ are the real and imaginary parts of the frequency characteristic of element [1.2], we obtain

$$\varphi = \alpha_3\alpha_m^2 \sin^2 \omega_m t + 2\alpha_3\alpha_m(x + \lambda_1) \sin \omega_m t + \alpha_3(x + \lambda_1)^2 + \lambda \qquad [1.5]$$

where

$$a_m = a_m' \sqrt{V^2(\omega_m) + V^{*2}(\omega_m)}$$

It is seen from this expression that only the second term

---

Translated from *Izvestiia Akademii Nauk SSSR, Otdelenie Tekhnicheskikh Nauk, Energetika i Avtomatica* (Bull. USSR Acad. Sci., Div. Tech. Sci., Power and Automation), no. 1, 1960, pp. 90–101. Translated by J. George Adashko.

[1] The practical construction of optimal regulators with synchronous detectors is described in (1–4).[2]

[2] Numbers in parentheses indicate References at end of paper.

contains the required information concerning the position of the system relative to the extremum $(x + \lambda_1)$, since the third term does not contain the sign of this deviation.

The second term of Equation [1.5] will be rewritten

$$\varphi' = 2\alpha_3 a_m |x + \lambda_1| \cos [\omega_m t - \tfrac{1}{2}\pi \operatorname{sign} (x + \lambda_1)] \quad [1.6]$$

from which it is seen that the controlled object phase-modulates the output signal along with changing its amplitude. To obtain a voltage proportional to the deviation from the extremum $(x + \lambda_1)$, the output quantity is applied to a demodulator (synchronous detector).

The equation of the synchronous detector is written in the form

$$y = \varphi \sin \omega_m t \quad [1.7]$$

Solving [1.6 and 1.7] simultaneously, we obtain

$$y = \alpha_3 a_m (x + \lambda_1) + \lambda \sin \omega_m t + [\alpha_s a_m (x + \lambda_1) \sin 2\omega_m t + \tfrac{3}{4}\alpha_3 a_m^2 \sin \omega_m t - \tfrac{1}{4}\alpha_3 a_m^2 \sin 3\omega_m t + \alpha_3 (x + \lambda_1)^2 \sin \omega_m t] \quad [1.8]$$

To prevent false switching of the servomotor by harmonics of the detector output voltage, it is necessary, in a real system, to employ past the low frequency filter an amplifier with a backlash zone of a width such that the amplitude of the higher harmonics at the amplifier output is less than backlash zone.

If this condition is satisfied, the exact Equation [1.8] can be replaced by the following approximate equation

$$y \approx \alpha_3 a_m (x + \lambda_1) + \lambda \sin \omega_m t \quad [1.8a]$$

The equation of the low frequency filter is written in the form

$$L_2(p) z = y \quad [1.9]$$

The equation of the nonlinear amplifier is

$$u = F(z) \quad [1.10]$$

The equation of the servomotor is

$$L_5(p) \mu_p = \alpha_5 u \quad [1.11]$$

Let us investigate the interference immunity of this system with the feedback loop open, under the assumption that the perturbation $\lambda(t)$ is a stationary random function,[3] observed in the interval $(O, T)$ and with a known correlation function $R_\lambda(\tau)$. We represent the function $\lambda(t)$ in the form of a canonical expansion (9,10)

$$\lambda(t) = \sum_{n=0}^{\infty} (A_n \cos n\omega_1 t + B_n \sin n\omega_1 t) \quad \left(\omega_1 = \frac{\pi}{T}\right) \quad [1.12]$$

where $A_n$ and $B_n$ are uncorrelated random quantities with zero mean values, and with dispersions

$$D[A_n] = D[B_n] = D_n \qquad \sigma_n = \sqrt{D_n} \quad [1.13]$$

The dispersions $D_n$ for different $n$ are determined as the coefficients of the Fourier expansion of the correlation function $R_\lambda(\tau)$

$$D_0 = \frac{1}{T}\int_0^\infty R_\lambda(\tau)\, d\tau \quad [1.14]$$

$$D_n = \frac{1}{T}\int_0^\infty R_\lambda(\tau) \cos n\,\omega\tau d\tau \quad [1.15]$$

Let us determine the interference immunity of an open-loop optimal system under the assumption that the random

[3] As can be seen from Equations [1.1 and 1.8], the perturbation $\lambda$ acts like any other perturbation fed directly to the input of the synchronous detector, and we shall henceforth consider it applied to the input of the detector.

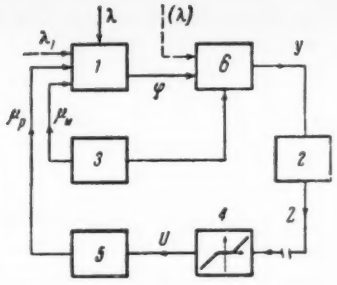


**Fig. 1 Block diagram of an optimal control system employing a synchronous detector. 1-controlled member, 2-filter, 3-pulse generator, 4-nonlinear amplifier, 5-servomotor, 6-synchronous detector. Translations: $\mu_M = \mu_m$; $\mu_p = \mu_r$**

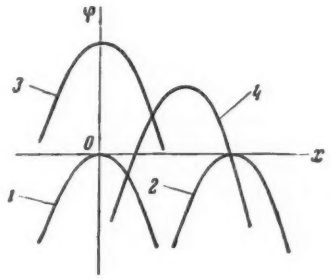


**Fig. 2 Characteristics of the controlled object. 1) $\lambda = \lambda_1 = 0$; 2) $\lambda = 0$, $\lambda_1 \neq 0$; 3) $\lambda \neq 0$, $\lambda_1 = 0$; 4) $\lambda \neq 0$, $\lambda_1 \neq 0$**

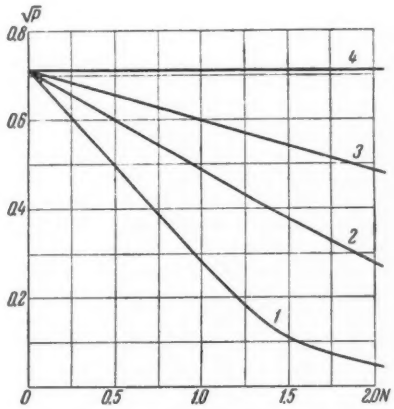


**Fig. 3 Dependence of the error probability in an optimal system with a single detector on the signal-to-nose ratio; $\alpha_3 a_m = 1$. 1) $x = 1$; 2) $x = 0.5$; 3) $x = 0.25$; 4) $x = 0$**

quantities $A_n$ and $B_n$ have normal distributions and that the system contains an ideal low-pass filter which blocks all frequencies above $\omega_m$. Since the d-c component of the voltage $y$ at the output of the synchronous detector is produced only by that synchronous component of $\varphi(t)$ which coincides in phase with the control signal sin $\omega_m t$, the detector in fact separates the d-c useful signal $\alpha_3 a_m x$ (for $\lambda_1 = 0$) from an oscillation of the form

$$\varphi'(t) = (\alpha_3 a_m x + B_k) \sin \omega_m t \qquad (\text{if } k\omega_1 = \omega_m) \quad [1.16]$$

It is seen from [1.16] that the fluctuation noise $\lambda(t)$ will cause errors (distortion) if $B_k > \alpha_3 a_m x$. Therefore the proba-

bility $p$ of the appearance of an error, i.e., the probability of the appearance of a noise $B_k > \alpha_3 a_m x$, is

$$p = \frac{1}{\sigma_k \sqrt{2\pi}} \int_0^\infty \exp\left(-\frac{B^2}{2\sigma_k^2}\, dB\right) = \frac{1}{2}[1 - \Phi(N)] \qquad [1.17]$$

where

$$\Phi(N) = \frac{2}{\sqrt{\pi}} \int_0^N \exp(-t^2) dt$$

is the probability integral, and $N = \alpha_3 a_m x / \sqrt{2}\ \sigma_k$ is the ratio of the effective voltages of the useful signal and of the noise at the detector output.

Figure 3 shows the dependence of the error probability $p$ on the signal-to-noise ratio. Since, when the characteristic of the object is approximated by the parabola [1.1], the value of the useful signal depends not only on the amplitude $a_m$ of the modulating signal but also on the magnitude itself of the deviation $x$ of the system from the optimum (for $\lambda_1 = 0$), then the probability of the error (for constant $a_m$) will increase upon approaching the optimum, and when $x \to 0$ we obtain $p \to 0.5$ (see Fig. 3). Since the error probability can be reduced by increasing the modulation amplitude $a_m$ only at the cost of increased hunting (increase in the d-c component of $\varphi(t)$, due to the modulating action), such a method of increasing the interference immunity of the system is not desirable. In references (1 and 2) a method was proposed of using a more complex modulation signal to improve the interference immunity of an optimal system without increasing hunting.

## 2 Investigation of the Interference Immunity of an Optimal System With the Feedback Loop Open, Using Two Modulating Signals of Different Frequency

To increase the interference immunity of optimal control systems, we have proposed one specific method of compounding the signal, namely simultaneous transmission of two modulating signals $\mu_m'$ and $\mu_m''$ with different frequencies $\omega_m'$ and $\omega_m''$, and detection of the output of the controlled object with the aid of two synchronous detectors, controlled respectively by signals of frequency $\omega_m'$ and $\omega_m''$. A block diagram of such a system is shown in Fig. 4.

Assume that the modulating signals are of the form

$$\mu_m' = a_{m1}' \sin(\omega_m' t + \theta')$$
$$\mu_m'' = a_{m2}' \sin(\omega_m'' t + \theta'') \qquad [2.1]$$

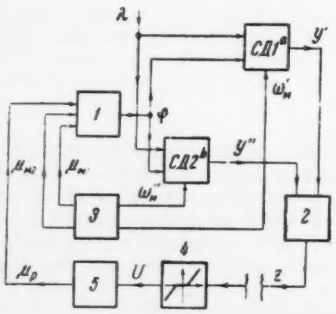


**Fig. 4 Block diagram of an optimal control system with two modulation inputs and two detectors SD1 and SD2 (see Fig. 1 for symbols). Translations: [a] SD1; [b] SD2; $M = m$; $p = r$. Reviewer's note: $\mu_{m1}$ should be $\mu_m'$ and $\mu_{m2}$ should be $\mu_m''$ to be consistent with text**

where

$$\theta' = \tan^{-1}\frac{(V\omega_m')}{U(\omega_m')} \qquad \theta'' = \tan^{-1}\frac{V(\omega_m'')}{U(\omega_m'')}$$

and the equations of the synchronous detectors SD1 and SD2 are respectively

$$y' = \varphi \sin \omega_m' t$$
$$y'' = \varphi \sin \omega_m'' t \qquad [2.2]$$

The frequency ratio of the modulating signals is assumed to be 1:2. Such a ratio is convenient both from the point of view of selection of the low-pass filter parameters, and from many other practical considerations in the construction of the actual system (4).

Solving [1.1, 1.2 and 2.2] simultaneously and taking into consideration the remarks made in the foregoing, we find that (for $\lambda_1 = 0$) each of the detectors actually separates a useful d-c signal from an oscillation of the form

$$\varphi'(t) = (\alpha_3 a_{m1} x + B_k) \sin \omega_m' t$$
$$\varphi''(t) = (\alpha_3 a_{m2} x + B_{k+1}) \sin 2\omega_m' t \qquad (\text{if } \omega_c = \omega_m') \qquad [2.3]$$

where

$$a_{m1} = a_{m1}' \sqrt{U^2(\omega_m') + V^2(\omega_m')}$$
$$a_{m2} = a_{m2}' \sqrt{U^2(2\omega_m'') + V^2(2\omega_m'')}$$

The probability that a fluctuating noise $\lambda(t)$ can produce an error (a change in the polarity of the detector output voltage) is equal to the probability that $B_k > \alpha_3 a_{m1} x$ and correspondingly $B_{k+1} > \alpha_3 a_{m2} x$. The probability of the appearance of an error in each of the detectors SD1 and SD2, each considered separately, is determined from Equation [1.17].

We now determine the probability of a simultaneous appearance of errors in both detectors. The probability of simultaneous appearance of two independent events is equal to the product of the probabilities of each event. Since, by definition, the random quantities $B_k$ and $B_{k+1}$ are uncorrelated, the probability of simultaneous appearance of errors in the detector, under the influence of fluctuations, is

$$p_{12} = p_1 p_2$$

where $p_1$ and $p_2$ are the error probabilities determined from [1.17]. Assuming the amplitudes of both modulating signals to be equal, i.e., $a_{m1} = a_{m2} = a_{m12}$, and considering the dispersion of the noise at the frequencies $\omega_m$ and $2\omega_m''$ also to be equal, we find that the probabilities of a simultaneous appearance of errors in the detectors SD1 and SD2 will be

$$p_{12} = \tfrac{1}{4}[1 - \Phi(N)]^2 \qquad [2.4]$$

A comparison of the probabilities of the errors of both systems shows that at equal hunting errors, the compounding of the modulating signal increases considerably the interference immunity of the optimal system.

Naturally, any further compounding of the modulating system by introducing a third and even higher harmonics and using detectors tuned to these harmonics, makes it possible to increase the interference immunity even further without increasing the hunting. But in many cases the limited bandwidth of the controlled object does not permit the use of more than two or three harmonics in the modulating signal.

## 3 Investigation of the Interference Immunity of a Closed-Loop Optimal System

In the foregoing, we investigated the interference immunity of an open-loop optimal system and took into account only the error induced by the noise at zero frequency, i.e., we studied only the d-c component of the output voltage of the synchronous detector, assuming the low-pass filter to be ideal. In practice, real low-pass filters of a definite bandwidth are used. The behavior of the closed-loop system is also affected by the fluctuation of the voltage at the output of the synchronous detector, resulting from the beats between the noise and the reference voltage of the detector. These detector output voltage oscillations are fed, in final analysis, to the input of the servomotor and cause it to operate falsely. Therefore, to obtain a better evaluation of the quality of an optimal system it is necessary to investigate it with a real filter, in the presence of noise, and with the feedback loop closed.

Let us consider the passage of a signal (regular component) and of noise through the nonlinear element of the control object, and let us establish the connection between the characteristics of the random quantities at the output and input of such an element (11).

Let the nonlinear part of the control object be described, as before, by Equation [2.1], where

$$x = x_r + a_m \sin \omega_m t$$

We shall assume henceforth the perturbation $\lambda_1(t)$ (see Eq. [1.1]) to be a specified function of the time, and the quantity $x_r(t)$ to be a stationary random function, defined within a certain interval of variation of the argument $t$. We represent it in the form

$$x_r(t) = m_x(t) + x_r^\circ(t)$$

where $m_x(t)$ is the mean value of the random quantity $x_r(t)$ and $x_r^\circ(t)$ is a random component with zero mean value and an autocorrelation function $R_x(\tau)$.

We denote the regular component at the input of the nonlinear element by $v$

$$v = m_x(t) + \lambda_1(t) + a_m \sin \omega_m t \qquad [3.1]$$

Then Equation [1.1] of the nonlinear element can be rewritten

$$\varphi = -\alpha_3(x_r^\circ + v)^2 \qquad [3.2]$$

from which we obtain, by averaging, an expression for the expectation value $m_\varphi$ of the output of the nonlinear element

$$m_\varphi = -\alpha_3(\sigma_x^2 + v^2) \qquad [3.3]$$

where $\sigma_x^2 = R_x(0)$ is the intensity of the fluctuation $x_r^\circ$.

The fluctuations at the output of the nonlinear element are determined by the difference

$$\varphi^\circ = \varphi - m_\varphi = -\alpha_3(x_r^2 - \sigma_x^2 + 2x_r v) \qquad [3.4]$$

For the autocorrelation function we can now write, on the basis of [3.4]

$$R_\varphi(\tau) = \overline{\varphi^\circ \varphi_\tau^\circ} = \alpha_3^2(x_r^2 - \sigma_x^2 + 2x_r v)\,(x_{r\tau}^2 - \sigma_x^2 + 2x_{r\tau}v_\tau) = \alpha_3^2\overline{[(x_{1r}^2 - \sigma_x^2)(x_{r\tau}^2 - \sigma_x^2)]} + 4v\overline{v_\tau x_r x_{r\tau}} + 2\alpha_3^2[v(\overline{x_{r\tau}^2} - 1)x_r + v(\overline{x_r^2} - 1)x_{1\tau}] \qquad [3.5]$$

The last term in the square brackets vanishes, since

$$\bar{x}_r = \bar{x}_{r\tau} = 0 \qquad \overline{x_r^2 x_{r\tau}} = \overline{x_{r\tau}^2 x_r} = 0$$

When $\overline{x_r x_{r\tau}} = R_x(\tau)$ we find that the autocorrelation function is

$$R_\varphi(\tau) = 2\alpha_3^2[R_x^2(\tau) + 2vv_r R_x(\tau)] \qquad [3.6]$$

Let us analyze the passage of a random function $\varphi(t)$ through a synchronous detector, the input of which receives also random noise $\lambda(t)$. The detector output voltage is

$$y(t) = \varphi(t) \sin \omega_m t + \lambda(t) \sin \omega_m t \qquad [3.7]$$

It is seen from [3.7] that even though the random functions $\varphi(t)$ and $\lambda(t)$ are stationary random quantities, the random function $y(t)$ is no longer a stationary random process, since its autocorrelation function [i.e., the statistical average of the product $y(t)y(t+\tau)$] and its spectral density depend on the time. The quantity of practical importance is the average (over the time) value of the spectral density. This quantity, which we denote by $S_y(\omega)$, is connected with the average (with respect to time) autocorrelation function by

$$\overline{\overline{yy_\tau}} = \overline{\overline{\varphi\varphi_\tau}}\,\overline{\overline{ff_\tau}} + \overline{\overline{\lambda\lambda_\tau}}\,\overline{\overline{ff_\tau}} \qquad (f = \sin \omega_m t) \qquad [3.8]$$

by the same relations that hold for the spectral density of the functions $\varphi$, $\lambda$ and the autocorrelation functions $R_\varphi(\tau)$, $R_\lambda(\tau)$

$$S_b(\omega) = \frac{2}{\pi}\int_0^\infty \overline{\overline{yy_\tau}} \cos \omega\tau d\tau = \frac{2}{\pi}\int_0^\infty R_\varphi(\tau)\overline{\overline{ff_\tau}} \cos \omega\tau d\tau + \frac{2}{\pi}\int_0^\infty R_\lambda(\tau)\overline{\overline{ff_\tau}} \cos \omega\tau d\tau \qquad [3.9]$$

Let us consider the first component of the spectrum in [3.9], which, considering [3.6 and 3.8], can be written in the following manner

$$\overline{\overline{R_\varphi(\tau)\,ff_\tau}} = [2\alpha_3^2 R_x^2(\tau) + 4\alpha_3^2\overline{vv_\tau}R_x(\tau)]\overline{\overline{ff_\tau}} = \alpha_3^2 R_x^2(\tau)\cos \omega_m(\tau) + \frac{\alpha_3^2 a_m^2}{2} R_x(\tau) + \frac{\alpha_3^2 a_m^2}{2} R_x(\tau) \cos 2\omega_m\tau \qquad [3.10]$$

Considering that

$$\overline{\overline{ff_\tau}} = \tfrac{1}{2}\cos \omega_m\tau \qquad \overline{\overline{vv_\tau}} = \tfrac{1}{2}a_m^2 \cos \omega_m\tau \qquad [3.11]$$

Let us use furthermore the following relations

$$S(\omega) = \frac{2}{\pi}\int_0^\infty [R(\tau) \cos \omega_0\tau] \cos \omega\tau d\tau = \frac{1}{4}[S'(\omega - \omega_0) + S'(\omega + \omega_0)] \qquad [3.12]$$

if

$$S'(\omega) = \frac{2}{\pi}\int_0^\infty R(\tau)\cos\omega\tau d\tau$$

Taking [3.12, 3.9 and 3.10] into consideration we obtain for the spectral density at the detector output the following expression

$$S_y(\omega) = \frac{\alpha_3^2 a_m^2}{2} S_x(\omega) + S_\lambda'(\omega) + \alpha_3^2 a_m\left\{\frac{1}{8}[S_x(\omega - 2\omega_m) + S_x(\omega + 2\omega_m)] + \frac{2}{a_m^2\pi}\int_0^\infty R_x^2(\tau)\cos\omega_m\tau\cos\omega\tau d\tau\right\} \quad [3.13]$$

where

$$S_x(\omega) = \frac{2}{\pi}\int_0^\infty R_x(\tau)\cos\omega\tau d\tau \quad [3.14]$$

$$S_\lambda(\omega) = \frac{2}{\pi}\int_0^\infty R_\lambda(\tau)\cos\omega\tau d\tau \quad [3.15]$$

$$S_\lambda'(\omega) = \tfrac{1}{4}[S_\lambda(\omega - \omega_m) + S_\lambda(\omega + \omega_m)] \quad [3.16]$$

It is seen from this expression that the spectral densities at the output of the detector and the input of the nonlinear element are connected by nonlinear relations, so that it is impossible to investigate accurately the closed-loop control system in general form. We shall assume henceforth that the spectrum of the noise $\lambda(t)$, causing the fluctuations in the closed-loop control system, is uniform over the bandwidth of the system. We shall also assume for an approximate solution of the problem of interest to us that the spectrum at the detector output is determined only by the first two terms of expression [3.13], i.e.

$$S_y(\omega) \approx \frac{\alpha_3^2 a_m^2}{2} S_x(\omega) + S_\lambda'(\omega) \quad [3.17]$$

The basis for replacing Equation [3.3] by the approximate Equation [3.17] is the following argument. The spectrum of the fluctuation $S_x(\omega - 2\omega_m)$, corresponding to the high frequency oscillations, is outside the bandwidth of the system, and can therefore be disregarded. The greatest error resulting from going from [3.13] to [3.17] is due to neglecting the spectrum of the high frequency fluctuations $S_x(\omega + 2\omega_m)$ (which are adjacent to $\omega = 0$), but the spectral density of these fluctuations does not amount in any case to more than 0.25 of the spectral density of the principal term $S_x(\omega)$.

The spectrum corresponding to the last term of the curly brackets in [3.13] can also be represented in the form of a sum of low frequency and high frequency fluctuations. When the optimal system under consideration (which, like ordinary control systems, is a low-pass filter) is acted upon by a random function with a spectrum that is uniform within the bandwidth of the system, the autocorrelation function of the variable $x$ can be represented (although approximately) in the form

$$R_x(\tau) = \exp(-\alpha|\tau|)\cos\beta\tau \quad [3.18]$$

which corresponds to a spectral density

$$S_x(\omega) = \frac{1}{\pi}\left[\frac{\alpha}{\alpha^2 + (\omega + \beta)^2} + \frac{\alpha}{\alpha^2 + (\omega - \beta)^2}\right] \quad [3.19]$$

Taking [3.14, 3.18 and 3.19] into account, the spectral density $S_x''(\omega)$, corresponding to the autocorrelation function $1/a_m^2 R_x^2(\tau)\cos\omega_m\tau$, can be written in the form

$$S_x''(\omega) = \frac{1}{8a_m^2}[S_x'(\omega - \omega_m) + S_x'(\omega + \omega_m)] + \frac{1}{16a_m^2}[S_x'(\omega - 2\beta + \omega_m) + S_x'(\omega + 2\beta - \omega_m)] + \frac{1}{16a_m^2}[S_x'(\omega - 2\beta - \omega_m) + S_x'(\omega + 2\beta + \omega_m)] \quad [3.20]$$

where

$$S_x'(\omega) = \frac{1}{\pi}\left[\frac{2\alpha}{4\alpha^2 + (\omega + \beta)^2} + \frac{2\alpha}{4\alpha^2 + (\omega - \beta)^2}\right]$$

is the spectral density corresponding to the autocorrelation function $R_x'(\tau) = \exp(-2\alpha|\tau|)$.

The high frequency components of the spectrum $S_x''(\omega)$ lie outside the bandwidth and can be disregarded. As to the low frequency fluctuations, adjacent to $\omega = 0$, it is seen from [3.20] that they amount to not more than 0.15—0.2 of the spectral density of the principal term of [3.13].

The expectation value of the regular component at the output of the detector is determined from [1.7 and 3.3]

$$m_y = m_\varphi \sin\omega_m t \quad [3.21]$$

Substituting [3.3] in [3.21] we obtain, after averaging over the time

$$\tilde{m}_y = -\alpha_3 a_m(m_x + \lambda_1) \quad [3.22]$$

which corresponds to the previously obtained expression [1.8].

Thus, from the point of view of the transformation of the expectation values, the nonlinear portion of the controlled object and the synchronous detector are equivalent to a linear inertialess element that satisfies Equation [3.22], and it follows from [3.16 and 3.17] that, from the point of view of the transformation of random components, these elements can also be approximated by a linear element satisfying the equation

$$y^\circ(t) = -\frac{\alpha_3 a_m}{\sqrt{2}} x^\circ(t) + \lambda(t)\sin\omega_m t \quad [3.23]$$

We now establish a quantitative connection between the characteristics of the random functions for the input and output quantities of the nonlinear amplifier with the characteristics [3.2].

We use for this purpose the method of statistical linearization (12), which is at the present time the only method that allows an investigation of the accuracy of systems containing elements with discontinuous functions.

The principal idea of this method is to choose such an approximate linearized connection between the output and the input of the nonlinear inertialess element, that the expectation values of the autocorrelation functions of the actual function and of its approximation be sufficiently close to each other.

Thus, if the random functions $u(t)$ and $z(t)$ are connected by a functional relationship

$$u(t) = F[z(t)]$$

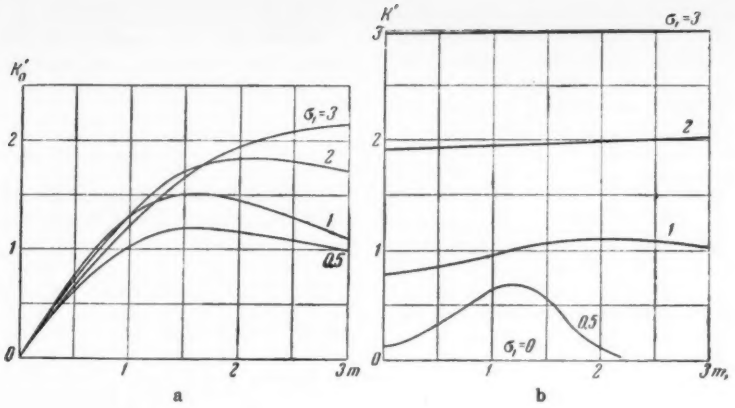


Fig. 5 a—**Dependence of the statistical transfer factor $k_0'$ of the regulator component on $m_1$, $\sigma_1$, for $F(z)$ given by Equation [3.27]**

$$k_0 = \frac{\alpha_4}{m_z}\psi_0(m_1, \sigma_1) \qquad m_1 = \frac{m_z}{\Delta} \qquad \sigma_1 = \frac{\sigma_z}{\Delta}$$

b—**Dependence of the statistical transfer coefficient $k_1$ of the random component on $m_1$, $\sigma_1$, for $F(z)$ given by Equation [3.27]**

$$k_1 = \frac{\alpha}{\sigma_z}\psi_1(M_1, \sigma_1)$$

then the transformed random function is represented in the form

$$u(t) \approx k_0 m_z + k_1 z^\circ(t) \qquad [3.24]$$

where $k_0$ and $k_1$ are the static transfer functions of the nonlinear element with respect to the regular ($m_z$) and random ($z^\circ$) components.

For an approximate determination of the coefficients $k_0$ and $k_1$, two methods have been proposed in (12), one of which [called the second method in (12)] consists of determining $k_0$ and $k_1$, starting out with the requirement that the expectation value of the difference of the two functions, the true and the approximating one, be a minimum. Since this method yields too high values for the coefficients $k_0$ and $k_1$ (by up to 20 per cent), and since we have discarded several terms to obtain the approximate equation [3.17], it is better to employ for partial compensation of this error the somewhat overestimated values of $k_0$ and $k_1$, obtained by calculation with the second method of (12).

The statistical transfer functions are simplest to determine when the input function has a normal distribution. We shall use henceforth the curves for $k_0$ and $k_1$, calculated in (12), by making precisely this assumption. The physical basis for using statistical transfer functions calculated from the normal distribution is the fact that the nonlinear element is connected in series with the inertial linear elements. On the other hand, as the linear part of the system transforms the random functions, it transforms the distribution law and makes it closer to normal.

We can now write, on the basis of the results obtained from [1.2, 3.22, 2.9, 3.24 and 2.11], the following equation for the expectation value of the coordinate $z$ in the closed-loop system

$$[L_1(p)L_2(p)L_5(p) + \alpha_3\alpha_5 a_m k_0(m_z, \sigma_z)]m_z = -\alpha_3 L_1(p)L_5(p)\lambda_1 \qquad [3.25]$$

and the following equation for the random components on the basis of [1.2, 3.23, 3.24, 2.9 and 2.11]

$$[L_1(p)L_2(p)L_5(p) + \frac{\alpha_3\alpha_5 a_m}{\sqrt{2}} k_1(m_z, \sigma_z)]z^\circ = L_1(p)L_5(p)\lambda \sin \omega_m t \qquad [3.26]$$

Equations [3.25 and 3.26] make it possible to analyze the closed-loop optimum system and to select, by calculating several variants, the optimum parameters of the system and, particularly, to obtain the optimum value of the amplitude of the modulating signal.

Equations [3.25 and 3.26] determine the unknown values of $m_z$ and $\sigma_z^2$. However, the right halves of these equations contain also the quantities $m_z$ and $\sigma_z$, through the expressions for $k_0(m_z, \sigma_z)$ and $k_1(m_z, \sigma_z)$, and they must therefore be determined by successive approximation or graphically, using curves of the functions $k_0$ and $k_1$. After determining $m_z$ and $\sigma_z$ by solving [3.25 and 3.26], we can then determine the mathematical expectation and the dispersion of any other variable system.

To illustrate the procedure developed in the foregoing, let us consider the example which follows.

*Example:* Let the transfer functions of the elements of a system have the following form

$$L_1(p) = (\tau_1 p + 1) \qquad L_2(p) = (\tau_2 p + 1)$$

$$L_5(p) = p \qquad F(z) = \begin{cases} +\alpha_0 \text{ for } z > \Delta \\ 0 \text{ for } |z| < \Delta \\ -\alpha_0 \text{ for } z < -\Delta \end{cases} \qquad [3.27]$$

We assume, furthermore, that $\lambda_1(t) = 0$, i.e., we investigate the behavior of a system with a fixed optimum point (on the $x$ axis) under the influence of a random noise $\lambda(t)$, which has a spectral density $S_\lambda(\omega) = 2c^2$ ("white noise").

The purpose of further investigation is the determination of the optimum value of the amplitude of the modulating signal $a_m^\circ$, at which an expectation value is attained for the deviation of the system from the optimum point $(m_\varphi)_{\min}$, for a constant overall gain of the entire system.

We assume furthermore that the closed-loop system is stable for the selected values of the parameter [a stability

test can be performed by the method of harmonic linearization; see, for example, (3)]. The backlash zone of the nonlinear amplifier and the parameters of the low-pass filter are chosen here such that for the assumed amplitude of the modulating signal, the conditions under which [1.8a] is valid are satisfied. As follows from [3.25], $m_z = 0$ when $\lambda_1(t) = 0$.

The amplitude-phase characteristic of the system, for variable $z$, becomes in this example

$$W_z(j\omega) = \frac{j\omega(1 + j\omega\tau_1)}{-j\omega^3\tau_1\tau_2 - \omega^2(\tau_1 + \tau_2) + j\omega + \frac{1}{\sqrt{2}}\,\alpha_3\alpha_5 a_m k_1(\sigma_z)}$$

Using the well-known relations (9,13), we find that the mean squared error $\sigma_z^2$ is

$$\sigma_z^2 = \frac{1}{2\pi j}\int_{-\infty}^{\infty} \frac{[j\omega(1 + j\omega\tau_1)]^2}{\left[-j\omega^3\tau_1\tau_2 - \omega^2(\tau_1 + \tau_2) + j\omega + \frac{1}{\sqrt{2}}\,\alpha_3\alpha_5 a_m k_1(\sigma_z)\right]^2} S_\lambda'(\omega)\,d\omega$$

where $S_\lambda'(\omega)$, on the basis of [3.16], is given in this case by

$$S_\lambda'(\omega) = c^2$$

Using the handbook tables (13,9), we finally obtain

$$\sigma_z^2 = c^2 \frac{\tau_1\tau_2 - \tau_1^2}{2\tau_1\tau_2\left[\tau_1 + \tau_2\frac{\tau_1\tau_2}{\sqrt{2}}\,\alpha_1^2\alpha_3\alpha_5 a_m k_1(\sigma_z)\right]}$$

For the given numerical values of the system parameters, solving this equation by trial and error [using the curves of Figs. 12 and 14 of reference (12)], it is easy to determine the numerical values of $\sigma_z^2$ and $k_1(\sigma_z)$.

Since the further investigation of the optimal value of $a_m$ is based on the assumption that the varied parameters are the quantities $a_m$ and $\alpha_0$, and that the overall gain of the system does not change, i.e.

$$\alpha_\Sigma = \frac{1}{\sqrt{2}}\,\alpha_3\alpha_5 a_m k_1(\sigma_z) = \frac{\alpha_0\alpha_3\alpha_5 a_m \psi_1(\sigma_1)}{\sqrt{2}\,\sigma_z} = \text{const}$$

where

$$k_1(\sigma_z) = \frac{\varkappa_0}{\sigma_z}\,\psi_1(\sigma_1)$$

$$\sigma_1 = \frac{\sigma_z}{\Delta}$$

and $\psi_1(\sigma_1)$ is determined from the curves of reference (12), it is not necessary to calculate the numerical value of $k_1(\sigma_z)$ to obtain the optimum value of $a_m$, since $k_1(\sigma_z)$ and $\sigma_z$ remain constant with varying $a_m$ and for $\alpha_\Sigma = \text{const}$.

Substituting $p = j\omega$ in the transfer function of the system relative to the variable $x$, we obtain for our example the following amplitude-phase characteristic

$$W_x(j\omega) = \frac{\alpha_0\alpha_5 k_1(\sigma_z)}{-j\omega^3\tau_1\tau_2 - \omega^2(\tau_1 + \tau_2) + j\omega + \frac{\alpha_0\alpha_3\alpha_5 a_m(\sigma_z)}{\sqrt{2}}}$$

For the mean squared error $\sigma_x^2$ we obtain

$$\sigma_x^2 = \frac{1}{2\pi j}\int_{-\infty}^{\infty} \frac{[\alpha_0\alpha_5 k_1(\sigma_z)]^2 S_\lambda'(\omega)}{\left[-j\omega^3\tau_1\tau_2 - \omega^2(\tau_1 + \tau_2) + j\omega + \frac{1}{\sqrt{2}}\,\alpha_3\alpha_5 a_m k_1(\sigma_z)\right]^2} d\omega$$

which, when integrated, yields

$$\sigma_x^2 = c^2 \frac{\alpha_0\alpha_5 k_1(\sigma_z)(\tau_1 + \tau_2)}{\sqrt{2}\,\alpha_3\alpha_5\left[\tau_1 + \tau_2 - \tau_1\tau_2\frac{\alpha_0\alpha_3\alpha_5 a_m k_1(\sigma_z)}{\sqrt{2}}\right]}$$

where $k_1(\sigma_z)$ can be considered as a constant.

Substituting the resultant expression into [3.3] for the expectation value $m_\varphi$ and taking [3.1] into account, we obtain after averaging

$$\tilde{m}_\varphi = \alpha_3^2\left[\frac{\alpha_\Sigma(\tau_1 + \tau_2)c^2}{\alpha_1\alpha_3^2 a_m^2(\tau_1 + \tau_2 - \tau_1\tau_2\alpha_\Sigma)} + \frac{a_m^2}{2}\right]$$

A test for the minimum of the resultant expression shows that the minimum of $\tilde{m}_\varphi$ is obtained when

$$a_m^\circ = \sqrt[4]{2A}$$

where

$$A = c^2\,\frac{\alpha_\Sigma(\tau_1 + \tau_2)}{\alpha_1\alpha_3^2(\tau_1 + \tau_2 - \tau_1\tau_2\alpha_\Sigma)}$$

Under optimum choice of the amplitude of the modulating signal, i.e., when $a_m = a_m^\circ$, we have

$$(m_\varphi)_{\min} = \alpha_3^2\sqrt{2A} = c\alpha_3\sqrt{\frac{2\alpha_\Sigma(\tau_1 + \tau_2)}{(\tau_1 + \tau_2 - \tau_1\tau_2\alpha_\Sigma)\alpha_1}}$$

Putting $\tau = 0$ in [3.4] and averaging [3.6] over the time, we find that the average mean squared error is

$$\tilde{\sigma}_\varphi^2 = 2\alpha_3^2\sigma_z^2(\sigma_z^2 + \alpha_1^2 a_m^2)$$

Comparing this relation with the expression for the minimum of $\tilde{m}_\varphi$, it is easy to note that the minimum of $\tilde{\sigma}_\varphi^2$ is reached when $a_m = \sqrt[4]{A}$.

## References


1 Ivakhnenko, A. G., "Basic Problems in the General Theory of Cybernetic Automatic Control Systems," Parts II, III, *Avtomatika* (Automation) no. 4, 1950; no. 1, 1959.

2 Ivakhnenko, A. G., "Tekhnicheskaya Kibernetika" (Technical Cybernetics), Gostekhizdat UkrSSR, Kiev, 1959.

3 Kuntsevich, V. M., "Investigation of Optimal Control Systems With Synchronous Detector," *Avtomatika* (Automation), no. 3, 1959.

4 Krug, E. K., "On One Method of Optimum Control," Conference on Theory and Application of Discrete Automatic Systems, Moscow, 1958.

5 Fel'dbaum, A. A., "Effect of Random Factors on the Process of Automatic Search," *ibid.*

6 Serdengecti, Sedat, "Optimalizing Control in the Presence of Noise Interference," Jet Propulsion, vol. 26, no. 6, June 1956, pp. 465–473.

7 Fel'dbaum, A. A., "Steady State in the Simplest Discrete Optimalizing System in the Presence of Random Noise," *Avtomatika i Telemekhanika* (Automation and Remote Control), vol. 20, no. 8, 1959.

8 Kryzhanovskii, O. M. and Kuntsevich, V. M., "Transients in Optimal Control Systems," *Izvestiia Akad. Nauk SSSR, Otd. Tekh. Nauk, Energetika i Avtomatika* (Bull. USSR Acad. Sci., Div. Tech. Sci., Power and Automation), no. 3, 1959. (Translated in ARS Journal, vol. 30, no. 1, Jan. 1960, pp. 86–92.)

9 Pugachev, V. S., "Teoriya Sluchainykh Funktsii i ee Primenenie k Zadacham Avtomaticheskovo Upravleniya" (Theory of Random Functions and Its Application to Problems of Automatic Control), State Pub- 86–92.)

lishing House of Theoretical and Technical Literature, Moscow, 1957.
10 Ventsel', E. S., "Teoriye Véroyatnostei," (Theory of Probability), Moscow, 1958.
11 Bunimovich, V. I., "Fluctuation Processes in Radio Receiving Devices," "Soviet Radio" Press, Moscow, 1951.
12 Kazakov, I. E., "Approximate Probability Method of the Accuracy of Essentially Nonlinear Automatic Systems," *Avtomatika i Telemekhanika* (Automation and Remote Control), vol. XVII, no. 5, 1956.
13 James, H. M., Nichols, N.B. and Phillips, R.S., "Theory of Servomechanisms," McGraw-Hill Book Co., New York, 1947.

*—Original received October 2, 1959*

### Reviewer's Comment

The author considers a class of extremum-seeking control systems in which sinusoidal modulation is employed in conjunction with a synchronous detector to detect the deviation from the extremal condition. The paper extends the work in this field to the case where the dynamics of the system elements may be considered, as well as the effect of a random disturbance occurring within the system. The results of the development in the paper permit the selection of the amplitude of the modulating signal in order to minimize (in the mean square sense) the effect of the random disturbance on the extremum searching function of the control system. A numerical example is presented to illustrate the technique. The paper further indicates an intensive effort in the field of optimalizing control in the USSR, an effort which was particularly notable at the Moscow IFAC Congress.

—JOHN G. TRUXAL
Department of Electrical Engineering
Polytechnic Institute of Brooklyn

# Problem of Nearly Self-Similar Unsteady Motion

T. G. KOLDOBSKAYA

MANY RECENT papers on gasdynamics are devoted to methods of investigating self-similar gas motion (1–6).[1] As is well known, a self-similar motion is defined analytically by means of a system of equations in which the number of independent variables can be reduced by a change of variables. This property of self-similar motion simplifies considerably the principal equations and affords solutions to many problems of practical importance, which otherwise would entail insurmountable difficulties.

In this connection, interest attaches to problems involving flow which is nearly self-similar. Each particular flow of this class is associated, in accordance with a definition which will be given in the following, with a nearly equivalent self-similar flow. The elements of the self-similar flow, which we shall call the basic flow, are assumed known.

The purpose of the present work is to obtain the hydrodynamic elements of a plane or axially symmetric unsteady nearly self-similar motion, i.e., to obtain the corrections to the known self-similar solution.

In this case, if some self-similar problem can be solved for a wedge (or cone) of arbitrary angle (or if a corresponding series of experimental data is available), it can be assumed that the solution of this problem will give us, in some unique linear formulation, a flow of the same kind about any cylindrical (or axially symmetric) body, with a profile such that the derivative of the contour lines does not change too rapidly.

Translated from *Vestnik Leningradskovo Universiteta* (Bulletin of the Leningrad University), no. 1, 1960, pp. 111–122. Translated by J. George Adashko.

[1] Numbers in parentheses indicate References at end of paper.

## 1 Unsteady Plane Flow About a Nearly Wedge-Shaped Body. Formulation of the Problem

The degree to which the surface of a given cylindrical body is close to that of a certain wedge is judged by the following conditions.

1 The generatrices of the cylindrical surface of the body are parallel to those of the wedge.

2 The profile of the wedge is tangent to the profile of the given body at the nose.

3 The angles between the wedge and the tangent to the profile of the body are assumed to be small everywhere.

We choose a Cartesian coordinate system such that the profile of the body lies in the $(x, y)$ plane and the origin coincides with the nose of the profile. For simplicity we assume the profile to be symmetrical about the $x$ axis and consider only its upper half (Fig. 1).

In all further investigations we make the usual gasdynamic assumptions and consider the gas to move adiabatically and to be free of internal friction.

### Equations of Motion

The equations of unsteady plane gas motion are of the form

$$\frac{\partial u}{\partial t} + u\frac{\partial u}{\partial x} + v\frac{\partial u}{\partial y} + \frac{1}{\rho}\frac{\partial p}{\partial x} = 0$$

$$\frac{\partial v}{\partial t} + u\frac{\partial v}{\partial x} + v\frac{\partial v}{\partial y} + \frac{1}{\rho}\frac{\partial p}{\partial y} = 0$$

$$\frac{\partial \rho}{\partial t} + u\frac{\partial \rho}{\partial x} + v\frac{\partial \rho}{\partial y} + \rho\left(\frac{\partial y}{\partial x} + \frac{\partial v}{\partial y}\right) = 0$$

$$\frac{\partial}{\partial t}\left(\frac{p}{\rho^\kappa}\right) + u\frac{\partial}{\partial x}\left(\frac{p}{\rho^\kappa}\right) + v\frac{\partial}{\partial y}\left(\frac{p}{\rho^\kappa}\right) = 0$$

.....[1.1]

where

$u, v$ = projections of the velocity on the $x$ and $y$ axes, respectively
$p$ = pressure
$\rho$ = density
$\kappa$ = ratio of specific heats.

Let $u_0$, $v_0$, $p_0$ and $\rho_0$ be the corresponding hydrodynamic elements of flow about a wedge.

We assume that a small deviation in the shape perturbs the principal flow (about the wedge) slightly, i.e., we assume that

$$\begin{aligned} u(x, y, t) &= u_0(x, y, t) + u_1(x, y, t) \\ v(x, y, t) &= v_0(x, y, t) + v_1(x, y, t) \\ p(x, y, t) &= p_0(x, y, t) + p_1(x, y, t) \\ \rho(x, y, t) &= \rho_0(x, y, t) + \rho_1(x, y, t) \end{aligned}$$

.....[1.2]

where the new unknown functions $u_1$, $v_1$, $p_1$, $\rho_1$ and their first derivatives are small quantities (of first order) compared with $u_0$, $v_0$, $p_0$ and $\rho_0$. We neglect small quantities of second order. Linearizing Equations [1.1] under this assumption, we obtain a system of four linear equations with variable coefficients.

All the coefficients of this system will be, as hydrodynamic elements of self-similar flow, the functions of two independent variables

$$\xi = \frac{x}{t} \qquad \eta = \frac{y}{t}$$

Therefore, changing the resultant linear system from the variables $x$, $y$ and $t$ to the variables $\xi$, $\eta$ and $t$ and introducing the following notation [see, for example, (4)]

$$\begin{aligned} u_0(\xi, \eta) - \xi &= U_0(\xi, \eta) \\ v_0(\xi, \eta) - \eta &= V_0(\xi, \eta) \end{aligned}$$

.....[1.3]

we obtain a system of equations of motion in the form

$$t\frac{\partial u_1}{\partial t} + U_0\frac{\partial u_1}{\partial \xi} + V_0\frac{\partial u_1}{\partial \eta} + \frac{1}{\rho_0}\frac{\partial p_1}{\partial \xi} = -\left(\frac{\partial U_0}{\partial \xi} + 1\right)u_1 - \frac{\partial U_0}{\partial \eta}v_1 + \frac{1}{\rho_0^2}\frac{\partial p_0}{\partial \xi}\rho_1$$

$$t\frac{\partial v_1}{\partial t} + U_0\frac{\partial v_1}{\partial \xi} + V_0\frac{\partial v_1}{\partial \eta} + \frac{1}{\rho_0}\frac{\partial p_1}{\partial \eta} = -\frac{\partial V_0}{\partial \xi}u_1 - \left(\frac{\partial V_0}{\partial \eta} + 1\right)v_1 + \frac{1}{\rho_0^2}\frac{\partial p_0}{\partial \eta}\rho_1$$

$$t\frac{\partial \rho_1}{\partial t} + U_0\frac{\partial \rho_1}{\partial \xi} + V_0\frac{\partial \rho_1}{\partial \eta} + \rho_0\left(\frac{\partial u_1}{\partial \xi} + \frac{\partial v_1}{\partial \eta}\right) = -\frac{\partial \rho_0}{\partial \xi}u_1 - \frac{\partial \rho_0}{\partial \eta}v_1 - \left(\frac{\partial U_0}{\partial \xi} + \frac{\partial V_0}{\partial \eta} + 2\right)\rho_1$$

$$t\frac{\partial p_1}{\partial t} + U_0\frac{\partial p_1}{\partial \xi} + V_0\frac{\partial p_1}{\partial \eta} + \kappa p_0\left(\frac{\partial u_1}{\partial \xi} + \frac{\partial v_1}{\partial \eta}\right) = -\frac{\partial p_0}{\partial \xi}u_1 - \frac{\partial p_0}{\partial \eta}v_1 - \kappa\left(\frac{\partial U_0}{\partial \xi} + \frac{\partial V_0}{\partial \eta} + 2\right)p_1$$

.....[1.4]

The fact that the problem formulated is close to self-similar, together with the form of the system [1.4], gives grounds for seeking a solution in a special form, as is done, for example, for certain types of flow in (7, 8 and 9). We shall seek a particular solution for our system in the form proposed for different systems by Stanyukovich (9)

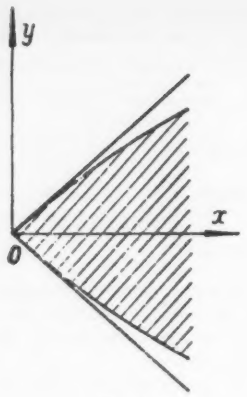


Fig. 1

$$\begin{aligned} u_1(\xi, \eta, t) &= t^{\alpha-1}\bar{u}(\xi, \eta) & v_1(\xi, \eta, t) &= t^{\alpha-1}\bar{v}(\xi, \eta) \\ p_1(\xi, \eta, t) &= t^{\alpha-1}\bar{p}(\xi, \eta) & \rho_1(\xi, \eta, t) &= t^{\alpha-1}\bar{\rho}(\xi, \eta) \end{aligned}$$

.....[1.5]

where

$\alpha$ = a certain constant satisfying the inequality $\alpha \geq 1$
$\bar{u}, \bar{v}, \bar{p}, \bar{\rho}$ = new unknown functions

Substituting Equation [1.5] in [1.4] we get

$$U_0\frac{\partial \bar{u}}{\partial \xi} + V_0\frac{\partial \bar{u}}{\partial \eta} + \frac{1}{\rho_0}\frac{\partial \bar{p}}{\partial \xi} = -\left(\frac{\partial U_0}{\partial \xi} + \alpha\right)\bar{u} - \frac{\partial U_0}{\partial \eta}\bar{v} + \frac{1}{\rho_0^2}\frac{\partial p_0}{\partial \xi}\bar{\rho}$$

$$U_0\frac{\partial \bar{v}}{\partial \xi} + V_0\frac{\partial \bar{v}}{\partial \eta} + \frac{1}{\rho_0}\frac{\partial \bar{p}}{\partial \eta} = -\frac{\partial V_0}{\partial \xi}\bar{u} - \left(\frac{\partial V_0}{\partial \eta} + \alpha\right)\bar{v} + \frac{1}{\rho_0^2}\frac{\partial p_0}{\partial \eta}\bar{\rho}$$

$$U_0\frac{\partial \bar{\rho}}{\partial \xi} + V_0\frac{\partial \bar{\rho}}{\partial \eta} + \rho_0\left(\frac{\partial \bar{u}}{\partial \xi} + \frac{\partial \bar{v}}{\partial \eta}\right) = -\frac{\partial \rho_0}{\partial \xi}\bar{u} - \frac{\partial \rho_0}{\partial \eta}\bar{v} - \left(\frac{\partial U_0}{\partial \xi} + \frac{\partial V_0}{\partial \eta} + 1 + \alpha\right)\bar{\rho}$$

$$U_0\frac{\partial \bar{p}}{\partial \xi} + V_0\frac{\partial \bar{p}}{\partial \eta} + \kappa p_0\left(\frac{\partial \bar{u}}{\partial \xi} + \frac{\partial \bar{v}}{\partial \eta}\right) = -\frac{\partial p_0}{\partial \xi}\bar{u} - \frac{\partial p_0}{\partial \eta}\bar{v} - \kappa\left(\frac{\partial U_0}{\partial \xi} + \frac{\partial V_0}{\partial \eta} + 2 + \frac{\alpha - 1}{\kappa}\right)\bar{p}$$

.....[1.6]

This system for the determination of $\bar{u}$, $\bar{v}$, $\bar{p}$ and $\bar{\rho}$ contains only functions of two variables ($\xi$ and $\eta$), and $t$ does not enter explicitly. Consequently we can seek a particular solution of the system [1.4] in the form [1.5].

**Boundary Conditions**

Any initial condition of the system [1.4] can be satisfied with the aid of the particular solution [1.5], upon suitable choice of the fundamental flow (about the wedge), since, according to Equation [1.5] we have for $t = 0$

$$u_1 = v_1 = p_1 = \rho_1 = 0 \qquad (\alpha \geq 1)$$

and

$$u = u_0 \qquad v = v_0 \qquad p = p_0 \qquad \rho = \rho_0$$

It is easy to show that for a solution of the form [1.5] to satisfy the flow condition [1.4], it is necessary and sufficient that the equation of the profile of the body be represented, with the necessary degree of accuracy, in the form

$$y = \tan \omega \cdot x + c_1 x^\alpha \qquad [1.7]$$

where $\alpha \geq 1$ and $c_1$ are certain constants chosen to match the form of the profile and to satisfy the condition that $c_1 x^\alpha$, together with its first derivative, be small functions, over the entire interval of the values of $x$ under consideration.

With this, the condition of flow for the system [1.4], referred to the surface of the wedge (in view of the small distance), is transformed into a boundary condition for the functions $\tilde{u}(\xi, \eta)$ and $v(\xi, \eta)$ and becomes

$$\left[\frac{\tilde{v} - \tilde{u}\tan\omega}{u_0}\right]_{\eta = \tan\omega\cdot\xi} = c\xi^{\alpha-1} \qquad [1.8]$$

where $c = \alpha c_1$. For a solution of the form [1.5] to satisfy the conditions on the surface of a strong discontinuity, it is necessary and sufficient that its equation be representable in the form

$$y = tf(\xi) + t^\alpha \tilde{\varphi}(\xi) \qquad (1.9)$$

where $\eta = f(\xi)$ is the equation of the surface of the strong discontinuity of the fundamental flow, $\alpha$ is determined by the form of the profile, and the function $t^\alpha\tilde{\varphi}(\xi)$ together with its first derivative are small quantities of order not lower than the first.

We then obtain for the functions $\tilde{u}$, $\tilde{v}$, $\tilde{p}$, and $\tilde{\rho}$ boundary conditions written (in view of the smallness of the distance) on the line $\eta = f(\xi)$ in the form

$$\begin{aligned}
\tilde{u}_+ &= A_1\tilde{\varphi}_\xi' + \alpha B_1\tilde{\varphi} + C_1\tilde{u}_- + D_1\tilde{v}_- + E_1\tilde{p}_- + F_1\tilde{\rho}_- \\
\tilde{v}_+ &= A_2\tilde{\varphi}_\xi' + \alpha B_2\tilde{\varphi} + C_2\tilde{u}_- + D_2\tilde{v}_- + E_2\tilde{p}_- + F_2\tilde{\rho}_- \\
\tilde{p}_+ &= A_3\tilde{\varphi}_\xi' + \alpha B_3\tilde{\varphi} + C_3\tilde{u}_- + D_3\tilde{v}_- + E_3\tilde{p}_- + F_3\tilde{\rho}_- \\
\tilde{\rho}_+ &= A_4\tilde{\varphi}_\xi' + \alpha B_4\tilde{\varphi} + C_4\tilde{u}_- + D_4\tilde{v}_- + E_4\tilde{p}_- + F_4\tilde{\rho}_-
\end{aligned} \qquad [1.10]$$

where the primes denote the corresponding derivatives; the subscripts minus and plus denote the values of the functions ahead of and past the strong discontinuity, respectively; $A_i$, $B_i$, $C_i$, $D_i$, $E_i$ and $F_i$ are functions of $\xi$, known on $\eta = f(\xi)$, defined by the formulas

$$\begin{aligned}
A_1 &= \frac{2}{\varkappa+1}\frac{1}{g_0^3}\left[\frac{f'm_0^-}{g_0}M_1 - \Theta_0^- M_2\right]\Big|_{\eta=f(\xi)} \\
B_1 &= -\frac{2}{\varkappa+1}\frac{f'M_1}{g_0^2}\Big|_{\eta=f(\xi)} \\
C_1 &= 1 + \frac{2}{\varkappa+1}\frac{f'^2M_1}{g_0^2}\Big|_{\eta=f(\xi)} \\
D_1 &= \frac{2}{\varkappa+1}\frac{f'M_1}{g_0^2}\Big|_{\eta=f(\xi)} \\
E_1 &= -\frac{2}{\varkappa+1}\frac{f'\Theta_0^-}{g_0\rho_0^-}(M_1-1)|_{\eta=f(\xi)} \\
F_1 &= \frac{2}{\varkappa+1}\frac{f'\Theta_0^-}{g_0\rho_0^-}(M_1-1)|_{\eta=f(\xi)} \\
A_2 &= -\frac{2}{\varkappa+1}\frac{1}{g_0^3}\left[f'\Theta_0^- M_2 + \frac{m_0^-}{g_0}M_1\right]\Big|_{\eta=f(\xi)} \\
B_2 &= \frac{2}{\varkappa+1}\frac{M_1}{g_0^2}\Big|_{\eta=f(\xi)} \\
C_2 &= \frac{2}{\varkappa+1}\frac{f'M_1}{g_0^2}\Big|_{\eta=f(\xi)} \\
D_2 &= 1 - \frac{2}{\varkappa+1}\frac{M_1}{g_0^2}\Big|_{\eta=f(\xi)} \\
E_2 &= \frac{2}{\varkappa+1}\frac{\Theta_0^-}{g_0\rho_0^-}(M_1-1)|_{\eta=f(\xi)} \\
F_2 &= -\frac{2}{\varkappa+1}\frac{\Theta_0^-}{g_0\rho_0^-}(M_1-1)|_{\eta=f(\xi)} \\
A_3 &= \frac{4}{\varkappa+1}\rho_0^-\Theta_0^-\frac{m_0^-}{g_0^3}\Big|_{\eta=f(\xi)} \\
B_3 &= -\frac{4}{\varkappa+1}\frac{\rho_0^-\Theta_0^-}{g_0}\Big|_{\eta=f(\xi)} \\
C_3 &= -\frac{4}{\varkappa+1}\frac{\rho_0^-\Theta_0^- f'}{g_0}\Big|_{\eta=f(\xi)} \\
D_3 &= \frac{4}{\varkappa+1}\frac{\rho_0^-\Theta_0^-}{g_0}\Big|_{\eta=f(\xi)} \\
E_3 &= -\frac{\varkappa-1}{(\varkappa+1)p_0^-}\Big|_{\eta=f(\xi)} \\
F_3 &= \frac{\varkappa-1}{(\varkappa+1)\rho_0^-}\Big|_{\eta=f(\xi)} \\
A_4 &= \frac{4(\varkappa+1)m_0^-\rho_0^-(M_1-1)}{g_0^3\Theta_0^-(2M_1+\varkappa-3)^2}\Big|_{\eta=f(\xi)} \\
B_4 &= -\frac{4(\varkappa+1)\rho_0^-(M_1-1)}{g_0\Theta_0^-(2M_1+\varkappa-3)^2}\Big|_{\eta=f(\xi)} \\
C_4 &= -\frac{4(\varkappa+1)f'\rho_0^-(M_1-1)}{g_0\Theta_0^-(2M_1+\varkappa-3)^2}\Big|_{\eta=f(\xi)} \\
D_4 &= \frac{4(\varkappa+1)\rho_0^-(M_1-1)}{g_0\Theta_0^-(2M_1+\varkappa-3)^2}\Big|_{\eta=f(\xi)} \\
E_4 &= -\frac{4\varkappa(\varkappa+1)}{\Theta_0^{-3}(2M_1+\varkappa-3)^2}\Big|_{\eta=f(\xi)} \\
F_4 &= \frac{\varkappa+1}{(2M_1+\varkappa-3)^2}\left[\varkappa+1+\frac{4(M_1-1)}{\Theta_0^-}\right]\Big|_{\eta=f(\xi)}
\end{aligned} \qquad [1.11]$$

where the subscript "0" denotes elements of the fundamental flow. The following symbols are used

$a$ = velocity of sound
$\Theta$ = velocity of propagation of line of strong discontinuity
$g_0 = \sqrt{1+f'^2}$
$m_0^- = (\xi + f\cdot f') - (u_0^- + f'v_0^-)$
$M_1 = \left(\frac{a_0^-}{\Theta_0^-}\right)^2 + 1$
$M_2 = \left(\frac{a_0^-}{\Theta_0^-}\right)^2 - 1$

It must be noted that the latter conditions are valid only for strong discontinuities of not too low an intensity, the propagation velocity of which differs from the velocity of sound by an amount whose square can no longer be neglected. For shock waves that are too weak (for which $M_2$ is a quantity of first order of smallness), the small values of $\tilde{u}$, $\tilde{v}$, $\tilde{p}$ and $\tilde{\rho}$ may lead nevertheless to a value of $\tilde{\varphi}$ which is no longer small, thus contradicting the basic assumption that our flow is nearly self-similar.

It is obvious that in order for a solution in the form [1.5] to satisfy the conditions on the line of stationary discontinuity, its equation must be representable in the form

$$y = tF(\xi) + t^\alpha\tilde{\chi}(\xi) + \chi_0(t) \qquad [1.12]$$

where $\eta = F(\xi)$ is the equation of the line of stationary dis-

continuity of the fundamental flow, and the sum $t^{\alpha}\tilde{\chi}(\xi) + \chi_0(t)$ is, together with its partial derivatives, a quantity of first order of smallness over the entire range of variation of the independent variables of interest to us.

Then the boundary conditions, written on $\eta = F(\xi)$, become

$$[\bar{\rho}] = 0$$

$$[\bar{v} - F'\bar{u}] = \frac{\tilde{\chi}'}{F'},\ v_0]$$

..... [1.13]

where the primes denote the derivatives, and the difference in the values of any function $b(\xi, \eta)$ on both sides of the discontinuity line is denoted, as usual, by $[b]$. Conditions [1.13], like conditions [1.8 and 1.10], do not contain $t$ and are the boundary conditions for the system [1.6].

The problem posed has thus been reduced to a solution of the system [1.6] in the plane of the two independent variables $(\xi, \eta)$ subject to boundary conditions which, depending on the specific formulation of the problem, are a suitable combination of conditions [1.8, 1.10 and 1.13].

If the equation of the profile of the body cannot be represented with sufficient degree of accuracy in the form [1.7], or if the degree of approximation to the form of the discontinuity line as given by Equations [1.9 and 1.12] is insufficient, a more precise formulation of the problem becomes necessary.

**More Precise Formulation of the Problem**

The problem can be formulated in practice with any necessary degree of accuracy if, by starting with the linearity of the system of equations of motion [1.4], the particular solution for it is sought in the form of a sum of an arbitrary number of terms in the form [1.5], i.e., in the form

$$u_1(\xi, \eta, t) = \sum_{i=1}^{n} t^{\alpha_i - 1}\bar{u}_i(\xi, \eta)$$

$$v_1(\xi, \eta, t) = \sum_{i=1}^{n} t^{\alpha_i - 1}\bar{v}_i(\xi, \eta)$$

$$p_1(\xi, \eta, t) = \sum_{i=1}^{n} t^{\alpha_i - 1}\bar{p}_i(\xi, \eta)$$

$$\rho_1(\xi, \eta, t) = \sum_{i=1}^{n} t^{\alpha_i - 1}\bar{\rho}_i(\xi, \eta)$$

..... [1.14]

where

$\alpha_i$ = certain constants, satisfying the inequalities $\alpha_i \geq 1 (i = 1, 2, 3, \ldots, n)$

$\bar{u}_i, \bar{v}_i, \bar{p}_i, \bar{\rho}_i$ = $4n$ new unknown functions

Turning to the boundary conditions of the system [1.4], we find that if they are to be satisfied with the aid of the solution [1.14], the equation of the profile of the body must be representable in the form

$$y = \tan\omega \cdot x + \sum_{i=1}^{n} c_i x^{\alpha_i} \qquad [1.15]$$

The equation of the line of strong discontinuity must be representable in the form

$$y = tf(\xi) + \sum_{i=1}^{n} t^{\alpha_i}\bar{\varphi}_i(\xi) \qquad [1.16]$$

The equation of the line of stationary discontinuity must be representable in the form

$$y = tF(\xi) + \sum_{i=1}^{n} t^{\alpha_i}\bar{\chi}_i(\xi) + \chi_0(t) \qquad [1.17]$$

where $c_i$ and $\alpha_i$ are constants determined on the basis of the form of the profile, and the sums

$$\sum_{i=1}^{n} c_i\chi^{\alpha_i} \qquad \sum_{i=1}^{n} t^{\alpha_i}\varphi_i(\xi) \qquad \sum_{i=1}^{n} t^{\alpha_i}\bar{\chi}_i(\xi) + \chi_0(t)$$

and their first derivatives are small quantities, the squares of which can be neglected over the entire range of variation of the independent variables.

The problem of the unsteady plane flow about profiles of the type [1.15] with discontinuity lines of the type [1.16 and 1.17] is reduced in this case to solving $n$ similar problems, each of which is analogous to the problem of flow about the profile [1.7].

Without raising any principal difficulties, this refinement merely increases the volume of representative computational work.

We shall therefore deal from now on only with the solution of the problem as formulated for profiles of the type [1.7].

## 2 Type of the System of Equations [1.6] and Methods of Solving the Problem

The characteristics of the system [1.6] in the $(\xi, \eta)$ plane can be readily determined by the usual methods (8).

The characteristics of the first family $\eta = \eta_1(\xi)$ are given by the equations

$$\eta_1' = \frac{U_0V_0 + a_0\sqrt{W_0^2 - a_0^2}}{U_0^2 - a_0^2} \qquad [2.1]$$

$$U_0d\bar{v} - V_0d\bar{u} + \sqrt{\frac{W_0^2}{a_0^2} - 1}\,\frac{d\bar{p}}{\rho_0} =$$

$$(Q_1\bar{u} + R_1\bar{v} + S_1\bar{\rho} + T_1\bar{p})d\xi \qquad [2.2]$$

The characteristics of the second family, $\eta = \eta_2(\xi)$ are given by

$$\eta_2' = \frac{U_0V_0 - a_0\sqrt{W_0^2 - a_0^2}}{U_0^2 - a_0^2} \qquad [2.3]$$

$$U_0d\bar{v} - V_0d\bar{u} - \sqrt{\frac{W_0^2}{a_0^2} - 1}\,\frac{d\bar{p}}{\rho_0} =$$

$$= (Q_2\bar{u} + R_2\bar{v} + S_2\bar{\rho} + T_2\bar{p})d\xi \qquad [2.4]$$

For the third family $\eta = \eta_3(\xi)$ we have

$$\eta_3' = (V_0/U_0) \qquad [2.5]$$

$$U_0d\bar{u} + V_0d\bar{v} + \frac{d\bar{p}}{\bar{\rho}_0} = (Q_3\bar{u} + R_3\bar{v} + S_3\bar{\rho})d\xi \qquad [2.6]$$

$$dp - a_0^2d\bar{\rho} = (Q_4\bar{u} + R_4\bar{u} + S_4\bar{\rho} + T_4\bar{p})d\xi \qquad [2.7]$$

We use the following notation: $W_0^2 = U_0^2 + V_0^2$, and $Q_i$, $R_i$, $S_i$, $T_i$ $(i = 1, 2, 3, 4)$ are functions of $\xi$, known from the corresponding characteristics, namely

$$Q_{1,2} = \left[\eta'_{1,2}\left(\frac{\partial U_0}{\partial\xi} + \alpha - \frac{U_0}{\varkappa p_0}\frac{\partial p_0}{\partial\xi}\right) - \frac{\partial V_0}{\partial\xi} + \frac{V_0}{\varkappa p_0}\frac{\partial p_0}{\partial\xi}\right]_{\eta=\eta_{1,2}(\xi)}$$

$$R_{1,2} = \left[\eta'_{1,2}\left(\frac{\partial U_0}{\partial\eta} - \frac{U_0}{\varkappa p_0}\frac{\partial p_0}{\partial\eta}\right) - \frac{\partial V_0}{\partial\eta} - \alpha + \frac{V_0}{\varkappa p_0}\frac{\partial p_0}{\partial\eta}\right]_{\eta=\eta_{1,2}(\xi)}$$

$$S_{1,2} = \left[\frac{1}{\rho_0^2}\left(\frac{\partial p_0}{\partial\eta} - \eta'_{1,2}\frac{\partial p_0}{\partial\xi}\right)\right]_{\eta=\eta_{1,2}(\xi)}$$

$$T_{1,2} = \left[\frac{(V_0 - \gamma'_{1,2}U_0)}{p_0}\left(\frac{\partial U_0}{\partial \xi} + \frac{\partial V_0}{\partial \eta} + 2 + \frac{\alpha - 1}{\varkappa}\right)\right]_{\eta=\eta_{1,2}(\xi)}$$

$$Q_3 = -\left[\frac{\partial U_0}{\partial \xi} + \alpha + \frac{V_0}{U_0}\frac{\partial V_0}{\partial \xi}\right]_{\eta=\eta_3(\xi)}$$

$$R_3 = -\left[\frac{\partial U_0}{\partial \eta} + \frac{V_0}{U_0}\left(\frac{\partial V_0}{\partial \eta} + \alpha\right)\right]_{\eta=\eta_3(\xi)}$$

$$S_3 = \left[\frac{1}{\rho_0^2}\left(\frac{\partial p_0}{\partial \xi} + \frac{V_0}{U_0}\frac{\partial p_0}{\partial \eta}\right)\right]_{\eta=\eta_3(\xi)}$$

$$Q_4 = -\left[\frac{1}{U_0}\left(\frac{\partial p_0}{\partial \xi} - a_0^2\frac{\partial \rho_0}{\partial \xi}\right)\right]_{\eta=\eta_4(\xi)}$$

$$R_4 = -\left[\frac{1}{U_0}\left(\frac{\partial p_0}{\partial \eta} - a_0^2\frac{\partial \rho_0}{\partial \eta}\right)\right]_{\eta=\eta_4(\xi)}$$

$$S_4 = \left[\frac{a_0^2}{U_0}\left(\frac{\partial U_0}{\partial \xi} + \frac{\partial V_0}{\partial \eta} + 1 + \alpha\right)\right]_{\eta=\eta_4(\xi)}$$

$$T_4 = -\left[\frac{\varkappa}{U_0}\left(\frac{\partial U_0}{\partial \xi} + \frac{\partial V_0}{\partial \eta} + 2 + \frac{\alpha - 1}{\varkappa}\right)\right]_{\eta=\eta_4(\xi)} \quad \ldots\ldots [2.8]$$

The slopes of the characteristics, and consequently the boundary that separates the elliptic and hyperbolic regions of the system [1.6]

$$(u_0 - \xi)^2 + (v_0 - \eta)^2 = a_0^2 \quad [2.9]$$

coincide completely with the corresponding expressions for the basic self-similar flow (4).

For a real flow, Equation [2.9] gives a certain closed curve in the $(\xi, \eta)$ plane. The system [1.6], like the system of equations of motion of the fundamental flow near the wedge, will be completely hyperbolic outside this curve when $U_0^2 + V_0^2 - a_0^2 > 0$, and can be solved here by the method of characteristics.

The linearity of the system [1.6], which expresses itself in the fact that the slope of the characteristics and the coefficients of the equations on these characteristics are determined only by elements of the fundamental flow, i.e., are certainly known at each point of the field, simplifies considerably the application of the method of characteristics, reduces the volume of the computational work and reduces the error of the method. In all other respects the calculation by the method of characteristics in the $(\xi, \eta)$ plane is quite analogous to the corresponding calculation for steady-state flow in the $(x, y)$ plane. In the calculations it is convenient here to start out with the scheme proposed by Vallander (8) for the method of characteristics. This scheme makes use of all three available families of characteristics and leads to a construction of a uniform grid of characteristics in which the length of each cell is approximately equal to a preselected value. In our case, both the boundary of the hyperbolic region and the entire grid of characteristics can be plotted beforehand, and the density of the grid can be made arbitrary depending on the necessary accuracy in the computation.

Inside the line [2.9], the system [1.6] becomes elliptic. On those portions of the boundary line which separate the regions of real and imaginary characteristics, all the unknowns can be determined by the method of characteristics. The other parts of the boundary consist, in the general case, of solid walls and lines, which separate the perturbed region of the flow from the unperturbed one. The flow parameters on these sections of the boundary line are determined from various physical considerations, depending on the specific conditions of the problem. Then the problem of determining the flow inside the indicated boundary, within its elliptic region, reduces to solving a definite boundary value problem for a system of linear elliptic equations. This problem can be solved approximately, for example by the method of nets.

## 3 Axially Symmetric Unsteady Flow Around a Nearly Conical Body

In analogy with the definition given in the plane case, the surface of an axially symmetric body is considered to be close to that of a certain cone if:

1 The symmetry axes of the two bodies are the same.

2 The generatrix of the cone coincides with the tangent to the generatrix of our body at the nose.

3 The angle between the generatrix of the cone and the tangents to the generatrix of our axially symmetric body are assumed to be everywhere small.

We introduce a cylindrical system of coordinates $(r, z, \vartheta)$ with origin located at the nose of the body. The $z$ axis is directed along the symmetry axis of the body. Since the problem has an axial symmetry, we shall confine ourselves henceforth to an examination of the flow in a meridional plane, i.e., where it intersects the $(r, z)$ plane (Fig. 2).

Almost all the conclusions and deductions of this section are derived analogously to the corresponding conclusions of the plane case. This analogy will be emphasized by introducing a similar notation, but it must be constantly kept in mind that the same symbols have different meanings in the plane and axially symmetric cases.

To keep repetition to a minimum, we shall omit details in the arguments where they are obvious from the preceding sections.

Let

$u$ = projection of steam velocity on $z$ axis
$v$ = projection of stream velocity on $r$ axis
$p$ = pressure
$\rho$ = density
$\kappa$ = ratio of specific heat
$u_0, v_0, p_0$ and $\rho_0$ = corresponding hydrodynamic elements of flow about a cone that is nearly equivalent to the given axially symmetric body

In the equations for the axially symmetric unsteady motion, we change to new independent variables $\xi = z/t$, $\eta = r/t$ and $t$. We seek a particular solution, analogous to the plane case, in the form

$$\begin{aligned} u(\xi, \eta, t) &= u_0(\xi, \eta) + t^{\alpha-1}\bar{u}(\xi, \eta) \\ v(\xi, \eta, t) &= v_0(\xi, \eta) + t^{\alpha-1}\bar{v}(\xi, \eta) \\ p(\xi, \eta, t) &= p_0(\xi, \eta) + t^{\alpha-1}\bar{p}(\xi, \eta) \\ \rho(\xi, \eta, t) &= \rho_0(\xi, \eta) + t^{\alpha-1}\bar{\rho}(\xi, \eta) \end{aligned} \quad \ldots\ldots [3.1]$$

where $\alpha$ is a certain constant, satisfying the inequality $\alpha \geq 1$, and $\bar{u}$, $\bar{v}$, $\bar{p}$ and $\bar{\rho}$ are new independent functions.

The second terms of the right halves and their derivatives are small functions, so that their squares can be neglected.

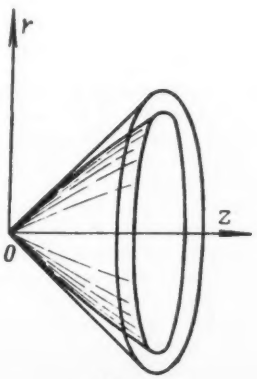


Fig. 2

To determine the four new unknown functions, we obtain a system of four linear equations with variable coefficients in the plane of the two independent variables $(\xi, \eta)$

$$U_0 \frac{\partial \bar{u}}{\partial \xi} + V_0 \frac{\partial \bar{u}}{\partial \eta} + \frac{1}{\rho_0} \frac{\partial \bar{p}}{\partial \xi} =$$
$$-\left(\frac{\partial U_0}{\partial \xi} + \alpha\right) \bar{u} - \frac{\partial U_0}{\partial \eta} \bar{v} + \frac{1}{\rho_0^2} \frac{\partial p_0}{\partial \xi} \bar{\rho}$$

$$U_0 \frac{\partial \bar{v}}{\partial \xi} + V_0 \frac{\partial \bar{v}}{\partial \eta} + \frac{1}{\rho_0} \frac{\partial \bar{p}}{\partial \eta} =$$
$$-\frac{\partial V_0}{\partial \xi} \bar{u} - \left(\frac{\partial V_0}{\partial \eta} + \alpha\right) \bar{v} + \frac{1}{\rho_0^2} \frac{\partial p_0}{\partial \eta} \bar{\rho}$$

$$U_0 \frac{\partial \bar{\rho}}{\partial \xi} + V_0 \frac{\partial \bar{\rho}}{\partial \eta} + \rho_0 \left(\frac{\partial \bar{u}}{\partial \xi} + \frac{\partial \bar{v}}{\partial \eta}\right) =$$
$$-\frac{\partial \rho_0}{\partial \xi} \bar{u} - \left(\frac{\partial \rho_0}{\partial \eta} + \frac{\rho_0}{\eta}\right) \bar{v} - \left(\frac{\partial U_0}{\partial \xi} + \frac{\partial V_0}{\partial \eta} + \frac{V_0}{\eta} + 2 + \alpha\right) \bar{\rho}$$

$$U_0 \frac{\partial \bar{p}}{\partial \xi} + V_0 \frac{\partial \bar{p}}{\partial \eta} + \varkappa p_0 \left(\frac{\partial \bar{u}}{\partial \xi} + \frac{\partial \bar{v}}{\partial \eta}\right) =$$
$$-\frac{\partial p_0}{\partial \xi} \bar{u} - \left(\frac{\partial p_0}{\partial \eta} + \frac{\varkappa p_0}{\eta}\right) \bar{v} - \varkappa \left(\frac{\partial U_0}{\partial \xi} + \frac{\partial V_0}{\partial \eta} + \frac{V_0}{\eta} + 3 + \frac{\alpha - 1}{\varkappa}\right) \bar{p} \qquad [3.2]$$

where

$$U_0(\xi, \eta) = u_0(\xi, \eta) - \xi$$
$$V_0(\xi, \eta) = v_0(\xi, \eta) - \eta$$

Satisfying with the aid of the solution [3.1] the possible boundary conditions of the initial system, we obtain, exactly as in a plane case, the corresponding boundary conditions with a system [3.2] in the $(\xi, \eta)$ plane.

Now the equation of the profile of the meridional section through the body can be represented in the form

$$r = \tan \omega \cdot z + c_1 z^\alpha \qquad [3.3]$$

where $\omega$ is the angle between the generatrix and the symmetry axis of the fundamental cone, and $\alpha$ and $c_1$ are constants ($\alpha \geq 1$), chosen in accordance with the shape of the profile, but under the condition that $c_1 z^\alpha$ is a small quantity, together with its first derivatives, for all values of $z$ under consideration.

The equation of the surface of strong discontinuity should now be represented in the form

$$r = tf(\xi) + t^\alpha \bar{\varphi}(\xi) \qquad [3.4]$$

where

$\eta = f(\xi)$ = equation of surface of strong discontinuity in flow around a cone

$t^\alpha \bar{\varphi}(\xi)$ = small function together with its first derivative

The equation of the surface of the stationary discontinuity should be represented, with the required degree of accuracy, in the form

$$r = tF(\xi) + t^\alpha \bar{\chi}(\xi) + \chi_0(t) \qquad [3.5]$$

where $\eta = F(\xi)$ is the equation of the corresponding surface of the stationary discontinuity of the basic self-similar flow. The expression $t^\alpha \bar{\chi}(\xi) + \chi_0(t)$, like its first derivative, is a small quantity, the square of which can be neglected.

We obtain now the conditions of the system [3.2] in the form [1.8, 1.10 and 1.13], in which the symbols now correspond to those introduced for the axially symmetric flow.

We can now formulate the problem of unsteady flow around an axially symmetric body, the equation for the profile of the meridional section of which can be written with sufficient accuracy in the form [3.3], and whose flow discontinuity lines can be written in the form [3.4 and 3.5]. The problem consists of solving the system [3.2], of four first-order linear equations for the four unknown functions of two independent variables, subject to boundary conditions which are a combination of the conditions [1.8, 1.0 and 1.13].

As in the plane case, this formulation of the problem can be refined to any desired degree of accuracy, by expressing the small additions to the particular solution of the system of equations in the form of a sum of an arbitrary number $(n)$ of small additions to Equation [3.1].

For an axially symmetric nearly conical body, the problem reduces here to a solution of $n$ identical problems, each of which is quite analogous to the problem of flow about a body with a profile of type [3.3].

The equations that determine the slopes of the characteristics of the system [3.2] in the $(\xi, \eta)$ plane will have formally the same appearance as in the planar case, namely [2.1, 2.3 and 2.5], where the symbols introduced at the beginning of this section are to be used for the axially symmetric case.

The relations on the characteristics differ from the corresponding relations of the planar case only in the coefficients of $d\xi$ and are the same as Equations [2.2, 2.4, 2.6 and 2.7], where $Q_i$, $R_i$, $S_i$ and $T_i$ are known functions of $\xi$, also of the same form as the corresponding expression [2.8] of the preceding section, with the exception of the coefficients

$$R_{1,2} = \left[\eta'_{1,2}\left(\frac{\partial U_0}{\partial \eta} - \frac{U_0}{\varkappa p_0}\frac{\partial p_0}{\partial \eta} - \frac{U_0}{\eta}\right) - \frac{\partial V_0}{\partial \eta} - \alpha + \frac{V_0}{\varkappa p_0}\frac{\partial p_0}{\partial \eta} + \frac{V_0}{\eta}\right]_{\eta = \eta_{1,2}(\xi)}$$

$$T_{1,2} = \left[\frac{(V_0 - \eta'_{1,2} U_0)}{p_0}\left(\frac{\partial U_0}{\partial \xi} + \frac{\partial V_0}{\partial \eta} + \frac{V_0}{\eta} + 3 + \frac{\alpha - 1}{\varkappa}\right)\right]_{\eta = \eta_{1,2}(\xi)}$$

$$S_4 = \left[\frac{a_0^2}{U_0}\left(\frac{\partial U_0}{\partial \xi} + \frac{\partial V_0}{\partial \eta} + \frac{V_0}{\eta} + 2 + \alpha\right)\right]_{\eta = \eta_3(\xi)}$$

$$T_4 = \left[-\frac{\varkappa}{U_0}\left(\frac{\partial U_0}{\partial \xi} + \frac{\partial V_0}{\partial \eta} + \frac{U_0}{\eta} + 3 + \frac{\alpha - 1}{\varkappa}\right)\right]_{\eta = \eta_3(\xi)} \qquad [3.6]$$

As in the planar case, the boundary line of the system [3.2], separating the hyperbolic region of the system from the elliptic one, is given by the equation

$$(u_0 - \xi)^2 + (v_0 - \eta)^2 - a_0^2 = 0 \qquad [3.7]$$

In the entire $(\xi, \eta)$ plane outside this curve (which is closed for a real flow) our system [3.2] will be completely hyperbolic and can be solved, up to a limit close to the line [3.7], by the method of characteristics, following a procedure which is formally analogous to the corresponding scheme used in the planar case. The same analogy with the planar case is observed also in the elliptic region inside the curve [3.7].

The axially symmetric problem can also be solved approximately, for example by the method of nets.

One specific problem which can be solved advantageously by the method described in this paper is that of Mach reflection of a plane shock wave by a body whose shape is nearly that of a wedge or a cone.

In conclusion, I take this opportunity to express my great gratitude to lecturer A. A. Grib for guiding this work and to Professor S. V. Vallander for valuable advice.

## References

1 Sedov, L. I., "Metody Podobiya i Razmernosti v Mekhanike" (Methods of Similarity and Dimensionality in Mechanics), Gostekhizdat (State Technical Press), Moscow, 1957.

2 Stanyukovich, K. P., "Neustanovivsheesya Dvizheniya Sploshnoi Sredy," GITTL (State Press for Technical and Theoretical Literature), Moscow, 1955.

3 Keller, J. B. and Blank, A., *Communications Pure and Appl. Math.*, vol. 4, 1951, pp. 75–94.

4 Ludloff, H. F. and Friedman, M. B., *J. Aeronaut. Sci.*, vol. 1, 1955, pp. 27–34.
5 Ryzhov, O. S. and Khristianovich, S. A., *Prikladnaya Matematika i Mekhanika* (Applied Mathematics and Mechanics), vol. 22, 1958, pp. 586–599.
6 Samogonyan, A. Ya., *Vestnik MGU* (Bull. Moscow State University), no. 12, 1953, pp. 63–68.
7 Grib, A. A., *Doklady Akad. Nauk SSSR* (Proc. USSR Acad. Sci.), vol. 102, no. 2, 1955, pp. 225–227.
8 Vallander, S. V., *Vestnik LGU* (Bull. Leningrad State University), no. 19, 1959, pp. 106–112.
9 Stanyukovich, K. P., *Doklady Akad. Nauk SSSR* (Proc. USSR Acad. Sci.), vol. 112, no. 4, 1957, pp. 595–598.

*—Original received January 28, 1959*

## Reviewer's Comment

Unsteady nearly self-similar motion is analyzed by perturbing basic self-similar flow and linearizing the resulting equations. A transformation is used to make the new flow self-similar by reducing the number of independent variables. The technique is discussed for nearly wedge-shaped and nearly conical bodies.

It should be noted that the conditions of self-similar motion include a restriction on the equation of state of the fluid. For the motion of an ideal compressible gas to be self-similar it is in general necessary that the equation of state be of the form $pv/T = F(S)$, with constant specific heats when $F(S)$ is constant (1). Also, when shock waves are present in the flow, it is necessary that $F(S)$ be constant. Fulfillment of this condition is implied by the form of the energy equation in Equation [1.1] which is valid only for a perfect gas with constant specific heats.

Two of Koldobskaya's references have recently appeared in English translation (2,3) and contain much basic material on self-similar motions.

—Myron S. Wecker
Gas Dynamics Laboratory
Princeton University

1 Wecker, M. S. and Hayes, W. D., "Self-Similar Fluids," Princeton University, Department of Aeronautical Engineering Rep. 518 (to be published).
2 Sedov, L. I., "Similarity and Dimensional Methods in Mechanics," English translation (M. Holt, Ed.), Academic Press, New York, 1959.
3 Stanyukovich, K. P., "Unsteady Motion of Continuous Media," English translation (M. Holt, Ed.), Pergamon Press, New York, 1960.

# Determination of the Preliminary Orbits of Artificial Satellites From Observations With Time Approximately Known

YU. V. BATRAKOV

**The problem of determining the preliminary unperturbed orbit of a close Earth satellite is considered for the case when the instants of certain observations are known with rough approximation. The usual assumption, that the observations lie on one loop and cover not too large a section of the orbit, is made. It is shown that the problem can be solved only if there are more than three observations. Equations are obtained for topocentric distances and for the quantities $n_i^0$ which are used to determine the time intervals between observations.**

**A numerical example is given wherein the orbit is calculated from four observations with only two exact time values.**

THE USE of the Gauss classical method for determining the orbits of an artificial Earth satellite from three observations requires that the observations give the exact coordinates of the moving body on the celestial sphere, and also that the instants of observation be accurately fixed. Before there were artificial satellites, all these requirements could be satisfied, as a rule without great difficulty, since the observed objects (small planets or comets) had a slow apparent motion over the celestial sphere, and the error in the fixation of the instant observation, though sometimes amounting to several minutes, could not play any role whatever. The situation

Translated from *Byulleten' Instituta Teoreticheskoi Astronomii* (Bull. Institute of Theoretical Astronomy), vol. 7, no. 7 (90), 1960, pp. 570–580. Translated by J. George Adashko.

changed radically with the first Earth satellites. The motion of the satellites over the celestial sphere is so rapid that within 1 sec the satellite can describe an apparent arc of approximately 1 deg. It is therefore clear that the accuracy of time determination should be very high. For example, if it is desirable to obtain the position of the satellite accurate to 1 or 2 sec of arc the accuracy of time reading should be on the order of 0.001 sec.

An exact determination of the time of observation is possible only at well-equipped observatories which have special apparatus for maintaining and measuring time. At most observing sites, the time is bound to be determined with errors greater than those corresponding to the possible accuracy of satellite coordinates, as measured on photographic plates.

On the other hand, since the number of first-class observatories is much smaller than the total number of observing sites, the normal situation is that many fewer observations are obtained at exactly fixed instants of time than at approximate times. Observations with the time considerably in error are also possible, even though the satellite position on the celestial sphere may be measured with sufficient accuracy. This raises the question of utilizing such observations to determine the orbit.

In this article we consider the problem of determining the initial unperturbed orbit from observations with approximate times. Also considered is the number of observations necessary to determine the preliminary orbit in the case when certain observations are given with approximate values of the time, and in the more general case, when the observation yields instead of a pair of coordinates $\alpha$ and $\delta$ only one coordinate, either $\alpha$ or $\delta$.

## 1 Derivation of Equations for Topocentric Distances

The problem of determining the preliminary orbit can be divided in a natural manner into two stages: The calculation of the topocentric distances and the calculation of the orbital elements. If the calculations pertaining to the first stage are completed and sufficiently accurate values of the topocentric distances are obtained, then the second stage presents no difficulty, since the procedure of determining the orbital elements from two geocentric positions has been sufficiently developed and is taught in almost all courses of theoretical astronomy. A successful overcoming of the difficulties of the first stage is therefore essential to the solution of the entire problem.

We shall consider the case when $n$ satellite positions on the orbit are separated by instants of time which are small compared with the period of revolution. We introduce the following notation:

$\mathbf{r}_i$ = geocentric radius vector of the satellite
$\mathbf{R}_i$ = geocentric radius vector of the point of observation
$\boldsymbol{\varrho}_i$ = topocentric radius vector of the satellite at the instant $t_i$ $(i = 0, 1, \ldots, n-1)$

We can then write the vector equation

$$\mathbf{r}_i = \boldsymbol{\varrho}_i + \mathbf{R}_i \qquad (i = 0, 1, \ldots, n-1) \qquad [1]$$

In addition, expanding $\dot{\mathbf{r}}_i$ in a Taylor series about $t = t_0$ we obtain

$$\mathbf{r}_i = F_i\mathbf{r}_0 + G_i\dot{\mathbf{r}}_0 \qquad (i = 1, 2, \ldots, n-1) \qquad [2]$$

where the scalar coefficients $F_i$ and $G_i$ are determined from the equations

$$F_i = 1 - \frac{1}{2}u_0\tau_i^2 - \frac{1}{6}u_0'\tau_i^3 + \frac{1}{24}(u_0^2 - u_0'')\tau_i^4 + \ldots$$

$$G_i = \tau_i - \frac{1}{6}u_0\tau_i^3 - \frac{1}{12}u_0'\tau_i^4 + \frac{1}{120}(u_0^2 - 3u_0'')\tau_i^5 + \ldots$$

$$u_0 = r_0^{-3} \qquad \tau_i = \sqrt{fm}\,(t_i - t_0) \qquad [3]$$

Here $f$ is the gravitational constant and $m$ is Earth's mass.

We can eliminate $\dot{\mathbf{r}}_0$ from Equations [2]. For this purpose we express $\dot{\mathbf{r}}_0$ in terms of $\mathbf{r}_0$ and $\mathbf{r}_i$ and substitute in the remaining $n-2$ equations of [2], obtaining

$$n_i\mathbf{r}_1 - \mathbf{r}_0 + n_i'\mathbf{r}_i = 0 \qquad (i = 2, 3, \ldots, n-1) \qquad [4]$$

where we denote for simplicity

$$n_i = \frac{-G_i}{F_iG_1 - F_1G_i} \qquad n_i' = \frac{G_1}{F_iG_1 - F_1G_i} \qquad [5]$$

The coefficients [5] can be represented by series in powers of the time, using expansions [3]. We have

$$n_i = \frac{\tau_i}{\tau_i'}\left[1 + \frac{u_0}{6}(\tau_i'^2 - \tau_i^2) + \ldots\right]$$

$$n_i' = -\frac{\tau_1}{\tau_i'}\left[1 + \frac{u_0}{6}(\tau_i'^2 - \tau_1^2) + \ldots\right]$$

$$(i = 2, 3, \ldots, n-1) \qquad [6]$$

where we put

$$\tau_i' = \tau_i - \tau_1 \qquad [7]$$

Introducing the notation

$$n_i^0 = \frac{\tau_i}{\tau_i'}$$

$$\kappa_i = 1 + (u_0/6)(\tau_i'^2 - \tau_i^2) + \ldots$$
$$\kappa_i' = 1 + (u_0/6)(\tau_i'^2 - \tau_1^2) + \ldots \qquad [8]$$

we obtain shorter and more convenient final formulas

$$n_i = n_i^0\kappa_i \qquad n_i' = (1 - n_i^0)\kappa_i' \qquad [9]$$

We now substitute $\mathbf{r}_i$ from [1] in [4], and obtain

$$n_i\boldsymbol{\varrho}_i - \boldsymbol{\varrho}_0 + n_i'\boldsymbol{\varrho}_i = -(n_i\mathbf{R}_1 - \mathbf{R}_0 + n_i'\mathbf{R}_i)$$
$$(i = 2, 3, \ldots, n-1) \qquad [10]$$

which is of fundamental significance for the determination of the topocentric distances.

The vector equations [10] are equivalent to the following scalar equations

$$\begin{aligned} n_i\lambda_1\rho_1 - \lambda_0\rho_0 + n_i'\lambda_i\rho_i &= -(n_iX_1 - X_0 + n_i'X_i) \\ n_i\mu_1\rho_1 - \mu_0\rho_0 + n_i'\mu_i\rho_i &= -(n_iY_1 - Y_0 + n_i'Y_i) \\ n_i\nu_1\rho_1 - \nu_0\rho_0 + n_i'\nu_i\rho_i &= -(n_iZ_1 - Z_0 + n_i'Z_i) \end{aligned}$$
$$(i = 2, 3, \ldots, n-1) \qquad [11]$$

where $\lambda_k$, $\mu_k$, $\nu_k$ and $\rho_k (k = 0, 1, \ldots, n-1)$ are the direction cosines and magnitudes of the vectors $\boldsymbol{\varrho}_k$, and $X_k$, $Y_k$ and $Z_k$ are the projections of the vector $\mathbf{R}_k$ on the coordinate axes. The direction cosines are connected with the spherical coordinates $\alpha$ and $\delta$ by the well-known formulas

$$\begin{aligned} \lambda_k &= \cos\alpha_k\cos\delta_k \\ \mu_k &= \sin\alpha_k\cos\delta_k \\ \nu_k &= \sin\delta_k \end{aligned}$$
$$(k = 0, 1, \ldots, n-1)$$

Equations [10] relate the topocentric distances $\rho_k$. These equations are rather complicated in structure, since the unknowns $\rho_k$ enter into $n_i$ and $n_i'$. Fortunately, in the case considered, when all the $\tau_i$ are small, the factors $\kappa_i$ and $\kappa_i'$ in terms of which the $\rho_k$ are expressed by $n_i$ and $n_i'$, depend little on $r_k$ and are almost equal to unity (see Eqs. [8]). Therefore Equations [11] are best reduced to a different form, by solving [11] with respect to those $\rho_k$ which enter [11] linearly.

Taking Equation [9] into account and introducing

$$\xi_i = \kappa_i'X_1 - \kappa_1X_1 \qquad \xi_i' = \kappa_i'X_i - X_0$$
$$\eta_i = \kappa_i'Y_i - \kappa_iY_1 \qquad \eta_i' = \kappa_i'Y_i - Y_0$$
$$\zeta_i = \kappa_1'Z_i - \kappa_iZ_1 \qquad \zeta_i' = \kappa_i'Z_i - Z_0$$

$$\Delta_i = \begin{vmatrix} \lambda_1 & \lambda_0 & \lambda_i \\ \mu_1 & \mu_0 & \mu_i \\ \nu_1 & \nu_0 & \nu_i \end{vmatrix}$$

$$a_i = \begin{vmatrix} \xi_i & \lambda_0 & \lambda_i \\ \eta_i & \mu_0 & \mu_i \\ \zeta_i & \nu_0 & \nu_i \end{vmatrix} \qquad a_i' = \begin{vmatrix} \xi_i' & \lambda_0 & \lambda_i \\ \eta_i' & \mu & \mu_i \\ \zeta_i' & \nu_0 & \nu_i \end{vmatrix}$$

$$b_i = \begin{vmatrix} \lambda_1 & \xi_i & \lambda_i \\ \mu_1 & \eta_i & \mu_i \\ \nu_1 & \zeta_i & \nu_i \end{vmatrix} \qquad b_i' = \begin{vmatrix} \lambda_1 & \xi_i' & \lambda_i \\ \mu_1 & \eta_i' & \mu_i \\ \nu_1 & \zeta_i' & \nu_i \end{vmatrix}$$

$$c_i = \begin{vmatrix} \lambda_1 & \lambda_0 & \xi_i \\ \mu_1 & \mu_0 & \eta_i \\ \nu_1 & \nu_0 & \zeta_i \end{vmatrix} \qquad c_i' = \begin{vmatrix} \lambda_1 & \lambda_0 & \xi_i' \\ \mu_1 & \mu_0 & \eta_i' \\ \nu_1 & \nu_0 & \zeta_i' \end{vmatrix}$$

. . . . . [12]

we obtain, after solving the system [11] with respect to the quantities $\rho_0$, $\rho_1$ and $\rho_i$, which enter it linearly, the following final system of equations

$$\rho_1 = (a_in_i^0 - a_i')/n_i^0\kappa_i\Delta_i$$
$$\rho_0 = (-b_in_i^0 + b_i')/\Delta_i$$
$$\rho_i = (c_in_i^0 - c_i')/(1 - n_i^0)\kappa_i'\Delta_i$$
$$(i = 2, 3, \ldots, n - 1)$$

. . . . . [13]

The system [13], which consists of $3n - 6$ equations, can be considered as the analog of the Lagrange-Gauss equations used in the usual method of determining the orbit from three observations. In the case when exact instants of time are given for all three observations, and consequently the $n_i^0$ are known, the use of Equations [13] for the determination of the topocentric distances may be just as convenient as the use of the Lagrange-Gauss equations. We note that in the case of three observations with exact instants of time the topocentric distances are obtained from [13] unambiguously.

The denominators of the right-hand sides of Equations [13] contain the determinants $\Delta_i$, which may vanish at certain combinations of observations. In particular, the $\Delta_i$ vanish when all points of observation are in the plane of the orbit at the instant of observation. In this particular case, Equations [13] cannot be used, and the initial system [11] must be employed. In this case the equations

$$n_i\nu_1\rho_1 - \nu_0\rho_0 + n_i'\nu_i\rho_i = -(n_iZ_1 - n_0 + n_i'Z_i)$$
$$(i = 2, 3, \ldots, n - 1)$$

can be considered as consequences of the remaining equations of [11], and the system [11] will contain only $2n - 4$ linearly independent equations.

## 2 Number of Observations Required to Determine the Orbit

In the ideal case each observation should yield two exact satellite coordinates ($\alpha$, $\delta$) on the celestial sphere and the exact instant of observation. However, as already noted, these requirements cannot always be satisfied, particularly in regard to the exact instant of observation. Theoretically, one can also have the case when the observations yield not the two satellite coordinates that fix its position on the celestial sphere, but only one of these, $\alpha$ or $\delta$, together with the instant of observation.[1]

Let us consider the number of observations needed to determine the unperturbed orbit in cases of this kind. The particular cases when Equations [13] are not suitable for the determination of $\rho_i$ will not be considered at present.

Equations [13] relate the unknown $\rho_s (s = 0, 1, \ldots, n - 1)$ with the observed $\alpha_s$, $\delta_s$ and $t_s$. Assume that this set of data includes $k$ unknown values of $\alpha_s$, $m$ unknown values of $\delta_s$, and $l$ unknown values of $t_s$. Then Equations [13] will contain in general $n + k + m + l$ unknowns. All these unknowns, generally speaking, can be determined if the number of equations is equal to the number of unknowns. From this we obtain the following condition for the number of observations $n$

$$n = (k + m + l)/2 + 3 \qquad [14]$$

The minimum number of observations $n = 3$ occurs when $k = m = l = 0$, that is, when all the $\alpha$, $\delta$ and $t$ are known. This is the well-known case of three observations, considered by Gauss. In all the remaining cases, the number of observations must be greater than three. We note that the total number of additional unknowns must be even.

In practice, apparently, only the following cases can occur:

**a** All the $\delta$ and $t$ are known ($m = l = 0$). Then condition [14] yields the following possible combinations

1) $k = 0$ $\quad n = 3$
2) $k = 2$ $\quad n = 4$
3) $k = 4$ $\quad n = 5$
4) $k = 6$ $\quad n = 6$

A further increase in $k$ is of no use, since it yields combinations that reduce to the foregoing ones. Thus, in this case the maximum number of observations must be six. If there are six observations, then all the $\alpha$ can be unknown, and the orbit can be determined from $\delta$ and $t$ alone.

**b** All the $\alpha$ and $t$ are known ($k = l = 0$). This case is analogous to the preceding one. The maximum number of observations is six. The orbit can be determined from $\alpha$ and $t$ alone from six observations.

**c** All the $\delta$ and $t$ are known ($k = n = 0$). The following combinations are possible

1) $l = 0$ $\quad n = 3$
2) $l = 2$ $\quad n = 4$
3) $l = 4$ $\quad n = 5$
4) $l = 6$ $\quad n = 6$

A further increase in $l$ yields combinations that reduce to the foregoing ones.

Consequently, in this case, it is possible to determine the orbit from four, five or six observations, depending on the number of instants of time which are known accurately. In the most unfavorable case, when all the times are known approximately, it is necessary to have six satellite positions on the celestial sphere to determine its orbit.

## 3 Solution of the Equations for Topocentric Distances in the Case of Four Observations With Two Unknown Instants of Time

Let us consider the problem of determining the topocentric distances by means of four observations, two of which contain values of time known to be in error, and the remaining two are determined without error. We denote the known instants by $t_1$ and $t_0$. The quantity $\tau_1 = \sqrt{fm}\,(t_1 - t_0)$ is consequently known. The quantities $\tau_2$ and $\tau_3$ are unknown and must be determined along with the topocentric distances. However, calculating $\tau_2$ and $\tau_3$ is equivalent to calculating $n_2^0$ and $n_3^0$, since we have from [7 and 8]

$$\tau_i = -[n_i^0/(1 - n_i^0)]\tau_1 \qquad [15]$$

Thus, we can select as the unknowns in this problem the following quantities: $\rho_0$, $\rho_1$, $\rho_i$ and $n_i^0$ ($i = 2, 3$). Eliminating

[1] An analogous case occurs when the observation is carried out with the aid of a radio interferometer. In this case the observations yield directly only the values of the azimuth of the satellite at different instants of time (Burt, 1958).

from the left-hand sides of [13] the quantities $\rho_0$ and $\rho_1$ and defining

$$A_i = \frac{a_i}{\kappa_i \Delta_i} \qquad A_i' = \frac{a_i'}{\kappa_i \Delta_i}$$

$$B_i = -\frac{b_i}{\Delta_i} \qquad B_i' = \frac{b_i'}{\Delta_i} \qquad \ldots\ldots [16]$$

we obtain the following equations for the determination of $n_i^0$

$$\frac{A_2'}{n_2^0} - \frac{A_3'}{n_3^0} = A_3 - A_2 \qquad B_2 n_2^0 - B_3 n_3^0 = B_3' - B_2' \quad [17]$$

We note that the coefficients $A_i$, $A_i'$, $B_i$ and $B_i'$ depend on $n_i^0$ not only through $\kappa_i$ and $\kappa_i'$, but also through the rectangular coordinates of the observation sites with indexes $i = 2, 3$. In fact we have following relations

$$X_i = X_i^0 \cos \mu\omega(t_i - t_0) - Y_i^0 \sin \mu\omega(t_i - t_0)$$
$$Y_i = Y_i^0 \cos \mu\omega(t_i - t_0) + X_i^0 \sin \mu\omega(t_i - t_0)$$
$$\ldots\ldots [18]$$

where

$X_i^0, Y_i^0$ = coordinates of the corresponding points of observations at the instant $t_i = t_0$
$\omega$ = angular velocity of the rotation of Earth about its axis
$\mu$ = converts the mean time into sidereal time

The differences $t_i - t_0$ are expressed in terms of $\tau_i$ by means of [3] and in terms $n_i^0$ by means of [15]. The coefficients of Equations [17] depend also on $\rho_k$ through $\kappa_i$ and $\kappa_i'$.

The final system of equations for the determination of all the unknowns of the problem consists of [13 and 17]. In this case two equations in [13] are redundant and can serve as a check on the calculations.

Equations [13 and 17] are best solved by the method of successive approximations. The calculations can be performed in the following sequence.

#### First Approximation

**1** In the first approximation we can put $\tau_i = 0$, $\kappa_i = \kappa_i' = 1$ $(i = 2, 3)$. These values of $\tau$, $\kappa$ and $\kappa'$ are used to calculate the constants in [12 and 16].

**2** The system [17] is solved, and this yields, as a rule, two solutions for $n_2^0$ and $n_3^0$, and consequently also for $\tau_2$ and $\tau_3$. Which of the solutions is correct can sometimes be ascertained by calculating $\rho_k$ from [13], for the resultant values of $\rho_k$ should be positive and have reasonable values. If the instants of observations are known approximately, the necessary solution can be selected by calculating $\tau_i$ and comparing it with the observed values.

**3** Equations [15] are used to calculate $\tau_i$ and Equations [13] are used to calculate $\rho_k$.

#### Second Approximation

**1** The coordinates are calculated of those points of observation for which instants of observations are not given, using [18] and the values of $\tau_i$ obtained from the first approximation.

**2** The values of $\kappa_i$ and $\kappa_i'$ are calculated from the approximate formulas

$$\kappa_i = 1 + \frac{1}{6} u_0(\tau_i'^2 - \tau_i^2) \qquad \kappa_i' = 1 + \frac{1}{6} u_0(\tau_i'^2 - \tau_1^2)$$

where

$$u_0 = r_0^{-3}$$
$$r_0^2 = \rho_0^2 + 2(\lambda_0 X_0 + \mu_0 Y_0 + \nu_0 Z_0) + R_0^2$$

or from the exact formulas

$$\kappa_i = \frac{\eta_{1i}}{\eta_{0i}} \qquad \kappa_i' = \frac{\eta_{1i}}{\eta_{10}} \qquad [19]$$

where $\eta_{kl}$ is the ratio of the areas of the elliptical sector and the triangle, included between the geocentric radii vectors $r_k$ and $r_l$. The topocentric distances $\rho_k$ necessary for the calculation of $u_0$ or $\eta_{kl}$ are taken from the first approximation.

The values of $\eta_{kl}$ are conveniently calculated by the formula due to Purtskhavanidze, indicated on p. 120 of the text by Subbotin (1941). In our notation, this formula can be rewritten

$$\eta_{kl} = 1 + \beta_{kl}\left(1 + \frac{12}{5}\alpha_{kl} - \frac{11}{10}\beta_{kl}\right) + \Delta\eta_{kl}$$

where

$$\alpha_{kl} = 1 - [\psi_{kl}/(r_k + r_l)]$$
$$\beta_{kl} = \frac{4}{3}\frac{\tau_{kl}^2}{(r_k + r_l)^3}$$
$$\psi_{kl}^2 = 2(r_k r_l + x_k x_l + y_k y_l + z_k z_l)$$
$$\tau_{kl} = \sqrt{fm}(t_l - t_k)$$
$$r_k^2 = x_k^2 + y_k^2 + z_k^2$$
$$x_k = \rho_k \lambda_k + X_k$$
$$y_k = \rho_k \mu_k + Y_k$$
$$z_k = \rho_k \nu_k + Z_k$$

and where $\Delta\eta_{kl}$ is a small correction, which can be obtained from the table given on p. 121 of the cited book, or which can be calculated from the formula

$$\Delta\eta = \beta(3.9443\alpha^2 + 5.52\alpha^3 + \ldots) - \beta^2(5.2286\alpha + 14.73\alpha^2 + \ldots) + \beta^3(2.3714 + 16.87\alpha + 69\alpha^2 + \ldots) + \ldots$$

**3** The constants [12 and 16] are calculated.
**4** The system [17] is solved.
**5** $\tau_i$ and $\rho_k$ are calculated.

#### Third and Higher Approximations

The sequence of calculations of the second approximation is repeated, except that $\kappa_i$ and $\kappa_i'$ must be calculated by the exact formulas.

The convergence of the process of successive approximations is insured by the fact that the intervals between observations are considered small compared with the period of rotation of the satellite around Earth.

We note that the solution of Equations [13 and 17] can be obtained much faster if approximate values of the instants of observations are known. Then the process of successive approximation can be started not with $\tau_1 = 0$, but with the indicated approximate values of $\tau_i$.

Once sufficiently accurate values of the topocentric distances $\rho_k$ and of the time intervals between observation $\tau_i$ are found, the orbit elements can be determined in accordance with the well-known rules (Subbotin, 1941).

### 4 Case of Five Observations and One Known Value of Time

In this case, the unknowns are $\rho_0$, $\rho_1$, $\rho_i$, $n_i^0$ $(i = 2, 3, 4)$ and some value of $\tau$, for example $\tau_1$. Eliminating $\rho_0$ and $\rho_1$ from the left-hand sides of [13] we obtain equations analogous to [17]

$$\frac{A_2'}{n_2^0} - \frac{A_i'}{n_i^0} = A_i - A_2$$
$$B_2 n_2^0 - B_i n_i^0 = B_i' - B_2'$$
$$(i = 3, 4)$$
$$\ldots\ldots [20]$$

which can be used in principle to determine $n_i^0$ $(i = 2, 3, 4)$

**Table 1**

| | Number of the observation | | | |
|---|---|---|---|---|
| | 1 | 0 | 2 | 3 |
| $t$ | $17^h58^m30^s.700$ | $18^h00^m04^s.000$ | $18^h02^m23^s.500$ | $18^h03^m38^s.500$ |
| $\alpha$ | 297°20′21.″8 | 256°32′59.″8 | 337°09′20.″7 | 277°23′24.″1 |
| $\delta$ | −8°41′40.″6 | 14°15′27.″7 | 25°22′23.″9 | 37°39′16.″1 |
| $\varphi$ | 28°30′08.″0 | 32°10′56.″0 | 39°30′02.″0 | 43°11′36.″0 |
| $\lambda_W$ | $2^h48^m13^s.133$ | $2^h19^m05^s.600$ | $2^h24^m29^s.000$ | $1^h46^m42^s.733$ |
| $\lambda$ | 0.453861 | −0.225433 | 0.832665 | 0.101831 |
| $\mu$ | −0.877852 | −0.942615 | −0.350777 | −0.785126 |
| $\nu$ | −0.152925 | 0.246283 | 0.428514 | 0.610908 |
| $\rho$ | 520.91 | 539.10 | 572.19 | 507.41 |
| $t-t_0$ | −90.s300 | 0 | 139.s500 | 214.s500 |

and $\tau_1$. However, $\tau_1$ enters into [20] only through $\kappa_i$, $\kappa_i'$ and $X$, $Y_i$, $(i = 1, 2, 3, 4)$, which undergo changes of the order of $\tau_1 \cdot \Delta\tau_1$, when $\tau_1$ is varied an amount by $\Delta\tau_1$. Consequently, $\tau_1$ can be expected beforehand to be determined very poorly, and the calculations will lose much in accuracy. Therefore the case of five observations with one known time can hardly be of practical interest. An exception can be made only for remote satellites, whose period of rotation is of the same order of magnitude as the period of rotation of Earth about its own axis. In this case one can hope to obtain a sufficiently accurate value of $\tau_1$, owing to the rapid change in the coordinates of the points of observation.

## 5 Example of Calculation of the Orbit From Four Observations With Two Unknown Values of the Time

To verify the procedure developed here, we calculated the orbit from four observations with two unknown instants of time. The computation is given to illustrate the procedure, and also to give a certain idea of the speed of convergence of the successive approximations.

The following fictitious system of elements of a typical satellite orbit is used, referred to the equatorial system of coordinates:

$a$ = 7408.22 km
$e$ = 0.0838781
$i$ = 63°26′06.0″
$\Omega$ = 273°52′17.0″
$\omega$ = 20°13′48.0″
$M_0$ = 7°32′28.0″
$t_0$ = 1957 Nov. 20, 17 hr, 58 min, 30.700 sec., universal time

where $\Omega$ is measured from the equinox of 1957.0. For the constant $fm$ we assumed the value

$$fm = 1.688370 \cdot 10^{16} \text{km}^3 \text{ deg}^2 \text{ hr}^{-2}$$

which gives the value $n = 203.78068$ for the average motion of the satellite per hour.

Using elements [21] we calculated four apparent positions of the satellite for selected points on Earth's surface at certain nearly equal instants of time. It was assumed here that Earth is an exact sphere of radius $R = 6378.39$ km. The calculated positions of the satellite, together with the chosen coordinates of the observation points and with the chosen instant of time, are listed Table 1. The same table gives the value of the direction cosines and the topocentric distances of the satellite at these instants of time, to the assumed order of accuracy. The differences $t_i - t_0$ are also given.

We shall assume that the four pairs of values of $\alpha$ and $\delta$ listed in Table 1, along with two values of $t_0$ and $t_1$, are all the data yielded by the observations. The instants $t_2$ and $t_3$ of the last two observations will be considered erroneous.

Table 2 lists certain intermediate and the final results of the four successive approximations, carried out in solving Equations [13 and 17]. The calculations are to six significant figures. The following notation is used

$$C_i = \frac{c_i}{\kappa_i' \Delta_i} \qquad C_1' = -\frac{c_i'}{\kappa_i' \Delta_i}$$

**Table 2**

| | Numbers of observations | | | | | | | | | |
|---|---|---|---|---|---|---|---|---|---|---|
| | First approximation | | | | Second approx. | | Third approx. | | Fourth approx. | |
| | 1 | 0 | 2 | 3 | 2 | 3 | 2 | 3 | 2 | 3 |
| $t_i$ | $17^h58^m30^s.700$ | $18^h00^m04^s.000$ | $18^h00^m04^s.000$ | $18^h00^m04^s.000$ | $18^h02^m09^s.069$ | $18^h03^m15^s.669$ | $18^h02^m21^s.830$ | $18^h03^m35^s.973$ | $18^h02^m23^s.276$ | $18^h03^m38^s.128$ |
| $X_i$ | 1642.61 | 2256.81 | 1951.77 | 2519.46 | 1992.89 | 2573.84 | 1997.08 | 2579.57 | 1997.47 | 2580.18 |
| $Y_i$ | −5359.24 | −4904.03 | −4518.14 | −3908.48 | −4500.15 | −3872.88 | −4498.29 | −3869.07 | −4498.13 | −3868.66 |
| $Z_i$ | 3043.72 | 3397.22 | 4057.20 | 4365.77 | 4057.20 | 4365.77 | 4057.20 | 4365.77 | 4057.20 | 4365.77 |
| $x_i$ | — | — | 1 | 1 | 1.006761 | 1.009383 | 1.007227 | 1.010149 | 1.007334 | 1.010266 |
| $x_i$ | — | — | 1 | 1 | 1.008224 | 1.015297 | 1.009411 | 1.017860 | 1.009564 | 1.018120 |
| $A_i$ | — | — | −1905.83 | −730.462 | −1895.81 | − 681.659 | −1896.28 | − 675.267 | −1896.37 | − 674.517 |
| $A_i'$ | — | — | 1448.02 | 909.994 | 1447.17 | 842.144 | 1448.32 | 834.183 | 1448.49 | 833.218 |
| $B_i$ | — | — | 325.093 | 3777.43 | − 291.513 | 3969.25 | − 290.862 | 3996.24 | − 290.907 | 3999.31 |
| $B_i'$ | — | — | 710.213 | −2016.66 | 711.104 | −2218.86 | 713.010 | −2244.60 | 713.403 | −2247.75 |
| $C_i$ | — | — | 1498.12 | 3504.08 | 1533.66 | 3600.30 | 1539.33 | 3616.50 | 1539.92 | 3618.54 |
| $C_i'$ | — | — | 615.210 | −2170.64 | − 683.766 | −2340.67 | − 692.332 | −2364.36 | − 693.308 | −2367.47 |
| $n_i^{0(1)}$ | — | — | 0.572741 | 0.672596 | 0.596331 | 0.694372 | 0.598841 | 0.696515 | 0.599151 | 0.696834 |
| $n_i^{(2)}$ | — | — | 18.0433 | −0.830956 | — | — | — | — | — | — |
| $\dot{r}_i^{(1)}$ | 622.40 | 524.01 | 568.33 | 551.10 | 571.77 | 521.15 | 572.05 | 509.37 | 572.10 | 508.14 |
| $\dot{r}_i^{(2)}$ | −1825.58 | −5155.54 | −1549.92 | −2775.80 | — | — | — | — | — | — |
| $t_i - t_0$ | — | — | 125.s069 | 191.s669 | 137.s830 | 211.s973 | 139.s276 | 214.s128 | 139.s456 | 214.s452 |

Table 3

| | Number of the observation | | | |
|---|---|---|---|---|
| | 1 | 0 | 2 | 3 |
| $\Delta\alpha$ (O—C) . . . . | —0.″1 | —1′19.″3 | +2′58.″7 | —0.″6 |
| $\Delta\delta$ (O—C) . . . . | +0.1 | — 47.″6 | — 48.″1 | 0.0 |

It was assumed in the first-approximation calculations that the second and third observations, the times of which are known, were made simultaneously with the zero-order observations. In each successive approximation the unknown instants of time were assigned the values obtained from the preceding approximation.

Equations [17] yield in the first approximation two systems of values of $n_i^0$, designated by the indexes (1) and (2) over the corresponding letters in Table 2. The calculation of $\rho_1$ for the two systems of $n_i^0$ shows that the second system of solutions should be discarded, since it yields negative topocentric distances. Therefore, in the subsequent approximations we retain only the values corresponding to the system of solutions $n_i^{0(1)}$.

We note that in calculating $n_i^0$ from [17] it is necessary to subtract nearly equal numbers which leads to the loss of accuracy. This can be offset by using a few additional significant figures in the later approximations.

From the rate of convergence of the successive approximations one can conclude that the fifth approximation changes the values of the time by several hundredths of a second and the values of the topocentric distances by several hundredths of a kilometer. Since such an accuracy can be considered excessive in the calculation of the initial orbit, the fourth approximation can be considered as final.

The values of $\rho_1$ and $\rho_0$ in the fourth approximation, not listed in Table 2, are

$$\rho_1 = 521.20 \text{ km} \qquad \rho_0 = 539.11 \text{ km}$$

Since the topocentric distances and the unknown instants of observations have already been determined, further calculations reduce to a determination of the orbital element from two geocentric positions.

To determine the elements we use the first and third observations, since they are separated by a time interval greater than the remaining intervals, and one can hope to determine more accurately the eccentricity and the longitude of the perigee.

Calculations yield the following system of elements

$a$ = 7412.80 km
$e$ = 0.0844343
$i$ = 63°26′25.2″
$\Omega$ = 273°52′32.5″
$\omega$ = 20°12′04.3″
$M_0$ = 7°34′15.2″
$t_0$ = 1957 Nov. 20, 17 hr, 58 min, 30.700 sec, universal time

The differences between the observed positions of the satellite and those calculated on the basis of this system of elements are given in Table 3.

Considerable discrepancies between the observed and calculated positions for the two middle instants of time which reach 2 min of arc are explained by the fact that in the calculation of the geocentric distances we confined ourselves only to the fourth approximation. With this, the instants of observation were determined to the accuracy of 0.05 sec, which is equivalent to an error of about 2 or 3 min of arc in the apparent position of the satellite. A more accurate calculation of the unknown instants will reduce these discrepancies considerably. However, even such a representation of observations can be considered satisfactory for an initial orbit.

The author considers it his duty to express his gratitude to E. N. Lemekhova, staff member of the Institute of Theoretical Astronomy of the USSR Academy of Science, for help with the calculations of the example.

## References

Subbotin, M. F., "A Course in Celestial Mechanics," vol. 1, 1941, Leningrad-Moscow.

Burt, E. G. C., 1958, "The Computation of Orbit Parameters From Interferometer and Doppler Data," Proc. Roy. Soc., vol. A 248, 1252, pp. 48–55.

*—Original received March 17, 1959*

# Method for Improving Orbits of Artificial Satellites of the Earth Using Observations With Approximate Values of Time

D. K. KULIKOV and
YU. V. BATRAKOV

**A method is developed for improving the elements of orbits of artificial satellites in the case when the observation times are only approximately known. Corresponding equations of condition are set up, one of which is independent of the time error. It is shown that certain orbit elements can be determined from equations that are independent of the time errors. An analysis of the optimum conditions for the determination of these elements is made. Equations of condition are also obtained for the corrections to the absolute coordinates of the observation stations, and an analysis is made of these equations. The procedure developed to improve the orbit elements of artificial satellites is illustrated with an example.**

IT IS well known that the task of improving an orbit consists of determining a system of elements that best fits all the available observations. The criterion of optimum representation of a set of observations employed here is that the sum of the squares of the deviations of calculated positions of the celestial body from its observed positions is a minimum, that is

$$\sum_i [(\alpha - \alpha_c)^2 \cos^2 \delta + (\delta - \delta_c)^2]_i = \min$$

where $\alpha$ and $\delta$ are the observed equatorial coordinates of the body at the instant $t$; $\alpha_c$ and $\delta_c$ are the calculated equatorial coordinates of the body at the instant of observation.

This problem is solved by setting up equations of condition that relate $(\alpha - \alpha_c) \cos \delta$ and $(\delta - \delta_c)$ with the corrections for the orbit elements. These equations are then solved by the least-squares method.

There are many methods for improving orbit elements, depending on the choice of the unknowns and of the coordinate systems. It is not our task to review methods of orbit correction. These are described in sufficient detail in well-known texts on theoretical astronomy (Dubyago, 1949; Subbotin, 1941; Bauschinger, 1906; Oppolzer, 1880; etc.). Mention should also be made of the work by Professor N. S. Samoilova-Yakhontova (1949), which contains a classification and systematization of the principal methods of correcting elliptic orbits.

All the classical methods of orbit correction, developed for the study of the motion of natural bodies in the solar system, can be applied in their entirety to artificial satellites. It becomes necessary, however, to take into account the peculiarities of the motion of the satellite. Accordingly, certain modifications must be introduced in the classical methods of orbit improvement.

First, additional unknowns must be introduced into the equations of condition. It is known, for example, that atmospheric drag causes considerable secular perturbations in the mean daily motion, the coefficients of which cannot as yet be determined theoretically. Therefore in the expression for the mean anomaly

$$M = M_0 + nt + n't^2 + n''t^3 + \ldots$$

the coefficients $n'$, $n''$, . . ., which take into account the influence of the atmosphere on the motion of the satellite, should be determined from observations.

Another peculiarity of the motion of an artificial Earth satellite is that, owing to the small distance between the satellite and the Earth's surface, the angular displacement of the satellite relative to the observer is quite large and may reach 2.5° per sec of time, amounting to 10″ in 0.001 sec.

Under these conditions, the errors that enter the determination of the instants of time assume great significance.

We note that in the development of classical methods of correction of the orbits of planets and comets, this fact has no particular significance, since then the angular displacement does not exceed 0.1″ per sec of time and consequently the error in time is practically zero.

At the present time the influence of errors in the fixation of time on the determination of the orbit elements of artificial satellites is reduced by increasing the number of observations. It is known, however, that this method can reduce the errors only to a definite limit. Obviously, the direct way of solving this problem is to increase the accuracy of fixation of the instants of observation of artificial satellites. Much has already been done in this direction, and there is no doubt that the technique of observations will be further improved in the future.

However, apart from this, the influence of these errors on the determination of certain unknowns can be substantially reduced by using a suitable method of data reduction. We now proceed to an examination of this problem.

## 1 Derivation of the Equations of Condition

We use a stationary equatorial system of coordinates $xyz$, with the $z$ axis directed toward the north pole of the Equator, the $x$ axis toward the vernal equinox, and the $y$ axis chosen to

Translated from *Byulleten' Instituta Teoreticheskoi Astronomii* (Bull. Institute of Theoretical Astronomy), vol. 7, no. 7 (90), 1960, pp. 554–569. Translated by J. George Adashko.

make the system a right-handed one.

Let

$\mathbf{r}(x, y, z)$ = radius vector of the satellite relative to Earth's center of inertia

$\mathbf{R}(X, Y, X)$ = radius vector of the observer relative to the same origin

$\boldsymbol{\varrho}(\xi, \eta, \zeta)$ = radius vector of the satellite relative to the observer

We can then write

$$\boldsymbol{\varrho} = \mathbf{r} - \mathbf{R} \qquad [1]$$

We note that the radius vector $\mathbf{r}$ is a function of the elements of the satellite orbit ($i$, $\Omega$, $\omega$, $M_0$, $n$, $e$) and the time $t$, whereas the radius vector $\mathbf{R}$ depends on the spherical coordinates of the observer, ($R$, $\varphi$, $\lambda$) and the time.

The effect of the errors in the coordinates of the observer's position, and in the time on $\boldsymbol{\varrho}$ is obtained by varying Equation [1]. We have

$$\Delta\boldsymbol{\varrho} = \Delta\mathbf{r} + \mathbf{r}\Delta t - \Delta\mathbf{R} - \dot{\mathbf{R}}\Delta t = \Delta\mathbf{r} - \Delta\mathbf{R} + \dot{\boldsymbol{\varrho}}\Delta t \qquad [2]$$

where

$\Delta\mathbf{r}$ = $\sum(\partial\mathbf{r}/\partial E_i)\Delta E_i$, the error in $\mathbf{r}$ due to inaccuracy in the elements $E_i$

$\Delta\mathbf{R}$ = error in the position of the observer relative to Earth's center of inertia

$\Delta t$ = error in the fixation of time

$\Delta\mathbf{R}$ is small quantity, and will be neglected for the sake of simplicity. We shall thus deal henceforth with the equation

$$\Delta\boldsymbol{\varrho} = \Delta\mathbf{r} + \dot{\boldsymbol{\varrho}}\Delta t \qquad [3]$$

We introduce an auxiliary system of coordinates, having its origin at the instantaneous position of the satellite. The coordinate axes are directed along the vector $\boldsymbol{\varrho}$, along the tangent to the diurnal parallel and along the tangent to the declination circle. Denoting the unit vectors by $\mathbf{j}_\rho$, $\mathbf{j}_\alpha$ and $\mathbf{j}_\delta$, respectively (Fig. 1), we can write

$$\mathbf{j}_\rho = \frac{\boldsymbol{\varrho}}{\rho} \qquad \mathbf{j}_\alpha = \frac{[\mathbf{j}_\zeta \times \boldsymbol{\varrho}]}{\sqrt{\xi^2 + \eta^2}} \qquad \mathbf{j}_\delta = -[\mathbf{j}_\rho \times \mathbf{j}_\alpha] \qquad [4]$$

where $\mathbf{j}_\zeta$ is a unit vector directed along the $\zeta$ axis.

Using the components of $\Delta\boldsymbol{\varrho}$ along $\mathbf{j}_\rho$, $\mathbf{j}_\alpha$ and $\mathbf{j}_\delta$, Equation [3] becomes

$$\mathbf{j}_\rho\Delta\rho + \mathbf{j}_\alpha\rho\cos\delta\Delta\alpha + \mathbf{j}_\delta\rho\Delta\delta = \Delta\mathbf{r} + \dot{\boldsymbol{\varrho}}\Delta t \qquad [5]$$

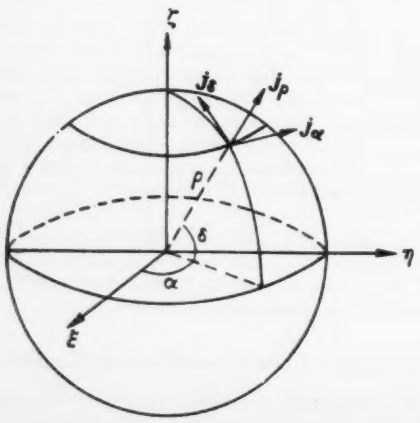


Fig. 1

The quantities $\Delta\alpha$ and $\Delta\delta$ are determined by comparing the observed positions of the satellite with its calculated positions. The quantity $\Delta\rho$ is unknown.

In classical methods of improving orbits, the unknown $\Delta\rho$ is eliminated by taking scalar products of Equation [5] with $\mathbf{j}_\alpha$ and with $\mathbf{j}_\delta$. This yields two equations of condition, one for the right ascension and one for the declination; in addition it is assumed that $\Delta t = 0$.

In our case it is necessary to eliminate the time error $\Delta t$ along with $\Delta\rho$ in at least one of the two equations.

For this purpose we take a scalar product of Equation [5] with a certain unit vector $\mathbf{j}_\varrho$ and stipulate that

$$(\mathbf{j}_\varrho \cdot \mathbf{j}_\rho) = 0 \qquad (\mathbf{j}_\varrho \cdot \dot{\boldsymbol{\varrho}}) = 0 \qquad [6]$$

We then have the following equation of condition

$$(\mathbf{j}_\varrho \cdot \mathbf{j}_\alpha)\rho\cos\delta\Delta\alpha + (\mathbf{j}_\varrho \cdot \mathbf{j}_\delta)\rho\Delta\delta = (\mathbf{j}_\varrho \cdot \Delta\mathbf{r}) \qquad [7]$$

It follows from relations [6] that the unit vector $\mathbf{j}_\varrho$ will be perpendicular to $\boldsymbol{\varrho}$ and $\dot{\boldsymbol{\varrho}}$. The plane of the vectors $\boldsymbol{\varrho}$ and $\dot{\boldsymbol{\varrho}}$ will henceforth be called the plane of the apparent orbit. Thus, the unit vector $\mathbf{j}_\varrho$ can be defined as

$$\mathbf{j}_\varrho = [\boldsymbol{\varrho} \times \dot{\boldsymbol{\varrho}}]/\rho v \qquad [8]$$

where $v$ is the component of the velocity $\dot{\boldsymbol{\varrho}}$ along a perpendicular to the vector $\boldsymbol{\varrho}$, that is

$$v^2 = \dot{\xi}^2 + \dot{\eta}^2 + \dot{\zeta}^2 - \dot{\rho}^2 \qquad [9]$$

We now choose a second unit vector $\mathbf{j}_G$ such that

$$\mathbf{j}_G = [\mathbf{j}_\varrho \times \mathbf{j}_\rho] \qquad [10]$$

It then follows from the vector Equation [5] that

$$(\mathbf{j}_G \cdot \mathbf{j}_\alpha)\rho\cos\delta\Delta\alpha + (\mathbf{j}_G \cdot \mathbf{j}_\delta)\rho\Delta\delta = (\mathbf{j}_G \cdot \Delta\mathbf{r}) + (\mathbf{j}_G \cdot \dot{\boldsymbol{\varrho}})\Delta t \qquad [11]$$

Taking Equations [4 and 8] into account, we can rewrite Equation [10] as

$$\mathbf{j}_G = \frac{\rho\dot{\boldsymbol{\varrho}} - \dot{\rho}\boldsymbol{\varrho}}{\rho v} = \frac{\mathbf{v}}{v} \qquad [12]$$

and consequently

$$(\mathbf{j}_G \cdot \dot{\boldsymbol{\varrho}}) = v$$

Setting

$$(\mathbf{j}_G \cdot \mathbf{j}_\alpha) = \cos\psi \qquad (\mathbf{j}_G \cdot \mathbf{j}_\delta) = \sin\psi \qquad [13]$$

we reduce the equations of condition [7 and 11] to the form

$$\rho\Delta g = (\mathbf{j}_\varrho \cdot \Delta\mathbf{r}) \qquad \rho\Delta G = (\mathbf{j}_G \cdot \Delta\mathbf{r}) + v\Delta t \qquad [14]$$

where

$$\begin{aligned} \Delta g &= \cos\psi\Delta\delta - \sin\psi\cos\delta\Delta\alpha \\ \Delta G &= \sin\psi\Delta\delta + \cos\psi\cos\delta\Delta\alpha \end{aligned} \qquad [15]$$

From Equations [13, 4, 8 and 12] we readily obtain

$$\cos\psi = \frac{\xi\dot{\eta} - \eta\dot{\xi}}{v\sqrt{\xi^2 + \eta^2}} \qquad \sin\psi = \frac{\rho\dot{\xi} - \zeta\dot{\rho}}{v\sqrt{\xi^2 + \eta^2}} \qquad [16]$$

The vector $\Delta\mathbf{r}$ is expressed in terms of the variations of the elements $\Delta i$, $\Delta\Omega$, $\Delta\omega$, $\Delta M_0$, $\Delta n$ and $\Delta e$ in accordance with the well-known Eckert-Brouwer equations (1937; see also Samoilova-Yakhontova, 1941; Kulikov, 1950)

$$\Delta\mathbf{r} = [\Delta\mathbf{i} \times \mathbf{r}] + [\Delta\boldsymbol{\Omega} \times \mathbf{r}] + [\Delta\boldsymbol{\omega} \times \mathbf{r}] + \dot{\mathbf{r}}\frac{\Delta M_0}{n} + \left(\dot{\mathbf{r}}t - \frac{2}{3}\mathbf{r}\right)\frac{\Delta n}{n} + \left(H\mathbf{r} + K\frac{\dot{\mathbf{r}}}{n}\right)\frac{\Delta e}{e} \qquad [17]$$

where

$$H = (r + p - 2a)/p$$

$$K = \frac{r + p}{p} \cdot \frac{r\dot{r}}{a^2 n}$$

$\Delta i$, $\Delta\Omega$ and $\Delta\omega$ are elementary rotations of the orbit about the line of nodes, the normal to the plane of the Equator and the normal to the plane of the orbit, respectively.

Thus, Equations [14], together with Equations [8, 12, 15, 16 and 17], yield an equation of condition in $g$ and $G$, the former being independent of the time error $\Delta t$.

The geometrical meaning of the auxiliary quantities $\Delta g$ and $\Delta G$, defined by Equation [15], is seen in Fig. 2. In this diagram $C$ is the observed position of the satellite; $O$ is the calculated position of the satellites; $\mathbf{j}_\alpha$, $\mathbf{j}_\delta$ and $\mathbf{j}_v$, $\mathbf{j}_G$ are unit vectors along the axes of the auxiliary coordinate systems discussed earlier.

Since, according to Equation [12], the axis $\mathbf{j}_G$ coincides with the apparent calculated orbit, the first equation of [14] is based on the deviation perpendicular to the apparent orbit and the second equation is based on deviation along the apparent orbit.

## 2 Summary of Working Formulas

We now give a complete summary of working formulas for the compilation of the equations of condition [14].

The rectangular geocentric equatorial coordinates and the velocity components of the satellites are calculated from the well-known formulas

$$\begin{aligned} x &= A_x(\cos E - e) + B_x \sin E \\ \dot{x} &= (an/r)(-A_x \sin E + B_x \cos E) \\ y &= A_y(\cos E - e) + B_y \sin E \\ \dot{y} &= (an/r)(-A_y \sin E + B_y \cos E) \\ z &= A_z(\cos E - e) + B_z \sin E \\ \dot{z} &= (an/r)(-A_z \sin E + B_z \cos E) \end{aligned} \quad \ldots\ldots [18]$$

$$\begin{aligned} E - e \sin E &= M_0 + n(t - t_0) \\ r &= a(1 - e \cos E) \qquad n = fm/\alpha^{3/2} \end{aligned} \quad \ldots\ldots [19]$$

$$\begin{aligned} A_x &= aP_x \qquad B_x = a\sqrt{1 - e^2}Q_x \\ A_y &= aP_y \qquad B_y = a\sqrt{1 - e^2}Q_y \\ A_z &= aP_z \qquad B_z = a\sqrt{1 - e^2}Q_z \end{aligned} \quad \ldots\ldots [20]$$

The direction cosines of the orbital axes $P_x$, $P_y$, $P_z$, $Q_x$, $Q_y$ and $Q_z$ are found from the relations

$$\begin{aligned} P_x &= \cos\Omega\cos\omega - \sin\Omega\sin\omega\cos i \\ Q_x &= -\cos\Omega\sin\omega - \sin\Omega\cos\omega\cos i \\ P_y &= \sin\Omega\cos\omega + \cos\Omega\sin\omega\cos i \\ Q_y &= -\sin\Omega\sin\omega + \cos\Omega\cos\omega\cos i \\ P_z &= \sin\omega\sin i \qquad Q_z = \cos\omega\sin i \end{aligned} \quad \ldots\ldots [21]$$

Here $i$, $\Omega$, $\omega$, $M_0$, $a$ and $e$ are the equatorial elements of the satellite orbit.

The rectangular geocentric equatorial coordinates and the velocity components of the observer are determined from the relations

$$\begin{aligned} X &= R\cos\varphi'\cos s \qquad \dot{X} = -2\pi(1 + \mu)Y \\ Y &= R\cos\varphi'\sin s \qquad \dot{Y} = 2\pi(1 + \mu)X \\ Z &= R\sin\varphi' \qquad\qquad \dot{Z} = 0 \end{aligned} \quad \ldots\ldots [22]$$

where $s$ is the local sidereal time.

The factor $1 + \mu = 1.00273791$ is the duration of the mean day expressed in sidereal days and is introduced to refer the velocities to the mean day as the time unit.

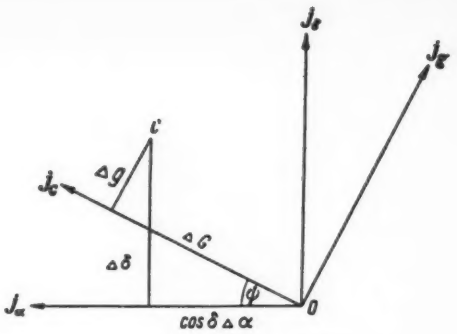


Fig. 2

The topocentric coordinates and velocity components of the satellite are readily found from the equation

$$\begin{aligned} \rho\cos\delta\cos\alpha &= \xi = x - X \qquad \dot{\xi} = \dot{x} - \dot{X} \\ \rho\cos\delta\sin\alpha &= \eta = y - Y \qquad \dot{\eta} = \dot{y} - \dot{Y} \\ \rho\sin\delta &= \zeta = z - Z \qquad \dot{\zeta} = \dot{z} - \dot{Z} \end{aligned} \quad \ldots\ldots [23]$$

The absolute terms of the equations of condition $\Delta g$ and $\Delta G$ are calculated from the formulas

$$\begin{aligned} \Delta g &= \cos\psi(\delta_{obs} - \delta_{calc}) - \sin\psi\cos\delta(\alpha_{obs} - \alpha_{calc}) \\ \Delta G &= \sin\psi(\delta_{obs} - \delta_{calc}) + \cos\psi\cos\delta(\alpha_{obs} - \alpha_{calc}) \end{aligned} \quad \ldots\ldots [24]$$

$$\cos\psi = \frac{\xi\dot{\eta} - \eta\dot{\xi}}{v\sqrt{\xi^2 + \eta^2}} \qquad \sin\psi = \frac{\rho\dot{\zeta} - \zeta\dot{\rho}}{v\sqrt{\xi^2 + \eta^2}}$$

$$v^2 = \dot{\xi}^2 + \dot{\eta}^2 + \dot{\zeta}^2 - \dot{\rho}^2 \qquad \rho\dot{\rho} = \xi\dot{\xi} + \eta\dot{\eta} + \zeta\dot{\zeta} \quad \ldots\ldots [25]$$

Finally, the coefficients of the equations of condition are determined from Equations [14] with allowance for Equations [8, 12 and 17]. Projected along the coordinate axes, these relations assume the form

$$\Delta g = \frac{1}{\rho^2 v}[(\eta\dot{\zeta} - \zeta\dot{\eta})\Delta x + (\zeta\dot{\xi} - \xi\dot{\zeta})\Delta y + (\xi\dot{\eta} - \eta\dot{\xi})\Delta z]$$

$$\Delta G = \frac{1}{\rho^2 v} \times$$

$$[(\rho\dot{\xi} - \xi\dot{\rho})\Delta x + (\rho\dot{\eta} - \eta\dot{\rho})\Delta y + (\rho\dot{\zeta} - \zeta\dot{\rho})\Delta z] + \frac{v}{\rho}\Delta t \quad \ldots\ldots [26]$$

with

$$\Delta x = z\sin\Omega\Delta i - y\Delta\Omega - (y\cos i + z\sin i\cos\Omega)\Delta\omega + \frac{\dot{x}}{n}\Delta M_0 + \left(\dot{x}t - \frac{2}{3}x\right)\frac{\Delta n}{n} + \left(Hx + K\frac{\dot{x}}{n}\right)\frac{\Delta e}{e}$$

$$\Delta y = -z\cos\Omega\Delta i + x\Delta\Omega + (x\cos i - z\sin i\sin\Omega)\Delta\omega + \frac{\dot{y}}{n}\Delta M_0 + \left(\dot{y}t - \frac{2}{3}y\right)\frac{\Delta n}{n} + \left(Hy + K\frac{\dot{y}}{n}\right)\frac{\Delta e}{e}$$

$$\Delta z = (y\cos\Omega - x\sin\Omega)\Delta i + (x\cos\Omega + y\sin\Omega)\sin i\Delta\omega + \frac{\dot{z}}{n}\Delta M_0 + \left(\dot{z}t - \frac{2}{3}z\right)\frac{\Delta n}{n} + \left(Hz + K\frac{\dot{z}}{n}\right)\frac{\Delta e}{e} \quad \ldots\ldots [27]$$

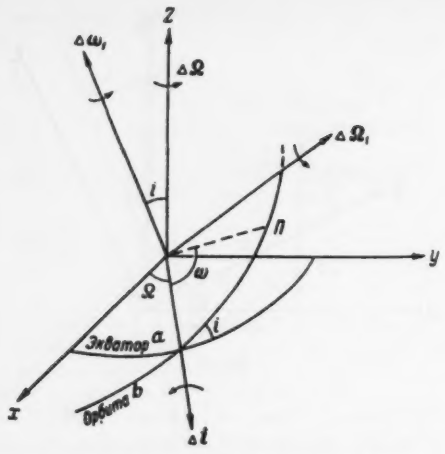


Fig. 3 Translations: [a] Equator; [b] orbit

where

$$H = (r + p - 2a)/p$$
$$K = (r + p)(x\dot{x} + y\dot{y} + z\dot{z})/pna^2$$
$$p = a(1 - e^2)$$

## 3 Analysis of the Equations of Condition

Let us consider the question of how to distribute the observations and how to use the equations of condition in $g$ and $G$ for the optimum determination of the unknowns, recalling that the first equation of [26] is independent of the errors in time.

It is well known that one of the most important conditions for the best determination of corrections to the orbit element is to insure that the observations cover a considerable portion of the orbit.

As applied to satellite, this requirement can be satisfied in the best manner if the observation stations are located in the latitude belt from $+i$ to $-i$.

On the other hand, the reliable determination of the foregoing unknowns is significantly affected by the distribution of observations of satellites on the apparent celestial sphere.

The general analytical solution of this problem is quite complicated. We shall therefore confine ourselves to an investigation of the equations of condition for certain particular cases, using for this purpose geometrical methods.

In these investigations we shall neglect in the coefficients of the equations of condition the eccentricity of the satellite orbit and the speed of rotation of Earth, since such assumptions do not change the qualitative picture of the cases investigated.

We first write out the vector $\Delta\mathbf{r}$, which enters the equations of condition [14] and which is determined by Equation [17] in the following form

$$\Delta\mathbf{r} = [\Delta\mathbf{i}\,\mathbf{x}\,\mathbf{r}] + [\Delta\boldsymbol{\Omega}_1\,\mathbf{x}\,\mathbf{r}] + [\Delta\boldsymbol{\omega}_1\,\mathbf{x}\,\mathbf{r}] + \frac{\dot{\mathbf{r}}}{n}\Delta M_0 + \left(\dot{\mathbf{r}}t - \frac{2}{3}\mathbf{r}\right)\frac{\Delta n}{n} + \left(H\mathbf{r} + K\frac{\dot{\mathbf{r}}}{n}\right)\frac{\Delta e}{e} \quad [28]$$

$\Delta\mathbf{i}$, $\Delta\boldsymbol{\Omega}_1$ and $\Delta\boldsymbol{\omega}_1$ are elementary rotations of the orbit about the line of nodes, a line located in the plane of the orbit perpendicular to the line of nodes, and the normal to the plane of the orbit, respectively (Fig. 3).

The magnitudes of the vectors $\Delta\boldsymbol{\Omega}_1$ and $\Delta\boldsymbol{\omega}_1$ are determined by the relations

$$\Delta\Omega_1 = \Delta\Omega \sin i \qquad \Delta\omega_1 = \Delta\omega + \Delta\Omega \cos i \quad [29]$$

Table 1

| | $\Delta i$ | $\Delta\Omega$ | $\Delta\omega_1$ | $\frac{\Delta M_0}{n}$ | $\frac{\Delta n}{n}$ | $\frac{\Delta e}{e}$ |
|---|---|---|---|---|---|---|
| $(\mathbf{n}, \Delta\mathbf{r})$ | $r \sin u$ | $r \sin i \cos u$ | 0 | 0 | 0 | 0 |
| $(\mathbf{s}, \Delta\mathbf{r})$ | 0 | 0 | 0 | 0 | $-\frac{2}{3}r$ | $Hr$ |
| $(\boldsymbol{\tau}, \Delta\mathbf{r})$ | 0 | 0 | $r$ | $\lvert\dot{\mathbf{r}}\rvert$ | $\lvert\dot{\mathbf{r}}\rvert t$ | $(K/n)\lvert\dot{\mathbf{r}}\rvert$ |

Let us project the vector $\Delta\mathbf{r}$ on three mutually perpendicular directions: The normal to the plane of the orbit, the radius vector, and a perpendicular to the radius vector in the plane of the orbit. Denoting the unit vectors along these directions by $\mathbf{n}$, $\mathbf{s}$ and $\boldsymbol{\tau}$ respectively, we obtain a table for the projections of the vector $\Delta\mathbf{r}$ (Table 1).

Consider now the equations of condition

$$\rho\Delta g = (\mathbf{j}_g \cdot \Delta\mathbf{r}) \qquad \rho\Delta G = (\mathbf{j}_G \cdot \Delta\mathbf{r}) + v\Delta t \quad [30]$$

as applied to certain particular cases.

**a** The plane of the orbit passes through the zenith of the observer (zenith passages). In this case the plane of the apparent orbit coincides with the plane of the actual orbit.

Let us turn to Fig. 4, in which $O$ is the center of the Earth, $M$ the location of the observer on the Earth's surface and $C$ the position of the satellite in the orbit at the instant of observation.

It follows directly from Fig. 4 that

$$\mathbf{j}_g = \mathbf{n} \qquad \cos\gamma = (R/r)\sin z \qquad \mathbf{j}_G = \boldsymbol{\tau}\sin\gamma + \mathbf{s}\cos\gamma \quad [31]$$

where $\gamma$ is the angle between the velocity vector and the direction to the observer, as measured at the satellite.

It is thus seen from Equations [31 and 32] and Table 1 that the equation in $g$ will contain two unknowns: $\Delta i$ and $\Delta\Omega$, whereas the equation in $G$ will contain four unknowns: $\Delta\omega_1$, $\Delta M_0$, $\Delta n$ and $\Delta e$.

Since in practice only passages close to, but not exactly through, the zenith can occur both equations will contain all six unknowns. In this case, however, the coefficients of the missing unknowns will be small, and the unknowns can be determined from the equations in $g$ and $G$ separately, using the method of successive approximations. The solution procedure reduces to the following. We first determine the unknowns $\Delta i$ and $\Delta\Omega$ from $\Delta g$ by setting all the other unknowns equal to zero. We then substitute the resultant values of $\Delta i$ and $\Delta\Omega$ in the equations in $G$, from which we then determine the unknowns $\Delta\omega_1$, $\Delta M_0$, $\Delta n$ and $\Delta e$. These values are then substituted in the equations in $g$, and the values of $\Delta i$ and $\Delta\Omega$ again determined. We proceed in this manner until the desired accuracy of solution is obtained.

Thus, passages near the zenith are quite suitable for the de-

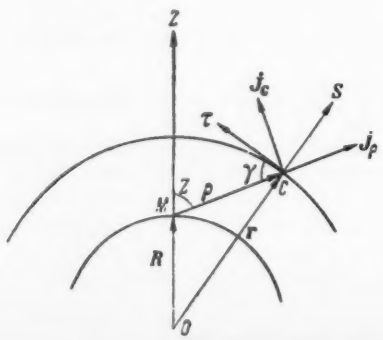


Fig. 4

termination of the inclination and the longitude of the ascending node of the orbit, since the latter are determined reliably from equations that are free of time errors. We note that the error resulting from the effect of the atmosphere on the motion of the satellite does not influence the determination of these elements, since this effect, as can be seen from the expression for the mean anomaly (see introductory paragraphs), is equivalent to a time error.

As is well known, the elements $\Omega$ and $i$ are of prime significance in the determination of the oblateness of Earth from observations of artificial satellites.

b The plane of the satellite orbit does not pass through the zenith of the observer (inclined passages). We first consider the case when the observations are taken at the highest point above the horizon. Fig. 5 shows a section through the center of the Earth $O$, the point of observation $M$, and the satellite position $C$. Since the point $C$ is the highest one, the unit vector $\mathbf{j}_G$ and $\boldsymbol{\tau}$ will be directed along the line of intersection of the plane of the apparent orbit with the plane of the actual orbit of the satellite. In Fig. 5 the line of intersection of these planes is perpendicular to the plane of the drawing.

Let $z_0$ be the zenith distance of the highest point. Then, we can write on the basis of Fig. 5

$$\begin{aligned} \mathbf{j}_g &= \mathbf{n}\cos\psi + \mathbf{s}\sin\psi \\ \mathbf{j}_G &= \boldsymbol{\tau} \quad\ \sin\psi = (R/r)\sin z_0 \end{aligned} \qquad \ldots\ldots\ldots\ldots\ldots\ldots\ldots\ldots\ldots\ldots\ldots\ldots [32]$$

where $\psi$ is the angle between the plane of the apparent orbit and the plane of the actual orbit.

Relations [32 and 30] and Table 1 show that the equation in $g$ will contain the unknowns $\Delta i$, $\Delta\Omega$, $\Delta n$ and $\Delta e$, whereas the equation in $G$ will contain the unknowns $\Delta\omega_1$, $\Delta M_0$, $\Delta n$ and $\Delta e$.

We now consider the case when the observations are taken at points other than the highest one.

In Fig. 6, the plane passing through $\mathbf{r}$ and $\boldsymbol{\tau}$ is the plane of the actual orbit, and the plane passing through $\boldsymbol{\varrho}$ and $\boldsymbol{\tau}$ is the plane of the apparent orbit. Denoting, as earlier, the angle between these planes by $\psi$, we can write

$$\begin{aligned} \mathbf{j}_g &= \mathbf{n}\cos\psi + \mathbf{s}\sin\psi \\ \mathbf{j}_G &= \boldsymbol{\tau}\sin\gamma + \mathbf{s}\cos\gamma\cos\psi - \mathbf{n}\cos\gamma\sin\psi \end{aligned} \qquad \ldots\ldots\ldots\ldots\ldots\ldots\ldots\ldots\ldots\ldots\ldots\ldots [32']$$

where $\gamma$ is the angle between the velocity vector and the direction to the observer, measured at the satellite (for the highest point, $\gamma = 90$ deg).

Equations [32 and 30] and Table 1 show that the equation in $g$ will, as before, contain the four unknowns $\Delta i$, $\Delta\Omega$, $\Delta n$ and $\Delta e$, whereas the equation in $G$ will contain all six unknowns.

Thus, the observations obtained in the case of inclined passages, both near the highest point and away from it, allow us to determine $\Delta i$, $\Delta\Omega$, $\Delta n$ and $\Delta e$ from equations that are free of time errors and also free of errors resulting from the influence of the atmosphere on the motion of the satellite.

The unknowns should be determined separately with respect to $\Delta g$ and $\Delta G$, by successive approximations, similar to the procedure previously indicated for the case of zenith passages.

Other variants are also possible, but they can be formulated more specifically only after sufficient experience has been acquired in the application of this procedure and the reduction of the observational data. For the purpose of illustration, in Section 5 we give an example of improving the orbit elements by the method just developed.

## 4 Use of Artificial Satellites for Geodetic Purposes

Artificial Earth satellites can be used, in principle, to solve certain geodetic problems. It is known, for example, that geodetic measurements on Earth's surface are usually based

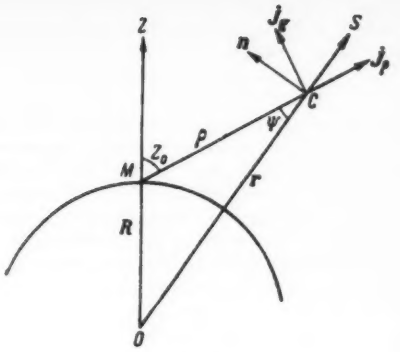


Fig. 5

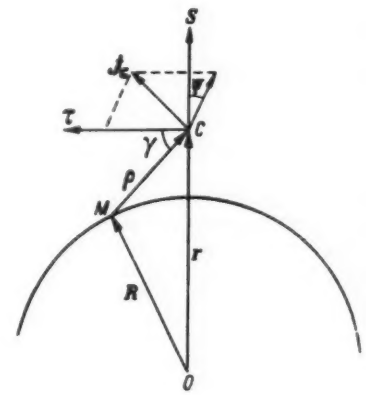


Fig. 6

on some reference ellipsoid which best fits a given section of the dry land. Individual reference ellipsoids are frequently not interrelated, particularly if they pertain to different continents. Therefore the mutual positions of the continents are not known with sufficient accuracy from independent triangulation networks. Our knowledge of the positions of the centers of the reference ellipsoids relative to the center of inertia of Earth is equally unreliable. The problem of interrelating individual reference ellipsoids and the determination of the position of the center of inertia of Earth are very important geodetic problems, and it is hoped that their solution will be substantially advanced through the use of artificial Earth satellites.

Let us consider first the problem of determining absolute coordinates of a point on Earth's surface, under the assumption that the origin is placed at the center of inertia of Earth and that the elements of the satellite orbit, referred to this system of coordinates, are known. Setting in Equation [2] $\Delta r = 0$, we obtain

$$\Delta\boldsymbol{\varrho} = -\Delta\mathbf{R} + \Delta\dot{\boldsymbol{\varrho}}t \qquad [33]$$

where $\Delta t$ is the error in the determination of the instant of observation.

We now resolve the resultant equation along the directions $\mathbf{j}_g$ and $\mathbf{j}_G$. Taking relations [8 and 12] into account, we obtain

$$\begin{aligned} \rho\Delta g &= -(\mathbf{j}_g\cdot\Delta\mathbf{R}) = -(1/\rho v)[(\eta\dot{\zeta} - \zeta\dot{\eta})\Delta X + \\ &\qquad (\zeta\dot{\xi} - \xi\dot{\zeta})\Delta Y\ (\xi\dot{\eta} - \eta\dot{\xi})\Delta Z] \\ \rho\Delta G - v\Delta t &= -(\mathbf{j}_G\cdot\Delta\mathbf{R}) = -(1/\rho v)[(\rho\dot{\xi} - \xi\dot{\rho})\Delta X + \\ &\qquad (\rho\dot{\eta} - \eta\dot{\rho})\Delta Y + (\rho\dot{\zeta} - \zeta\dot{\rho})\Delta Z] \end{aligned} \qquad \ldots\ldots\ldots\ldots\ldots\ldots\ldots\ldots\ldots\ldots\ldots\ldots [34]$$

where $\Delta X$, $\Delta Y$ and $\Delta Z$ are the corrections to the coordinates of the point on Earth's surface in the inertial system of coordinates. Owing to Earth's rotation, these corrections depend on time. It is therefore advantageous to use, instead of the coordinates $X$, $Y$ and $Z$, which are stationary in space, a rotating system of coordinates $X'$, $Y'$ and $Z'$, in which the $X'$ axis is constantly directed to the point of intersection of the Greenwich meridian with the Equator, the $Z'$ axis passes through the North Pole of Earth, and the $Y'$ axis is perpendicular to the other two and completes the right-handed system. The center of the new system of coordinates again coincides with Earth's center of inertia. The connection between the old and the new system of coordinates is given by the formulas

$$\begin{aligned} X &= X'\cos s_0 - Y' \sin s_0 \\ Y &= X' \sin s_0 + Y' \cos s_0 \\ Z &= Z' \end{aligned}$$

where $s_0$ is the sidereal time at Greenwich.

Denoting the corrections of the new coordinates by $\Delta X'$, $\Delta Y'$ and $\Delta Z'$, we can rewrite Equations [34] in the form

$$\begin{aligned} \Delta g &= -(1/\rho^2 v)\{[(\eta\dot{\zeta} - \zeta\dot{\eta}) \cos s_0 + (\zeta\dot{\xi} - \xi\dot{\zeta}) \sin s_0]\Delta X' + [-(\eta\dot{\zeta} - \zeta\dot{\eta}) \sin s_0 + (\zeta\dot{\xi} - \xi\dot{\zeta}) \cos s_0]\Delta Y' + [\xi\dot{\eta} - \eta\dot{\xi}]\Delta Z'\} \\ \Delta G &= -(1/\rho^2 v)\{[(\rho\dot{\xi} - \xi\dot{\rho}) \cos s_0 + (\rho\dot{\eta} - \eta\dot{\rho}) \sin s_0]\Delta X' + [-(\rho\dot{\xi} - \xi\dot{\rho}) \sin s_0 + (\rho\dot{\eta} - \eta\dot{\rho}) \cos s_0]\Delta Y' + \\ &\qquad [\rho\dot{\zeta} - \zeta\dot{\rho}]\Delta Z'\} + (v/\rho)\Delta t \end{aligned} \qquad [35]$$

The system of Equations [35] makes it possible, generally speaking, to determine the corrections $\Delta X'$, $\Delta Y'$ and $\Delta Z'$ of the coordinates of a point on Earth's surface separately, if there are not less than two observations and $\Delta t = 0$. To employ Equations [35], it is necessary to know precisely both the coordinates of the satellite and instants of observations. But it has already been noted in the foregoing that the instant of observation can be determined with only a limited accuracy. The error in time influences most strongly the quantity $\Delta G$ but hardly affects $\Delta g$. It is therefore more advantageous to determine the corrections $\Delta X'$, $\Delta Y'$ and $\Delta Z'$ not from the entire system [35], but only from the equations that contain $\Delta g$. This will exclude almost completely the influence of erroneous instants of observation on the corrections to the observer's coordinates. The minimum number of observations necessary to determine the corrections $\Delta X'$, $\Delta Y'$ and $\Delta Z'$ is three.

Let us perform a certain analysis of the conditions that favor the determination of particular corrections to the observer's coordinates. For this purpose it is advantageous to change over from corrections to the coordinates $X'$, $Y'$ and $Z'$ to corrections in a different system of rectangular coordinates, namely, to a system where the axes are directed along the radius vector of the point of observation, along the tangent to the diurnal parallel, and along the perpendicular to the first two axes. The corrections to the coordinates in this system will be respectively $\Delta R$, $R \cos \varphi' \Delta\lambda$ and $R\Delta\varphi'$, where $R$ is the magnitude of the geocentric radius vector of the point of observation, $\varphi'$ the geocentric latitude and $\lambda$ the longitude, which is positive in the eastern direction.

Then the first equation of [34], with allowance for relations [22], becomes

$$\begin{aligned} \rho^2 v\Delta g = &-[(\eta\dot{\zeta} - \zeta\dot{\eta}) \cos s \cos \varphi' + \\ &(\zeta\dot{\xi} - \xi\dot{\zeta}) \sin s \cos \varphi' + (\xi\dot{\eta} - \eta\dot{\xi}) \sin \varphi']\Delta R + \\ &[(\eta\dot{\zeta} - \zeta\dot{\eta}) \sin s - (\zeta\dot{\xi} - \xi\dot{\zeta}) \cos s]R \cos \varphi'\Delta\lambda + \\ &[(\eta\dot{\zeta} - \zeta\dot{\eta}) \cos s \sin \varphi' + (\zeta\dot{\xi} - \xi\dot{\zeta}) \sin s \sin \varphi' - \\ &(\xi\dot{\eta} - \eta\dot{\xi}) \cos \varphi']R\Delta\varphi' \end{aligned} \qquad [36]$$

where $s$ is the local sidereal time.

Introducing the unit vectors $\mathbf{j}_R$, $\mathbf{j}_\lambda$ and $\mathbf{j}_\varphi$, directed along the axes of the foregoing system of coordinates, we can rewrite Equation [36] in the following form

$$\begin{aligned} \rho^2 v\Delta g = -([\boldsymbol{\rho} \times \dot{\boldsymbol{\rho}}]\cdot\Delta\mathbf{R}) = &-\{([\boldsymbol{\rho} \times \dot{\boldsymbol{\rho}}]\cdot\mathbf{j}_R)\Delta R + ([\boldsymbol{\rho} \times \dot{\boldsymbol{\rho}}]\cdot\mathbf{j}_\lambda)R \\ &\cos \varphi'\Delta\lambda + ([\boldsymbol{\rho} \times \dot{\boldsymbol{\rho}}]\cdot\mathbf{j}_\varphi)R\Delta\varphi'\} \end{aligned} \qquad [37]$$

The coefficients of $\Delta R$, $R \cos \varphi\Delta\lambda$ and $R\Delta\varphi'$ in [37] involve cross products, and they reach a maximum when all three vectors are mutually perpendicular.

To determine the correction $\Delta R$ it is best to have its coefficient as large as possible; that is, the vector $\mathbf{j}_R$ should deviate as much as possible from the plane of the vectors $\boldsymbol{\rho}$ and $\dot{\boldsymbol{\rho}}$. It follows from this that to determine $\Delta R$ it is necessary to observe such passages of the satellites in which the highest point is located far away from the zenith, and the most suitable observations are those made near this highest point.

To determine the correction $R \cos \varphi'\Delta\lambda$ it is necessary to have a maximum value for the coefficient of $([\boldsymbol{\rho} \times \dot{\boldsymbol{\rho}}]\cdot\mathbf{j}_\lambda)$; this is obtained by observations at the zenith. The most suitable orbits are those passing through the poles or those with considerable inclinations to the plane of the Equator.

For the best determination of the correction $R\Delta\varphi'$ it is also convenient to make the observations in the zenith, and the inclination of the orbit to the plane of the Equator should equal the latitude of the point of observation.

Thus, the best conditions for the determination of all corrections are produced when there are two orbits, one passing through the poles of Earth, and the other with an inclination approximately equal to the latitude of the place of observation. It is possible, however, to make use of only one orbit, if the passages are observed on the ascending and descending loops, both in the zenith and away from it in the vicinity of the highest point. A combination of such data makes it possible to determine simultaneously the unknown quantities. The orbit used here should be so inclined to the plane of the Equator that the parallel at the latitude of the point of observation intersects the orbit at an angle close to 45 deg. This makes it possible to determine the corrections $R \cos \varphi'\Delta\lambda$ and $R\Delta\varphi'$ with approximately the same accuracy.

Formulas [34 and 35] have been derived under the assumption that the elements of the orbits are known accurately. In practice, apparently, one cannot make such an assumption. Therefore the inaccurate elements must be improved simultaneously with the coordinates of the points of observation. The equations of condition are then written in the form of [14], to the right-hand sides of which are added the right-hand sides of Equations [36].

We now turn to the case when the coordinates of the points of observation relative to the center of the reference ellipsoid are known, and the position of the center of the reference ellipsoid relative to the center of inertia of Earth is unknown. For simplicity we assume that the coordinates of the satellite relative to Earth's center of inertia are known.

This case is analogous to the preceding one, with the only difference that now the corrections to the coordinates for all the observation stations will be the same. Equations of condition for the unknown corrections $\Delta X'$, $\Delta Y'$ and $\Delta Z'$, arising from the fact that the center of the reference ellipsoid does not coincide with Earth's center of inertia, will have the form of [35]. As in the preceding case, it is advantageous to determine these corrections from equations that are free of time errors. It is desirable here that the observation points be more or less uniformly distributed over Earth's surface. As to the inclination of the orbit, its best value is close to the extreme values 0 and 90 deg.

In real cases, the position of the satellite with respect to Earth's center of inertia must be considered unknown, and therefore the corrections to the elements of its orbit must be obtained simultaneously with the corrections to the coordinates of the center of inertia. The equations of condition will have the form [14], to the right-hand side of which are added the right-hand sides of [35].

We note that this procedure for determining the corrections to the coordinates of the point on Earth's surface and of

Table 2 Epoch and equinox Nov. 20, 1957, 17 hr, 58 min, 30.700 sec, universal time

| | O | C | O—C |
|---|---|---|---|
| $a$ . . . | 7564.4654 | 7569.5500 | —5.0846 |
| $e$ . . . | 0.07967130 | 0.07937080 | 0.00030050 |
| $i$ . . . | 65°36233 | 65°50000 | —0°13767 |
| $\Omega$ . . . | 272°56135 | 272°46778 | 0°09357 |
| $\omega$ . . . | 23°59441 | 23°83472 | —0°24031 |
| $M_0$ . . . | 355°16533 | 354°82000 | 0°34533 |
| $n$ . . . | 197°49991 | 197°30096 | 0°19895 |

Note: All numbers given are expressed in km.

Earth's center of inertia makes it possible to exclude not only the influence of inaccuracies in the determination of the time, but also, to a certain extent, the irregular influences of the atmosphere, which cannot be taken into consideration theoretically or empirically. This leads to a possibility of using relatively low satellites for geodetic purposes, the motion of which is subject to the perturbing influence of atmosphreic drag.

If it is assumed that along with the elements of the satellite's orbit one also knows accurately the instants of observation, that is, $\Delta t = 0$, then the corrections to the coordinates of the observation points can be determined from the equations of condition [35], which contain $\Delta G$. An analysis of these equations shows that the correction $\Delta R$ is determined from them in the best manner only when the observations are carried out at a sufficient distance from the highest point. In addition in this case the apparent orbit of the satellite should pass through the zenith. To determine the correction $R \cos \varphi' \Delta\lambda$, the most suitable orbits are those with inclinations equal to the local latitude. The correction $R\Delta\varphi'$ is best determined with polar orbits. In the two last cases, the most accurate results are obtained from observations near the zenith.

## 5 Example of Improving Elements by Using Equations of Condition Independent of Time Errors

To verify the procedure developed here for improving the elements of satellite orbits, we have chosen a fictitious example which illustrates the procedure clearly and can be used to verify various other modifications of the method. It is therefore advisable to describe it in detail.

The first step is to obtain fictitious observations of the satellite. For this purpose we took a system of elements of a certain fictitious orbit, close to the orbits of the first Soviet satellites. This system is listed in the second column of Table 2 (the O system). Earth is assumed strictly spherical, and its radius is taken to be $R = 6378.3880$ km.

The product of Earth's mass and the gravitational constant is taken to be $fm = 1.6883740 \cdot 10^6$ km$^3$/hr$^2$.

The mean motion of the satellite per hour, obtained with this value of $fm$, is given in the last line of Table 2.

Using the elements listed in the second column of Table 2 and formulas [18–21], we calculated 19 positions of the satellite in the orbit, so as to cover more or less uniformly one loop of the orbit. We then calculated the right ascensions and declinations of the subsatellite points. The number of observation points was also taken to be 19, and the latitude and the local sidereal time at the instant of observation at each station were chosen arbitrarily, subject only to the condition that the deviations of the positions of the stations from the corresponding points under the satellite did not exceed approximately 10 or 15 deg in either coordinate. Then Equations [22] give the rectangular coordinates of the stations, and Equations [23] give the apparent positions of the satellite for each observation.

Since it was desirable to verify the suitability of the procedure for observations containing time errors, five instants of the 19 were changed in magnitude by 5 to 23 sec, and these modified instants were used as observations. Thus, there were considerable time errors in five out of 19 instants.

Table 3 lists the rectangular coordinates of the satellite, the rectangular coordinates of the observation stations and the apparent coordinates $\alpha_0$ and $\delta_0$ of the satellite calculated for the 19 instants $t_i$ from elements (O). The last column of Table 3 lists the corrections $\Delta t_i$ which must be added to the times $t_i$ in order to obtain the observed instant of time containing a time error. The coordinates $\alpha_0$ and $\delta_0$ as well as the instant $t_i$, with the corrections $\Delta t_i$ added, comprise the satellite observations which should be used to improve the initial system of preliminary elements.

As the initial system of elements, subject to improvement, we chose the system listed in the third column of Table 2 (system C). The differences between the elements of the systems that comprise the observations (O), and the preliminary system that is subject to improvement (C), is listed in the last column of Table 2.

Using the (C) system for the instant $t_i + \Delta t_i$, we calculated the coordinates $\alpha_c$ and $\delta_c$, needed for the formation of the dif-

Table 3 Observed values of coordinates and time for Nov. 20, 1957

| № | $t_i$ | $x$ | $y$ | $z$ | $X$ | $Y$ | $Z$ | $\alpha_0$ | $\delta_0$ | $\Delta t_i$ |
|---|---|---|---|---|---|---|---|---|---|---|
| 1 | 17$^h$58$^m$30$^s$.700 | +1187.892 | −6580.478 | +1946.291 | + 528.094 | −6004.050 | +2087.181 | 318°85814 | − 9°13550 | — |
| 2 | 18 02 23.500 | +1839.012 | −5772.628 | +3443.290 | +1046.160 | −5700.414 | +2663.579 | 354.79579 | +44.40291 | + 5.000 |
| 3 | 18 07 29.500 | +2513.018 | −4168.139 | +5067.766 | +1745.060 | −3471.948 | +5058.081 | 317.80618 | + 0.53533 | — |
| 4 | 18 13 44.100 | +2972.242 | −1623.626 | +6315.997 | + 936.351 | −1710.087 | +6073.112 | 2.43180 | + 6.79725 | — |
| 5 | 18 20 56.800 | +2952.328 | +1596.196 | +6586.359 | +2634.672 | +1841.417 | +5509.222 | 322.33290 | +69.56669 | +17.000 |
| 6 | 18 24 07.300 | +2766.807 | +2956.493 | +6314.803 | +2945.662 | +3117.536 | +4721.004 | 222.00022 | +81.41290 | — |
| 7 | 18 29 49.400 | +2205.835 | +5122.817 | +5303.969 | +2033.733 | +3601.855 | +4855.348 | 83.54425 | +16.33525 | + 9.000 |
| 8 | 18 35 01.700 | +1496.024 | +6653.853 | +3907.025 | + 274.622 | +5595.419 | +3049.542 | 40.91132 | +27.94840 | — |
| 9 | 18 42 36.200 | + 268.678 | +7926.156 | +1357.567 | + 220.993 | +6020.867 | +2093.838 | 88.56632 | −21.12226 | — |
| 10 | 18 46 00.900 | − 310.433 | +8097.377 | + 112.819 | − 777.369 | +6316.135 | + 431.245 | 75.31096 | − 9.81076 | — |
| 11 | 18 52 22.300 | −1355.573 | +7743.472 | −2198.213 | −1180.305 | +6244.798 | − 541.487 | 96.67037 | −47.67383 | −23.000 |
| 12 | 18 59 43.700 | −2369.962 | +6329.953 | −4545.510 | −1602.120 | +4128.327 | −4590.638 | 109.22676 | + 1.10878 | — |
| 13 | 19 02 13.800 | −2646.509 | +5630.559 | −5216 041 | −2853.570 | +3954.719 | −4111.105 | 82.95643 | −33.19900 | — |
| 14 | 19 05 51.000 | −2967.245 | +4455.352 | −6029.189 | −1965.951 | +2685.120 | −5441.416 | 119.49375 | −16.11948 | +10.000 |
| 15 | 19 12 01.400 | −3264.173 | +2109.213 | −6904.572 | −2289.405 | +1891.952 | −5644.730 | 167.43502 | −51.59585 | — |
| 16 | 19 15 32.500 | −3276.645 | + 653.694 | −7073.566 | −3160.366 | +1094.988 | −5431.107 | 255.23835 | −74.47200 | - |
| 17 | 19 25 17.000 | −2680.703 | −3325.811 | −6163.236 | −2136.904 | −3134.031 | −5127.896 | 199.42607 | −60.88465 | - |
| 18 | 19 30 07.600 | −2057.528 | −4987.142 | −4967.702 | −2111.742 | −5043.945 | −3283.747 | 46.33594 | −87.33013 | - |
| 19 | 19 37 11.600 | − 853.918 | −6614.989 | −2504.590 | + 38.670 | −5991.017 | −2188.618 | 214.95583 | −16.17916 | — |

Table 4 Coordinates and components of satellite velocity for Nov. 20, 1957

| № | $t_i + \Delta t_i$ | $x$ | $y$ | $z$ | $\dot{x}$ | $\dot{y}$ | $\dot{z}$ | $\alpha_c$ | $\delta_c$ |
|---|---|---|---|---|---|---|---|---|---|
| 1 | 17h58m30s700 | +1166.188 | −6595.889 | +1933.404 | +10725.512 | + 9278.281 | +24389.799 | 317°15375 | −10°02031 |
| 2 | 18 02 28.500 | +1828.434 | −5772.376 | +3463.030 | + 9215.284 | +15516.243 | +21668.347 | 354.70244 | +45.57583 |
| 3 | 18 07 29.500 | +2490.103 | −4196.335 | +5062.491 | + 6484.386 | +21827.962 | +16277.829 | 315.80536 | + 0.24316 |
| 4 | 18 13 44.100 | +2953.902 | −1657.466 | +6319.137 | + 2354.250 | +26291.466 | + 7645.194 | 1.49403 | + 6.95012 |
| 5 | 18 21 13.800 | +2931.251 | +1686.167 | +6585.390 | − 2630.835 | +26312.483 | − 3281.449 | 332.05897 | +72.54911 |
| 6 | 18 24 07.300 | +2762.579 | +2923.769 | +6332.549 | − 4340.443 | +24931.073 | − 7159.882 | 226.62395 | +80.60721 |
| 7 | 18 29 58.400 | +2192.683 | +5146.948 | +5293.232 | − 7200.318 | +20296.995 | −13867.316 | 84.03453 | +15.75436 |
| 8 | 18 35 01.700 | +1508.610 | +6634.913 | +3934.149 | − 8916.223 | +14852.176 | −18143.473 | 40.11031 | +28.73412 |
| 9 | 18 42 36.200 | + 290.740 | +7921.103 | +1385.776 | −10100.469 | + 5357.588 | −21636.715 | 87.89794 | −20.42362 |
| 10 | 18 46 00.900 | − 285.159 | +8099.049 | + 140.066 | −10102.608 | + 901.105 | −22062.458 | 74.56674 | − 8.94650 |
| 11 | 18 52 01.300 | −1266.934 | +7802.429 | −2040.271 | − 9357.336 | − 6752.192 | −21151.720 | 93.57175 | −43.87757 |
| 12 | 18 59 43.700 | −2340.494 | +6357.777 | −4530.293 | − 7139.147 | −15456.315 | −17111.243 | 108.32441 | + 1.47147 |
| 13 | 19 02 13.800 | −2617.982 | +5662.526 | −5204.307 | − 6151.234 | −17850.770 | −15171.701 | 82.14575 | −32.37942 |
| 14 | 19 06 01.000 | −2953.528 | +4434.676 | −6055.923 | − 4442.051 | −20946.286 | −11717.190 | 119.37482 | −17.00502 |
| 15 | 19 12 01.400 | −3244.767 | +2153.382 | −6909.936 | − 1300.967 | −24273.867 | − 5145.491 | 164.69595 | −51.94383 |
| 16 | 19 15 32.500 | −3262.571 | + 700.026 | −7086.282 | + 708.193 | −25152.023 | − 823.848 | 255.49172 | −76.15355 |
| 17 | 19 25 17.000 | −2685.837 | −3282.891 | −6198.239 | + 6335.694 | −22624.279 | +11751.953 | 195.17260 | −62.01471 |
| 18 | 19 30 07.600 | −2073.452 | −4952.487 | −5013.475 | + 8760.341 | −18413.281 | +17465.277 | 67.28279 | −86.71960 |
| 19 | 19 37 11.600 | − 884.334 | −6601.216 | −2562.390 | +11149.184 | − 9007.921 | +23590.887 | 213.47003 | −18.66499 |

ferences $\alpha_0 - \alpha_c$ and $\delta_0 - \delta_c$, which enter into the right-hand sides of the equations of condition. Tables 4 and 5 contain the rectangular coordinates and components of the satellite velocity necessary for the calculation of the coefficients of the equations of condition; these coefficients were calculated from the elements (C). They also contain the coordinates and the velocity components of the observation stations at the instant $t_i + \Delta t_i$, but the observer velocity along the $Z$ axis is not given, since it is always equal to zero. The last two columns of Table 4 list also the coordinates $\alpha_c$ and $\delta_c$.

Tables 6 and 7 contain all the coefficients and the right-hand sides of the equations of condition both in terms of $g$ and in terms of $G$.

According to the conclusions derived in Section 3 in the analysis of the equations of condition, the equation of condition free of time errors makes it possible to determine more or less reliably four corrections, namely $\Delta i$, $\Delta\Omega$, $\Delta n$, $\Delta e$; the other two corrections, $\Delta\omega$ and $\Delta M_0$ will be determined much less accurately, since their coefficients in the equation of condition are small. We therefore put $\Delta\omega = 0$ and $\Delta M_0 = 0$ in the equations of condition for $\Delta g$. The normal system for $\Delta g$ then assumes the following form

| $\Delta i$ | $\Delta\Omega$ | $\Delta n$ | $\Delta e$ | $\Delta g$ |
|---|---|---|---|---|
| 202.80956 | −2.09144 | −4.55610 | −37.36308 | −31.11462 |
| | 151.83729 | 12.51195 | 61.09388 | 18.76082 |
| | | 4.27331 | 15.16709 | 3.06410 |
| | | | 98.82677 | 16.08684 |

Solving this normal system we obtain the following corrections

$$\Delta i = -0°.14500 \qquad \Delta n = +0°.23662$$
$$\Delta\Omega = +0°.09748 \qquad \Delta e = +0.0001986$$
$$\ldots\ldots\ldots\ldots\ldots\ldots\ldots\ldots\ldots\ldots\ldots\ldots\ldots\ldots\ldots\ldots\ldots\ldots [38]$$

We now substitute [38] in the equations of condition for $\Delta G$ and obtain the corresponding normal system for the determination of the unknown $\Delta\omega$ and $\Delta M_0$. We get

| $\Delta\omega$ | $\Delta M_0$ | $\Delta G - \Sigma$ |
|---|---|---|
| 415.6895 | 427.4171 | −1.762498 |
| | 445.2800 | −1.283101 |

Table 5 Coordinates and components of observer velocity for Nov. 20, 1957

| № | $t_i + \Delta t_i$ | $X$ | $Y$ | $Z$ | $\dot{X}$ | $\dot{Y}$ |
|---|---|---|---|---|---|---|
| 1 | 17h58m30s700 | + 528.094 | −6004.050 | +2087.181 | +1576.160 | +138.633 |
| 2 | 18 02 28.500 | +1048.239 | −5700.033 | +2663.579 | +1496.351 | +275.180 |
| 3 | 18 07 29.500 | +1745.060 | −3471.948 | +5058.081 | + 911.442 | +458.106 |
| 4 | 18 13 44.100 | + 936.351 | −1710.087 | +6073.112 | + 448.925 | +245.807 |
| 5 | 18 21 13.800 | +2632.386 | +1844.682 | +5509.222 | − 484.259 | +691.044 |
| 6 | 18 24 07.300 | +2945.662 | +3117.536 | +4721.004 | − 818.404 | +773.284 |
| 7 | 18 29 58.400 | +2031.368 | +3603.189 | +4855.348 | − 945.895 | +533.267 |
| 8 | 18 35 01.700 | + 274.622 | +5595.419 | +3049.542 | −1468.888 | + 72.093 |
| 9 | 18 42 36.200 | + 220.993 | +6020.867 | +2093.838 | −1580.575 | + 58.014 |
| 10 | 18 46 00.900 | − 777.369 | +6316.135 | + 431.245 | −1658.088 | −204.072 |
| 11 | 18 52 01.300 | −1169.830 | +6246.769 | − 541.487 | −1639.878 | −307.099 |
| 12 | 18 59 43.700 | −1602.120 | +4128.327 | −4590.638 | −1083.753 | −420.582 |
| 13 | 19 02 13.800 | −2853.570 | +3954.719 | −4111.105 | −1038.178 | −749.108 |
| 14 | 19 06 01.000 | −1967.909 | +2683.684 | −5441.416 | − 704.511 | −516.608 |
| 15 | 19 12 01.400 | −2289.405 | +1891.952 | −5644.730 | − 496.668 | −601.006 |
| 16 | 19 15 32.500 | −3160.366 | +1094.988 | −5431.107 | − 287.452 | −829.647 |
| 17 | 19 25 17.000 | −2136.904 | −3134.031 | −5127.896 | + 822.734 | −560.972 |
| 18 | 19 30 07.600 | −2111.742 | −5043.945 | −3283.747 | +1324.117 | −554.366 |
| 19 | 19 37 11.600 | + 38.670 | −5991.017 | −2188.618 | +1572.739 | + 10.152 |

Table 6 Tentative equations in g

| № | $\Delta i$ | $\Delta\Omega$ | $\Delta\omega$ | $\Delta M_0$ | $\Delta n$ | $\Delta e$ | $\Delta g$ |
|---|---|---|---|---|---|---|---|
| 1 | +1°.708171 | −4°.949448 | −0°.221485 | −0°.311155 | −1°.073770 | −5°.938921 | −1°.064975 |
| 2 | +2.868870 | −4.126900 | −0.281976 | −0.284837 | −0.663833 | −3.663327 | −1.010572 |
| 3 | +3.997286 | −2.939709 | −0.310058 | −0.174736 | −0.895557 | −4.557890 | −1.073062 |
| 4 | +1.730268 | −0.485239 | −0.195230 | −0.016588 | −0.591606 | −2.298758 | −0.398281 |
| 5 | +6.329346 | +1.318126 | +0.187858 | +0.111772 | +0.246345 | +0.591446 | −0.917426 |
| 6 | +3.570418 | +1.437516 | +0.311858 | +0.116850 | +0.531234 | +0.711453 | −0.251158 |
| 7 | +3.604797 | +2.913583 | +0.161868 | +0.155134 | +0.083238 | +0.304901 | −0.192414 |
| 8 | +2.088047 | +2.905154 | +0.049479 | +0.171963 | −0.274437 | +1.103220 | −0.004071 |
| 9 | +0.732151 | +3.535726 | +0.191038 | +0.204881 | −0.014341 | +0.870378 | +0.267243 |
| 10 | +0.077243 | +3.782594 | +0.197887 | +0.218055 | −0.111614 | +1.405307 | +0.375010 |
| 11 | −0.994756 | +3.259652 | +0.218465 | +0.197803 | −0.025456 | +1.015647 | +0.459739 |
| 12 | −2.031627 | +2.446508 | +0.121595 | +0.121853 | +0.313892 | −0.939313 | +0.573181 |
| 13 | −2.579133 | +2.446045 | +0.188849 | +0.122569 | −0.168542 | +1.212236 | +0.573621 |
| 14 | −3.022002 | +1.904076 | +0.050206 | +0.089236 | +0.322711 | −0.967635 | +0.655776 |
| 15 | −4.621400 | +1.279521 | +0.025884 | +0.083034 | +0.301579 | −0.679921 | +0.856327 |
| 16 | −4.282242 | +0.491922 | +0.172843 | +0.054904 | −0.237472 | +0.473083 | +0.569517 |
| 17 | −5.604808 | −2.455347 | −0.207731 | −0.178175 | −0.180067 | +0.425965 | −0.572571 |
| 18 | −2.618674 | −2.091268 | +0.024343 | −0.162370 | −0.713584 | −0.795598 | −0.207939 |
| 19 | −1.765340 | −3.922852 | −0.439576 | −0.237089 | +0.411256 | +3.654954 | +0.052670 |

From this we obtain the following values of the missing corrections

$$\Delta M_0 = +0°.09116 \qquad \Delta\omega = -0°.09797 \qquad [39]$$

Comparing the corrections [38 and 39] with the differences of the elements as given in the column (O—C) of Table 2, we see that [38] is quite close to the corresponding differences (O—C), whereas [39] differs much more from the corrections corresponding to (O—C).

This situation is quite natural, since the time error does not influence the corrections in [38], whereas the corrections $\Delta\omega$ and $\Delta M_0$, determined from the equations for $\Delta G$, depend to a considerable extent on the time errors contained in individual observations (Table 3).

We note here that there is a possibility, at least in principle, of determining the corrections to the instants of observation simultaneously with determining the corrections to the elements. In this case the equations of condition for $\Delta g$ can be used to determine the corrections to the elements, while the equations for $\Delta G$ can be used to determine the corrections for the instants of observation. This procedure is, however, hardly realistic, since the observed positions of the satellite and the coordinates of the observation stations must in this case be known with an accuracy that considerably exceeds the

Table 7 Tentative equations in G

| № | $\Delta i$ | $\Delta\Omega$ | $\Delta\omega$ | $\Delta M_0$ | $\Delta n$ | $\Delta e$ | $\Delta G$ |
|---|---|---|---|---|---|---|---|
| 1 | −0°.105587 | +3°.556741 | +7°.852742 | +9°.222153 | −0°.128490 | −2°.459677 | +1°.574944 |
| 2 | +1.425220 | −0.241181 | +4.222212 | +4.904265 | +1.052943 | +5.449785 | −0.599110 |
| 3 | −1.252964 | +3.450780 | +6.196438 | +7.249114 | +0.657246 | +4.061048 | +1.713716 |
| 4 | +0.429623 | +1.350275 | +3.498146 | +3.884549 | +0.992583 | +5.689652 | +0.855475 |
| 5 | +0.195167 | +2.582480 | +6.135230 | +6.579331 | +2.042008 | +11.709248 | −4.425251 |
| 6 | +0.759196 | +1.999449 | +4.150727 | +4.355913 | +1.513179 | +8.300620 | +1.030864 |
| 7 | −0.108328 | +1.606210 | +4.079519 | +3.742857 | +2.442439 | +7.038610 | −0.722337 |
| 8 | −0.358222 | +1.188375 | +4.059046 | +3.827744 | +2.105018 | +7.324991 | +1.057589 |
| 9 | +0.042617 | +1.661009 | +3.519737 | +3.027495 | +2.575808 | +2.504174 | +0.897437 |
| 10 | −0.002598 | +1.667782 | +4.321895 | +3.751188 | +3.009293 | +3.361319 | +1.069626 |
| 11 | −0.066507 | +1.634087 | +3.429548 | +2.923408 | +2.909151 | −0.521797 | +4.307384 |
| 12 | −0.248165 | +1.523733 | +2.968579 | +2.521817 | +2.234451 | +0.204986 | +0.785639 |
| 13 | +0.425980 | +1.189735 | +3.811974 | +3.273110 | +3.288107 | −1.792501 | +0.896015 |
| 14 | −0.392867 | +1.664883 | +3.424353 | +2.940497 | +2.985280 | −2.174060 | −0.605964 |
| 15 | +0.120129 | +2.004387 | +4.912954 | +4.487114 | +5.587337 | −7.599263 | +1.510948 |
| 16 | −0.362971 | +1.835872 | +4.341164 | +4.138984 | +5.596460 | −8.122773 | +1.583625 |
| 17 | −0.296047 | +2.303555 | +5.856612 | +5.769858 | +7.957620 | −11.832230 | +2.287462 |
| 18 | +0.153681 | +2.286825 | +3.282067 | +3.301979 | +4.616010 | −7.057272 | +1.132059 |
| 19 | −0.748592 | +0.745793 | +5.623387 | +6.217398 | +9.944277 | −9.561718 | +2.865796 |

accuracy that is attainable at the present time.

The authors consider it their duty to express deep gratitude to the staff members of the Institute of Theoretical Astronomy of the USSR Academy of Sciences, R. P. Ermenko and O. A. Sizova, for taking the trouble to calculate the examples given here.

## Bibliography

Dubyago, A. D., "Opredelenie Orbit" (Determination of Orbits), M-L, 1949.

Kulikov, D. K., "Numerical Methods of Celestial Mechanics as Applied to the Study of the Motion of Jupiter's 8th Satellite," *Bull. Inst. Theoret. Astronomy*, vol. 4, no. 7, 1960.

Samoilova-Yakhontova, N. S., 1941, "Correction of Elliptic Orbits," *Bull. Inst. Theoret. Astronomy*, vol. 3, 1953.

Samoilova-Yakhontova, N. S., 1949, "On the Question of Improving the Elements of Elliptic Orbits," *Bull. Inst. Theoret. Astronomy*, vol. 4, no. 6, 1959.

Subbotin, M. F., "Kurs Nebesnoi Mekhaniki" (Course of Celestial Mechanics), vol. 1, M-L, 1941.

Bauschinger, J., "Die 'Bahnbestimmung der Himmelskorper," Leipzig, 1906.

Eckert, W. and Brouwer, D., "The Use of Rectangular Coordinates in the Differential Correction of Orbits," *Astron. J.*, vol. 46, 1937.

Oppolzer, T., "Lehrbuch zur Bahnbestimmung der Kometen und Planeten," vol. 2, Leipzig, 1880.

*—Original received June 27, 1959*

---

## Reviewer's Comment

The problem treated in the two preceding articles is that of determining the preliminary and improved orbits of an artificial Earth satellite from data taken at times which are imperfectly known.

The need for a data processing scheme which utilizes measurements of time which are in error is discussed very clearly by the authors in the introduction to each paper. Methods developed in these translations may be of considerable interest to those concerned with problems of orbital mechanics, since, to the best knowledge of this reviewer, no comparable treatment has appeared in the open literature of this country.

It must be pointed out that the problem is formulated from the astronomical point of view. Thus the data consists only of the angular directions of the object as seen by the observer at different times. Techniques employed in obtaining a preliminary orbit from observational data of this kind are, as a rule, modifications of methods originally developed by Laplace and Gauss. Description of these techniques are scattered throughout the astronomical literature which is neither readily available nor too well-known to most people presently engaged in orbit computation. Basic principles as well as detailed treatment of certain fundamental methods can be found in (1–4).

The exposition in the papers presented here follows closely methods of Laplace and Gauss. Perhaps the most significant difference between standard methods and that of Batrakov and Kulikov is the fact that instants of time which are known to be in error are treated as unknown quantities of the problem. Unfortunately time enters the solution through some well-known series expansions (1 and 2). Difficulties and limitations arising from this fact are considered by Batrakov in the first paper.

Improvement of the orbit proceeds according to principles well-known to most astronomers. For an excellent basic description of these the reader is referred to (2). In the case of satellites, however, certain modifications must be introduced. These arise from the high angular rates of satellites with respect to the observing station as well as from the existence of certain perturbations which are not tractable theoretically at present. These modifications are discussed in the second paper.

Finally it is worthwhile to call the readers' attention to detailed numerical examples accompanying both papers. These are extremely helpful in mastering the techniques presented in these papers. The attractive feature of the presentation is that all working formulas as well as steps involved in actual computation are collected in one place.

—Igor Jurkevich
Space Sciences Laboratory
General Electric Co.

1 Moulton, F. R., "An Introduction to Celestial Mechanics," Macmillan Co., N. Y., 1914.

2 Herget, P., "The Computation of Orbits," published privately by the author, 1948.

3 Crawford, R. C., "Determination of Orbits of Comets and Asteroids," McGraw-Hill Book Co., Inc., N. Y., 1930.

4 Williams, K. P., "The Calculation of the Orbits of Asteroids and Comets," The Principia Press, Inc., Bloomington, Ind., 1934.

# Dependence of the Internal Energy of Air on the Pressure and Density at High Temperatures

S. S. KVASHNINA

THE CONNECTION between the internal energy of a medium, the pressure and the density is called the caloric equation of state, $\epsilon = \epsilon(p, \rho)$. In the case of an ideal gas, the internal energy depends on one parameter $z = p/\rho$, and the caloric equation has the form

$$\epsilon = \frac{z}{\gamma - 1} \quad \left(\gamma = \frac{c_p}{c_v}\right)$$

At high temperatures, on the order of several thousands and tens of thousands of degrees, dissociation and ionization greatly affect the thermodynamic properties of air (1).[1] In this case the internal energy is determined by two parameters, pressure and density.

The thermodynamic functions of air at temperatures from 6000 to 20,000 K and pressures from 0.001 to 9000 atm have been calculated and tabulated (2,3). But to solve different gasdynamic problems it is more convenient to use analytic relations than tabular data. Such relations can be obtained by approximating the tables.

The results of approximation of the dependence $\epsilon = \epsilon(p, \rho)$, based on the tables of (3) in the temperature interval from 12,000 to 20,000 K and pressures from 1 to 1000 atm are given in the present article. The figure shows the dependence $\epsilon(z)$ for different pressures $p$ (all the quantities are referred to values of the corresponding parameters at $p = 1$ atm, $T = 12{,}000$ K). For comparison we give here the linear variation of $\epsilon(z)$ for an ideal gas with $\gamma = 1.4$ (dotted line). The curves obtained can be approximated by straight lines of different slopes with different intercept on the $\epsilon$ axis. The deviations from the straight line at the ends of the segments can be taken into account by additional terms in the form of $\exp az$. The following general formula can be proposed for the approximation

$$\epsilon = a_1 z + a_2 + a_3 \exp a_4 z + a_5 \exp a_6 z$$

$$(a_i = a_{i1}p^2 + a_{i2}p + a_{i3}) \qquad (i = , \ldots , 16)$$

If $p$ is in atmospheres, $\rho$ in gm/cm³, $\epsilon$ in cal/gm, then the values of $a_{ik}$ $(k = 1, 2, 3)$ are as follows

$$1 \leqslant p \leqslant 10 \qquad 6.993 \leqslant z \cdot 10^{-4} \leqslant 21.88$$

$$a_{11} = 0.2182 \cdot 10^{-3} \qquad a_{12} = -0.5633 \cdot 10^{-2} \qquad a_{13} = 0.2152$$
$$a_{21} = 0.7602 \cdot 10 \qquad a_{22} = 0.2292 \cdot 10^{2} \qquad a_{23} = -0.2821 \cdot 10^{4}$$
$$a_{31} = a_{32} = a_{33} = a_{41} = a_{42} = a_{43} = 0$$
$$a_{51} = -0.2269 \qquad a_{52} = 0.3364 \cdot 10 \qquad a_{53} = -0.1104 \cdot 10^{2}$$
$$a_{61} = -0.7711 \cdot 10^{-7} \qquad a_{62} = 0.2935 \cdot 10^{-5} \qquad a_{63} = 0.2672 \cdot 10^{-4}$$

$$10 < p < 60, \qquad 6.727 \leqslant z \cdot 10^{-4} \leqslant 19.14$$

$$a_{11} = 0 \qquad a_{12} = -0.6420 \cdot 10^{-3} \qquad a_{13} = 0.1884$$
$$a_{21} = 0 \qquad a_{22} = 0.3334 \cdot 10^{2} \qquad a_{23} = -0.2551 \cdot 10^{4}$$
$$a_{31} = 0 \qquad a_{32} = -0.3927 \qquad a_{33} = +0.9912 \cdot 10^{3}$$
$$a_{41} = 0 \qquad a_{42} = 0.3600 \cdot 10^{-7} \qquad a_{43} = -0.1230 \cdot 10^{-4}$$
$$a_{51} = 0 \qquad a_{52} = 0.1272 \cdot 10^{-2} \qquad a_{53} = -0.3816 \cdot 10^{-1}$$
$$a_{61} = 0 \qquad a_{62} = 0.3403 \cdot 10^{-5} \qquad a_{63} = 0.6408 \cdot 10^{-5}$$

$$60 \leqslant p \leqslant 300, \qquad 6.253 \leqslant z \cdot 10^{-4} \leqslant 15.67$$

$$a_{11} = 0.2643 \cdot 10^{-6} \qquad a_{12} = -0.1712 \cdot 10^{-3} \qquad a_{13} = 0.1735$$
$$a_{21} = -0.7191 \cdot 10^{-2} \qquad a_{22} = 0.6616 \cdot 10 \qquad a_{23} = -0.2069 \cdot 10^{4}$$
$$a_{31} = 0.1118 \cdot 10^{2} \qquad a_{32} = 0.2039 \cdot 10^{4} \qquad a_{33} = -0.5660 \cdot 10^{5}$$
$$a_{41} = 0.6698 \cdot 10^{-9} \qquad a_{42} = -0.4546 \cdot 10^{-6} \qquad a_{43} = -0.4496 \cdot 10^{-4}$$
$$a_{51} = a_{52} = a_{53} = a_{61} = a_{62} = a_{63} = 0$$

$$300 < p \leqslant 1000 \qquad 5.637 \leqslant z \cdot 10^{-4} \leqslant 13.46$$
$$a_{11} = 0 \qquad a_{12} = 0.6464 \cdot 10^{-5} \qquad a_{13} = 0.1249$$
$$a_{21} = 0 \qquad a_{22} = -0.1380 \cdot 10 \qquad a_{23} = 0.1589 \cdot 10^{4}$$
$$a_{31} = a_{32} = a_{33} = a_{41} = a_{42} = a_{43} = a_{51} = a_{52} = a_{53} = a_{61} = a_{62} = a_{63} = 0$$

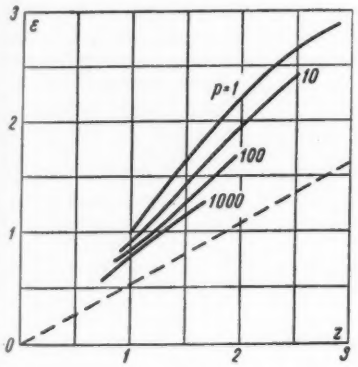


The possible relative error in using the data of the approximate equations does not exceed 4 per cent.

Translated from *Izvestiia Akademii Nauk SSSR, Otdelenie Tekhnicheskikh Nauk, Mekhanika i Mashinostroenie* (Bull. USSR Acad. Sci., Div. Tech. Sci., Mechanics and Machine Building), no. 1, 1960, pp. 178–179. Translated by J. George Adashko.

[1] Numbers in parentheses indicate References at end of paper.

## References

1 Stupochenko, E. V., Stakhanov, I. P., Samuilov, E. V., Pleshanov, A. S. and Rozhdestvenskii, I. B., "Thermodynamic Properties of Air in the

Temperature Interval From 1000 to 12,000° K and in the Pressure Interval 0.001 to 1000 Atm," "Fizicheskaya Gazodinamika" (Physical Gasdynamics), USSR Acad. Sci., 1959. Translation in ARS JOURNAL, vol. 30, no. 1, Jan. 1960, pp. 98–112.

2 Predvoditelev, A. S., Stupochenko, E. V., Samuilov, E. V., Stakhanov, I. P., Pleshanov, A. S. and Rozhdestvenskii, I. B., "Tables of Thermodynamic Functions of Air for Temperatures from 6000 to 12,000°K and Pressures from 0.001 to 1000 Atm," USSR Acad Sci. Press, 1957.

3 Predvoditelev, A. S., et al., "Tables of Thermodynamic Functions of Air for Temperatures from 12,000 to 20,000°K and Pressures from 0.001 to 1000 Atm," USSR Acad. Sci. Press, 1959.

*—Original received October 16, 1959*

### Reviewer's Comment

The empirical equations presented by this author are a compact representation of extensive Russian tables of the thermodynamic properties of air at high temperatures. The work will be of particular value in connection with computations carried out on high speed computers since the coefficients of the empirical equations can be more compactly stored than can the entries of the table from which they are derived, and since the evaluation of the empirical equations will require no more programing effort than a table look-up operation.

—STUART R. BRINKLEY JR.
Combustion and Explosives Research, Inc.
Pittsburgh, Pennsylvania

# Technical Comment

## Comments on "Condensation Shocks in Supersonic Nozzles"

R. M. HEAD

U. S. Naval Postgraduate School, Monterey, California

STEPCHKOV'S paper (1)[1] presents the results of some apparently quite carefully made experiments on condensation of water vapor in supersonic nozzles, without, however, presenting anything that extends the state of the knowledge beyond that which existed ten years ago. His curves and discussion pertaining to droplet radii $< 10^{-6}$ cm are open to question since the equations he utilizes are not valid in that range. Except for the two examples presented in Fig. 2, there are insufficient data available to enable calculations of the temperature gradient along the various nozzles to be made. If the temperature gradients were utilized as an additional parameter in the presentation of the data of Figs. 4, 5 and 6, the apparently large amount of scatter in the points would undoubtedly be reduced markedly, inasmuch as large temperature gradients have a pronounced effect in delaying the onset of condensation. The theoretical discussion presented in the paper has been covered in considerably greater detail in a number of earlier papers, but ones of which the author was apparently unaware. [See, for example (2–4)].

Please note that the ordinate of Fig. 10 should be labeled $S/S_{cs}$.

[1] Numbers in parentheses indicate References at end of paper.

### References

1 Stepchkov, A. A., "Condensation Shocks in Supersonic Nozzles," ARS JOURNAL, vol. 30, no. 7, July 1960, pp. 695–699.

2 Wegener, P. P. and Mack, L. M., "Condensation in Supersonic and Hypersonic Wind Tunnels," "Advances in Appl. Mech.," Academic Press, Inc., New York, 1958, vol. 5, pp. 307–447.

3 Stever, G. H., "Condensation of High Speed Flows," in "Fundamentals of Gas Dynamics," edited by H. W. Emmons, vol. III of the series "High Speed Aerodynamics and Jet Propulsion," Princeton Univ. Press, Princeton, N. J., 1958.

4 Head, R. M., "Investigation of Spontaneous Condensation Phenomena," Cal. Tech. thesis, 1949.

# Digest of Translated Russian Literature

The following abstracts have been selected by the Editor from translated Russian journals supplied by the indicated societies and organizations, whose cooperation is gratefully acknowledged. Information concerning subscriptions to these publications may be obtained from these societies and organizations.

## *AUTOMATION AND REMOTE CONTROL (Avtomatika i Telemekhanika).* Published by Instrument Society of America, Pittsburgh, Pa.

**A Precision Multiplier,** by L. N. Fitsner, vol. 20, no. 1, Jan. 1959, pp. 56–62.

*Abstract:* A description is given of a multiplier with a static error not exceeding 0.01 to 0.02 per cent of the full scale of output voltage, and with the ordinary high speed of electronic components. The low value of error is made possible by constructing the multiplier of a "rough" and an "exact" part.

*Summary:* The circuits we have been considering for multipliers with "rough" and "exact" portions have greater accuracy and speed of action than do existing circuits. They are simple to adjust, and the elements comprising them are simple. Experimental investigation of a number of circuits of multipliers constructed in accordance with the principles here considered were carried out as early as 1952, and gave good results. The static errors of such MU's did not exceed 0.01 to 0.02 per cent of the output voltage scale. Subsequently these components were manufactured as parts of nonlinear electronic models.

**The Analysis and Synthesis of Certain Discrete Contactless Circuits,** by B. I. Rameev and Yu. A. Shreider, vol. 20, no. 1, Jan. 1959, pp. 63–70.

*Abstract:* The article treats of the code circuits, based on diodes, which are used in the Strela computer. Algebraic methods for analyzing and synthesizing such circuits are considered. The possible ways of constructing these circuits economically are discussed. Use is made of a logical symbolism close to the ordinary Boolean algebra.

**Chain Matrixes and Substitution Circuits for Electromagnetic-Type Electromechanical Transformers,** by A. Ya. Mel'nichuk, vol. 20, no. 1, Jan. 1959, pp. 71–76.

*Abstract:* Different variations of four-terminal substitution circuits for electromagnetic-type electromechanical transformers are considered. The possible methods of estimating the influence of "negative rigidity" on transformer operation are discussed.

**On the Possibility of Certain Types of Oscillations in Sampled-Data Control Systems,** by Shao Da-Chuan, vol. 20, no. 1, Jan. 1959, pp. 77–82.

**Choice of an Optimum Amplification Factor for a Self-Aligning Control System,** by I. I. Perel'man, vol. 20, no. 2, Feb. 1959, pp. 177–184.

*Abstract:* A method is given for determining the optimum (from the point of view of reducing the mean-square control error) amplification factor in a control system with a self-aligning program, when a cyclic disturbance at its input is described statistically.

**The Optimal Parameters for Noise Stability in a Telemetry System,** by V. A. Kashirin, vol. 20, no. 2, Feb. 1959, pp. 216–226.

*Abstract:* The stability of telemetry signals against weak and fairly strong fluctuation noise is calculated for pulse-time (PT) and pulse-width (PW) systems. It is shown that there are optimal transmission parameters, which insure minimal referred root-mean-square error for a given noise level. The various types of modulation are compared from the point of view of noise stability.

**Noise Stability in Pulse-Width and Pulse-Time Telemetry Subject to Strong Fluctuation Noise,** by N. V. Pozin, vol. 20, no. 2, Feb. 1959, pp. 227–235.

*Abstract:* Noise stability in pulse-width and pulse-time telemetry subject to strong fluctuation noise is examined; the main methods of transmission are considered. The mean and mean-square errors are used as tests of the noise stability. Errors in the leading edges of pulses are neglected, but allowance is made for errors caused by fluctuation noise which splits up the pulses or the spaces between them. The signal is sampled for analysis. Formulas for evaluating the noise stability are deduced. The noise stabilities of certain specific telemetry systems are compared.

**Concerning the Realization of Optimum Weighting Functions of Pulse Servo Systems,** by V. P. Perov, vol. 20, no. 3, March 1959, pp. 276–284.

*Abstract:* Simple techniques for the approximate realization of optimum weighting functions of pulse servo systems are given for several particular cases.

**A Fast Transistorized Magnetic Push-Pull Amplifier for a Servo Drive,** by V. S. Volodin, E. D. Larin, M. A. Rozenblat and G. V. Subbotina, vol. 20, no. 3, March 1959, pp. 307–313.

*Abstract:* It is shown that a high speed amplifier for a servo drive can be made by combining magnetic and transistor amplifiers. Test data are given for such an amplifier designed to control a two-phase asynchronous motor; the transient duration is 1–1.5 cycles at the supply frequency, and the power gain is $1.5 \times 10^6$.

**Choice of Characteristic for Nonlinear Rate Feedback in Position Servos,** by B. N. Naumov, vol. 20, no. 3, March 1959, pp. 319–329.

*Abstract:* A method for choosing the characteristic for nonlinear rate feedback in a position servo is given; this feedback is to provide a transient very similar to the desired one with a pre-set structure for the system. It is shown that the characteristic can be chosen from the experimental response curve for the initially unstabilized servo.

**Methods of Studying Stability in Automatic Control Systems With Distributed Parameters,** by Ya. B. Kadymov, vol. 20, no. 3, March 1959, pp. 330-333.

**An Integral Estimate for Selecting the Optimum Parameters of an Automatic Control System With a Given Overshoot,** by A. I. Tupitsyn, vol. 20, no. 4, April 1959, pp. 394–402.

*Abstract:* A combined integral estimate is used to find the optimum parameters of an automatic control system with a given overshoot. Formulas are given which define the response time approximately. Examples are given.

**Use of an Integral-Square Estimate to Determine the Optimal Parameters of an Autopilot With Rate Feedback,** by V. D. Matytsin and V. A. Ryapolov, vol. 20, no. 4, April 1959, pp. 403–408.

*Abstract:* The stabilization of an aircraft by an autopilot with rate feedback is studied. Analytic formulas are deduced which define the optimum values of the transfer numbers for the autopilot in terms of the aircraft's aerodynamic parameters and flight conditions. Lag in the controls is allowed for. The integral-square estimate is minimized to yield the optimum stabilization parameters.

**Compensation of a Continuous Automatic Control System by Means of a Delay Element Filter,** by Wang Sin-Min, vol. 20, no. 4, April 1959, pp. 421–430.

*Abstract:* Methods are considered for the design of a delay element filter for compensating a continuous automatic control system. The filter parameters are determined for a few simple cases.

**Investigation of the Characteristics of Pneumatic Jet Elements,** by L. A. Zalmanzon and A. I. Semikova, vol. 20, no. 4, April 1959, pp. 431–448.

*Abstract:* The article deals with an investigation of pneumatic jet elements, the operation of which is based on the utilization of the characteristics of pressure changes obtained when the impact tube is moved through different sections of the jet flowing from a nozzle. Examples are given of the possible applications of such elements in pneumatic devices.

**Machine Analysis of Switching Circuits,** by P. P. Parkhomenko, vol. 20, no. 4, April 1959, pp. 465–475.

*Abstract:* Algorithms for the mechanization of the structural analysis of switching circuits and for the sequential determination of the action of their elements are presented. The realization of the algorithms in a special logical machine is described. The machine performs a complete analysis of switching circuits of practically any complexity much better and more rapidly than man does. The results of the analysis are recorded manually or automatically. The machine may be used for the analysis of switching circuits with solid-state elements and for the solution of logical and other types of problems. The principles involved can be used for automatic quality control in the production of relay devices and other electrical apparatus.

**A Peak-Holding Regulator That Follows the Peak,** by N. V. Grishko, vol. 20, no. 4, April 1959, pp. 497–499.

*Abstract:* A peak-holding regulator that follows the peak is described. It consists of two main parts, one of which measures the distance from the peak, and the other of which is a sampled data followup device. Test results are given; these tests had as object to find parameters optimal in the sense that the root-mean-square followup error is minimal.

**Methods of Studying the Stability of Automatic Control Systems With Distributed Parameters, With Allowance for Losses,** by Ya. B. Kadymov, vol. 20, no. 4, April 1959, pp. 500–503.

*Abstract:* The stability criterion for systems with distributed parameters is extended to systems with losses.

## *BULL. ACAD. SCI. USSR, PHYSICAL SERIES (Izvestiia Akademii Nauk SSSR, Seriia Fizicheskaya).* Published by Columbia Technical Translations, White Plains, N. Y.

**Luminescence Mechanism in Plastic Scintillators,** by I. M. Rozman, E. A. Andreeshchev and S. F. Kilin, vol. 23, no. 1, 1959, pp. 99–103.

*Conclusions:* The fact that the temperature quenching of fluorescence of polystyrene agrees with the temperature quenching of its scintillation indicates at any rate that the additional quenching in the process of scintillation has a very high rate ($>10^{10}$ sec$^{-1}$). On the other hand, the specific scintillation response is only about five times smaller than the value that might be expected in the case of complete absence of additional quenching. We see only two ways in which these facts can be reconciled: 1 We can assume the presence of "instantaneous" quenching for some fraction of the primary activations, for example, because of "inactive" absorption or owing to local temperature rises, or 2 we can assume the presence of bimolecular quenching for some fraction of the primary activations, as we have done herein. The second assumption leads to differences between the decay laws for scintillation and fluorescence. The experimental data now available are not in conflict with this conclusion, but, unfortunately, are not adequate to substantiate it unambiguously.

**Fluorescence Spectra of "Motorenes" (Engine Fuels),** by C. Mihul, C. Ruscior, V. Pop, F. R. Shvartz and G. A. Redulescu, vol. 23, no. 1, 1959, pp. 117–120.

*Introduction:* In the present report we give the results of our investigation of the fluorescence spectra of "motorenes" (engine fuels) obtained from Rumanian petroleum. The spectra were photographed on panchromatic films by means of an Hilger E-3 spectrograph and scanned on a microphotometer of our own design. Except as noted, the fluorescence was excited by the integral radiation of a mercury tube. We studied the spectra of a number of fuels of different origin. Here we shall describe the spectra of four samples we designated as $A_{1spec}$ (special), $A_1$, $A_2$ and C.

**Characteristics of fuel samples**

| Sample | Specific gravity at 20 C | Index of refraction $n_D^{20}$ | Viscosity at 50 C, *cSt* | Initial boiling point, °C | Volume distilled At 300° | Volume distilled At 360° |
|---|---|---|---|---|---|---|
| $A_{1spec}$ | 0.902 | 1.5041 | 4.5 | 239 | 50 | 97 |
| $A_1$ | 0.897 | 1.4998 | 4.5 | 240 | 51 | 96 |
| $A_2$ | 0.876 | 1.4891 | 4.1 | 230 | 50 | 97 |
| C | 0.859 | 1.4811 | 3.7 | 240 | 56 | 94 |

**Luminescence Spectra of High Molecular Weight Petroleum Hydrocarbons,** by Kh. I. Mamedov, vol. 23, no. 1, 1959, pp. 121–124.

*Introduction:* At the Fourth All-Union Conference on Luminescence we reported on the results of an investigation of the luminescence spectra of the kerosene fraction of petroleum. While there is little difficulty in investigating the low temperature fractions of petroleum by conventional spectroscopic methods, when it comes to high molecular weight fractions ordinary analytic procedures become ineffective owing to the large number of complex molecular groupings; hence, development of new techniques is imperative. In the present work, for the purpose of determining the nature of the substances in an oil fraction of petroleum, we had recourse to combined investigation of the luminescence and absorption spectra.

**Properties of the investigated crystalline substances separated from petroleum**

| Sample no. | Appearance | Melting point, deg C | Molecular weight |
|---|---|---|---|
| 1 | White crystalline substance | 235 | 299 |
| 2 | White crystalline substance | 199 | 316 |
| 3 | Pale yellow crystalline substance | 260 | ... |
| 4 | Yellow crystalline substance | 290–292 | 460 |

**High Frequency Ferromagnets,** by L. I. Rabkin, vol. 23, no. 3, 1959, pp. 309–313.

*Introduction:* The growing need for magnetic materials suitable for use in radio-frequency circuits led to the discovery and development of three classes of high frequency ferromagnets, which differ as regards structure, properties and fabrication procedure. The first class comprises metallic ferromagnets which are prepared by the usual procedures of metallurgy. The second class includes ferrites—nonmetallic ferromagnets, which are prepared primarily by ceramic techniques. These materials are frequently called magnetic or ferrous ceramics. The third class of ferromagnets consists of magnetodielectrics, heterogeneous substances, consisting of mixtures of ferromagnetic powders and insulating materials. Cores and components of this class are fabricated by techniques similar to those employed in the plastics industry.

**Some Attributes of Ferrites Under Pulse Conditions,** by N. A. Smol'kov and V. F. Belov, vol. 23, no. 3, 1959, pp. 345–347.

*Introduction:* Memories—information storage devices—are fundamental to modern engineering cybernetics. Of all such devices, the most reliable, economical and quick acting are memories based on ferrite cores with rectangular hysteresis loops. Magnesium-manganese ferrites, sometimes doped with CaO, ZnO, etc., are extensively used in computer memories. Inasmuch as

the external conditions, in particular the ambient temperature, under which such devices are operated may differ, the variation of the properties of ferrites as a function of the external conditions is of considerable interest. Albers-Schoenberg and Eckert investigated the influence of temperature on the hysteresis loop of Mg-Mn ferrites; Van der Heide et al. studied the temperature dependence of the pulse characteristics of Cu-Mn ferrites. In the present work we investigated the temperature dependence of the pulse characteristics of some Mg-Mn ferrites.

**Ferromagnetic Semiconductors in Super-High Frequency Fields,** by A. G. Gurevich, vol. 23, no. 3, 1959, pp. 348–353.

*Introduction:* One of the principal fields of application of ferromagnetic semiconductors is super-high frequency (hereinafter *shf*) engineering. Until relatively recently, ferromagnetic materials were not used in this range. The need for such materials arose at the end of the 1940's, when development of *shf* electronics brought two new acute problems: 1 Rapid regulation of component parameters, and 2 the development of systems not governed by the reciprocity principle. Only through the use of magnetized ferromagnetic materials could these problems be solved by simple means insuring good stability, an unlimited service life and the capacity to handle high *shf* powers. Ferromagnetic metals cannot be used efficiently in the *shf* range. Both the indicated problems can however, be solved by means of ferromagnetic semiconductors with low conductivity, for example, some ferrites. The introduction of ferromagnetic semiconductors brought a revolution in *shf* engineering. Recent advances in radar, radio relay communications and allied fields would be impossible without ferromagnetic semiconductors. The present report is a brief survey of the properties of ferromagnetic semiconductors in *shf* fields with particular attention to premagnetized materials, the behavior of which is of great interest from both the theoretical and practical standpoints.

**Some Properties of Ferrites at Super-High Frequencies,** by N. A. Smol'kov and E. I. Fomenko, vol. 23, no. 3, 1959, pp. 363–365.

## *INDUSTRIAL LABORATORY* (*Zavodskaya Laboratoriya*). Published by Instrument Society of America, Pittsburgh, Pa.

**Heat Resisting Strain Gage Wire Grids on a Laminated Fiber Glass Base,** by V. A. Golovin and V. D. Nessonov, vol. 25, no. 1, Jan. 1959, pp. 126–128.

*Introduction:* A considerable number of different types of strain gage wire grids has been developed for measuring at elevated temperatures. However, their measuring ranges and characteristics are as yet not satisfactory. The DK type strain gage grids wound on a paper base impregnated with synthetic resin are widely used in measuring dynamic and static strains at ordinary temperatures. When the temperature rises to 150–200 C the paper base becomes carbonized, which affects the adherence of wire to the metal. Tests showed that laminated fiber glass, a material consisting of two layers of glass fibers with BF-2 adhesive, is the best base for strain gage wire grids.

**Strain Gage for Measuring Strains Caused in a Specimen by the Combined Action of Axial Forces and Torque,** by N. M. Domarev and V. F. Latyshev, vol. 25, no. 1, Jan. 1959, pp. 129–130.

*Introduction:* The mechanical strain gage suggested here is simple and convenient in operation. It enables a simultaneous measurement to be made of axial and angular strains in specimens ranging in diameter from 10 to 30 mm in both the elastic and elastic-plastic regions, and makes possible the determination of the first three figures of the modulus of elasticity $E$ and of shear $G$, and also the determination of the Poisson's ratio. The requirements of accuracy are satisfied. The strain gage consists of two main parts which are secured on the specimen by means of blades 1 and 2 (U8 steel) hardened to $R_C = 64$, and can be handled independently of one another. The axial strain is measured on the gage length of 100 mm by means of two indicators 3 and 4 with $\mu$-divisions. These indicators are mounted on the top of the strain gage and are in contact with flat platform 5.

**Annulus Dynamometer With Electric Strain Gages,** by N. F. Cherepnin, vol. 25, no. 1, Jan. 1959, pp. 130–131.

*Introduction:* We have developed, for measuring tensile stresses in the foundation bolts of supporting structures in mines, an annulus dynamometer with electric indicator. The circuit of the measuring unit consists of two parts: A resistance dynamometer and electric indicator which, in turn, consists of an a-c generator, an unbalance compensator and the zero indicator.

**Investigation of Chromatographic Gas Analyzers,** by T. G. Garnova, L. É. Elotnikov, M. B. Moshinskaya, N. G. Paradzhanova and V. P. Shvartsman, vol. 25, no. 2, Feb. 1959, pp. 167–168.

**A Method of Investigation of Metal Corrosion During Condensation,** by I. L. Rozenfel'd and K. A. Zhigalova, vol. 25, no. 2, Feb. 1959, pp. 182–184.

*Introduction:* Observations show that the distinctive feature of corrosion accompanying condensation is the nonuniformity of its distribution, which can be explained only by the fact that the condensation occurring on all commercial metals is mainly in drop form. The investigations of corrosion processes accompanying condensation, as well as short-time tests, must be carried out with due regard to the amount of moisture condensing on the metal surface. In doing so, it is necessary to take into account that, at a given relative humidity, the changes in the water vapor content of air with temperature are nonlinear. For this reason, equal temperature changes produce, at low temperatures (for example, at 5–10 C), and at higher temperatures (35–40 C), the condensation of different quantities of water.

**Elimination of Errors Occurring in Measurements With Q-Meters,** by I. S. Pavlov and A. S. Marchenko, vol. 25, no. 2, Feb. 1959, pp. 184–189.

*Introduction:* The sources of errors occurring during measurements with Q-meters can be divided into three groups: 1 Errors of calculation equations; 2 errors due to the unsatisfactory design of the instrument; and 3 errors introduced by additional devices (various attachments, thermostats, specimen holders, etc.). It has often been pointed out in technical literature that the errors in determining the Q-factor are relatively high. The calculation with equations known for the theory of errors often produces a relative error of the order of 30 per cent and more. This error is of the maximum size permissible in single tests. The actual error due to the scatter of measurement results is determined by the deviation of the individual values from the mean value, as obtained in large-scale tests. These tests are carried out in absolutely identical conditions. Experience shows that, if this condition is fulfilled, then the scatter of results of individual tests is not very high. However, it is difficult to obtain identical test conditions. The second group of causes of possible errors is represented by design and construction defects of the instrument itself, which affect the measurement accuracy.

**Recording of the Impact Testing Process of Welded Joints With an Oscillograph,** by M. N. Gapchenko, vol. 25, no. 2, Feb. 1959, pp. 203–207.

*Introduction:* As a method which makes possible the recording of quick processes taking place during an impact test, oscillographic investigation has been in use for a long time. Apart from their advantages, the existing methods also have some disadvantages, mainly inadequate sensitivity and accuracy, complexity of the plant, etc. We recorded the impact test on a loop oscillograph using an accelerometer as the pickup.

**Experimental Apparatus for the Study of the Corrosion Behavior of Materials in Highly Corrosive Media,** by V. I. Ginzburg, vol. 25, no. 2, Feb. 1959, pp. 233–235.

*Introduction:* We designed and constructed, from molybdenum glass, an apparatus which imitates the production process of the actual manufacturing unit. The equipment is intended for the study of corrosion behavior or the chemical resistance of metallic and nonmetallic materials at high temperatures in continuous contact with highly corrosive liquid or gaseous agents. For the accommodation of test specimens, any of the devices with the continuous circulation of gas can be employed. The plant was successfully used in the study of the corrosion behavior of nickel-chromium steels at temperatures up to 100 C in a flow of concentrated sulfuric acid (85–98 per cent), saturated with various gases ($O_2$, $N_2$ and $C_2H_2$). Of particular interest was the study of the type and causes of the point-pit corrosion of nickel-chromium steel in conditions approximating their service conditions: The variation of speed and quantity of the gas circulated through the system, the intensity of agitation of the liquid corrosive medium, the temperature of the solution, etc.

**Hydraulic Strain Gage for Measuring Strain During Tension and Compression,** by K. K. Likharev, vol. 25, no. 3, March 1959, pp. 376–377.

*Introduction:* We developed a hydraulic strain gage based on the principle of the "hydraulic level ratio." The strain gage is easy to operate and gives stable readings of high accuracy.

**High Sensitivity Flame Spectrophotometer With a Photomultiplier,** by A. L. Osherovich and G. A. Sheinina, vol. 25, no. 3, March 1959, pp. 380–382.

*Introduction:* The main requirements which flame spectrophotometers have to meet are: A spectral sensitivity within 3800–9200 A; the optical system should be able to separate as narrow as possible a spectral interval; the sensitivity range and the dynamical range of the photoelectrical equipment should permit the recording of very weak as well as very strong fluxes. We developed a simple highly sensitive flame spectrophotometer which meets these requirements.

**Determination of the Modulus of Elasticity $E$ by the Electrical Method,** by Yu. D. Sofronov, vol. 25, no. 4, April 1959, pp. 489–491.

*Introduction:* The application of the radiophysical method for the determination of elastic constants, requires the use of complex electronic equipment. In order to simplify the construction of apparatus and its servicing in the excitation of vibrations of specimens, we applied the industrial alternating current. In this, we changed the testing method as, in this case, the resonance is achieved by changing the free length of the specimen.

**A Simple and Highly Sensitive Thermocouple for the Measurement of Body-Surface Temperature,** by G. I. Berezin, vol. 25, no. 4, April 1959, pp. 502–503.

**A Device With a Split Block for the Determination of the Friction Coefficient,** by A. A. Presnyakov and A. A. Vinnitskii, vol. 25, no. 4, April 1959, p. 505.

*Introduction:* We developed a device with a split block permitting the determination of contact friction forces arising in setting, and also the actual specific pressure at the surface in contact. The latter provided the possibility of studying the friction distribution in the deformation nucleus and calculating the coefficient of friction. The layout of the device is described.

**An Electrolytical Bridge for the Investigation of Electro Osmosis Under Hydrostatic Pressure,** by É. M. Gutman, vol. 25, no. 4, April 1959, p. 507.

## *INSTRUMENTS AND EXPERIMENTAL TECHNIQUES* (*Pribory i Tekhnika Eksperimenta*). Published by Instrument Society of America, Pittsburgh, Pa.

**Studies on Slow Neutron Counters,** by V. Ya. Savel'ev and V. A. Kononenko, no. 1, Jan.–Feb. 1959, pp. 66–69.

*Abstract:* A simplified theory is presented for the processes in $BF_3$-filled slow neutron counters. Formulas are deduced that relate the pulse height, efficiency and threshold to voltage, pressure and dimensions. Experimental results are given, particularly on the relations between the main parameters, e.g., the threshold, amplitude, efficiency, plateau position, pressure, potentials on the electrodes, discrimator settings, and dimensions. The simplified theory gives results that are in reasonable agreement with experiment.

**Thermal Stabilities of Halogen Counters,** by V. G. Chaikovskii, no. 1, Jan.–Feb. 1959, pp. 69–71.

*Abstract:* A design for thermally stable halogen-filled counters has been sought. It has been found that these counters change their characteristics at high temperatures because products formed by the halogens reacting with the materials in the counter evaporate. The counters can be made stable up to 170–200 C if these products are first removed.

**Nonoverloading Linear Amplifier for High Speed Counting,** by A. S. Melioranskii and Yu. M. Ostanevich, no. 1, Jan.–Feb. 1959, pp. 77–80.

*Abstract:* Description of a linear, nonoverloading amplifier to work with a scintillation transducer for counting speeds up to $10^5$ pulses per sec.

**Modulation Method of Identifying Weak Pulse Signals,** by A. G. Gorelik and V. V. Kostarev, no. 1, Jan.–Feb. 1959, pp. 80–85.

*Abstract:* A device for identifying weak signals in pulse working at aerological radio location stations is described. For decreasing the effect of the instability of supplies, tube characteristics variations and changes in circuit parameters, a modulation averaging method was used. With an averaging time of 2.5 sec a gain of 17 db in the signal to noise ratio was obtained as compared with a conventional radio location station.

**Methods and Apparatus for Low Temperature Optical and Spectral Investigations,** by V. P. Babenko, V. L. Broude, V. S. Medvedev and A. F. Prikhot'ko, no. 1, Jan.–Feb. 1959, pp. 119–124.

*Abstract:* Metal cryostats were developed for optical and spectral investigations at the temperature of liquid hydrogen and liquid helium. The design features of the cryostats made it possible to obtain the lowest and most stable temperatures of the samples and also to reduce considerably the consumption of hydrogen or helium used for cooling. The cryostats were adapted for the application of microprojection methods of the absorption and luminescence of crystals in the free and stressed state and for crystallo-optical and photoelectric low temperature measurements.

**Behavior of Certain Type Photomultipliers in Weak Magnetic Fields,** by L. I. Zlobin, Yu. A. Nemilov and A. N. Pisarevskii, no. 1, Jan.–Feb. 1959, pp. 145–146.

*Abstract:* Data on the variation of the general sensitivity, amplitude, resolution and the pulse rise time in weak longitudinal magnetic fields for photomultipliers FÉU-11, FÉU-15, FÉU-8 and FÉU-V are given.

**Installation for Obtaining Powerful Magnetic Fields of Short Duration,** by V. R. Karasik, no. 1, Jan.–Feb. 1959, pp. 147–150.

*Abstract:* The construction of devices for obtaining powerful magnetic fields of short duration is described in detail. Fields of $3 \times 10^5$ oersteds in a volume of 0.7 $cm^3$ are obtained by discharging a bank of capacitors. The discharge is oscillatory with a period of $2 \times 10^{-4}$ sec. The construction of the solenoid, its manufacture and assembly are described in detail.

**Measurement of Particle Distribution by the Amplitudes of Radial-Phase Vibrations,** by K. A. Belovintsev and B. N. Yablokov, no. 2, March–April 1959, pp. 188–191.

*Abstract:* A method is given for measuring the distribution of accelerated particles by the amplitudes of radial-phase vibrations. This distribution was found experimentally. A relation was obtained between the half width of the accelerated bunch and the energy and period, for which the accelerating voltage operates; this relation shows satisfactory agreement with theory.

**A New Radio Telescope of High Resolving Power,** by S. É. Khaikin and N. L. Kaidanovskii, no. 2, March–April 1959, pp. 195–199.

*Abstract:* The reflector is made up of separate flat strips tangential to the paraboloid, whose axis is directed to the point of observation; the points of contact lie in a horizontal plane passing through the focal point of the paraboloid. The reflecting surface is made highly accurate in form by adjusting each strip individually. A plane wave is transformed to a cylindrical one with its axis vertical. A second mirror (a paraboloidal cylinder) transforms the latter wave to a spherical one. The axis of the telescope may be set in any direction by adjusting the positions of the strips and of the radiator. The horizontal dimension is 120 m, the vertical one 3 m; this gives a beam with a divergence of 1.2′ in azimuth and 1° about the line of sight at 3-cm wave length. A telescope with a reflecting area of $10^4$–$10^5$ $m^2$ can be built for centimeter wave lengths on this principle.

**Experience With Adjusting a Large Radio Telescope,** by N. A. Esepkina, no. 2, March–April 1959, pp. 200–201.

*Abstract:* A description is given of an experimental test of a proposed method of measuring the parameters of a narrow beam antenna within the Fresnel zone. Measured patterns and gain factors are given for systems with apertures of about 1000 and 2000 λ. The effects of some errors in the surfaces are examined.

**Remote Controlled Device for Measuring the Intensity of a Magnetic Field,** by L. N. Gertsiger, no. 2, March–April 1959, pp. 208–211.

*Abstract:* A device for measuring the intensity of permanent magnetic fields within the limits of 0.3–20 kilo-oested based on the nuclear magnetic resonance method and designed for measurements in the gaps of large magnets is described. Control of the frequency of a vacuum tube oscillator by means of a piezoelectric capacitor is employed in the system.

**Apparatus for Automation of the Measurements of the Multiple Scattering of Particles,** by G. E. Belovitskii, L. N. Korablev, L. V. Sukhov and I. V. Shtranikh, no. 2, March–April 1959, pp. 267–271.

*Abstract:* An instrument which makes both readings and calculating operations automatically during measurements of multiple Coulomb scattering is described. The instrument also permits the automation of measurements of lengths. The instrument contains transducers installed on a microscope and an electronic calculating device operating on the discrete counting principle. The use of this instrument speeds the measurement of scattering by more than five times and increases the accuracy of measurement and reliability of calculations. The instrument can be used for the automation of similar measurements in bubble chambers and cloud chambers.

**Selection of the Optimum Passband in an Amplifier Operating With an Ionization Chamber,** by A. A. Vorob'ev, V. A. Korovlev and G. E. Solyakin, no. 2, March–April 1959, pp. 275–284.

*Abstract:* The optimum passband of an amplifier with two differentiating circuits was calculated. It was shown that the introduction of a second differentiating circuit completely removes the influence of the microphonic effect and low frequency interference without impairing the signal to noise ratio.

**Transformation of Sinusoidal Signals Into Short Pulses,** by V. I. Nikitenko and A. N. Pegoev, no. 2, March–April 1959, pp. 289–291.

*Abstract:* A converter of sinusoidal signals into short pulses is described. Experimental data of converting which provides a far greater accuracy in transformation are given. The error of transformation is less than $10^{-4}$ of the original sinusoidal signal period with a change in its amplitude by a factor of 2. Oscillograms illustrating the operation of the circuit are appended.

**A Way of Increasing the Stability of Scintillation Counters,** by A. M. Ivanchenko, no. 2, March–April 1959, pp. 330–332.

*Abstract:* As a result of long-standing work with scintillation counters designed to measure the luminescence yield and the amplitude resolution of scintillators, it was established that, despite the application of high stability feed sources and magnetic protection of the photomultiplier, the results of repeated measurements often do not coincide. The necessity of keeping the photomultiplier in darkness for a comparatively long time after the change of scintillators causes a scattering of measurement results for the luminescence yield and the resolution of the crystal phosphor. This article proposes a method which is based on the principle of automatic amplification control of the whole linear channel (including the photomultiplier and the amplifier) by means of the control signal.

**A Resonance Modulator of Light Beams,** by A. A. Meier and K. P. Tissen, no. 2, March–April 1959, pp. 332–333.

*Abstract:* This article describes a simple light beam modulator in which a high stability of modulation frequency is achieved by the application of mechanical resonance. Two variants of the modulator (working at a frequency of approximately 70 cps) were applied to the investigation of electrical properties of semiconductors.

## *JOURNAL OF APPLIED MATHEMATICS AND MECHANICS (Prikladnaia Matematika i Mekhanika).* Published by Pergamon Institute, New York, in conjunction with American Society of Mechanical Engineers.

**A Method of Solving the Basic Integral Equation of Statistical Theory of Optimum Systems in Finite Form,** by V. S. Pugachev, vol. 23, no. 1, 1959, pp. 1–16.

*Abstract:* We present the application of the general formula for solving a linear integral equation of the first kind, encountered in solving a number of problems of statistical theory of optimum systems, to the case when the kernel of the equation represents a correlation function of a random function and is related to white noise by linear differential equation. A case of an infinite observation interval is treated first, and the results obtained are then applied to the case when the observation interval is finite. Finally, on the basis of the author's general formula, a solution for the nonstationary case given by Laning is derived in a straightforward manner. From this solution there follow previously known solutions of specific problems by Dolph and Woodbury, Zadeh and Ragazzini, and Semenov. It has been shown that the known results by Wiener and Booton for the case of infinite observation interval can be obtained from the author's general formula as special cases. Consequently, the results of this article complete the proof that all the known methods of determining optimum linear systems may be very simply obtained through the application of one general method, that of canonic representations of random functions.

**On the Autonomous Determination of Position of a Moving Object by Means of a Space Gyrocompass, a Directional Gyroscope and an Integrating Device,** by A. Iu. Ishlinskii, vol. 23, no. 1, 1959, pp. 75–82.

*Abstract:* A theoretical solution of the problem of the determination of position of a moving object by means of gyroscopes, accelerometers and integrating devices has been presented in another paper. The scheme of combining the computed elements as shown in it could be modified in many different ways. This work presents one of the variants of a somewhat different solution of the problem with the use of the properties of Geckeler's gyrocompass. This variant of a solution of the problem of an autonomous determination of position of an object moving on a spherical Earth requires the use of a directional gyroscope and of a device integrating a system of three nonlinear differential equations of the first order.

**Magnetodynamics of Plane and Axisymmetric Flows of a Gas With Infinite Electrical Conductivity,** by M. N. Kogan, vol. 23, no. 1, 1959, pp. 92–106.

*Abstract:* In this paper we investigate flows of an ideal gas with infinite conductivity in a magnetic field which is parallel to the velocity of the approaching stream. It is shown that there exist two hyperbolic flow regimes, one of which occurs at subsonic velocities. In this flow regime shock waves are inclined upstream. For certain values of the ratio between magnetic and hydrodynamic pressures, there exists an elliptic type of flow at supersonic velocities. In this regime weak shock waves do not occur, but there are strong shock waves whose angles of inclination start from the perpendicular. We work out the simple waves for the hyperbolic regimes and construct the solutions for the problem of flow around bodies, in the linearized and second-order approximations.

**Analysis of Weak Discontinuities in Magnetohydromechanics,** by V. N. Zhigulev, vol. 23, no. 1, 1959, pp. 107–113.

**Integro-Differential and Integral Equations of Equilibrium of Thin Elastic Shells,** by N. A. Kil'Chevski, vol. 23, no. 1, 1959, pp. 165–178.

*Abstract:* In the following we present a method based on application of the work reciprocity theorem for deriving integro-differential and integral equations of equilibrium of thin elastic shells in terms of displacements. This is a modification of the well-known Somiglian method, from which it differs by a special choice of the system of the "auxiliary" displacements; this choice allows us to represent the displacement of a point of the middle surface of the shell by the sum of two displacements: The displacement of the corresponding point of the middle plane of a plate—the "map" of the middle surface of the shell—and a supplementary displacement depending in particular on the curvature of the middle surface of the shell. In the case of cylindrical shells the method was used by the author over 10 years ago. In the present paper it is extended to the treatment of shells of any form of the middle surface.

**On the Motion of Gyroscopic Systems,** by V. S. Novoselov, vol. 23, no. 1, 1959, pp. 242–246.

*Abstract:* In examining the motion of a gyroscopic system, we usually omit the second derivatives of Lagrangian coordinates in the linearized equations. For the steady motion of gyroscopic systems in which damping is not present, such an operation was justified by Merkin. In this paper we consider the case of a gyroscopic system with variable coefficients. The method

suggested is based on ordinary substitution for the independent variables; this method is also of interest for the steady gyroscopic system.

**Steady-State Flow of Detonating Gas Around a Cone,** by S. S. Kvashnina and G. G. Chernyi, vol. 23, no. 1, 1959, pp. 252–259.

**The Solution of the Equation of Magnetohydrodynamics Describing the One-Dimensional Axisymmetrical Motion of a Gas in a Gravitational Field,** by E. V. Riazanov, vol. 23, no. 1, 1959, pp. 260–265.

*Abstract:* We consider the one-dimensional axisymmetrical unsteady motion of an electrically conducting perfect gas, subject to the force of Newtonian gravitation. We will assume the conductivity of the gas to be infinite, the magnetic field perpendicular to the trajectory of the gas molecules, and the viscosity and thermal conductivity negligible.

**On the Similarity of Hypersonic Viscous Flows Around Slender Bodies,** by V. V. Luniev, vol. 23, no. 1, pp. 273–280.

*Abstract:* The equations of the laminar boundary layer on sharp flat and axisymmetric bodies are considered for high flight Mach numbers $M$. For the flat plate, similar equations have been studied by Shen and Lees. Criteria for the extent of the influence of the boundary layer on the outer inviscid flow are established for $M \gg 1$. For thin bodies, conditions for the similarity of the flows are determined.

**Selfsimilar Motions of Gas With Shock Waves, Spreading With Constant Speed Into Gas at Rest,** by G. L. Grozdovskii, A. N. Diukalov, V. V. Tokarev and A. I. Tolstykh, vol. 23, no. 1, 1959, pp. 281–286.

**On a Problem of Optimum Control of Nonlinear Systems,** by N. N. Krasovskii, vol. 23, no. 2, 1959, pp. 303–332.

**On the System of Differential Equations of Equilibrium of Shells of Revolution Under Bending Loads,** by V. S. Chernin, vol. 23, no. 2, 1959, pp. 372–382.

**Flow Problems in Magnetohydrodynamics,** by M. D. Ladizhenskii, vol. 23, no. 2, 1959, pp. 419–427.

**A Point Source of Luminous Radiation in a Scattering Medium,** by L. A. Galin, vol. 23, no. 2, 1959, pp. 428–435.

*Abstract:* This paper establishes the distribution of luminous radiation from a point source located in a scattering medium. It is assumed that the scattering is isotropic: That is, that any element of the medium emits radiation in all directions with equal intensity. This problem was first considered in a paper by Ambartsumian. Some problems of a similar type have been considered in connection with the diffusion of neutrons.

**Solutions of Singular Cases of Point Explosions in a Gas,** by V. P. Korobeinikov and E. V. Riazanov, vol. 23, no. 2, 1959, pp. 539–544.

**On the Conditions at Elastic Wave Fronts Propagating in a Nonhomogeneous Medium,** by A. A. Gvozdev, vol. 23, no. 2, 1959, pp. 556–561.

*Abstract:* Two types of waves can be propagated independently from one another in a homogeneous elastic medium. In the longitudinal waves the displacements $\mathbf{u}$ are such that there are no element rotations (rot $\mathbf{u} = 0$), and in transverse waves there are no volume changes (div $\mathbf{u} = 0$). In a nonhomogeneous elastic medium no independent longitudinal and transverse waves exist. Volume changes as well as element rotations are simultaneously present in these wave motions. This article deals with the study of the character of the displacements near the wave front (a surface at which the displacements undergo a finite discontinuity), which moves in an ideally elastic nonhomogeneous medium. Fronts with such discontinuities may correspond to sources of waves with a time dependence of the type of a step force (Heaviside functions), or an integral of it.

**A Generalization of a Proposition by Liapunov on the Existence of Periodic Solutions,** by S. N. Shimanov, vol. 23, no. 2, 1959, pp. 583–587.

**Equations of Perturbed Motion in the Kepler Problem,** by A. I. Lur'e, vol. 23, no. 2, 1959, pp. 588–591.

**On the Stationary Distribution of Mutually Attracting Particles,** by A. N. Gerasimov, vol. 23, no. 2, 1959, pp. 592–596.

*Introduction:* The well-known barometric formula of Laplace $p = p_0 \exp[-(mgh/kT)]$ is a particular, and by no means complete, example of the application of Boltzmann's general formula $\rho = \rho_0 \exp[-(\Pi/kT)]$ where $\Pi$ is the potential energy of the particle and $T$ the absolute temperature, identical for all the parts of the region, to which the distribution of the density $\rho$ is related. However, the state of the system, though stationary in the thermal sense, need not necessarily be isothermal. We will investigate an infinite body whose particles are subjected only to forces of mutual attraction in accordance with Newton's law. The equation of state need not be specified, it can be arbitrary. In the end some state of the system will be established, and it will necessarily possess spherical symmetry (we assume an infinite number of particles). A nonlinear integral equation is derived, connecting distribution of temperature with distributon of density. Knowing the distribution of the one, the distribution of the other can be obtained from this equation. For the Clapeyron state the problem can easily be carried through to completion. The formulas above are obtained as particular cases for the isothermal state.

## *MEASUREMENT TECHNIQUES* (*Izmeritel'naya Tekhnika*). Published by Instrument Society of America, Pittsburgh, Pa.

**Error of the Measurement of the Intensity of a Magnetic Field by the Method of Nuclear Magnetic Resonance,** by A. V. Kubarev, no. 1, Jan. 1959, pp. 44–48.

*Introduction:* The method of nuclear magnetic resonance finds wide use for the measurement of the intensity of a constant magnetic field with high precision. It is sufficient to point out that the results achieved now permit one to raise the question about transfer to a new testing plan of magnetic measurements whose basis will be the value of the gyromagnetic ratio of the proton and the method of nuclear resonance. The analysis of the errors of the method and corresponding measuring apparatus arouses interest. The presence of nonuniformities of the field measured and the measuring circuit with narrow band amplification of the resonant signal, are taken into account in the analysis.

**A Photoelectric Instrument for Measuring Torques,** by M. D. Konovalov, V. A. Rikhter and V. N. Tarapin, no. 2, Feb. 1959, pp. 113–114.

*Introduction:* This instrument was developed by Professor S. A. Strelkov's design for measuring the torques in the shafts of building and road-making machines; the two designs were made to work a loop oscillograph without requiring current leads. The first design was meant for use with shafts that could be withdrawn in order to mount the device; the second (demountable) design was meant for use with shafts that could not be withdrawn.

*Summary:* Tests have shown that the calibration stays unchanged (within the error of measurement) for up to a year; the error of measurement under field conditions is 3–4 per cent, but can be reduced to 2 per cent under laboratory conditions; the unit works well at temperatures from −20 to +35 C. These units have been in use for several years on excavators, snow-clearing machines, road rollers and other such machines. From the Editor: V. I. Zelinskii has used the principle described here to make the torsion gage described as "A photoelectric torque torsiometer" in no. 1 for 1958.

**A Ballistic Pendulum for Calibrating Acceleration Transducers,** by V. P. Nenyukov, A. S. Zhmur and G. L. Lyapin, no. 2, Feb. 1959, pp. 114–116.

*Introduction:* The ballistic pendulum consists of a framework, a striker, a release mechanism and a deflection meter. The striker is a steel cylinder held by four steel wires. It is fitted with a striking pad on one end and with lugs and chain to couple with the release mechanism on the other. The counterweight is made of cast aluminum and is suspended in the same way as the striker. The end facing the striker can be fitted with a disk of steel, plastic, etc. The other end carries a holder for the transducer. The weight is also fitted with a boss coupled to a wire that works the deflection indicator. We found by recording the signals from a piezoelectric transducer on an oscilloscope that vibrational oscillations were excited in the weight. The accelerations caused by these oscillations are superimposed on the general acceleration. A cleaner recording was produced by fitting a damping pad between the weight and the transducer holder. The shape of the acceleration pulse produced when the

impact disk is of bonded plastic is fairly close to half a sine wave (the area under the curve deviates from the area for the best-fit sine wave by not more than 4 per cent).

**An Improved Low Frequency Bandpass Filter Circuit,** by V. G. Zhelnov, no. 2, Feb. 1959, p. 138.

*Introduction:* The proposed circuit is a modernized version of a low frequency bandpass filter for the suppression of higher harmonics, described earlier by the author. In the original version of that circuit the frequency change of an LC circuit was accomplished by means of changing the equivalent inductance, which made it possible to obtain a frequency coverage coefficient of 3.

**Simple Method of Widening the Working Frequency Band of Film Bolometers in the Super-High Frequency Range,** by V. A. Yugov, no. 2, Feb. 1959, p. 139.

*Introduction:* Film bolometers for power measurements at super-high frequencies find ever increasing applications. The bandwidth, however, of an untuned bolometer head without a band widening system is insufficient for band measurements. As a result of investigations of different band widening methods, we have proposed a method of band widening by means of quartz tubes.

**Determining Ionization Work Done in Air by Gamma Radiations $Co^{60}$,** by K. K. Aglintsev, G. P. Ostromukhova and E. A. Khol'nova, no. 2, Feb. 1959, pp. 142–143.

*Introduction:* To date there are no precise experimental data giving the value of ionization work done in the sphere of hard gamma radiations. One can only mention a note in which the value of ionization work done is reported for gamma radiations $Co^{60}$ as being equal to 34.2 ev. We conducted an experimental investigation of the ionization work in air for gamma radiations $Co^{60}$. The value of ionization work done was measured by means of a preparation in a normal ionization chamber which determined the number of ion pairs and a gamma-calorimeter which gave the value of the absolute activity of the same preparation. The mean value of the ionization work done, obtained from measurements of four different $Co^{60}$ preparations, was found to equal $33.7 \pm 1.5$ ev.

**A General Approach to the Analysis of Static and Dynamic Errors,** by N. A. Chekhonadskii, no. 3, March 1959, pp. 156–160.

*Summary:*

1 The laws operating when measurements are carried out both statically and dynamically may be expressed by general relationships.

2 As a result of an application of the expressions obtained for the dynamic error analysis, it can be established that the dynamic error determined experimentally is, by its meaning, a systematic error of an apparatus operating dynamically. In addition to this error, a random error also arises when measurements are made dynamically.

3 Results of measurements carried out by the apparatus both statically and dynamically may be expressed by similar expressions containing the basic characteristics of the apparatus for these operating conditions; this should make it easier to resolve static and dynamic problems involved in the construction of apparatus.

**Convergence of Automatic Balancing in Measuring Circuits With Two Balancing Elements,** by V. Yu. Kneller, no. 3, March 1959, pp. 189–196.

*Introduction:* Both in production testing and laboratory practice there has been felt in recent years an increasing need for changing over from precision manual measurements of electrical a-c quantities to automatic measurements. Since the appearance of automatic balancers and a-c bridges—instruments which were most suitable for the purpose—more than 20 years have passed. During this period, many original circuits were proposed and sets made; to date, however, there have not been published any descriptions of a sound method for designing such devices, neither does there even exist a clear understanding of the process of automatic balancing and the manner in which it is affected by various bridge parameters. This hinders considerably the development and use of automatic balancers and bridges, in whose design one of the first questions raised is whether the measuring circuit will again balance itself automatically if the balance conditions are disturbed. If the answer is in the affirmative, there arises the question of the quality of the balancing process, i.e., of the speed of balancing, of the oscillations of the balancing elements, etc. The present article deals with analyzing these two problems for automatically controlled balancing by means of two parameters.

**Maximum Sensitivity of a Simple Bridge Circuit at Balance,** by V. A. Kochan, no. 3, March 1959, pp. 200–205.

*Introduction:* Many papers have been written on the problem of calculating optimum resistance values of simple bridge arms for maximum current, voltage or power. The present article provides a calculation of optimum bridge arm resistances with a given current $I_1$ and resistance $r_1$ for maximum sensitivity.

**A Standard Pulse-Series Generator for Checking Discrete-Operation Computers in Measuring Instruments,** by G. L. Grin, and M. A. Zemel'man, no. 3, March 1959, pp. 209–211.

**Dynamic Properties of Devices for Measuring Unstable Temperatures,** by G. P. Katys, no. 3, March 1959, pp. 230–236.

*Introduction:* The optical devices used for measuring temperatures for unstable flames and gaseous media are usually photoelectric systems operating under dynamical conditions. The accuracy of measurement of rapidly changing temperatures depends very much on the principle adopted for the measuring system of the device and on the dynamical properties of its components. However, in designing or examining such devices the dynamical properties of measuring systems are not usually taken into account. As a result, the dynamical errors may reach the size of the errors of the method and even exceed them.

**Some Problems Connected With the Application of Random Functions in Metrological Practice,** by G. S. Simkin, no. 4, April 1959, pp. 241–245.

*Introduction:* In estimating the accuracy of various means of measurement, one frequently uses the theory of random quantities or, what amounts to the same thing, the theory of random errors, whose characteristic property is the fact that they are independent of the parameters of the means of measurement. However, a closer study shows that such an approach is sometimes insufficient.

**A Device for Checking Wobble in Small Bearings,** by I. M. Efuné, no. 4, April 1959, p. 255.

## *OPTICS AND SPECTROSCOPY (Optika i Spektroskopiia).* Published by Optical Society of America, Inc., Washington, D. C.

**On the Question of the Buildup Time for Thermodynamic Equilibrium in the Plasma of an Arc Discharge,** by V. K. Prokof'ev, D. B. Gurevich, I. M. Belousova and Iu. A. Snigirev, vol. 7, no. 1, July 1959, pp. 7–10.

*Abstract:* This paper presents a method for measuring the buildup time for thermodynamic equilibrium in the plasma of an arc burning in air, as well as the results of the measurements. The method consisted of momentary electrical perturbations of the arc plasma. Equilibrium was taken as established when the temperatures, as measured from the atomic and molecular spectra, were equal. The times required to establish equilibrium turned out to be of the order of 20–25 microsec.

**Enhancement of the Sensitivity of the Optic-Acoustic Method of Gas Analysis by Using Cells With Multiple Passage of Radiation,** by Ia. I. Gerlovich and P. V. Slobodskaia, vol. 7, no. 1, July 1959, pp. 63–67.

*Abstract:* A method is described for enhancing the sensitivity of an optic-acoustic gas analyzer, based on using cells with multiple passage of radiation. Dependence of the signal developed by the receiver on the effective thickness of the absorbing layer of gas in the cells is examined. It is shown that increase in sensitivity of the gas analyzer depends on the reflection coefficient of the mirror and astigmatism of the pencils of radiation. Relations are obtained which enable one to determine the optimum number of passages. The dependence of the sensitivity of a gas analyzer on the amount of gas being determined in the comparison cell is established.

**Isotope Shift in the Uranium Spectrum,** by L. A. Korostyleva and G. A. Striganova, vol. 7, no. 2, Aug. 1959, pp. 89–90.

*Abstract:* A Fabry-Perot interferometer was used to study the isotope shift in the uranium spectrum. The shift was measured for 46 lines in the visible region of the spectrum. New data were

obtained on isotope shift in terms and on preliminary classification of uranium spectral lines.

**Influences on the Intensities of Spectral Lines in Flame Spectra,** by N. S. Tskhai and S. L. Mandel'shtam, vol. 7, no. 2, Aug. 1959, pp. 91–96.

*Abstract:* The causes of changes, observed in the practice of spectral analysis, in the intensities of spectral lines in the flame spectra of elements with changes in the form of compounds in which the elements are introduced to the flame, and with the introduction of additional compounds, have been investigated. The concentrations of Na and Sr atoms in the region of the flame and the temperature of the flame were measured; it was established that the observed changes of line intensities were caused by the joint action of the change in concentration of the atoms of the elements in the flame region as a consequence of the change of entrance speed of the solution into the flame, and of the change in the state of excitation of the atoms as a consequence of a change in the flame temperature.

**Investigation of the Temperature Dependence of the Intensity of Infrared Absorption Bands of Gases,** by V. N. Smirnov and P. A. Bazhulin, vol. 7, no. 2, Aug. 1959, pp. 123–127.

*Abstract:* Quantitative measurements of the intensity of infrared absorption bands of a series of substances in the gaseous phase were carried out at various temperatures. It was found that most of the bands show an increase in intensity with a rise in temperature. The effect of the gas pressure on the intensity of the infrared absorption was investigated. A discussion of the results obtained is given.

**Luminescence and Vavilov-Cherenkov Radiation in Solutions Bombarded by Gamma Rays,** by Z. A. Chizhikova, vol. 7, no. 2, Aug. 1959, pp. 141–145.

*Abstract:* The gamma luminescence is investigated of solutions in which energy transfer from the solvent to the solute does not exist. In such solutions the luminescence intensity is comparable to the Vavilov-Cherenkov radiation intensity. Vavilov-Cherenkov radiation was used as a standard to determine the luminescence excitation efficiency $\rho$ during bombardment by high speed electrons. The average value of $\rho$ is 3.9 $\pm$ 0.5 per cent for the solutions investigated.

**Infrared Absorption of Thin Films of Tin Dioxide,** by V. K. Miloslavskii, vol. 7, no. 2, Aug. 1959, pp. 154–156.

*Abstract:* The optical and electrical properties of thin films of tin dioxide have been investigated. Transmission and absorption in the 1–18$\mu$ range were measured, as well as the temperature dependence of these quantities between $-150$ and $+200$ C. The effects of various impurities were studied.

**On the Role of the Angle of Light Incidence in Observation of the Ultraviolet Minimum of Silver Reflectance,** by G. P. Skornikov and I. I. Sasovskaia, vol. 7, no. 2, Aug. 1959, p. 157.

*Introduction:* One of the singular features of metals is the dependence of their optical parameters on the angle of incidence. This is stated by Ketelaar's formulas, and is confirmed by experiment. In the light of these features it is of interest to trace the angular dependence of silver reflectance in the region of the ultraviolet minimum, where reflection attains a value characteristic of dielectrics. Here we may expect a change in the amount of reflection in the region of the minimum, but it is difficult to predetermine the tendency of the points of the minimum to shift on the wavelength scale.

**Investigation of Infrared Absorption Spectra of Hydrocarbons at Various Temperatures in the Liquid and Solid Phases,** by K. H. Kesler, Iu. A. Pentin, E. G. Treshchova and V. M. Tatevskii, vol. 7, no. 3, Sept. 1959, pp. 195–200.

*Abstract:* The infrared absorption spectra of a series of hydrocarbons were studied at room temperature in the liquid phase and at low temperatures (down to $-172$ C) in the solid phase in order to ascertain the changes which take place in the sectra in the transition from the liquid to the solid. From a study of these changes conclusions could be reached concerning the presence or absence of rotational isomers in each of the phases and concerning the change of concentration of rotational isomers with temperature.

*Conclusions:*

1 Infrared absorption spectra were obtained in the region $\sim$700–1800 cm$^{-1}$ at room temperature and at low temperatures (down to $-172$ C) for n-heptane; n-octane; 3-methylheptane; 2,3-dimethylheptane; 2-methylheptene-2; 3,3-dimethylheptene-1; 2,2,5,5-tetramethylhexane; 2,4-dimethylpentane; 2,5-dimethylhexane; the spectra of five of these were observed for the first time.

2 It was found that for 2,4-dimethylpentane and 2,5-dimethylhexane changes take place in the spectrum of the crystalline phase, which indicate that in this phase there is a smaller number of rotational isomers present than in the liquid phase; probably only the single isomer with the highest symmetry is present.

3 The different behavior of the hydrocarbons on solidification is discussed from the point of view of the possible rotational isomers. The suggestion is made that crystallization is possible for those substances for which, among the possible rotational isomers, there is one with an adequately high degree of symmetry; this isomer possesses an advantage over the others in the sense that it is able to form a regular molecular crystalline lattice.

**Optical Characteristics of Water and Ice in the Infrared and Radio Wave Regions of the Spectrum,** by L. D. Kislovskii, vol. 7, no. 3, Sept. 1959, pp. 201–206.

*Abstract:* Values of the optical constants of water and ice have been calculated on the basis of a method proposed by the author for a broad range of the infrared and radio frequency spectrum. Certain earlier well-known data and our own experimental data were employed for the calculations. The values of the optical constants which have been found are in satisfactory agreement with the experimental data available in the literature.

**Theory of the Linear Kerr Effect in the Region of Exciton Absorption of Light by Molecular Crystals,** by A. F. Lubchenko, vol. 7, no. 3, Sept. 1959, pp. 221–227.

*Abstract:* A theory is developed of the linear Kerr effect for molecular crystals in which excitons are formed when there is a weak coupling between exciton excitation and lattice vibrations and an arbitrary value of the absorption coefficient. Equations have been obtained which determine the propagation of light in the region of exciton absorption in a constant uniform external electric field; the third rank tensor has been calculated which specifies the optical anisotropy, and also the value of the double refraction for crystals of cubic and medium symmetry when light propagation is along the direction of the external electric field parallel to the axis of the highest order.

**Plastic Scintillators With Additions of Aryl Derivatives of 1,3,4-Oxadiazole,** by N. P. Shimanskaia, A. P. Kilimov, A. P. Grekov, L. M. Egupova and R. S. Azen, vol. 7, no. 3, Sept. 1959, pp. 239–241.

*Abstract:* The scintillation efficiency and luminescence and absorption spectra of solutions of eight 2,5-aryl derivatives of oxadiazole in polystyrene were measured. The data obtained were compared with that measured earlier for eight derivatives of oxadiazole. It was shown that, among the substituents examined, the biphenyl and 1-naphthyl groups have the most favorable effect on the scintillation efficiency. Estimation of the scintillation efficiency of polystyrene solutions, carried out by the method of Swank and Buck, shows that this characteristic of plastic scintillators is determined basically by the optical properties (absorption and luminescence spectra) of the monomer and additive used.

*Conclusions:*

1 Among derivatives of oxadiazole, the most suitable as scintillation additives in plastic scintillators are the following: BBD, $\alpha$N$\alpha$ND, MtPPD, $\alpha$NBD, $\alpha$NPD.

1) 2-phenyl-5-(1-naphthyl)-1,3,4-oxadiazole.
2) 2-(1-naphthyl)-5-(2-naphthyl)-1,3,4-oxadiazole.
3) 2-(4-biphenyl)-1,3,4-oxadiazole.
4) 2-(4-biphenyl)-5-(2-naphthyl)-1,3,4-oxadiazole.
5) 2-phenyl-5-(2-naphthyl)-1,3,4-oxadiazole.
6) 2,5-di-(4-methoxyphenyl)-1,3,4-oxadiazole.
7) 2-phenyl-5-(4-biphenyl)-1,3,4-oxadiazole.
8) 2-(1-naphthyl)-5(4-biphenyl)-1,3,4-oxadiazole.
9) 2,5-dibiphenyl-1,3,4-oxadiazole.

---

2 In the diarylsubstituted oxadiazole series, the derivatives with the best scintillation properties are those which contain 1-naphthyl or biphenyl groups.

3 Scintillation efficiency may be estimated (in relative units) for low concentrations on the basis of a method of Swank and Buck, in which calculation the overlapping of the luminescent

spectrum of the host and the absorption spectrum of the additive is taken into account, as well as the yield of photoluminescence of the additive and the sensitivity of the FEU phototube to the luminescence of the additive.

4 Scintillation efficiency of organic materials in plastic solutions is determined basically by three characteristics: a) absorption spectrum, b) luminescence spectrum, c) luminescence yield.

**On the Possibility of Resolving Two Light Sources of Sharply Differing Intensities,** by A. N. Riazanov, vol. 7, no. 3, Sept. 1959, pp. 269–270.

*Introduction:* Numerous recent reports have discussed the possibility of increasing the resolving power of optical systems by narrowing the central diffraction maximum and moving aside the satellites. These reports discuss resolving two point sources whose intensities are of the same order of magnitude. The problem of resolving two light sources of sharply differing intensities has its own specific peculiarities. It is well known that diffraction from the aperture of an objective gives a central maximum, surrounded by weaker secondary maxima whose intensities, with a slit objective, are 0.047, 0.017, 0.008, etc., times the intensity of the central maximum. If the difference in intensity of two point sources is of the same order as the intensity difference between the zero and first-order maxima, then such sources are impossible to resolve with the use of the usual uniform objective, even if the angular distance between them is somewhat larger than is required by the Rayleigh criterion. Consequently, for the resolution of two such light sources it is necessary to reduce the background around the zero order maximum. It is possible to achieve this at the price of some broadening of the central maximum.

**The Classification of Secondary Radiation,** by B. I. Stepanov and P. A. Apanasevich, vol. 7, no. 4, Oct. 1959, pp. 285–289.

*Abstract:* A quantum-electrodynamical analysis of the transformation of light by matter yields a systematic classification of secondary radiation, justifying its division into scattering or photoluminescence, depending on the absence or presence of intermediate processes between the disappearance and appearance of photons. The limits of adapting the criteria for duration and decay suggested by Vavilov are clarified.

**Dependence of the Intensity of Some Helium Lines on Pressure,** by V. E. Yakhontova and M. I. Kliot-Dashinskii, vol. 7, no. 4, Oct. 1959, pp. 290–293.

*Abstract:* The pressure dependence of the intensity of the 5016 and 3965 Å lines of helium in a discharge tube is examined theoretically. It is shown that, in the general case, the emission intensity and the gas pressure are related by a nonlinear expression which depends upon the existence in the discharge of self-absorption effects. It is shown that the theoretical relationships obtained are in quantitative agreement with the experimental results.

**On the Temperature Dependence of the Intensities of Vibrational Absorption Bands of Gases in the Case of Fermi Resonance,** by M. P. Lisitsa and V. L. Strizhevskii, vol. 7, no. 4, Oct. 1959, pp. 305–307.

*Abstract:* The question of the temperature dependence of the intensities of vibrational absorption bands in the presence of resonance interaction of energy levels has been considered. It has been shown that the theory developed leads to conclusions which agree satisfactorily with experiment.

**Optical Properties of Metal Films in the Region of Anomalous Skin Effect,** by Van-Si-Fu, V. P. Silin and E. P. Fetisov, vol. 7, no. 4, Oct. 1959, pp. 339–341.

*Abstract:* The optical properties of conducting films are considered for the case in which losses due to diffusion scattering of electrons at the surface of the conductor are not negligible.

**Thin Film Optics. V. The Properties of Silicon,** by M. P. Lisitsa and N. G. Tsvelykh, vol. 7, no. 4, Oct. 1959, pp. 341–344.

*Abstract:* The coefficients $T$, $R$ and $R'$ were measured for amorphous layers of silicon of thicknesses $0 < d < 1200$ Å, and for four wave lengths in the visible spectrum. On the basis of the experimental data, curves were plotted of the dependence of the fractional absorption of light on the film thickness. The index of refraction was calculated for the thicker films. The question of aging was also partially studied.

**The Vernier Effect in the Interferometric Measurement of the Thickness of Thick Layers,** by I. N. Shklyarevskii, E. T. Verkhovtseva and G. N. Polyakova, vol. 7, no. 4, Oct. 1959, pp. 349–350.

**Effect of Foreign Gases on the Absorption of Infrared Radiation by Water Vapors in the Region of an Individual Line in Band 2.7μ,** by K. P. Vasilevsky and B. S. Neporent, vol. 7, no. 4, Oct. 1959, pp. 353–354.

*Introduction:* The investigation of the effect of foreign gases on the integral absorption was carried out by us for an individual line of water vapor at 4025 $cm^{-1}$ (transition $v_3'' = 0$, $J'' = 5_{-5}$, $v_3' = 1$, $J' = 6_{-2}$). The dependence of the absorption in this line on the natural concentration of water vapor and on the length of path has been previously investigated by us, and it was found that under the given experimental conditions the line absorption is accurately represented by the equations given by Laudenburg and Reiche for lines of dispersion form; i.e., the integral absorption $A$ is equal to $A = \int [1 - (I/I_0)]d\nu = 2\sqrt{S\gamma l}$ for $x = Sl/2\pi\gamma \gg 1$.

**Registration of Spectra of the Aurora Borealis by Means of a Recording Spectrometer,** by I. G. Frishman, vol. 7, no. 4, Oct. 1959, pp. 354–355.

**Selective Modulation of Radiation by Periodical Variation of Gas Temperature,** by A. O. Sall', vol. 7, no. 4, Oct. 1959, pp. 355–356.

**Laws of the Absorption of Infrared Radiation in Thin Layers of Some Gases I. Coefficient of Absorption in Vibration-Rotation Bands,** by P. I. Bresler, vol. 7, no. 5, Nov. 1959, pp. 371–375.

*Abstract:* The laws of absorption of infrared radiation in gases for thicknesses of layers, which are generally dealt with in infrared absorption instruments, are examined. Approximate formulas for the determination of the coefficient of absorption and of the absorbed radiation in vibration-rotation bands of diatomic and some more complicated molecules are investigated.

**Laws of the Absorption of Infrared Radiation in Thin Layers of Some Gases II. Absorption of Radiation in the Vibration-Rotation Bands of Some Gases,** by P. I. Bresler, vol. 7, no. 5, Nov. 1959, pp. 375–377.

*Abstract:* Formulas are obtained connecting the intensity of radiation absorbed by a relatively thin layer of a gas, with the parameters of the particular vibration-rotation band of the gas. The limits of the application of the laws of the linear and of the quadratic roots of the absorption are determined.

**The Absorption Spectrum of Liquid and Solid Oxygen Under Pressure (12,600–3000 Å),** by V. I. Dianov-Klokov, vol. 7, no. 5, Nov. 1959, pp. 377–380.

*Abstract:* Measurements were made of the intensity of the absorption spectrum of condensed oxygen at $T = 86$ K and at densities from $\rho = 1.16$ gm/cm³ to $\rho = 1.6$ gm/cm³ (pressures up to 8000 atm). It was found that the dependence of the absorption intensity on $\rho$ is not the same for different groups of bands and is always high; for example, for wave length 6290 Å, $\epsilon_m \sim \rho^{4.9}$ in the region of the existence of a liquid phase. From the curve $\epsilon_m = f(\rho)$, an estimate was made of the change in volume for the transition, liquid $\rightarrow \gamma$ and $\gamma \rightarrow \beta$.

**The Long Wave Length Infrared Spectrum of $H_2O$ Vapor and the Absorption Spectrum of Atmospheric Air in the Region 20–2500μ (500–4cm$^{-1}$),** by N. G. Yaroslavsky and A. E. Stanevich, vol. 7, no. 5, Nov. 1959, pp. 380–382.

*Abstract:* The long wave length infrared (rotational) spectrum of $H_2O$ vapor in the region below 2500μ is discussed, as is the presence in the spectrum of an absorption band at 1634μ(6.12 $cm^{-1}$), corresponding to the rotational transistion $2_2 \rightarrow 3_{-2}$. Quantitative data are obtained concerning atmospheric room air in the region 20–2500 μ (500–4$cm^{-1}$) for a layer of air of thickness 10 m at a temperature of 20 C, pressure of 760 mm of mercury, and absolute humidity of 10.5 gm/m³.

**Determination of Spectrum Color Coordinates for 27 Normal Observers,** by N. I. Speranskaya, vol. 7, no. 5, Nov. 1959, pp. 424–428.

*Abstract:* The color coordinates of the spectrum were determined on the basis of purely colorimetric correlations with energy measurements for 27 normal observers with a visual field of 10 deg. It was shown that the results obtained as a whole agreed satisfactorily with the measurements of Stiles for a group of 50 observers, in spite of considerable difference in experimental conditions. The data obtained, together with those of Stiles,

were arranged basically in a table of values of the color coordinates of a spectrum with uniform energy distribution, presented for acceptance at the sessions of the International Illumination Commission (Brussels, 1959).

## *PROBLEMS OF CYBERNETICS* (*Problemy Kibernetiki*). Published by Pergamon Institute, N. Y.

**Certain General Problems in Cybernetics,** by A. A. Lyapunov, vol. 1, 1960, pp. 1–21.

**The Logical Structure of Programs,** by A. A. Lyapunov, vol. 1, 1960, pp. 48–81.

*Introduction:* In recent years the automatic high speed digital computer has undergone rapid development. These machines make it possible to change the nature of a computer service fundamentally. If, earlier, calculations involving a million arithmetic operations verged on the possible, today, with the help of computers, we can often solve problems requiring billions of arithmetic operations. The appearance of such machines produced a large number of new mathematical questions and new fields of mathematics. On the one hand, much new work has resulted in the field of computing methods; on the other, the necessity of developing the theory of applied algorithms, i.e., of rational methods of constructing programs for the solution of various problems with computers, has arisen. This subject has been given the name of programing. The aim of this article is to describe the logical principles of programing.

**The Logical Schemes of Algorithms,** by Yu. I. Yanov, vol. 1, 1960, pp. 82–140.

**Automatic Programing With a Programing Program,** by S. S. Kamynin, E. Z. Lyubimskii and M. R. Shura-Bura, vol. 1, 1960, pp. 149–191.

**Electronic Digital Computer TSEM-1,** by G. A. Mikhailov, B. I. Shitikov and N. A. Yavlinskii, vol. 1, 1960, pp. 214–227.

*Introduction:* There is an acute need for machines of medium size in addition to the large calculating machines necessary for computing centers. The price and running costs of these machines are nine to ten times less than the price of larger machines, and their technical specifications completely satisfy the requirements of scientific research institutes and design organizations. A machine of this class, the M-2 of the Control Mechanism Laboratory of the Academy of Sciences, is built according to the parallel principle (L 1), and the series machine *Ural* uses a magnetic drum (L 2) for high speed storage. The machine described in the present article is of the series type and has a fast-storage unit based on ultrasonic delay lines.

**A Method of Determining Grammatical Concepts on the Basis of Group Theory,** by O. S. Kulagina, vol. 1, 1960, pp. 228–242.

**Questions Involved in Distinguishing Homonyms When Translating from English Into Russian Using a Computer,** by T. N. Moloshnaya, vol. 1, 1960, pp. 243–250.

**Machine Translation From Hungarian to Russian,** by I. A. Mel'chuk, vol. 1, 1960, pp. 251–293.

## *RUSSIAN JOURNAL OF PHYSICAL CHEMISTRY* (*Zhurnal Fizicheskoi Khimii*).[1] Published by The Chemical Society, London.

**Reaction Kinetics of Peroxides in Solution. II. Kinetics of the Reaction Between Benzoyl Peroxide and Diphenylamine,** by O. A. Chaltykyan, E. N. Anatasyan, N. M. Beileryan and G. A. Marmaryan, no. 1, pp. 36–44.

**Effect of Ozone on Hydrocarbon Combustion. II. Ignition of Butylene With Oxygen,** by N. A. Slavinskaya, S. A. Kamenetskaya and S. Ya. Pshezhetskii, no. 1, pp. 45–49.

**Effect of Ozone on the Ignition of Hydrocarbons. III. Ignition of Cyclohexane With Oxygen,** by N. A. Slavinskaya, S. A. Kamenetskaya and S. Ya. Pshezhetskii, no. 2, pp. 271–275.

*Abstract:* A study has been made of the critical conditions for the ignition of cyclohexane with oxygen in a heated vessel. Ozone lowers the ignition temperature and the lower limit of cyclohexane pressure, and eliminates the induction period. These results conform with Semenov's heat ignition theory. It has been shown by calculation that ozone lowers the effective activation energy from 43 kcal to 9.2 kcal for mixtures containing 13.2 per cent ozone. The effect of ozone on the ignition of cyclohexane is similar to that of the ignition of butane, but is weaker than on the ignition of butylene.

**The Entropy of Gaseous Monatomic Ions,** by V. P. Vasil'ev, E. K. Zolotarev and K. B. Yatsimirskii, no. 2, pp. 328–330.

*Abstract:* Employing statistical thermodynamic equations, the entropies of ions in the gaseous state under standard conditions have been calculated.

**The Formation of Nitrogen Oxides in the Shock Wave of a Strong Explosion in Air,** by Yu. P. Raizer, no. 3, pp. 700–709.

*Abstract:* The kinetics of the formation of the nitrogen oxides NO and $NO_2$ are examined, and their distribution in air caught in a strong shock wave is calculated. An estimate is made of the total nitrogen oxidized during the strong explosion. It has been shown that the nitrogen oxide does not form in wave fronts with temperatures below 2000 deg. The basic mechanism in the formation of the dioxide at temperatures above 2000 deg has been shown to be the process $NO + O_2 = NO_2 + O$, and the rate of this reaction has been calculated with the aid of the activated complex method. The investigation was necessary to explain a number of optical phenomena observed in a strong explosion: Glow of the shock wave at temperatures 2000–7000 deg, the breaking away of the wave front from the fire ball and the characteristic intensity minimum of the latter. An interpretation of these effects has been given by the author in another report (*Zhur. Eksper. Teor. Fiz.*, vol. 34, 1958, p. 483).

**The Rate of Burning of Atomized Fuel in a Turbulent Flow,** by V. Ya. Basevich, no. 5, pp. 1080–1086.

*Abstract:* In a study of the burning of atomized fuel in a turbulent flow the rate constants of the process have been determined. The theoretical ratio between the rate of burning of the drops and the vapor phase of the fuel in the case of a noncombustible composition of the latter, has been checked. The minimum critical diameter of the drops, which under conditions of turbulent flow limits the diffusion region of combustion, has been established.

**Kinetic Analysis of Chain Reactions. V. New Solutions of the Basic Equations for the Chain Reaction Kinetics Involving Two Active Particles,** by S. S. Vasil'ev, no. 5, pp. 1100–1110.

*Abstract:* New solutions for the basic differential equations of chain reaction kinetics for the case of two active particles made it possible to obtain formulas that show directly how the values of the generalized rate constants of the initial kinetic equations, of the rates of the spontaneous formation of active particles, and of the initial concentration of these particles, affect the kinetic development of chain reactions. Analysis of the formulas obtained shows that this investigation has made possible the more precise statement of a number of principles in the theory of chain reactions that up till now have not been quite clear. Thus additional clarification has been made of the conditions of the "lower limit" of development of a chain reaction. Conditions have been indicated when a branching chain reaction in the course of its development may lead to a steady-state concentration of active particles.

**Studies on the Thermodynamic Properties of Binary Metallic Systems by the EMF Method. V. The Copper-Bismuth System,** by A. V. Nikol'skaya, A. L. Lomov and Ya. I. Gerasimov, no. 5, pp. 1134–1139.

*Abstract:* The thermodynamic properties of the copper-bismuth system in the liquid state have been studied by the emf method. The emf of the concentration cell $^{-}Cu_s/CuCl, KCl\text{–}NaCl|(Cu_NBi_{1-N})_{liq}{}^{+}$ with the mole fraction of copper in the melts 0.063–0.710 has been measured over the temperature range 1150–1225 K. From the emf's the activity coefficients of copper were calculated for 1150, 1175, 1200 and 1225 K. The following thermodynamic properties at 1200 K have been calculated for both components: Activity coefficients, partial and integral heats of mixing, and the excess entropy of mixing. The properties of the system are characterized by large positive deviations from Raoult's law ($\gamma$ = 1.2–3.0). Copper-bismuth

[1] Most of the following material is taken from a series of abstracts covering vol. 33, nos. 1–6 (Jan.–June 1959). The cover-to-cover translation program began with no. 7 (July 1959).

melts are formed with the absorption of heat: $\Delta H_{max} = 1600$ cal/g-at. The entropy of mixing is considerably larger than the ideal value $\Delta S_{exc}$ lying within the limits of 0.3–0.7 cal/deg g-at. Curves depicting the heats and entropies of mixing as functions of the composition of the melts exhibit segments with small changes in $\Delta H$ and particularly in $\Delta S_{exc}$. These occur at mole fractions of Cu 0.3–0.7. It is suggested that the effect is associated with the microheterogeneous structure of the melts.

**Wetting of Refractory Oxides by Liquid Metals,** by V. N. Eremenko and Yu. V. Naidich, no. 6, pp. 1238–1245.

*Abstract:* It has been demonstrated that the wettability of oxides increases with electrical conductivity. A correlation has been found between the electrical conductivity and thermodynamic stability (heat of formation). The contact angle of liquid metal on the oxide surface has been calculated and compared with the experimental value. The study was carried out in a specially designed vacuum apparatus.

**Liquid-Vapor Equilibria in Three-Component Systems,** by V. B. Kogan and V. M. Safronov, no. 6, pp. 1353–1359.

*Abstract:* A graphical-analytical method of calculating liquid-vapor equilibrium data in three-component systems from those for two-component systems has been proposed; it is based on the application of the equation

$$\log\left(\frac{\gamma_1}{\gamma_2}\right)_{av} = \int_0^1 \log\frac{\gamma_1}{\gamma_2}\,dX_1' = \frac{Q_{13} - Q_{23}}{1 - X_3}$$

derived in a previous communication (*Zhur. Fiz. Khim.*, vol. 32, 1958, p. 1095).

**Electrical Conductivity of Silica Films on Glass,** by A. Ya. Kuznetsov, no. 6, pp. 1374–1377.

*Abstract:* The electrical conductivity of silica films on glass in a humid atmosphere is due to the adsorbed water in the film pores. Filling of the pores increases the conductivity of the water by one or two magnitudes, owing to the appearance of additional capillary superconductivity. In time cations diffuse into the film from the underlying layers of glass and the conductivity increases further. The diffusion processes eventually come to a stop, however, and the surface conductivity of the glass assumes a constant value for a given humidity and temperature.

**Thermodynamics of Superstates (Short Communication),** by V. K. Semenchenko, no. 6, pp. 1440–1445.

*Abstract:* Superconductivity and superfluidity of materials at low temperatures are considered as basically similar thermodynamic properties, arising from the existence of truly reversible processes with finite velocities. The possible existence of other superstates is discussed.

**Calculation of Ionization Potentials,** by A. Ya. Lisyutin, no. 7, pp. 97–98.

*Summary:* It is shown that out of the four empirical equations for calculating ionization potentials, considered by Nemtsev as independent in terms of independent parameters, three may be derived from the remaining one. This points to a functional interdependence of the parameters used by Nemtsev.

**The Effect of Intramolecular Interaction on Molecular Refraction,** by N. N. Tyutyulkov, no. 7, pp. 98–99.

*Introduction:* The refraction $R$ of many organic molecules can be represented by the sum of the refractions $R_i$ of the individual bonds. In cases where deviations from additivity are observed, for example for molecules with conjugate bonds, it is necessary to introduce an increment $\Delta R$ specific to this deviation. In the present work the effect of the interaction of conjugate bonds of the refraction is investigated with the aid of an oscillatory model; for this purpose it is assumed that the interaction of the bonds can be approximately treated as the interaction of harmonic oscillators. A similar model was discussed from a somewhat different point of view in the work of Kuhn and in the monograph by Vol'kenshtein et al.

**The Variation of the Shape of the Electron Paramagnetic Resonance Spectrum With Temperature in Peroxide-Type Radicals,** by Yu. N. Molin and Yu. D. Tsvetkov, no. 7, pp. 102–104.

*Introduction:* The electron paramagnetic resonance (EPR) spectrum of Teflon has been investigated. It was shown that under the action of oxygen the radicals

$$\sim\!\!\sim CF_2—\dot{C}F—CF_2\sim\!\!\sim \qquad [1]$$

initially formed are changed into peroxide-type radicals

$$\sim\!\!\sim CF_2—\underset{\displaystyle |}{\overset{\displaystyle O—\dot{O}}{CF}}—CF_2\sim\!\!\sim \qquad [2]$$

The electron paramagnetic resonance spectrum of radical [2] is an asymmetric line and has no hyperfine structure, whose absence is due to the fact that the unpaired electron is localized mainly on the oxygen atoms, the nuclei of which do not have a magnetic moment.

## *SOVIET PHYSICS-JETP (Zhurnal Eksperimental, noi i Teoreticheskoi Fiziki).* Published by American Institute of Physics, Inc., N. Y.

**Reflection of Electromagnetic Waves From a Plasma Moving in Slow Wave Guides,** by O. G. Zagorodnov, Ya. B. Faĭnberg and A. M. Egorov, vol. 11, no. 1, July 1960, pp. 4–5.

*Abstract:* Electromagnetic wave reflections from a moving plasma were investigated experimentally. It was found that when the wave was greatly slowed down [(1/200)–(1/375)c] the double Doppler effect observed in reflection increased the frequency by 11–20 per cent. The measurements were carried out at 24.75 mc/s. The slow wave structure was a helix. The possibility is indicated of using this effect to amplify microwaves and to multiply their frequencies, to improve the dynamic stability of the plasma, and to perform measurements in plasma.

**Electrical Conductivy of Dielectrics in Strong Shock Waves,** by A. A. Brish, M. S. Tarasov and V. A. Tsukerman, vol. 11, no. 1, July 1960, pp. 15–17.

*Abstract:* The electrical conductivity of air, water and certain solid dielectrics subjected to strong shock waves has been measured by an electrical contact method. The measured values of the specific conductivity in the shock front are as follows: Air, 0.5 $\Omega^{-1}$ cm$^{-1}$; water, 0.2 $\Omega^{-1}$ cm$^{-1}$. At shock front pressures of approximately $1 \times 10^6$ kg/km$^2$ it is found that the electrical conductivity of Plexiglas or paraffin reaches 1 to $2 \times 10^2$ $\Omega^{-1}$ cm$^{-1}$, a value which approximates the conductivity of a metal.

**Influence of the Medium Density on Bremsstrahlung in Electron-Photon Showers in the Energy Range $10^{11}$–$10^{13}$ ev,** by A. A. Varfolomeev, R. I. Gerasimova, I. I. Gurevich, L. A. Makar'ina, A. S. Romantseva and S. A. Chueva, vol. 11, no.1, July 1960, pp. 23–32.

*Abstract:* Fifteen electron-photon showers in the energy range $10^{11}$–$10^{13}$ ev recorded in emulsion stacks were examined. The energies of the primary $\gamma$ rays initiating the showers were determined by measuring the energy spectrum of cascade electrons at the depth of 2.5–3 radiation units, and from the screening effect on the first pairs. The energy spectrum of pairs produced at a depth of up to 1.5 radiation units was measured. The results are in agreement with calculations carried out taking into account the influence of multiple scattering and of the polarization of the medium on the bremsstrahlung of high energy electrons.

**Ultra-High Energy Extensive Air Showers,** by A. T. Abrosimov, G. A. Bazilevskaya, V. I. Solov'eva and G. B. Khristiansen, vol. 11, no. 1, July 1960, pp. 74–79.

*Abstract:* Extensive air showers having from $5 \times 10^6$ to $10^8$ particles were investigated. Data are presented on the absolute shower intensity, the value spectrum exponent and on the lateral distributions of the electron-photon component and of the $\mu$ mesons of these showers. Data on the electron-photon component indicate either that there is no equilibrium between the electron-photon and the nuclear components in ultra-high energy showers in the lower layers of the atmosphere, or that the lateral distribution of the electrons on the periphery of the shower is determined not only by the coulomb scattering, but also by the particle angular divergence in the elementary nuclear cascade events.

**Comparison of Different Coordinate Conditions in Einstein's Gravitation Theory,** by V. A. Fock, vol. 11, no. 1, July 1960, pp. 80–84.

*Abstract:* In this paper it is shown that the first-order co-

ordinate conditions actually used by Einstein and Infeld in the problem of the motion of masses coincide with the harmonic ones and define a coordinate system in this order of approximation up to a Lorentz transformation. The difference between the Einstein-Infeld and the harmonic coordinate systems is characterized by the order of smallness of admissible non-Lorentz transformations. These differences may be found explicitly. They are so small that they cannot affect the form of the equations of motion in the first post-Newtonian approximation. On the basis of the results obtained a criticism is given on the general attitude of Einstein and Infeld to the problem of coordinates.

**Space and Time Reflections in Relativistic Theory,** by Yu. M. Shirokov, vol. 11, no. 1, July 1960, pp. 101–108.

*Abstract:* A complete classification has been obtained for the representations of the inhomogeneous Lorentz group, including space reflections and time reflections of the Wigner type. The question of the values of the squares of the various reflection operations for particles of half-integral spin is investigated in detail. The results are compared with those which are obtained when additional requirements are imposed on the theory, in particular the requirement of locality of the field operators. It is shown that, in addition to mass, spin and parity, elementary particles have still another purely geometrical characteristic, which might be called the symmetry type. The question of the symmetry type for real particles is discussed.

**Some General Relations in Statistical Quantum Electrodynamics,** by E. S. Fradkin, vol. 11, no. 1, July 1960, pp. 114–116.

*Abstract:* A number of general relations associated with the gage invariance of quantum electrodynamics are obtained.

**Possible Transmission of Electromagnetic Waves Through a Metal in a Strong Magnetic Field,** by O. V. Konstantinov and V. I. Perel', vol. 11, no. 1, July 1960, pp. 117–119.

*Abstract:* It is shown that an electromagnetic wave propagating along a magnetic field can penetrate a metal plate perpendicular to the field if the Larmor frequency is higher than the frequency of the propagating wave and much higher than the collision frequency, and if the electron Larmor radius is smaller than the wave length in the metal.

**Damping of Oscillations of a Disk in Rotating Helium II,** by Yu. G. Mamaladze and S. G. Matinyan, vol. 11, no. 1, July 1960, pp. 134–136.

*Abstract:* The interaction of an oscillating disk with rotating helium II is examined. An expression is obtained for the torsional moment acting on the surface of the disk, taking into account the presence of vortex lines, mutual friction between the normal and superfluid components, and the possibility of sliding of the vortex lines along the solid surface. A calculation of the damping of oscillations, which neglects sliding and is in linear approximation with respect to the mutual friction coefficients, is in qualitative agreement with the experimental data. It seems that quantitative agreement can only be obtained if sliding is taken into account.

**Effect of Conductivity Anisotropy in a Magnetic Field on the Structure of a Shock Wave in Magnetogasdynamics,** by S. A. Kaplan, vol. 11, no. 1, July 1960, p. 183.

**Isothermal Discontinuities in Magnetohydrodynamics,** by V. I. Tseplyaev, vol. 11, no. 1, July 1960, pp. 185–186.

**Number of Extensive Atmospheric Showers of Cosmic Rays Near Sea Level,** by S. I. Mishnev and S. I. Nikol'skii, vol. 11, no. 1, July 1960, pp. 186–187.

**Lateral Distribution Function of the Flux of Charged Particles in an Individual Extensive Atmospheric Shower,** by S. N. Vernov, N. N. Goryunov, V. A. Dmitriev, G. V. Kulikov, Yu. A. Nechin and G. B. Khristiansen, vol. 11, no. 1, July 1960, pp. 215–216.

**Several Possible Applications for the Resonant Scattering of Gamma Rays,** by I. Ya. Barit, M. I. Podgoretskii and F. L. Shapiro, vol. 11, no. 1, July 1960, pp. 218–219.

**On Gage Transformations in Quantum Electrodynamics,** by Yu. A. Gol'fand, vol. 11, no. 1, July 1960, pp. 223–224.

## *SOVIET PHYSICS-SOLID STATE* (*Fizika Tverdogo Tela*). Published by American Institute of Physics, Inc., N. Y.

**The Relationship Between Excess Noise in Germanium and Surface Traps,** by L. S. Sochava and D. N. Mirlin, vol. 2, no. 1, July 1960, pp. 18–20.

*Introduction:* According to McWhorter, "excess" noise in germanium is due to fluctuations in the extent to which surface traps are filled ("slow states"). In order to explain the noise spectrum, it is assumed that the relaxation time of the traps $\tau$ is distributed according to a $1/\tau$ law over a wide interval of time. This type of distribution function leads to the experimentally observed excess-noise spectrum. This model is supported by the experimental data of Kingston and McWhorter, who showed that the behavior of the field-effect frequency characteristics can be explained by the presence at the germanium surface of traps with relaxation times distributed in accordance with a law close to $1/\tau$ over a time interval from $10^{-3}$ to $10^{3}$ sec. In order to test the McWhorter model, we have compared the forms of the field effect frequency characteristics and the excess-noise spectrum for the same specimens.

**Thermal Expansion of Germanium at Low Temperatures,** by S. I. Novikova, vol. 2, no. 1, July 1960, pp. 37–38.

*Introduction:* The thermal expansion coefficient of silicon becomes negative at low temperatures. To elucidate the nature of this anomalous dependence of $\alpha$ on temperature, it would be desirable to know the behavior of the thermal expansion coefficient in substances similar to silicon in their physical and

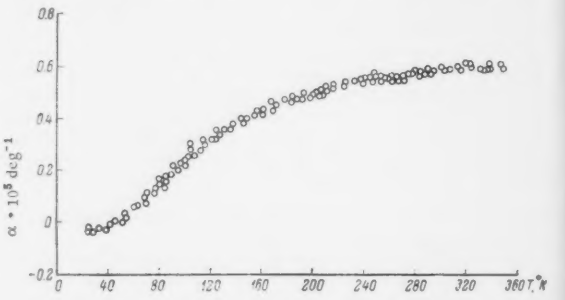


Fig. 1. The thermal expansion coefficient of germanium. Experimental values.

crystallographic properties. Such a substance is germanium, which is a semiconductor crystallizing out with the diamond-type lattice. Measurements were carried out using a slightly improved form of a quartz dilatometer described earlier. The thermal expansion coefficient $\alpha$ was calculated directly from the experimental results; the temperature intervals in these measurements did not exceed 10 deg.

**Dispersion of Light in Germanium,** by M. I. Kornfeld', vol. 2, no. 1, July 1960, pp. 42–43.

*Introduction:* The dependence of the refractive index of germanium on the light wave length was investigated by Briggs over the range from 1.8 to 2.6$\mu$, and more accurately by Salzberg and Villa in the region from 2 to 16$\mu$. In both cases, the measurements were made at room temperature. The present note gives the results of an investigation of light dispersion in germanium in the shorter wave region from 1.5 to 2.2$\mu$, over a wide temperature range from 80 to 460 K.

**The Voltage Sensitivity of Hall-EMF Probes,** by V. V. Galavanov, vol. 2, no. 1, July 1960, pp. 55–57.

(*Continued from page 832*)

The increase in the slope of each axial wall temperature distribution is probably due to the increase in resistivity with temperature (the resistivity at 4000 R is twice that at 2000 R). The large axial temperature gradients at the entrance and exit of the test section are the result of conduction losses to the connecting flanges, mixing tanks and electrical connectors.

### Friction Coefficients

The average friction coefficients for both the adiabatic and heated runs are shown in Figs. 5 and 6. The line representing the Kármán-Nikuradse relation between friction coefficient and Reynolds number for turbulent flow

$$\frac{1}{\sqrt{8f/2}} = 2 \log \left( Re \sqrt{\frac{8f}{2}} \right) - 0.8 \qquad [6]$$

and the laminar flow line

$$\frac{f}{2} = \frac{8}{Re} \qquad [7]$$

are included for comparison.

For Reynolds numbers above 6000, the average friction coefficients for adiabatic flow are in very good agreement with the turbulent flow line. In the lower Reynolds number region the coefficients drop off and approach the laminar flow line, as would be expected in the transition region. The extension of the transition region to a Reynolds number of 6000 was due to the effect of the bellmouth entrance.

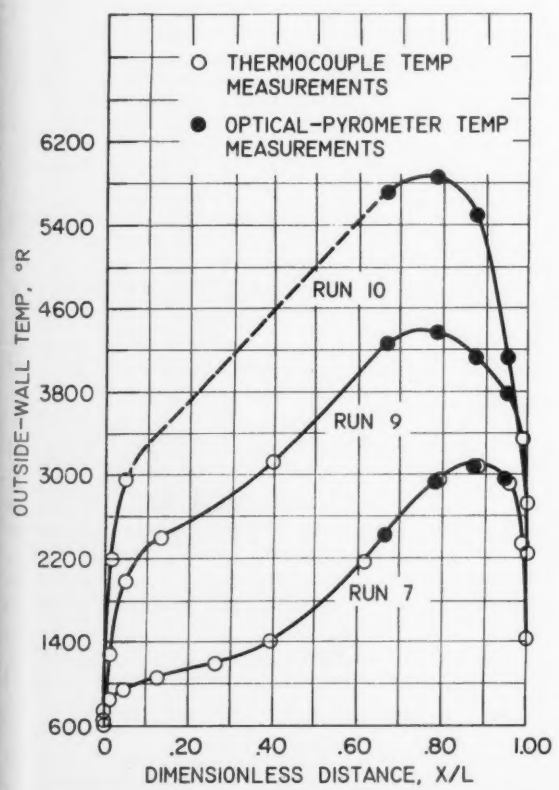


Fig. 4 **Representative outside wall temperature distribution for various amounts of heat input to helium. Tungsten tube; length-diameter ratio, 92**

The average friction coefficients with the density evaluated at bulk temperature (Eq. [2]) are shown in Fig. 5. The data from the present investigation are in fair agreement with the predicted line for the higher Reynolds number range.

In (1 and 7) it is indicated that average friction coefficients are best correlated with density evaluated at the film temperature and with a modified Reynolds number based on film temperature. Data from the present investigation and (7) are shown evaluated in this manner in Fig. 6. The friction coefficients are somewhat higher than the Kármán-Nikuradse line, but good agreement exists with the data of (7).

### Heat Transfer Coefficients

The results of (1) indicate that the average Nusselt number for various ratios of surface to bulk temperature and length to diameter is best represented by

$$(Nu_{av})_f = \frac{h_{av}D}{k_f} = 0.034\, Re_f^{0.8} Pr_f^{0.4} \left(\frac{L}{D}\right)^{-0.1} \qquad [8]$$

where all the physical properties and the density are evaluated at the film temperature, and the modified Reynolds number is used.

An alternative method of correcting for the effect of the length to diameter ratio is the use of the following equation

$$(Nu_{av})_f = \frac{h_{av}D}{k_f} = 0.021\, Re_f^{0.8} Pr_f^{0.4} \left[1 + \left(\frac{L}{D}\right)^{-0.7}\right] \qquad [9]$$

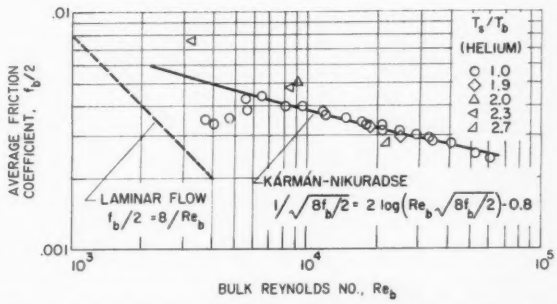


Fig. 5 **Correlation of average friction coefficients. Viscosity and density evaluated at bulk temperature $T_b$**

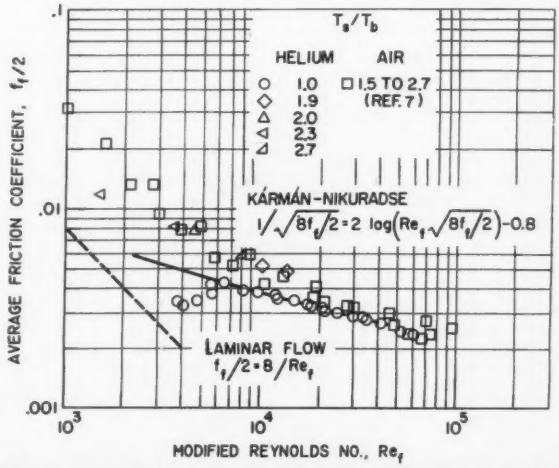


Fig. 6 **Correlation of average friction coefficients. Viscosity and density evaluated at film temperature $T_f$**

where the use of $[1 + (L/D)^{-0.7}]$ in place of $(L/D)^{-0.1}$, and the corresponding difference in constants, makes the relation more general, since it is applicable to all length-diameter ratios. The data of the present investigation with the properties evaluated at the film temperature are shown in Fig. 7 as a function of modified Reynolds number. For Reynolds numbers less than 10,000 the present data are in poor agreement with Equation [9]. Above a Reynolds number of 10,000 the data agree to within 10 per cent.

For the limited range of Reynolds number in this investigation, the average heat transfer data seem to be correlated better by evaluating the physical properties and density at the surface temperature. The results are shown in Fig. 8. Experimental data from (1) using air and a platinum test section at average tube surface temperatures from 980 to 3050 R are shown in both Figs. 7 and 8.

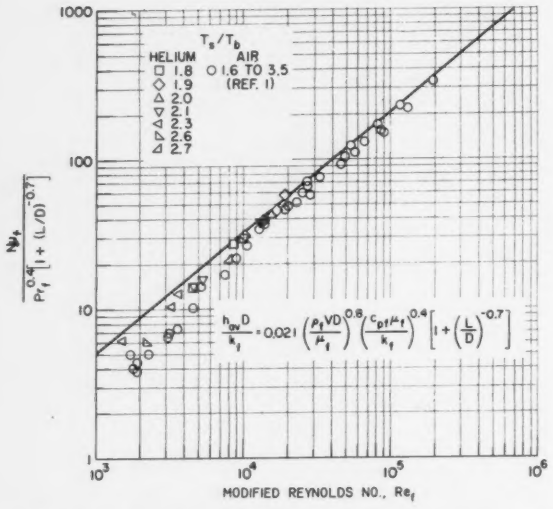


**Fig. 7 Correlation of average heat transfer coefficients with variable heat flux. Properties of helium evaluated at film temperature $T_f$**

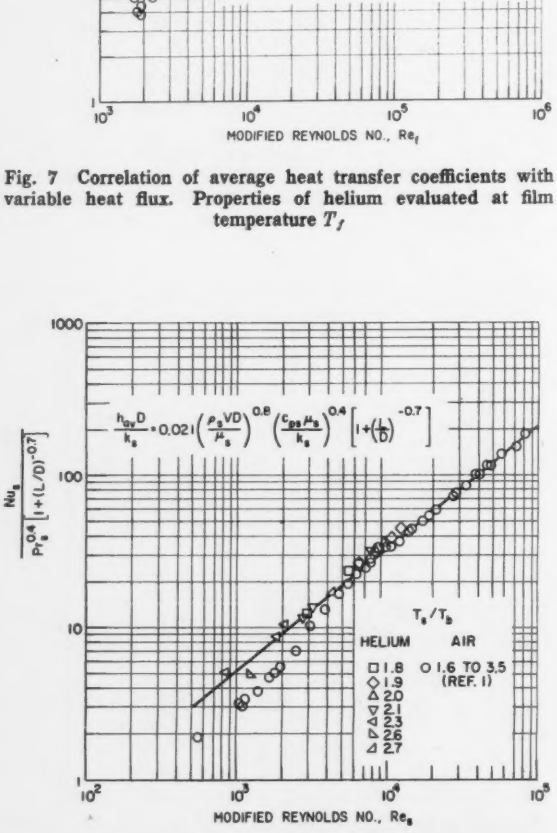


**Fig. 8 Correlation of average heat transfer coefficients with variable heat flux. Properties of helium evaluated at surface temperature $T_s$**

Since there could be some question as to the significance of average heat transfer coefficients when the heat flux varies as much as is indicated by the axial wall temperature distributions shown in Fig. 4, it seemed desirable to calculate local heat transfer coefficients. Ratios of local surface temperature to local bulk temperatures were considerably higher than ratios of the averages of these temperatures. Local heat transfer data are shown in Fig. 9, where the film Nusselt number is plotted as a function of modified Reynolds number. The data are in fair agreement with the line represented by the equation

$$Nu_f = hD/k_f = 0.021\ Re_f^{0.8} Pr_f^{0.4} \qquad [10]$$

The same data, shown in Fig. 10 with the physical properties and density evaluated at the surface temperature $T_s$, fall higher than the predicted line. However, the spread of the data is decreased from about 38 per cent in Fig. 9 to about 25 per cent in Fig. 10. Heat transfer coefficients for the first two increments and the last increment were not used because of entrance effects and the large end losses.

## Appendix: Method of Optical Pyrometry

As mentioned previously, the temperatures above approximately 3500 R were measured with an optical pyrometer. Since the insulated test section did not approximate a black body, it was necessary to correct the temperature readings of the pyrometer.

A relation between the true temperature of an object and the brightness temperature indicated by the optical pyrometer can be obtained from Wien's formula for black-body radiation

$$J_{bb} = C_1\lambda^{-5}e^{-C_2/\lambda T_{bb}} \qquad [A\text{-}1]$$

where

$J_{bb}$ = rate of emission of radiant energy at wave length $\lambda$ from a black body at temperature $T_{bb}$
$C_1, C_2$ = radiation constants

The same formula can be applied to a non-black body at true temperature $T_{bb}$ and can be written

$$J_{br} = \epsilon_\lambda C_1\lambda^{-5}e^{-C_2/\lambda T_{bb}} = C_1\lambda^{-5}e^{-C_2/\lambda T_{br}} \qquad [A\text{-}2]$$

where $T_{br}$ is the brightness temperature.

The ratio of $J_{br}$ to $J_{bb}$ is defined as the spectral emissivity $\epsilon_\lambda$ of the non-black body under consideration, as follows

$$\epsilon_\lambda = \frac{J_{br}}{J_{bb}} = \frac{C_1\lambda^{-5}e^{-C_2/\lambda T_{br}}}{C_1\lambda^{-5}e^{-C_2/\lambda T_{bb}}} \qquad [A\text{-}3]$$

Therefore

$$\ln \epsilon_\lambda = -\frac{C_2}{\lambda T_{br}} + \frac{C_2}{\lambda T_{bb}} = \frac{C_2}{\lambda}\left(\frac{1}{T_{bb}} - \frac{1}{T_{br}}\right) \qquad [A\text{-}4]$$

The interposition of a view window between the heated object and the optical pyrometer necessitates a modification of Equation [A-4] to include the spectral transmissivity $\tau_\lambda$ of the window. The spectral transmissivity is defined as the ratio of the transmitted radiant energy to the incident radiant energy for a given wave length

$$\tau_\lambda = \frac{J_\tau}{J_{br}} = \frac{C_1\lambda^{-5}e^{-C_2/\lambda T_\tau}}{C_1\lambda^{-5}e^{-C_2/\lambda T_{br}}} \qquad [A\text{-}5]$$

where

$T_\tau$ = temperature of a heated body measured with the optical pyrometer with the window interposed
$T_{br}$ = optical pyrometer brightness temperature measured under the same conditions with the exception that no window is interposed

Both measurements would be made while the black-body temperature remained constant. Equation [A-5] can also be expressed as

$$\ln \tau_\lambda = \frac{C_2}{\lambda}\left(\frac{1}{T_{br}} - \frac{1}{T_\tau}\right) \qquad [A\text{-}6]$$

Solving Equation [A-6] for $T_{br}$ gives

$$T_{br} = \frac{C_2/\lambda}{\ln \tau_\lambda + C_2/\lambda T_\tau} \qquad [A\text{-}7]$$

and substituting this expression for $T_{br}$ into Equation [A-4] gives

$$\ln (\epsilon_\lambda \tau_\lambda) = \frac{C_2}{\lambda}\left(\frac{1}{T_{bb}} - \frac{1}{T_\tau}\right) \qquad [A\text{-}8]$$

which can be written

$$T_{bb} = \frac{C_2/\lambda}{\ln (\epsilon_\lambda \tau_\lambda) + C_2/\lambda T_\tau} \qquad [A\text{-}9]$$

This expression can be used to calculate the actual temperature of a heated body if the spectral emissivity of the heated body $\epsilon_\lambda$ and the transmissivity of the window $\tau_\lambda$ are known, and the temperature $T_\tau$ is measured with an optical pyrometer.

The transmissivity of a view window can be determined very easily experimentally by measuring the temperature of a calibration lamp both with and without the window interposed and by inserting these values into Equation [A-6].

There are values of spectral emissivity for tungsten and molybdenum in the literature, but these values are for flat polished specimens with all radiation originating from the specimen. These conditions are not very closely approximated by most heat transfer test sections; for example, the test sections used in the present investigation were circular tubes whose surfaces did not remain polished because of grain growth and a small amount of oxidation; some of the radiation incident to the optical pyrometer was emitted and reflected from the hot radiation shield. As a matter of fact, it is more correct to say that it is the spectral emittance that is of interest. The method of determining this emittance was to measure the temperature of the test section with an optical pyrometer and thermocouple simultaneously, and then insert the values into [A-8] to obtain a value for ln $(\epsilon_\lambda \tau_\lambda)$.

This value could be used to compute $\epsilon_\lambda$, since $\tau_\lambda$ had been previously determined. The values of $\epsilon_\lambda$ could be plotted as a function of temperature up to the point where the thermocouples failed (about 3500 R) and then extrapolated to the higher temperatures. With these values of $\epsilon_\lambda$ and $\tau_\lambda$, Equation [A-9] could be used to determine the true wall temperature with the optical pyrometer.

The values for spectral emittance might have been in error, especially in the extrapolated region. The effect of an error in emittance on the test section wall temperature calculated by Equation [A-9] is shown in Table 4. From this table it can be seen that fairly large errors in spectral emittance do not seem to affect the wall temperature appreciably.

**Table 4 Effect of error in emittance on calculated test section wall temperature**

| Measured temperature $T_\tau$, R | Spectral emittance $\epsilon_\lambda$ | Calculated true temperature $T_{bb}$, R |
|---|---|---|
| 5460 | 0.5 | 6030 |
| 5460 | 0.6 | 5870 |
| 5460 | 0.7 | 5740 |

## Nomenclature

- $c_p$ = specific heat of helium at constant pressure, Btu/(lb) (R)
- $D$ = inside diameter of test section, ft
- $G$ = mass flow per unit cross-sectional area, lb/hr (ft²)
- $g$ = acceleration due to gravity, $4.17 \times 10^8$ ft/hr²
- $h$ = heat transfer coefficient
- $k$ = thermal conductivity of helium, Btu/(hr) (ft²) (R/ft)
- $L$ = heat transfer length of test section, ft
- $Nu$ = Nusselt number, $hD/k$
- $Pr$ = Prandtl number, $c_p\mu/k$
- $p$ = absolute static pressure, lb/ft²
- $\Delta p_{fr}$ = friction static pressure drop across test section, lb/ft²
- $Q$ = rate of heat transfer to gas, Btu/hr
- $Q_e$ = rate of electrical heat input to test section, Btu/hr
- $R$ = gas constant for helium, 386 ft-lb/(lb) (R)

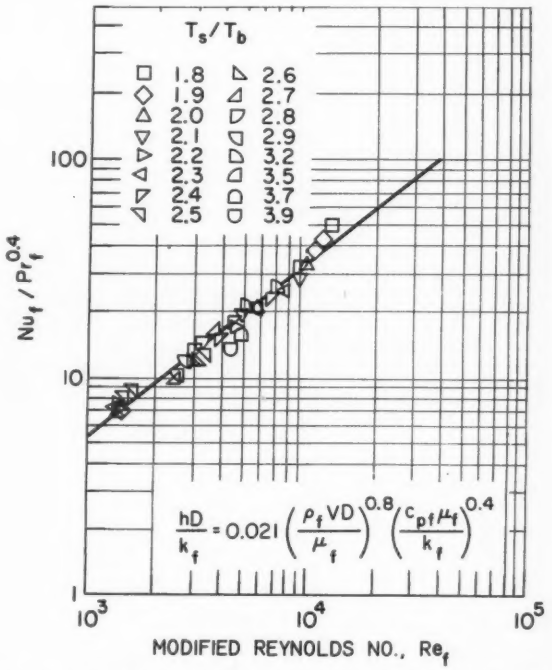


**Fig. 9 Correlation of local heat transfer coefficients with variable heat flux. Properties of helium evaluated at film temperature $T_f$**

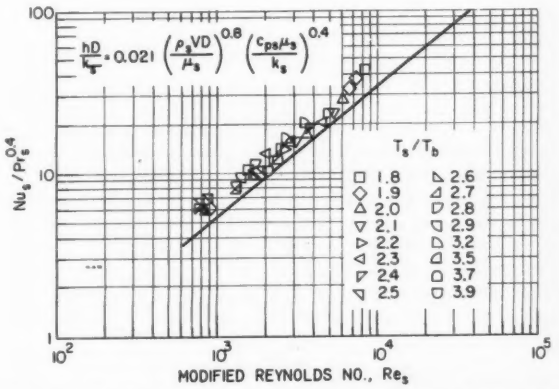


**Fig. 10 Correlation of local heat transfer coefficients with variable heat flux. Properties of helium evaluated at surface temperature $T_s$**

$Re$ = Reynolds number, $\rho VD/\mu$
$S$ = heat transfer area of test section, ft²
$T$ = total or stagnation temperature, R
$t$ = static temperature
$V$ = bulk velocity of gas, ft/hr
$w$ = helium flow, lb/hr
$x$ = distance from entrance of test section, ft
$\mu$ = absolute viscosity of helium, lb/(hr) (ft)
$\rho$ = density of helium, lb/ft³

***Subscripts***

$b$ = bulk (when applied to properties, indicates evaluation at average bulk temperature $T_b$)
$f$ = film (when applied to properties, indicates evaluation at average film temperature $T_f$)
$s$ = surface (when applied to properties, indicates evaluation at average surface temperature $T_s$)
1 = test section entrance
2 = test section exit

## References


1 Humble, L. W., Lowdermilk, W. H. and, Desmon, L. G., "Measurements of Average Heat-Transfer and Friction Coefficients for Subsonic Flow of Air in Smooth Tubes at High Surface and Fluid Temperatures," NACA Rep. 1020, 1951. (Supersedes NACA RM's E7L31, E8L03, E50E23 and E50H23.)

2 Durham, F. P., Neal, R. C. and Newman, H. J., "High Temperature Heat Transfer to a Gas Flowing in Heat Generating Tubes with High Heat Flux," presented at Reactor Heat Transfer Conf., Nov. 1957, TID-7529, pt. 1, book 2, pp. 502–514.

3 Woolley, H. W., "Helium," Table 6.10 of the NBS-NACA Tables of Thermal Properties of Gases," Nat. Bur. Standards, 1950.

4 Nuttall, R. L., "Helium," Table 6.39 of the NBS-NACA Tables of Thermal Properties of Gases," Nat. Bur. Standards, 1950.

5 Nuttall, R. L., "Helium," Table 6.42 of the NBS-NACA Tables of Thermal Properties of Gases, Nat. Bur. Standards, 1950.

6 Bernardo, E. and Eian, C. S., "Heat-Transfer Tests of Aqueous Ethylene Glycol Solutions in an Electrically Heated Tube," NACA ARR E5F07, 1945.

7 Weiland, W. F. and Lowdermilk, W. H., "Measurements of Heat-Transfer and Friction Coefficients for Air Flowing in a Tube of Length-Diameter Ratio of 15 at High Surface Temperatures," NACA RM E53E04, 1953.


# Controlled Recovery of Nonlifting Satellites


R. W. DETRA,[1]
F. R. RIDDELL[2] and
P. H. ROSE[3]

Avco-Everett Research Laboratory
Everett, Mass.



**This paper considers the problems of recovering, at a preselected site, satellites that are orbiting close to Earth (i.e., within a few hundred miles of Earth's surface). Considerations are limited to vehicles which accomplish re-entry into the atmosphere with drag devices. The discussion centers on two possible means of effecting controlled recovery of satellites: Recovery accomplished by a single perturbation of the satellite orbit as may be done with a single solid fuel retrograde rocket; and recovery accomplished by continuous application of a small force of controllable magnitude as may be done by varying the drag area of the vehicle provided it is orbiting in the outer fringes of the atmosphere. These two cases may be considered as extremes in the way in which the perturbing forces can be applied. The "intermediate" case of a controlled recovery by a series of impulsive forces (e.g., by a number of small retrorockets) is not considered.**


ANY MEANS of recovering a satellite at a desired location on Earth's surface must necessarily involve a perturbation of the original orbit. This part of the problem is in many ways similar to the general problem of transfer between orbits which has received considerable attention in the literature (1–6).[4] Both Hohmann (1) and Lawden (2) have shown that the optimum way to transfer between elliptical orbits is by means of impulsive forces which are applied at departure from one orbit and at arrival at the other. Such a procedure can be followed in practice by using chemical rockets; however, the weight penalties associated with this maneuver become large except for fairly small orbital changes. For this reason attention has also been given to the problem of orbital transfers by use of low thrust rocket motors (e.g., ion rockets) which operate continuously. Such analyses have been given by Stuhlinger (4) and by Irving and Blum (5). Another possible way of transferring between orbits is by the use of multiple impulses at a thrust level intermediate between that obtainable by chemical rockets and by continuous ion propulsion. An analysis of this approach has been made by Camac (6).

Similar considerations apply to the perturbation of satellite orbits in order to initiate controlled recovery. However, very little appears to have been written on the recovery of satellites even for what we might call the "classical" maneuver of using impulsive forces to transfer orbits. Hakes (7) has discussed recovery from a particular orbit by this method but did not generalize his results. In considering guidance problems of space vehicles, Wheelon (8) has developed a fairly general result for landing accuracy as a function of rocket impulse and alignment errors, for the case of recovery of satellites from circular orbits using a single impulse. However, no general analysis of the use of retrograde chemical rockets for the con-


Presented at the ARS Controllable Satellites Conference, MIT, April 30–May 1, 1959.


[1] Principal Staff Scientist. Member ARS.
[2] Technical Assistant to the President. Member ARS.
[3] Principal Research Scientist. Member ARS.
[4] Numbers in parentheses indicate References at end of paper.

trolled recovery of satellites appears to be in the literature. Other possibilities for controlled recovery, such as the use of multiple impulses as a means of control or the continuous application of force by a low thrust rocket motor or by atmospheric drag, have apparently received no attention at all.

In this paper we will consider the recovery of satellites from nearby orbits and show that, even without considering atmospheric effects, the special nature of the recovery problem leads to conclusions which are not included in the available analyses of transfer between orbits. In order to simplify consideration of the strong interaction with the atmosphere which occurs late in the recovery trajectory, our discussion will be limited to the problem of recovering nonlifting satellites. This problem is of current interest, since it is now generally recognized that the first satellites to be recovered will be of this type. Certainly this is the case for the NASA manned satellite Project Mercury, some details of which were made public last fall. We shall discuss some possible means of recovering drag vehicles at a desired recovery site, and point out some of the problems encountered in such controlled recovery.

In particular, analyses will be made of the retrograde rocket and drag modulation methods of recovery. In the usual concept the retrorocket achieves the perturbation of the satellite orbit in one short impulse producing a sudden change in the velocity and hence in the orbital path of the vehicle. In the drag modulation method, on the other hand, the velocity is perturbed over a long period of time by the continuous application of small forces. The variable drag approach is thus equivalent to a long burning retrorocket with a low level, controllable thrust. Alternatively, it is approximately equivalent to a large number of small retrorockets that can be fired at will over the whole recovery period. Neither of these retrorocket systems appears at present to be as practical as a variable drag surface, hence the choice of the terminology "drag modulation method." In the sense of this discussion the two approaches which are to be analyzed represent opposite extremes in the means of perturbing a satellite orbit to initiate recovery, and for this reason a comparative analysis is of interest. Each of these methods of recovery has certain inherent limitations. The retrorocket recovery system gets prohibitively heavy if the perigee altitude of the original orbit gets as large as 1000 miles. The drag recovery scheme is even more severely limited to an altitude range of about 80–140 miles. Nevertheless, there are many current satellite projects to which one or both methods could be applied.

There are other practical limitations, such as those imposed by the state of development of gyros and accelerometers which directly influence the attainable guidance and control accuracies. These are not discussed in any fine detail. Instead, the discussion is kept on general terms using the practical limitations of specific systems only as guide lines.

## Retrorocket Recovery

### General Remarks

Conceptually speaking, one of the simplest ways to recover a satellite from orbit is to perturb the orbit slightly using a small chemical rocket. It should be realized, of course, that because of the tremendous energy possessed by the satellite it is difficult to perturb the orbit greatly without investing a large part of the satellite weight in rocket fuel. If one remembers that the weight of rocket needed to launch a satellite is at present between 100 and 1000 times the weight of the satellite itself, then it is clear that a retrorocket which comprises only a few per cent of the satellite weight can effect only a very small perturbation upon the orbit. Nevertheless, for satellites that are flown near to Earth (i.e., within a few hundred miles of Earth's surface), it is practical from a weight viewpoint not only to induce the re-entry of the satellite by means of a retrorocket, but also to control its landing point to a reasonable degree of accuracy.

It is useful for the discussion here to look upon recovery and landing point control as two separate requirements. In this sense, recovery may be defined as a means of causing the orbit to interesect the atmosphere so that the vehicle will decelerate and drop to Earth's surface. Landing point control, on the other hand, is a means of causing the final deceleration to be accomplished at a desired location with an acceptable accuracy.

For a retrorocket system, recovery is accomplished with the smallest possible rocket if the rocket is fired forward in the flight direction as the satellite passes through apogee. Such a retrorocket firing causes the perigee to drop in altitude. With a sufficiently large rocket, the new perigee can be made to occur within the atmosphere so that on its next pass the satellite will re-enter the atmosphere and be decelerated. The relative weight of the rockets required to accomplish such a maneuver is well known, and it is generally recognized that the optimum way to execute this maneuver is to apply the perturbing force as a tangential impulse at apogee. The point of this present discussion is that, although such a maneuver may be satisfactory for recovery and require a minimum weight penalty of rockets, it does not effect satisfactory landing point control. The reason for this is fairly obvious. Since the local flight path angle is nearly horizontal when the vehicle is close to perigee, the slightest error in the resultant altitude of the satellite or a perturbation in the density of the upper atmosphere will cause a very large landing position error. In order to control the landing point accurately, it is desirable to have the perturbed orbit intersect the atmosphere at as large an angle as possible (9). A better way to accomplish this with minimum rocket weight is to fire the rocket at apogee, as discussed before, but to cause the perturbed ellipse to intersect the sensible atmosphere about one quarter of an orbit later rather than one half orbit later as suggested previously. In this way better landing point control can be obtained, but the retrorocket weight is roughly twice the minimum weight that is required to accomplish recovery alone.

The second point of general interest is the accuracy in total impulse and in firing direction which the retrorocket must meet to satisfy a given landing accuracy requirement. There is a requirement that the satellite position be known within a certain accuracy in space and in time if the vehicle is to be landed accurately. A complete analysis of rocket accuracy requirements can clearly be very complex, since they depend on the initial orbital altitude and eccentricity as well as on the total rocket impulse and the angle relative to the flight path at which the rocket is fired. We have not attempted a complete analysis of this problem in this paper but have confined our attention to what appear to be the most interesting results.

### Rocket Weight Requirements

For this discussion consider the coordinate system shown in Fig. 1. The notation which will be used in the following discussions is shown graphically in this figure.

It is interesting at the outset to examine simply some general retrorocket weight requirements. As was noted, the problem of orbit transfer based on impulsive forces has received considerable attention in the past, and some basic results are repeated here. A general result for the retrorocket size requirements for orbit transfer in a vacuum is given in Fig. 2. Here the relative velocity decrement is plotted against the relative change in perigee altitude for an impulse applied tangentially at apogee. The results were obtained by a linearized perturbation theory, which is valid for the near Earth satellite orbits that are considered in this paper. The relative change in velocity is related approximately to the retrorocket weight through the specific impulse by the formula

$$\frac{\Delta V}{Va} = \frac{V_{ex}}{Va}\frac{W_R}{W_I} = \frac{gI_{sp}}{Va}\frac{W_R}{W_I}$$

where

$V_{ex}$ = rocket exhaust velocity
$W_R$ = weight of rocket fuel
$W_I$ = initial total weight of vehicle
$I_{sp}$ = specific impulse

The increasing cost of using chemical retrorockets for returning from deeper space penetrations can be seen from Fig. 2. For orbits with perigees at altitudes of about one half an Earth radius (i.e., for recovery, $\Delta R_P/R_P = 2000/6000 = 0.33$), the retrorocket weight requirements become very severe (i.e., for a specific impulse of 250 sec, $W_R/W_I \approx 30$ per cent). The effect of course is a strong function of specific impulse, thus pointing to the importance of the high values of this parameter that may be achieved by employment of advanced space propulsion techniques.

Although these results give the minimum rocket weight necessary for recovering a satellite, a controlled recovery on Earth imposes additional conditions not necessarily met by these minimum retrorockets. A better idea of the requirements can be obtained by looking in greater detail at the flight conditions as the satellite begins to re-enter the atmosphere close to Earth. Fig. 3 shows the retrorocket weight requirements as a percentage of the vehicle weight for recovery from a circular orbit at an altitude of 100, 200 and 300 nautical miles. The weight requirements are based on the rockets being fired tangentially to the flight path with an $I_{sp}$ = 250 sec. Hence after the retrorocket impulse the satellite is at apogee of an elliptic orbit which then passes through the re-entry point ($h$ = 50 nautical miles) at the range indicated.

We note that the results given in Fig. 3 which correspond to recovery at a range of 180 deg give the lowest retrorocket weight for any particular initial altitude. However, we also note the resultant re-entry angles are very small. It will be shown that these small retrorockets and re-entry angles are not acceptable for a controlled satellite recovery. At smaller ranges the increasing trend of retrorocket weight with re-entry angle is clearly seen. The cases of re-entry at very small ranges can generally be ruled out either because of the large weight penalty of the retrorockets or, if the payload is fragile, the large decelerations associated with large re-entry angles. In general, however, if the retrorocket weight is limited to about 10 per cent of the initial weight, then the re-entry angle will be limited to less than about 5 deg for recovery from near-by satellite orbits.

It should be noted that a retrorocket system requires, in addition to the retrorocket itself, an orientation system which will locate the direction in which the rocket must be fired and an attitude control system to hold the vehicle steady while the rocket is firing. Hence retrorocket weight is only one of the criteria for the design of a satellite recovery system. It is of interest also to examine the accuracy requirements on the orientation and attitude control system, since these criteria will largely determine the weight and complexity of these subsystems.

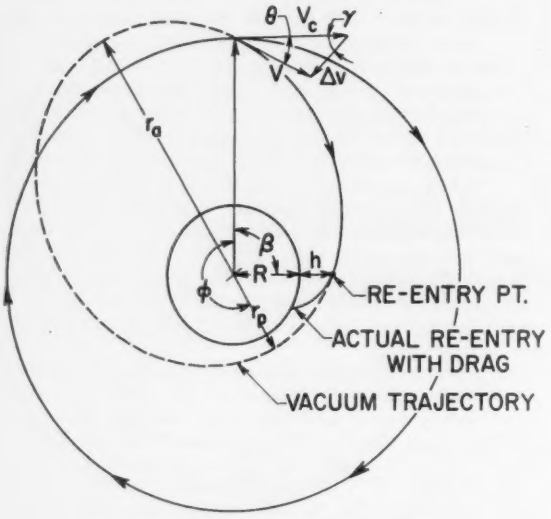


Fig. 1 Coordinate system and nomenclature

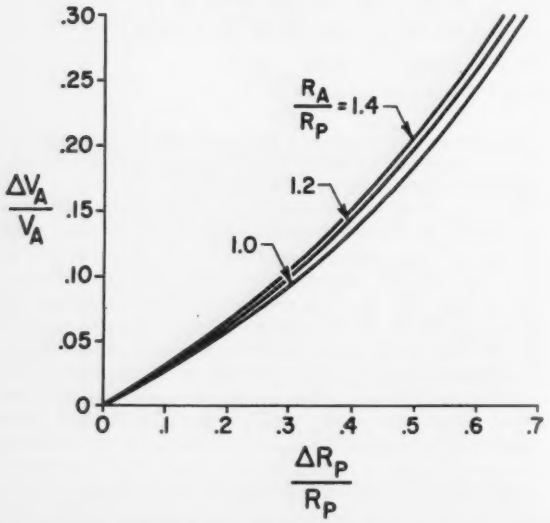


Fig. 2 Change in perigee altitude due to a velocity change at apogee

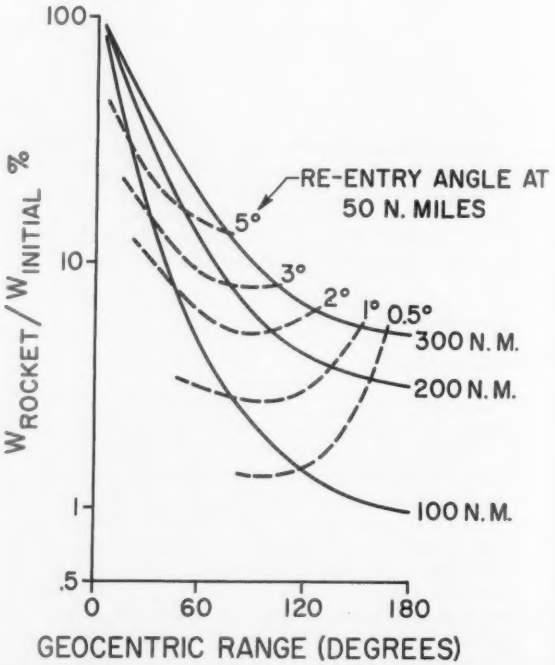


Fig. 3 Retrorocket weight requirements for satellite recovery. The weight requirements are based on recovery from a circular orbit with retrorockets, having an $I_{sp}$ = 250 sec, fired tangentially to the flight path

### Accuracy Requirements

When considering an accurately controlled satellite recovery the important considerations are the range sensitivity to errors produced in the operation of the retrorocket system and the accuracy with which the satellite's position in space is known when the retrorockets are fired.

Uncertainties of the satellite's position along its orbit can be treated separately, since they are related directly to range errors. For nearly circular orbits this can be interpreted in terms of a timing error in firing the retrorockets. Thus a timing error of 1 sec corresponds to a range error of approximately 5 miles at the landing point. These errors should not impose severe limitations on the recovery system.

The range sensitivity to the other variables can be evaluated from the relation between $\beta$, $\Delta V$, $h$ and $\gamma$ given by orbit mechanics. Wheelon (8) has derived such a relation for recovery from a circular orbit and it is given here for reference. (See Fig. 1 for notation.)

$$\frac{\Delta V}{V_c} = \frac{1}{2}\sec\gamma\left\{\frac{2\left(1+\frac{h}{R}-\cos\beta\right)+\tan\gamma\sin\beta-\left[\tan^2\gamma\sin^2\beta+4(1-\cos\beta)\left(1+\frac{h}{R}-\cos\beta+\tan\gamma\sin\beta\right)\right]^{1/2}}{\left(1+\frac{h}{R}-\cos\beta+\tan\gamma\sin\beta\right)}\right\}$$

Implicit differentiation of this equation yields the error coefficients which are used to evaluate the range sensitivity to errors in the retrorocket system operation.

Fig. 4 shows the range sensitivity at the re-entry point to velocity errors as a function of the retrorocket weight for the case of retrorockets fired tangentially to the flight path (i.e., $\gamma = 0$ deg). The curves asymptote vertically to the values of rocket weight given in Fig. 3 for a range of 180 deg. We note first that very small re-entry angles and the corresponding low weight retrorockets are not acceptable because of the high sensitivity of the range to velocity errors. This result combined with the results of Fig. 3 shows that for controlled satellite recovery the retrorocket weight must be larger than that given by the simple orbit transfer results shown in Fig. 2. In addition, range becomes sensitive to atmospheric variations at small re-entry angles. Detailed trajectory calculations indicate vacuum trajectories down to 50-nautical miles altitude are acceptable for re-entry angles of more than 1 deg, and further, provided the desired landing accuracy is of the order of ± 100 nautical miles, then range errors incurred in the atmosphere below 50 nautical miles may be neglected for nonlifting vehicles. If a landing accuracy of the order of ±10 nautical miles is required, then atmospheric effects must be considered more carefully.

Fig. 4 also shows that for a fixed sensitivity increased orbital altitudes require larger re-entry angles. In order to obtain these larger re-entry angles, larger retrorocket weights are needed. On the other hand, these larger re-entry angles present a problem for fragile payloads. It is well known that the re-entry deceleration increases sharply as the re-entry angle gets larger than 2 or 3 deg [e.g., Hakes (7)]. Human limitations to accelerations suggest the re-entry angle for manned drag vehicles should be limited to 3 deg or less. Thus it would appear that increased range sensitivity to velocity errors must be accepted if a satellite recovery with limited re-entry decelerations is to be made from the higher orbital altitudes under discussion. Of course, one solution to this problem is to use orbit transfer techniques to get to a lower orbital altitude while outside the atmosphere and then re-

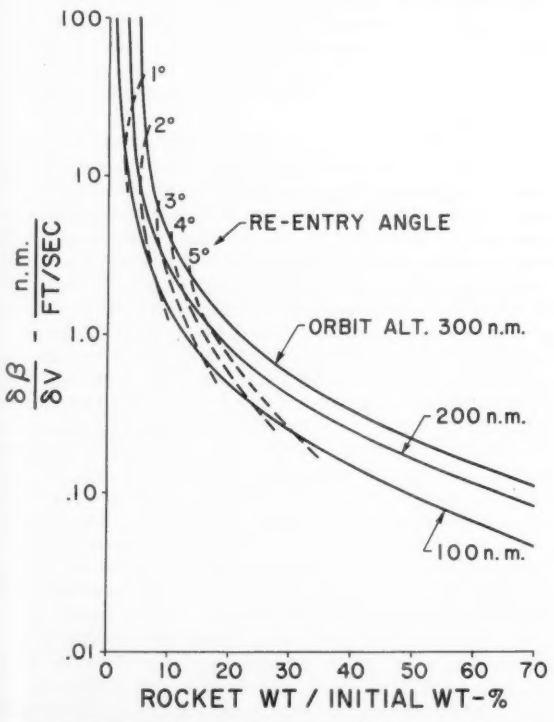


Fig. 4 Range sensitivity at the re-entry point to velocity errors. The sensitivities are given for recovery from circular orbits by retrorockets fired tangentially to the flight path (i.e., $\gamma = 0$). The rocket weight is based on an $I_{sp} = 250$ sec

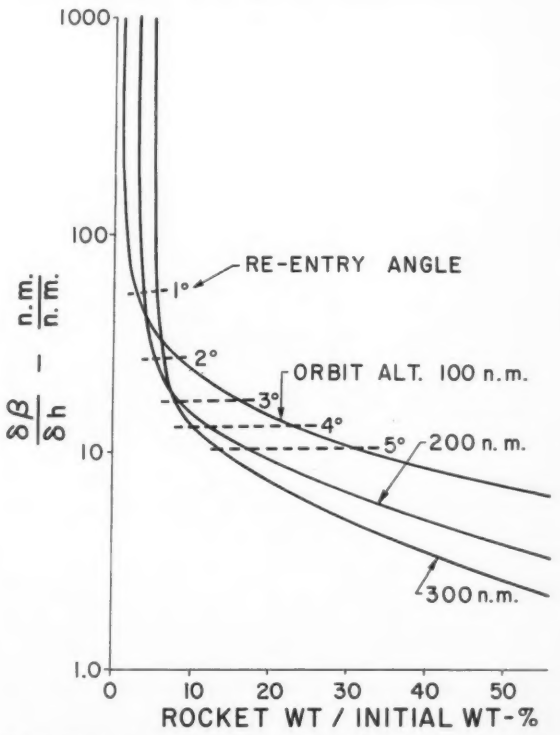


Fig. 5 Range sensitivity at the re-entry point to altitude errors. The range sensitivity is defined for recovery from circular orbits by retrorockets having an $I_{sp} = 250$ sec fired tangentially to the flight path

enter Earth's atmosphere from this low altitude orbit.

In Fig. 5 the range sensitivity at the re-entry point to altitude errors is shown as a function of retrorocket weight. The results shown here are based on the same conditions as used for Fig. 4—the recovery from a circular orbit is initiated by retrorockets ($I_{sp}$ = 250 sec) fired tangentially ($\gamma$ = 0 deg) to the flight path.

We see here, as in the previous case, that very small re-entry angles are not acceptable for a controlled satellite recovery because of the large range sensitivity to altitude uncertainties. In general, the orbit altitude must be known very accurately to get even reasonable landing accuracy except at very large retrorocket weight. The problem becomes more severe as the re-entry angle is limited to smaller values because of re-entry deceleration loads. As in the previous case, the curves approach asymptotically the minimum retrorocket weight for a range of 180 deg while the sensitivity approaches infinity.

Notice also that the range sensitivity varies very little at constant re-entry angle. Therefore a useful rule of thumb for retrorocket satellite recovery from circular orbits is that the range sensitivity to altitude errors is a function of the re-entry angle only.

Fig. 6 shows the range sensitivity to retrorocket impulse orientation errors as a function of retrorocket weight. The retrorocket weight is based on recovery from a circular orbit ($h$ = 300 nautical miles) and an $I_{sp}$ of 250 sec. The results shown in the figure are generally not considered in the usual orbit transfer problems.

We note first that the minimum retrorocket weight for a given range occurs at an impulse orientation angle different from zero ($\gamma \neq 0$) except for a range of 180 deg which is the "classical" result (i.e., $\beta$ = 180 deg, $\gamma$ = 0). Secondly, the range sensitivity is zero at this minimum rocket weight for any given range. It is clear then that retrorocket recovery systems which are designed for the optimum impulse orientation angle will simultaneously minimize the rocket weight requirements and the range sensitivity to impulse orientation errors.

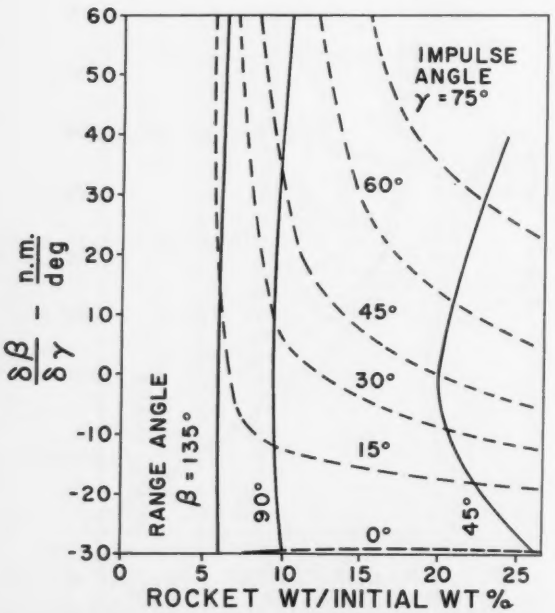


**Fig. 6 Range sensitivity to impulse orientation errors. The results are given for recovery from a 300-nautical mile altitude circular orbit with retrorockets having an $I_{sp}$ = 250 sec**

To avoid large rocket weights practical retrorocket satellite recovery systems will probably be designed for a re-entry range of about 90 deg. Although at this range there is not much weight saved by using the optimum value of $\gamma$, an impulse orientation angle different from zero ($\gamma \approx$ 24 deg) may be advantageous to minimize the range sensitivity to orientation errors.

To summarize these results, consider a practical retrorocket system operating in an exactly circular orbit at an altitude of 100 nautical miles. Let us say the desired range is 90 deg and the required landing accuracy ±100 nautical miles. Considering the case of tangentially fired retrorockets ($\gamma$ = deg) and considering each error separately, the following control requirements are established

$$\delta(\Delta V)/\Delta V = \pm 11 \text{ per cent}$$

$$\delta h = \pm 1.4 \text{ nautical miles}$$

$$\delta\gamma = \pm 3.3 \text{ deg}$$

Combined into a system having an accuracy of ±100 nautical miles, these maximum allowable errors would be reduced by a factor of $\sqrt{3}$. As noted, the range error due to $\delta\gamma$ could be reduced significantly by designing the system for $\gamma \approx$ 24 deg.

## Variable Drag Recovery

### General Remarks

In the previous section we discussed the recovery of satellites by perturbing the orbit with a single impulse. It is clear that although this method may be suitable for some applications, it is difficult to get a high degree of landing accuracy without an excessive weight penalty in rocket fuel. One might well ask, instead of using a single retrorocket, would it not be better if the retardation forces were applied in a series of impulses. As a limit of such a process one could consider continuously applying a small retardation force in order to cause a controlled landing at a selected point. This, in fact, may be done in practice with a vehicle that has a variable drag area. It is not the purpose of this paper to discuss how such a vehicle might be constructed, but simply to show that variable drag is conceivably a useful means of effecting controlled recovery of satellites.

It is certainly clear that a variable drag device must operate in the outer fringes of the atmosphere. For the present discussion we will consider a satellite that is flying in the altitude range of 80 to 140 miles. Lifetimes of satellites that do not exceed this range of altitudes may be from a few hours up to possibly a week or more. Flights beyond this altitude range utilizing variable drag control devices will not be considered here. It should be noted, however, that this altitude range is of itself interesting for some specialized satellite flights. For example, the NASA Mercury project will fly in this area.

There are two basic ideas that are needed in order to understand the variable drag landing point control system. The first of these is that to a first approximation, the lifetime of a satellite is proportional to its drag. This approximation breaks down near the end of the satellite's life, but it is still true that its lifetime can be controlled up to the very last moment by variation of its drag. The second point is that in flying nearly circular orbits in the specified altitude range, the orbital period is essentially independent of the exact orbital path. Hence the vehicle can be located along its track over Earth with great accuracy by simply a measurement of the time. Of course a reference time is required, but this may be supplied either at launch or subsequently by communicating a timing signal as the satellite crosses a given line of longitude. The basis of the variable drag recovery system is, therefore, to control the rate of descent of the satellite by varying the drag area and to do this with reference to a timing signal which continuously locates the satellite relative to its desired landing point.

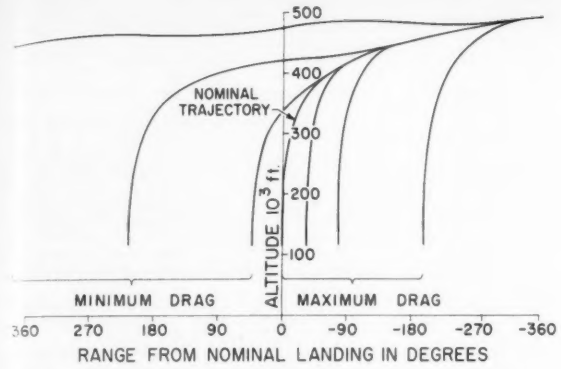


**Fig. 7a Range control for variable drag recovery from a circular orbit. Nominal ballistic drag parameter $W/C_DA$ = 7 lb/ft². Maximum drag is 20 times minimum drag**

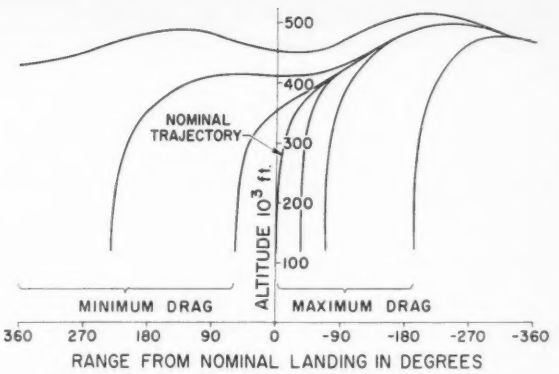


**Fig. 7b Range control for variable drag recovery from an elliptic orbit. Eccentricity, $\epsilon = 10^{-3}$. Same drag value as in Fig. 7a**

### Control Capabilities

The total variation in drag area that is required will depend on the specific purpose of the satellite that is to be flown. From practical considerations, it would seem that a drag variation of a factor of between 5 and 50 would be useful. To illustrate the control capability, Figs. 7 show the change in landing position that is possible for a satellite that can vary its drag by a factor of 20. The figures show the nominal landing trajectory which the satellite follows if the drag is held constant at a position midway between the maximum and minimum drag configuration. The nominal drag is taken as the geometric mean of the maximum and minimum drags. At various points along this nominal trajectory flight paths have been computed which resulted from either suddenly increasing the drag to its maximum value or suddenly decreasing it to its minimum value. These paths are also shown in the figures. In the computation that is plotted, the nominal ballistic drag parameter was 7 lb per ft² and the range of variation was by a factor of $\sqrt{20}$ above and below the nominal. The distance between the landing positions of the maximum drag and the minimum drag curves which start from the same point on the nominal trajectory represents the maximum landing point control that is available at this point. Curves are shown for a nominal re-entry from both circular and slightly elliptic orbits. A visual comparison shows that small ellipticities do not strongly affect the landing point control that is possible.

The control capabilities of this type of system are shown more generally in Fig. 8. Here the ratio of the control range to the nominal range is plotted against the nominal range for various drag variations about this nominal. This computation was done for values of the nominal ballistic drag parameter $W/C_DA$ of 7 and of 70 lb per ft², using an atmospheric model based on recent satellite and rocket data. The results were essentially independent of the nominal value of $W/C_DA$. Hence Fig. 8 may be considered valid for the interesting practical range of drag values for either instrumented or biological satellites.

Fig. 8 was plotted for recovery from purely circular orbits. The effect of ellipticity is shown in Fig. 9 which is a replot Fig. 8 for a nominal $W/C_DA = 7$ and a drag ratio of 20 but within various orbit ellipticities. The ellipticities that were chosen are consistent with the restriction of flying in the altitude range of 80 to 140 miles. It can be seen from Fig. 9 that such ellipticity introduces a perturbation on the effective control range but does not seriously degrade the control possibility.

It may be concluded from this discussion that the possibility of accurately controlling a satellite recovery by modulating the drag does exist.

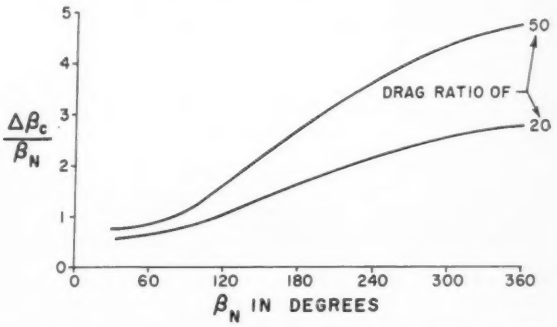


**Fig. 8 Ratio of the range control $\Delta\beta_c$ to the nominal range $\beta_N$ as a function of the nominal range, for the total drag variations of a factor of 20 and of 50**

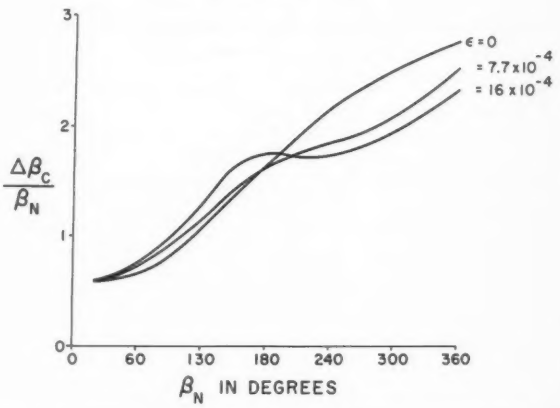


**Fig. 9 Effect of ellipticity on range control for a total drag ratio of 20, and different values of eccentricity $\epsilon$. The $\epsilon = 0$ curve is replotted from Fig. 8**

## Summary

The problem of recovering a satellite from a near Earth orbit with a single retrorocket impulse has been examined and some of the gross limitations in weight and accuracy requirements pointed out. It appears that the single retrorocket recovery method has certain inherent accuracy limitations unless one accepts large rocket weight penalties.

A brief examination of the possibility of recovering a satellite by modulating the drag has indicated that the basic capability of controlling the landing point in this manner does

exist. This analysis was subject to the restriction that the satellite fly in a nearly circular orbit in the outer fringes of the atmosphere.

These results indicate that recovery methods better than the single retrorocket impulse will soon be needed, and that such better methods may well be found by a continuous application of the retarding force as in the drag modulation method, or perhaps by a series of small rocket impulses, or by a combination of these methods.


### Acknowledgments

The authors would like to acknowledge the contributions of many members of the Avco-Everett Research Laboratory staff to the material in this paper. Special thanks are due to A. R. Kantrowitz, Director of the Laboratory and for the assistance of J. D. Teare, J. E. Hayes and H. K. Brown in the computations.


### References


1 Hohmann, W., "Die Erreichbarkeit der Himmelskorper," R. Oldenburg, Munich, 1925.

2 Lawden, D. A., "Minimal Rocket Trajectories," JOURNAL OF THE AMERICAN ROCKET SOCIETY, vol. 23, Nov.-Dec. 1953, p. 360.

3 Tsien, H. S., "Take-Off From Satellite Orbit," JOURNAL OF THE AMERICAN ROCKET SOCIETY, vol. 23, July-Aug. 1953, p. 233.

4 Stuhlinger, E., "Electrical Propulsion System for Space Ships with Nuclear Power Source, Parts I, II, and III, *J. Astron.*, Winter 1955, Spring 1956 and Summer 1956.

5 Irving, J. H. and Blum, E. K., "Comparative Performance of Ballistic and Low-Thrust Vehicles for Flight to Mars," Second Annual AFOSR Astronautics Symposium, Denver, Colo., April 1958.

6 Camac, M., "Reduction of Flight Time and Propellant Requirements of Satellites with Electrical Propulsion by the Use of Stored Electrical Energy," ARS preprint 721-58, 1958.

7 Hakes, R. C., "Some Fundamental Problems Associated with Injecting, Orbiting, and Recovering Man from Orbit," Presented at IAS 27th Annual Meeting, New York, N. Y., Jan. 26–29, 1959.

8 Wheelon, A. D., "Midcourse and Terminal Guidance," Space Technology Lectures, University of California, April 7–11, 1958.

9 Phillips, R. L. and Cohen, C. B., "The Use of Drag Modulation to Reduce Deceleration Loads During Atmospheric Re-entry," Rep. GM-TR-0165-00352, Space Technology Laboratories, Los Angeles, April 9, 1959.


# Technical Notes

## Escape in the Equatorial Plane of an Oblate Planet


MAURICE L. ANTHONY[1] and GEORGE E. FOSDICK[2]
The Martin Co., Denver, Colo.


RECENT investigations of planetary transfer have revealed that a ballistic transfer puts severe limitations on the burnout parameters. This note investigates the influence of oblateness on the escape path of a vehicle moving in the equatorial plane of a planet, and presents some numerical results pertinent to the case of Earth.

Fig. 1 indicates qualitatively the changes in an equatorial plane path brought about by oblateness (exaggerated for clarity). The speed at infinity $V_\infty$, the distance to the asymptote $p$ and the asymptotic direction $\varphi_\infty$ are the items of interest. As indicated by the figure, planetary oblateness tends to reduce the speed at infinity, increase the distance to the asymptote, and increase the angle $\varphi_\infty$. A quantitative discussion of these items follows.

#### Speed at Infinity

The speed at infinity may be found from the energy equation, where the potential $U$, given in (1)[3] is

$$U = -\frac{\mu}{r}\left[1 + \frac{J}{3}\left(\frac{R}{r}\right)^2\right] \qquad [1]$$

Comparison of initial energy with the energy at infinity yields

$$V_\infty^2 = V_0^2 - \frac{2\mu}{r_0}\left[1 + \frac{J}{3}\left(\frac{R}{r_0}\right)^2\right] \qquad [2]$$

By introducing the parameters $V_c$, $\eta$ and $c$ in the following way

$$1 + \eta = c^2 = \left(\frac{V_0}{V_c}\right)^2 = \frac{V_0^2 r_0}{\mu} \qquad [3]$$

Equation [2] may be written in the equivalent ways

$$V_\infty = V_c\left[\eta - 1 - \frac{2J}{3}\left(\frac{R}{r_0}\right)^2\right]^{1/2} \qquad [4]$$

$$V_\infty = \left[V_0^2 - \frac{2\mu}{r_0}\left(1 + \frac{JR^2}{3r_0^2}\right)\right]^{1/2} \qquad [5]$$

The oblate-free results may be obtained by setting $J = 0$ in Equations [4 and 5]

$$V_{s\infty} = V_c(\eta - 1)^{1/2} = (V_0^2 - 2\mu/r_0)^{1/2} \qquad [6]$$

Thus the difference between speeds at infinity is

$$\Delta V_\infty = V_c\left[\sqrt{\eta - 1} - \sqrt{\eta - 1 - \frac{2J}{3}\left(\frac{R}{r_0}\right)^2}\right] \qquad [7]$$

For given $J$ and $R$, $\Delta V_\infty$ is a maximum for $r_0 = R$ and $\eta = 1 + (2J/3)(R/r_0)^2$. This maximum is

$$\max \Delta V_\infty = \sqrt{2\mu J/3R} \qquad [8]$$

which is approximately 857 fps for Earth. Fig. 2 show $\Delta V_\infty$


Received March 18, 1960.


[1] Research Scientist, Applied Research Section. Member ARS.

[2] Design Engineer, Astronautics Section. Member ARS.

[3] Numbers in parentheses indicate References at end of paper.

EDITOR'S NOTE: The Technical Notes and Technical Comments sections of ARS JOURNAL are open to short manuscripts describing new developments or offering comments on papers previously published. Such manuscripts are usually published without editorial review within a few months of the date of receipt. Requirements as to style are the same as for regular contributions (see masthead page).

for Earth. The range of $V_\infty$ of practical interest for two-impulse interplanetary ballistic journeys extends from 8200 fps (for trajectories to Venus) to 39,000 fps (for Pluto) for which the corresponding values of $\eta$ (at $r_0 = R$) vary from about 1.09 to 1.25. For this range of $\eta$ the differences in speeds at infinity vary from 48 fps (Venus) to 9.1 fps (Pluto). For a minimum energy transfer orbit to Mars, starting at $r_0 = 1.1R$, the vehicle must escape from Earth with a relative speed of approximately 9600 fps with an allowable error of $\pm 1$ fps in order to impact Mars. If oblateness were not considered, $V_\infty$ would be 28.7 fps in error.

### Minimum Speed Required for Escape

To escape an oblate planet from a position in the equatorial plane, $V_\infty$ must be positive or zero. The minimum speed required for such an escape from $r_0$ is obtained from Equation [5] by setting $V_\infty = 0$. The resulting equation is

$$\bar{V} = \sqrt{\frac{2\mu}{r_0}\left(1 + \frac{JR^2}{3\,r_0^2}\right)} \qquad [9]$$

which is larger than the corresponding oblate-free speed, given by

$$\bar{V}_e = \sqrt{2\mu/r_0} \qquad [10]$$

Thus, to escape from the equatorial plane of an oblate planet with $V_\infty = 0$, the speed required exceeds the oblate-free minimum escape speed

$$\bar{V} - \bar{V}_e = \sqrt{\frac{2\mu}{r_0}}\left[\sqrt{1 + \frac{J}{3}\left(\frac{R}{r_0}\right)^2} - 1\right] \approx \frac{J}{6}\left(\frac{R}{r_0}\right)^2\sqrt{\frac{2\mu}{r_0}} \qquad [11]$$

The maximum of this difference occurs for $r_0 = R$, and for Earth it is approximately 10 fps.

### Distance to the Asymptote

In the equatorial plane, the distance $p$ (Fig. 1) may be found by using another first integral of the equation of motion, constant angular momentum. By comparing apsidal conditions and conditions at $\infty$

$$\frac{p}{r_0} = \frac{V_0}{V_\infty} = \left[1 - \frac{2\mu}{r_0 V_0^2}\left(1 + \frac{JR^2}{3r_0^2}\right)\right]^{-1/2} \qquad [12]$$

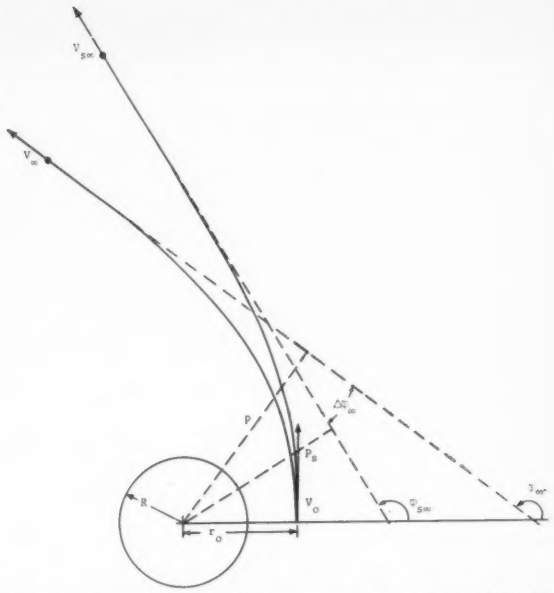


Fig. 1 Qualitative effects of oblateness on an escape path in the equatorial plane

Since oblateness decreases $V_\infty$, the distance to the asymptote increases with oblateness.

### Direction at Infinity

An analytic expression for the path is necessary to obtain the direction of the asymptote. Recent work by Anthony and Fosdick (2) has resulted in an approximate analytical determination of the path of a vehicle in the vicinity of an oblate planet, which is valid for large eccentricities. For the

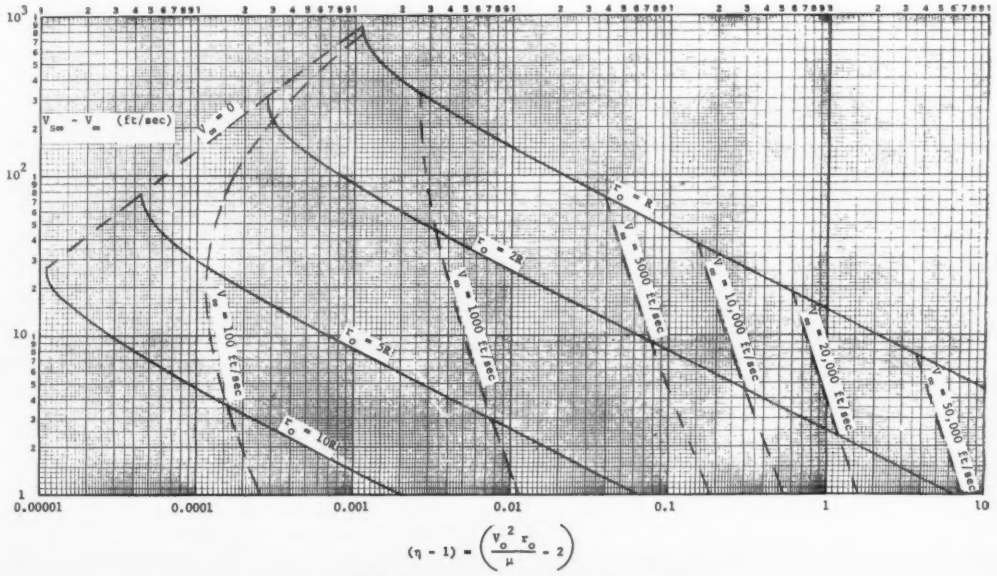


Fig. 2 Oblateness effects on the speed at infinity

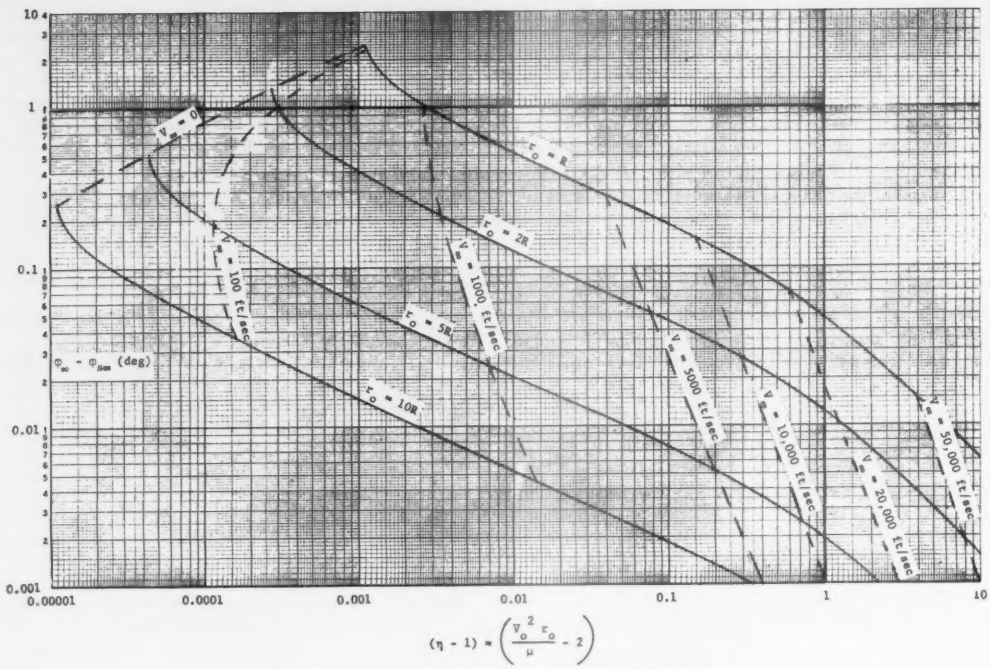


**Fig. 3 Oblateness effects on the direction at infinity**

equatorial plane, the path equation becomes

$$\frac{r_0}{r} = \frac{1}{c^2}\left\{1 + \eta\cos\xi + \frac{J}{c^4}\left(\frac{R}{r_0}\right)^2 \times \left[1 - \cos\xi + \frac{\eta^2}{6}(3 - 2\cos\xi - \cos 2\xi)\right]\right\} \quad [13]$$

where

$$\xi = \frac{\varphi}{1 + (J/c^4)(R/r_0)^2} \quad [14]$$

When $r \to \infty$, the left side of Equation [13] becomes zero. An approximate solution of this equation for $\cos\xi_\infty$, valid to first order in $J$, is

$$\cos\xi_\infty = -\frac{1}{\eta} - \frac{J}{3c^2\eta^2}\left(\frac{R}{r_0}\right)^2(3 - \eta + 2\eta^2) \quad [15]$$

For $\xi_\infty = 180$ deg, a first-order solution of Equation [15] yields

$$\bar{\eta} = 1 + \frac{2}{3}J\left(\frac{R}{r_0}\right)^2$$

as a minimum speed for escape, which is another way of expressing the exact result given by Equation [9].

Equations [14 and 15] yield

$$\varphi_\infty = \left[1 + \frac{J}{c^4}\left(\frac{R}{r_0}\right)^2\right] \times \arccos\left[-\frac{1}{\eta} - \frac{J}{3c^2\eta^2}\left(\frac{R}{r_0}\right)^2(3 - \eta + 2\eta^2)\right] \quad [16]$$

For an oblate-free planet

$$\varphi_{\infty\infty} = \arccos(-1/\eta) \quad [17]$$

so that

$$\Delta\varphi_\infty = \left[1 + \frac{J}{c^4}\left(\frac{R}{r_0}\right)^2\right]\arccos\left[-\frac{1}{\eta} - \frac{J}{3c^2\eta^2}\left(\frac{R}{r_0}\right)^2 \times (3 - \eta + 2\eta^2)\right] - \arccos\left(-\frac{1}{\eta}\right) \quad [18]$$

For $\eta$ not near unity

$$\Delta\varphi_\infty \approx \frac{J}{c^4}\left(\frac{R}{r_0}\right)^2\left[\arccos\left(-\frac{1}{\eta}\right) + \frac{1}{3\eta}(3 - \eta + 2\eta^2)\sqrt{\frac{\eta + 1}{\eta - 1}}\right] \quad [19]$$

Fig. 3 shows numerical results for escape from Earth. Maximum effects of oblateness again occur at $V_\infty = 0$ (about 2.5 deg for $r_0 = R$). For the range of practical interest for minimum energy interplanetary ballistic trajectories, beginning at $r_0 = R$, $\Delta\varphi_\infty$ varies between 0.19 and 0.019 deg for trajectories to Venus and Pluto, respectively.

### Nomenclature

- $c$ = $V_0/V_c$
- $G$ = Newton's gravitational constant
- $J$ = oblateness parameter (approximately $1.638 \times 10^{-3}$ for Earth)
- $M$ = mass of planet
- $p$ = distance from center of oblate planet to asymptote of path
- $R$ = equatorial radius of planet (approximately $2.092601 \times 10^7$ ft for Earth)
- $r$ = radial position on the path
- $V$ = speed along the path
- $V_c$ = $\sqrt{\mu/r_0}$, circular speed at initial radius for an inverse-square force field
- $\bar{V}$ = minimum escape speed
- $\Delta V_\infty$ = $V_{s\infty} - V_\infty$
- $\xi$ = $\varphi/[1 + (J/c^4)(R/r_0)^2]$
- $\eta$ = $c^2 - 1$ (for the non-oblate case, $|\eta|$ = eccentricity)

$\bar{\eta}$ = $(\bar{V}/V_c)^2 - 1$
$\mu$ = $GM$ (approximately $1.4076613 \times 10^{16}$ ft³/sec² for Earth)
$\varphi$ = central angle
$\Delta\varphi_\infty$ = $\varphi_\infty - \varphi_{r\infty}$

***Subscripts***

0 = initial values
$s$ = results obtained for a planet with a spherically symmetric mass distribution (inverse-square force field)
$\infty$ = conditions for $r = \infty$
$s\infty$ = results obtained from inverse-square force field for $r = \infty$

**References**


1 Jeffreys, H., "The Earth," Cambridge University Press, 1959.
2 Anthony, M. L. and Fosdick, G. E. "An Analytical Study of the Effects of Oblateness on Satellite Orbits," The Martin Co., Denver, Colo., Research Rep. R-60-2, April 1960.


# Geodetic Latitude and Altitude of a Satellite


W. J. BERGER[1] and J. R. RICUPITO[1]

Aeronutronic Div., Ford Motor Co., Newport Beach, Calif.



**With the geocentric position vector of a satellite given, the problem is to compute the geodetic latitude and the altitude of the satellite above the Earth spheroid. The Lagrange multiplier method is avoided by a geometric derivation of an exact trigonometric equation for the geodetic latitude. By series expansion of the exact equation, an analytic approximation is obtained for the correction term, which, by addition to the geocentric latitude, gives the geodetic latitude. The altitude of the satellite then follows from the law of cosines.**



Received March 24, 1960.

[1] Research Engineer.

IN A PREVIOUS paper (1)[2] our formula [54] for the geodetic latitude of a sub-satellite point is not strictly accurate. The formula there actually gives the geodetic latitude of the point where the geocentric position vector $\bar{R}$ (of the vehicle) intersects the surface of the Earth spheroid, and the computed value exceeds the true geodetic latitude of the satellite by a few minutes of arc. The problem of finding the normal to a spheroid from a given external point has sometimes been attacked by the use of the Lagrange multiplier method in the calculus of maxima and minima, usually with the result that a high-degree algebraic equation must be solved. Since this problem apparently is not directly considered in geodesy texts (2) or almanacs (3) although it is inherent in missile and satellite work, and since in this paper (by a geometric derivation) we avoid the Lagrange multiplier altogether, the solution presented here should be of interest and utility.

## Geometric Derivation

In geodesy (2) the surface of Earth is represented by an

[2] Numbers in parentheses indicate References at end of paper.

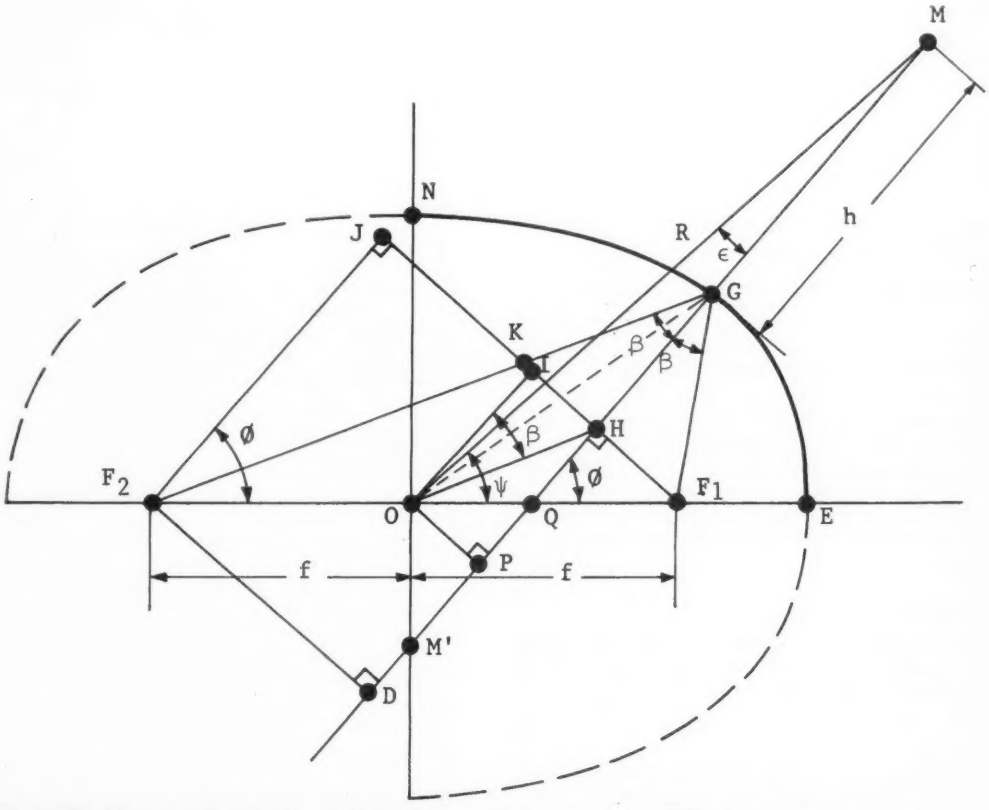


Fig. 1 Meridian section of Earth, containing the geocentric position vector $\overline{OM}$ of the satellite, geocentric latitude $\psi$, geodetic latitude $\phi$

ellipsoid of revolution, i.e., a spheroid. Hence, it suffices to consider the geometry in a meridian plane containing the position vector of the satellite. In Fig. 1, $NGE$ is a quadrant of the ellipse; $O$ is the center of Earth; $\overline{OE}$ is equal to $a$, the equatorial radius; $\overline{ON}$ is equal to $c$, the polar radius; $F_1$ and $F_2$ are the foci; and $\overline{F_2O} = \overline{OF_1} = f = ae$, where $e$ is the eccentricity. The satellite is at point $M$. We are given the geocentric distance $\overline{OM} = R$ and the geocentric latitude $\angle EOM = \psi$ of the satellite. From the vehicle $M$, the normal to the spheroid cuts the surface at $G$, the equatorial plane at $Q$, and the polar axis at $M'$. We wish to determine the geodetic latitude $\angle EQM = \phi$ and the altitude $\overline{GM} = h$. If $\angle OMQ = \epsilon$, then evidently $\phi$ is equal to $\psi + \epsilon$.

Suppose that $M$ is nearer to $F_1$ than to $F_2$. Construct the focal radii $F_1G$ and $F_2G$. Through $F_1$ construct a line normal to $MM'$ at $H$ and intersecting $F_2G$ at $K$. Complete the rectangles $F_2JHD$ and $OIHP$ as shown in the figure.

Since the focal radii $F_1G$ and $F_2G$ make equal acute angles $\beta$ with the normal $M'M$ at $G$, we have $\overline{F_1H} = \overline{HK}$; the line $OH$ thus joins the midpoints $O$ and $H$ of sides $F_2F_1$ and $KF_1$ in $\Delta F_2F_1K$. Hence, $OH$ is parallel to $F_2G$, with the result that $\angle IOH = \beta$.

Now $\overline{F_2F_1} \sin \phi = 2f \sin \phi = \overline{F_1J} = \overline{F_1H} + \overline{HJ}$, while $\overline{F_1H} = \overline{F_1G} \sin \beta$, and $\overline{HJ} = \overline{DF_2} = \overline{F_2G} \sin \beta$. Hence, $2f \sin \phi$ is equal to $(\overline{F_1G} + \overline{F_2G}) \sin \beta$. But $\overline{F_1G} + \overline{F_2G}$ is equal to $2\,OE = 2a$, and so we obtain

$$\sin \beta = (f/a) \sin \phi = e \sin \phi \qquad [1]$$

which establishes the relation between $\phi$ and $\beta$.

Next, we involve $\epsilon$, $\beta$ and $\phi$ in a single equation by noting that $\overline{OP} = R \sin \epsilon$, $\overline{OI} = f \cos \phi$, and $\overline{IH} = \overline{OI} \tan \beta$. But $\overline{OP}$ is equal to $\overline{IH}$, and hence $R \sin \epsilon = f \cos \phi \tan \beta$. By Equation [1], and the substitutions $f = ae$, $\epsilon = \phi - \psi$, the preceding equation becomes

$$R \sin (\phi - \psi) = ae^2 \sin 2\phi / 2\sqrt{1 - e^2 \sin^2 \phi} \qquad [2]$$

which is the basic equation for the geodetic latitude $\phi$.

**Series Expansion**

Rewriting Equation [2] in terms of $\epsilon$, we have, exactly

$$R \sin \epsilon = ae^2 \sin 2(\psi + \epsilon) / 2\sqrt{1 - e^2 \sin^2(\psi + \epsilon)} \qquad [3]$$

Evidently $\epsilon$ is quite small, so that for purposes of series expansion, $\sin \epsilon \approx \epsilon$, $\cos \epsilon \approx 1$. Since Earth has small eccentricity ($e \approx 0.082$), we shall neglect powers of $e$ higher than the fourth. Hence, by trigonometric and binomial expansion in Equation [3], we eventually obtain

$$\epsilon = \frac{e^2 \sin 2\psi + e^4 \sin^3 \psi \cos \psi}{2\{(R/a) - e^2 \cos 2\psi - (1/4)e^4 [1 + (1 - 2\cos 2\psi) \cos 2\psi]\}} \qquad [4]$$

After computing $\epsilon$ by Equation [4], we have the geodetic latitude given by

$$\phi = \psi + \epsilon \qquad [5]$$

**Height Above Spheroid**

The altitude $h = \overline{GM}$ of the satellite above the spheroid is given by the law of cosines in $\Delta OGM$ as

$$h = R \cos (\phi - \psi) - \sqrt{\overline{OG}^2 - R^2 \sin^2 (\phi - \psi)} \qquad [6]$$

where (2)

$$\overline{OG}^2 = (a^4 \cos^2 \phi + c^4 \sin^2 \phi)/(a^2 \cos^2 \phi + c^2 \sin^2 \phi) \qquad [7]$$

and

$$c = a\sqrt{1 - e^2}$$

**References**


1 Berger, W. J. and Ricupito, J. R., "Prediction Theory of Missile and Satellite Orbits," ARS JOURNAL, vol. 29, no. 6, June 1959, pp. 428–432.

2 Bomford, Brig. G., "Geodesy," Oxford University Press, London, 1952, pp. 392–403.

3 "American Ephemeris & Nautical Almanac, for the year 1960," U. S. Government Printing Office, Washington, D. C., 1958, pp. 465, 497.


# Terminal Guidance Technique for Satellite Interception Utilizing a Constant Thrust Rocket Motor


MARTIN L. NASON[1]

**Radio Corporation of America, Burlington, Mass.**



**The planar relative motion between a target and interceptor satellite is treated by perturbation techniques to obtain linearized equations of motion which are valid in the vicinity of a collision course. A terminal guidance law is formulated for attaining a collision course and for the achievement of satellite rendezvous using constant thrust rocket motors.**


**Motion Representation**

THE DIFFERENTIAL equations of motion of a mass particle confined to a plane which is acted upon by rocket forces are given in polar form

$$\ddot{R} - R(\dot{\sigma})^2 = F_R/(m_0 + \dot{m}t) \qquad [1]$$

$$R\ddot{\sigma} + 2\dot{R}\dot{\sigma} = F_\sigma/(m_0 + \dot{m}t) \qquad [2]$$

A polar coordinate representation of the relative motion was chosen, since guidance information for terminal control is usually available in this form. See Fig. 1. The apparent gravitational acceleration[2] is neglected. The force system can be achieved by either a one-motor or two-motor system. In the two-motor system a separate motor is used for both $F_R$ and $F_\sigma$. The relationship between the mass flow rate and the force components for a single-motor and a two-motor system are simply

$$\dot{m} = -\sqrt{F_R^2 + F_\sigma^2}/C \qquad \text{one-motor system} \qquad [3]$$

$$\dot{m} = -(F_R/C_R + F_\sigma/C_\sigma) \qquad \text{two-motor system} \qquad [4]$$

It is significant to note, however, that in the form written, Equations [1 and 2] are a valid representation for either a single or two-motor system.

It is convenient to nondimensionalize the range and time. Letting $r = R/R_0$ and $\tau = t/T$, Equations [1 and 2] become

$$r'' - r\dot{\sigma}^2 = a_r/(1 - \tau) \qquad [5]$$

$$r\ddot{\sigma} + 2\dot{r}\dot{\sigma} = a_\sigma/(1 - \tau) \qquad [6]$$

This is a reduced version of Preprint 777-59, presented at the ARS Controllable Satellites Conference, MIT, April 30–May 1, 1959.

[1] Engineering Scientist, Missile Systems Design. Member ARS.

[2] Hord, R. A., "Relative Motion in the Terminal Phase Interception of a Satellite or a Ballistic Missile," NACA TN 4399, Sept. 1958.

where

$$a_r = F_R T^2/m_0 R_0 \quad [7]$$

$$a_\sigma = F_\sigma T^2/m_0 R_0 \quad [8]$$

$$T = -m_0/\dot{m} \quad [9]$$

Since there is no known exact solution of Equations [5 and 6], an approximate solution based on perturbation techniques will now be generated. For the study of motion in the vicinity of a collision course, the most appropriate parameter to choose as the perturbation parameter is the nondimensional normal acceleration component $a_\sigma$. Thus the assumed solutions are of the form

$$r = r_1 + r_2 a_\sigma \quad [10]$$

$$\sigma = \sigma_1 + \sigma_2 a_\sigma \quad [11]$$

where $a_\sigma \ll 1$.

To complete the formulation of the problem, the initial conditions and the forcing function must be stated

$$r(0) = r_0 = 1 \qquad \sigma(0) = 0 \qquad a_r = \text{constant}$$

$$\dot{r}(0) = \dot{r}_0 \qquad \dot{\sigma}(0) = \dot{\sigma}_0$$

Substituting the assumed solutions into Equations [5 and 6] and carrying out the formal techniques for solving the sets of differential equations involving the variables $r_1$, $r_2$, $\sigma_1$ and $\sigma_2$, respectively, the following results

$$r = r_0 + \dot{r}_0 \tau + a_r[\tau + (1 - \tau)\ln(1 - \tau)] \quad [12]$$

$$\dot{\sigma} = (1/r^2)\left(\dot{\sigma}_0 - a_\sigma\{(\dot{r}_0 + 2a_r)\tau + [1 + \dot{r}_0 + a_r(2 - \tau)]\ln(1 - \tau)\}\right) \quad [13]$$

In the development of these solutions, the initial angular rate of rotation $\dot{\sigma}_0$ was placed as an initial condition on $\dot{\sigma}_2$ by setting $\dot{\sigma}_2(0) = \dot{\sigma}_0/a_\sigma$. This implies that in order for the power series solution to yield an acceptable approximation to the actual motion, $\dot{\sigma}_0$ must be of the order of $a_\sigma$ or less. Letting $\sigma_B = \int_0^{\tau_B} \dot{\sigma}\, d\tau$, where $\dot{\sigma}(\tau_B) = 0$, then it can be established that the restriction $\dot{\sigma}_0 < a_\sigma \ll 1$ implies that the condition $\sigma_B \ll 1$ is also satisfied. Thus, the angular rotation of the line of sight during the terminal maneuver will remain small if the assumptions on which the linearized solution were obtained are not violated.

A comparison of exact solutions of the relative motion equations [5 and 6], as obtained by an analog computer, with the approximate solutions given by Equations [12 and 13] has been performed for a few typical cases. The linearized solution for the angular rate was found to be reliable for values of the perturbation parameter of the order of 0.4. However, the linearized range rate solutions did not give acceptable approximations for values of $a_\sigma$ greater than 0.2.

### Formulation and Implementation of Guidance Law

Two distinct guidance problems will be considered. First, it will be required only that the interceptor satellite hit the target satellite, and, secondly, it will be required that a soft landing or rendezvous takes place.

For the first problem, if the time to impact is not considered, then it is sufficient to require that the relative range rate be negative and that the derivative $\dot{\sigma}$ vanish. Since only the component of relative velocity normal to the line of sight $r\dot{\sigma}$ must be erased (to achieve a collision course), it is readily apparent that the minimum value of impulsive velocity correction is obtained when its direction is normal to the relative range vector and equal to $r\dot{\sigma}$. Consequently, it doesn't appear to be unreasonable to require that the orientation of the rocket motor force also be normal ($F = F_\sigma$) to the relative range vector. Although this orientation does not correspond to minimum fuel expenditure primarily because of the coupling of the range motion into the angular

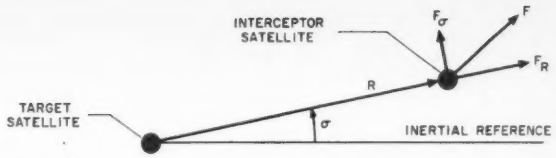


Fig. 1 Axis system for relative motion representation

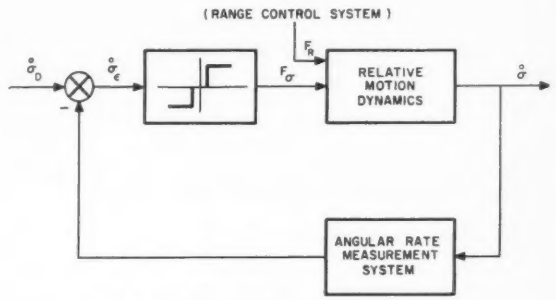


Fig. 2 Angular rate control system

motion, the propellant mass consumed approaches the minimum impulsive. Thus the terminal guidance law for collision course control will be based on this concept. In instrumenting this system, provision must be made for orientation control of the thrust vector, for measurement of the rate of change of the line of sight angle and for thrust termination when the conditions for a collision course have been satisfied. A block diagram of this system is shown in Fig. 2. The sign of the force $F_\sigma$ is given by the relationship

$$\text{sign of } F_\sigma = \text{sign of } (-\dot{\sigma}) \quad [14]$$

A dead space in the thrust controller is inserted to prevent overshoot and unnecessary hunting when the angular rate approaches zero.

To achieve rendezvous, a range control system is necessary. Examining Equation [12] it is apparent that the angular motion does not couple into the range motion within the limitations imposed on the solution. Differentiating Equation [12] with respect to $\tau$, solving the resulting expression for $\tau$ and substituting this expression back into Equation [12], the following relationship is obtained

$$r - r_0 = \dot{r}_0 + a_r - (\dot{r} + a_r)e^{(\dot{r}_0 - \dot{r})/a_r} \quad [15]$$

Regarding $a_r$ now as a variable depending on the instantaneous mass and range, the condition which must be satisfied for rendezvous ($\dot{r} = 0$) to be achieved at the range $r_D$ becomes simply

$$r - r_D = -\dot{r} + a_r(e^{\dot{r}/a_r} - 1) \quad [16a]$$

or

$$R - R_D = \frac{F_R m}{\dot{m}^2}\left(e^{-\dot{m}\dot{R}/F_R} + \frac{\dot{m}\dot{R}}{F_R} - 1\right) \quad [16b]$$

Equation [16a] was obtained from Equation [15] by letting $r = r_D$ and $\dot{r} = 0$, and then dropping the zero subscripts on the initial range and range rate variables. A block diagram of the range control system is shown in Fig. 3. The range control computer determines the sign of the force $F_R$ by the switching criterion

$$\text{sign of } F_R = \text{sign of } \left[\dot{R}\left|\frac{F_R m}{R\dot{m}^2}\right|\left(e^{-\left|\frac{\dot{m}\dot{R}}{F_R}\right|} + \left|\frac{m\dot{R}}{F_R}\right| - 1\right) - (R - R_D)\right] \quad [17]$$

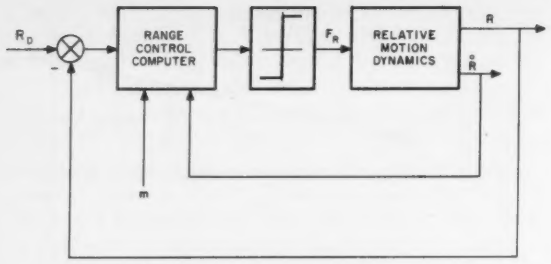


**Fig. 3 Range control system**

The angular rate control system must, of course, be operating during range control to minimize off-collision errors.

**Rocket Motor Fuel Requirements**

The rocket motor propellant required to place the interceptor on a collision course is obtained by defining $\tau_B$ such that $\dot{\sigma}(\tau_B) = 0$ and by noting that $\tau_B = m_{PF}/m_0$. Thus, from Equation [13]

$$\frac{\dot{\sigma}_0}{a_\sigma} = (\dot{r}_0 + 2a_r)\frac{m_{PF}}{m_0} + \left[r_0 + \dot{r}_0 + a_r\left(2 - \frac{m_{PF}}{m_0}\right)\right]\ln\left(1 - \frac{m_{PF}}{m_0}\right) \quad [18]$$

The restriction that range not vanish while this correction is being performed must be imposed. If the range control system is not functioning (only a hit desired), an explicit relationship between the minimum impulsive mass $m_{PI}/m_0$ and the constant thrust mass ratio $m_{PF}/m_0$ can be obtained. Setting $a_r = 0$ in Equation [18] and recognizing that $\dot{\sigma}_0/a_\sigma = C \ln (1 - m_{PI}/m_0)$ then

$$\frac{m_{PI}}{m_0} = 1 - \frac{(1 - m_{PF}/m_0)^{1-K}}{e^{K\, m_{PF}/m_0}} \quad [19]$$

where $K = \dot{R}_0 m_0/R_0\dot{m}$ = dimensionless burning parameter.

The range restriction, in this case, implies that $K\ m_{PF}/m_0$ be less than unity. As the burning parameter is decreased, the constant thrust mass ratio approaches the minimum impulsive mass ratio for the achievement of a collision course.

Integrating Equation [13] over the burning time $\tau_B$, the total angular rotation of the line of sight can be determined for $a_r = 0$

$$\sigma_B = \frac{a_\sigma}{K}\ln\left(\frac{1 - m_{PF}/m_0}{1 - m_{PI}/m_0}\right) \quad [20]$$

Since the total angular change must be small for the linearized solutions to be valid, Equation [20] indicates the relationship between the ratio $a_\sigma/K$ and the constant thrust and impulsive burning mass ratios which must be adhered to.

In computing the amount of propellant required to control the range, the change in range rate between switching points (change of sign of $F_R$) is the dominant parameter. Since $m_{PF_n}/m_0 = \Delta\tau_{B_n}$ where $\Delta\tau_{B_n} = \tau_{B_n} - \tau_{B_{n-1}}$ and $\dot{r}_{n-1} = \dot{r}(\tau_{B_{n-1}})$, $\dot{r}_n = \dot{r}(\tau_{B_n})$, by differentiating Equation [12] with respect to $\tau$ and making the appropriate substitutions, the constant thrust mass ratio becomes simply

$$\frac{m_{PF_n}}{m_0} = \sum_{n=1}^{n}\left(1 - e^{\frac{\dot{r}_{n-1} - \dot{r}_n}{a_{r_n}}}\right) \qquad n = 1, 2, 3 \ldots \quad [21]$$

where $n$ = number of switching points.

**Nomenclature**

| | | |
|---|---|---|
| $a$ | = | nondimensional acceleration |
| $C$ | = | effective exhaust velocity |
| $F$ | = | rocket motor force |
| $K$ | = | burning parameter |
| $m$ | = | mass of vehicle |
| $m_P$ | = | propellant mass |
| $R$ | = | relative range |
| $r$ | = | nondimensional relative range |
| $t$ | = | time |
| $\sigma$ | = | line of sight angle |
| $\tau$ | = | nondimensional time |
| $(^\circ)$ | = | differentiation with respect to $t$ |
| $(\cdot)$ | = | differentiation with respect to $\tau$ |

***Subscripts***

| | | |
|---|---|---|
| 0 | = | initial value |
| $R$ | = | along range |
| $\sigma$ | = | normal to range |

# Extension of the Transient Heating Charts

A. N. BAXTER[1]

**Space Technology Laboratories, Inc., Los Angeles, Calif.**

ALTHOUGH advances have been made toward protecting against high heating rates (notably in coatings and ablating material), it is sometimes more practicable to use the heat sink properties of a material to prevent it from debilitating, especially where the heating duration is short and the unit kinetic energy of the heating fluid is high.

Theoretically determined data have long been available for estimating the transient temperature conditions of the uninsulated surface of a semi-infinite slab (insulated on one side) subjected to a relatively low (constant) film coefficient and recovery temperature (1–4).[2] However, the environment generated by rocket jet or fluid dynamic shock wave impingement can make it necessary to use existing graphs in regions of dubious validity (5,6). For example, at Fourier modulus values less than 0.02, and at Biot modulus values on the order of 0.1, the temperature ratio data obtained by reading virtually any of the available charts are of questionable accuracy. The reported work was therefore undertaken several years ago to clarify and extend existing work in these regions; the results were used during the design of uncooled deflectors for rocket jets, but are believed to have more general application within the missile and propulsion fields.

The equation for one-dimensional heat flow relating temperature $t$, dimensional position within the slab $x$, exposure time $\tau$ and slab thermal diffusivity $\alpha$ is

$$\frac{\partial^2 t}{\partial x^2} = \frac{1}{\alpha}\frac{\partial t}{\partial \tau} \quad [1]$$

A solution, and more tractable condition is (1)

$$\frac{\theta_s}{\theta_0} = \frac{t_s - t_f}{t_i - t_f} = 2\sum_{n=1}^{\infty}\frac{\sin N_n}{N_n + \sin N_n \cos N_n}(e)^{-N_n^2(\alpha\tau/l^2)}\cos N_n \quad [2]$$

Received March 10, 1960.

[1] Member of the Technical Staff. Associate Member ARS.

[2] Numbers in parentheses indicate References at end of paper.

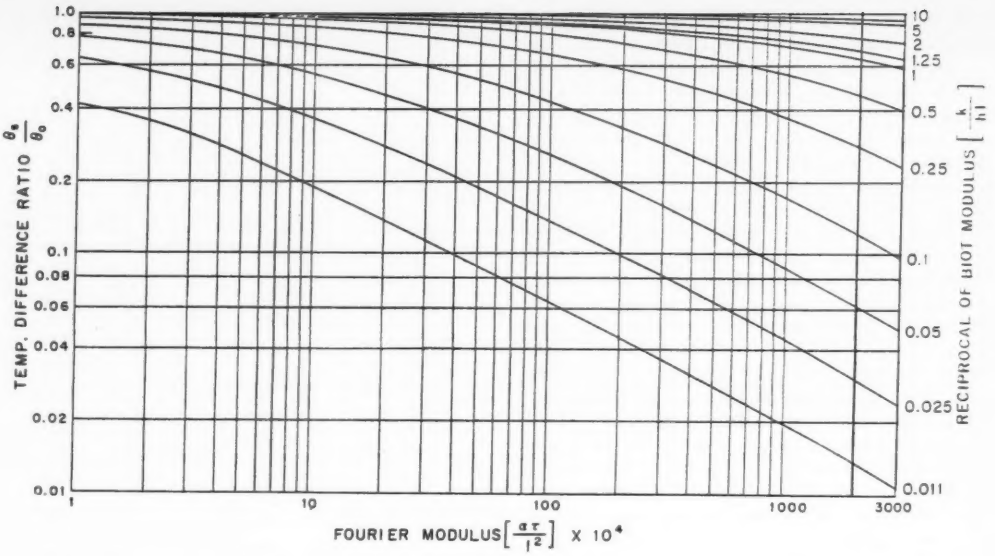


**Fig. 1 Temperature difference ratio vs. Fourier modulus for the heated surface of a semi-infinite slab**

where

$t_s$ = surface temperature of time $\tau$
$t_f$ = recovery temperature of the heating fluid
$t_i$ = initial temperature of the slab
$N_n$ = dimensionless quantity occurring in the expression $\cot N_n/N_n = k/hl$
$l$ = slab thickness
$\theta_s = t_s - t_f$
$\theta_0 = t_i - t_f$
$k$ = slab terminal conductivity (assumed constant)
$h$ = film coefficient (assumed constant)

For small values of exposure time $\tau$, the number of terms required to achieve satisfactory convergence is high (see Eq. [2]); most of the solutions reported herein required 30 terms. Calculations were performed on the Burroughs model no. E102.

Fig. 1 is a plot of some solutions in which the following ranges were investigated: Fourier modulus ($\alpha\tau/l^2$): 0.0001 to 0.30; reciprocal of Biot modulus ($k/hl$): 0.011 to 10.0. A complete presentation of expanded charts is available in (6). Sample problem solutions employing similar plots are found in the literature.


### Acknowledgment

The writer wishes to thank M. B. Rogers and G. E. Smith for the machine setup, and M. Moser and J. Poitz for coordinate geometrical work.


### References


1 Giedt, W. H., "Principles of Engineering Heat Transfer," Van Nostrand Co., Inc., N. Y., 1957, pp. 293–304.
2 McAdams, W. H., "Heat Transmission," McGraw-Hill Book Co., N. Y., 1942, 2nd ed., pp. 27–34.
3 Jakob, M., "Heat Transfer," John Wiley and Sons, Inc., N. Y., 1956, pp. 270–274.
4 Hatch, J. E., Schacht, R. L., Albers, L. U. and Saper, P. G., "Graphical Presentation of Difference Solutions for Transient Radial Heat Conduction in Hollow Cylinders With Heat Transfer at the Inner Radius and Finite Slabs With Heat Transfer at One Boundary," NASA TR R-56, 1960.
5 Baxter, A. N., "The Influence of Jet Properties on the Design of Uncooled Deflecting Surfaces," ARS preprint no. 625–58, 1958.
6 Baxter, A. N., "On the Extension of Transient-Heating Charts for the Semi-Infinite Slab," Space Technology Laboratories, Inc., STL/TN-59-0000-09355, Dec. 15, 1959.


# Stability of Some Potential Rocket Fuels in the Molten State


R. P. RASTOGI,[1] R. K. NIGAM[2] and HARBANS LAL[3]

**Panjab University, Chandigarh, India**


RECENTLY a very useful criterion for determining the stability of molecular complexes in the molten state has been developed which involves the knowledge of entropy of fusion from available freezing point composition data (1).[4]


Received Feb. 11, 1960.

[1] Reader in Chemistry, Chemistry Department.
[2] Research Assistant.
[3] M. Sc. student.
[4] Numbers in parentheses indicate References at end of paper.

It was thought interesting to examine the stability of diborane-ether complexes and hydrazine hydrate, which are potential rocket fuels. The phase equilibrium data for these have recently been obtained (2, 3).

For the region between the two eutectics, it follows from thermodynamics that for a binary mixture

$$\frac{\Delta_f h^\circ}{R}\left(\frac{1}{T} - \frac{1}{T_c}\right) = -\ln (\xi_A{}^l)^m(\xi_B{}^l)^n + \ln (\xi_A{}^l)_c{}^m(\xi_B{}^l)_c{}^n \quad [1]$$

where

$T_c$ = congruent melting point
$\Delta_f h^\circ$ = heat of fusion
$\xi_A{}^l$, $\xi_B{}^l$ = mole fractions of the species $A$ and $B$ in the liquid phase

The subscript $c$ refers to the composition at the congruent melting point. $\xi_A^l$ and $\xi_B^l$ are equal to stoichiometric mole fractions $x^1$ and $(1 - x^1)$ only when the compound $A_mB_n$ suffers complete dissociation. However, the qualitative deductions involve no error even if the stoichiometric mole fractions are substituted in Equation [1] for the general case. When $\ln (x^l)^m(1 - x^l)^n$ is plotted against $[(1/T) - (1/T_c)]$ a straight line should be obtained if Equation [1] is valid, and the slope should yield the value of the heat of fusion. This is done in Figs. 1 and 2. In this manner the heats of fusion were estimated for five systems by using earlier data (2, 3). The entropy of fusion for these are tabulated in Table 1.

It has been shown earlier (1) that if the entropy of fusion is of the order of 2, the compound is quite stable in the molten state. However, if the entropy of fusion is of the order of 20 cal/deg/mole, the complex formed would be unstable in the molten state. A perusal of the table therefore, reveals that diborane-tetrahydropyran and hydrazine-water complexes should be stable in the molten state. In fact the hydrazine-water complex is known to be quite stable. Complexes of diborane with methylethyl ether and diethyl ether should not be stable in the molten state. The freezing point curve of ether in the phase diagram can be analyzed to show whether it would be so. From thermodynamics it is known that this curve would be given by

$$-\ln \xi_B^l = \frac{\Delta_f h_B^\circ}{R}\left(\frac{1}{T} - \frac{1}{T_B^\circ}\right) + \frac{\Delta_f C_P^\circ}{R}\left(\ln \frac{T_B^\circ}{T} + 1 - \frac{T_B^\circ}{T}\right) \quad [2]$$

where

$\Delta_f h_B^\circ$ = heat of fusion of the component $B$
$T_B^\circ$ = melting point of the species $B$ which is ether in the present case
$\Delta_f C_P^\circ$ = difference in the heat capacity of ether in solid and liquid phases

From Equation [2], the true mole fraction of ether can be calculated and compared with the stoichiometric mole fraction of ether which would be the mole fraction when complete dissociation of the complex takes place. This was tested by using the known values of heats of fusion (4) and the extrapolated values of heat capacities from the data of Parks and Huffman (4). The mole fractions agree within experimental errors and show that the complex is dissociated to a large extent in the molten state.

Presently, four types of chemical reactions of boron hydrides are recognized. These are due to (5):

1 Symmetrical cleavage of the double-bridge bond.
2 Nonsymmetrical cleavage of the double-bridge bond.
3 Loss of proton from a hydrogen bridge bond.
4 Loss of molecular hydrogen from the molecule.

**Table 1 Entropy of diborane-ether complexes and hydrazine-hydrate**

| System | Nature of the compound formed | Congruent melting point, K | Heat of fusion, cal/gm | Entropy of fusion, cal/deg/mole |
|---|---|---|---|---|
| diborane-tetra-hydropyran | $AB_2$ | 227 | 390 | 1.7 |
| diborane-di-methyl ether | $AB_3$ | 217 | 910 | 4.2 |
| diborane-methylethyl ether | $AB$ | 134 | 1100 | 8.2 |
| diborane-diethyl ether | $AB_2$ | 149 | 2800 | 18.7 |
| | $A_3B_2$ | 147 | 3660 | 24.9 |
| hydrazine-water | $AB$ | 222 | 536 | 2.4 |

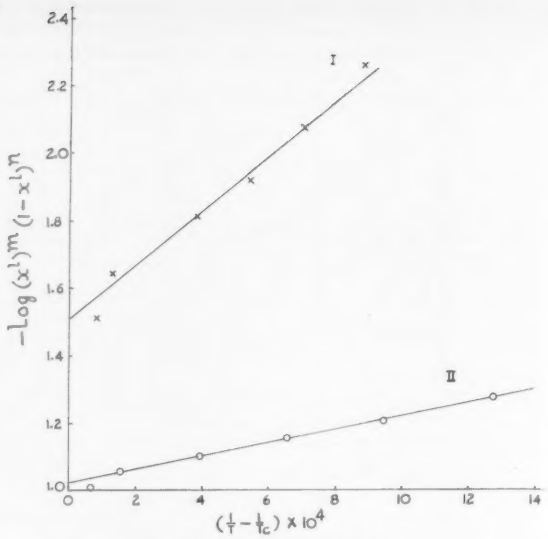


**Fig. 1 Estimation of heats of fusion of complexes:**
**I. Diborane-diethyl ether ($A_3B_2$)**
**II. Diborane-dimethyl ether**

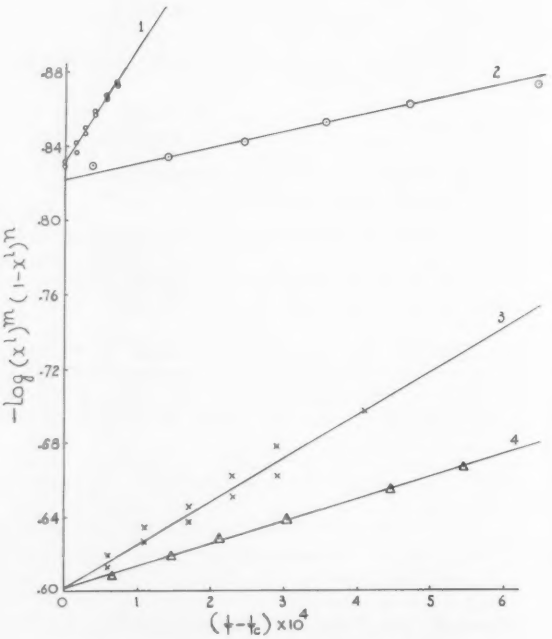


**Fig. 2 Estimation of heats of fusion of complexes:**
**1. Diborane-diethyl ether ($AB_2$)**
**2. Diborane-tetrahydropyran**
**3. Diborane-methylethyl ether**
**4. Hydrazine-water**

It is obvious that the type of reaction expected from a given molecule would depend on the position of the molecule in the systematic arrangement and on the geometry of the original boron hydride. It seems that for the formation of diborane-ether complexes, type 3 is more important and for this type the

following structure as suggested by Pitzer (6) is more plausible

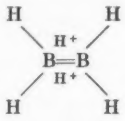

It is plausible that the complexes are formed by hydrogen bonding due to availability of protons. It is obvious then that the stability of the complexes formed would depend on the length of the ether molecules. This conclusion is verified by the construction of the models. This suggests instability of diborane complexes with diethyl ether. The given structure postulates the possibility of the existence of $AB$ or $AB_2$ complex, but it is difficult to explain how $AB_2$ complexes are formed.


**Acknowledgments**

The authors are grateful to the Indian Council of Scientific and Industrial Research for financing the investigation. They also thank Dr. Wirth for sending the detailed freezing point composition data for mixtures of ethers and diborane.


**References**


1 Rastogi, R. P. and Nigam, R. K., "Entropy of Fusion of Molecular Complexes," *J. Sci. Ind. Res., India*, vol. 18B, 1959, p. 305; *see also* "Thermodynamic Properties of Associated Mixtures," *J. Phys. Chem.*, 1960.

2 Wirth, H. E., Massoth, F. E. and Gilbert, D. X., "Complexes of Ethers With Diborane," *J. Phys. Chem.*, vol. 62, 1958, p. 870.

3 Hill, T. C. and Sumner, J. F., "The Freezing Point Diagram of the Hydrazine-Water System," *J. Chem. Soc.*, 1951, p. 838.

4 Parks, G. S. and Huffman, H. M., "Thermal Data on Organic Compounds—IV. The Heat Capacities, Entropies and Free Enerties of n-Propyl Alcohol, Ethyl Ether and Dulcitol," *J. Amer. Chem. Soc.*, vol. 48, 1926, p. 2788.

5 Parry, R. W. and Edwards, L. J., "Systematics in the Chemistry of Boron-Hydrides," *J. Amer. Chem. Soc.*, vol. 81, 1959, p. 3554.

6 Pitzer, K. S., "Electron Deficient Molecules—I. The Principles of Hydroboron Structures," *J. Amer. Chem. Soc.*, vol. 67, 1945, p. 1126.


# Insulation Temperature for the Transient Heating of an Insulated Infinite Metal Slab[1]


**WILLIAM H. HOLTER[2] and JOHN H. GROVER[3]**

**Atlantic Research Corp., Alexandria, Va.**



**The solution is given for the equation of transient heat conduction at the hot surface of the insulation of an infinite metal slab. A graphical representation of a simplified approximate solution of sufficient accuracy for engineering use is also given.**


IN A PREVIOUS paper (1),[4] the authors presented the generalized solution of the transient heat conduction equation for an insulated infinite metal slab and a graphical representation of a simplified approximate solution for the temperature of the metal slab. In some instances it is also desirable to determine the temperature of the insulation. The solution for the hot surface is given here.

The previously obtained (1) generalized solution is

$$\frac{T' - \bar{t}}{T' - T_0} = \sum_{i=1}^{\infty} \frac{2be^{-\alpha a_i^2 \theta}(a_i^2 + g^2)\,(b \sin a_i x + a_i \cos a_i x)}{a_i\{[(bg - a_i^2)^2 + a_i^2(b - g)^2]l + (bg + a_i^2)\,(b + g)\}} \qquad [1]$$

This equation is valid for an infinite slab of insulation with finite thermal conductivity, in contact at one surface with a slab of metal of infinite thermal conductivity and in contact at the other surface with hot flowing gases. Additional assumptions included:

1 Conduction of heat only in the direction normal to the plane of the slabs.

2 An initially uniform temperature throughout the slabs.

3 No heat transferred to the metal slab except by conduction through the insulation.

4 No thermal resistance between the two slabs.

5 A finite thermal film resistance between the hot flowing gases and the insulation.

6 Temperature of the flowing gases does not decrease in the direction of flow.

7 Thermal diffusivity $\alpha$ of the insulation is invariant with temperature.

The temperature of the hot surface of the insulation is obtained by letting $x$ equal zero in Equation [1] to yield

$$Y_s = \frac{T' - T_s}{T' - T_0} = \frac{2be^{-\alpha a_i^2 \theta}(a_i^2 + g^2)}{[(bg - a_i^2)^2 + a_i^2\,(b + g)^2]l + (bg + a_i^2)\,(b + g)} \qquad [2]$$

Equation [2] may be rearranged in terms of the dimensionless parameters $X$, $Y_s$, $m$, $n$ and $\beta_i$ to give

$$Y_s = \sum_{i=1}^{\infty} \frac{2e^{-X\beta_i^2 m}\,(1 + n^2\beta_i^2)}{(1 + m^2\,\beta_i^2)\,(1 + n^2\beta_i^2) + (m + n)\,(1 + mn\beta_i^2)} \qquad [3]$$

Equation [3] is the exact solution and can be used for determining the hot surface temperature. By again introducing the empirical parameter

$$\mu = m + n + mn \qquad [4]$$

the right-hand side of Equation [3] can be closely approximated in terms of one less parameter, as follows

$$Y' = \frac{\mu Y_s}{m(1 + n)} = \sum_{i=1}^{\infty} \frac{2\mu e^{-X\beta_i^2}}{1 + \mu + \mu^2\beta_i^2} \qquad [5]$$

Equation [5] is exact to within a few per cent, and its use allows the complete range of the numerical solutions to be presented in a single plot, thus avoiding double interpolation. The numerical solution of Equation [5] is shown in Fig. 1 for values of $\mu$ from 0.05 to 50. The curves in this figure


Received March 10, 1960.


[1] The figure and equations presented in this note were prepared under the sponsorship of the U. S. Navy, Bureau of Weapons.

[2] Mathematician.

[3] Head, Aerothermodynamics Group. Member ARS.

[4] Numbers in parentheses indicate References at end of paper.

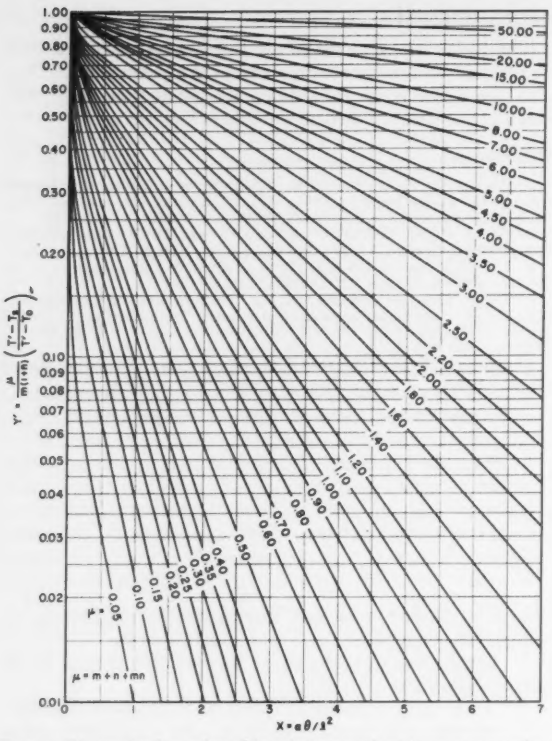


**Fig. 1 Dimensionless plot of insulation surface temperature rise vs. heating time for an insulated infinite metal slab**

correspond exactly to the Hottel chart for large slabs, for evaluation of surface temperature as given by McAdams (2).

### Nomenclature

$a_t$ = positive roots of $\tan a_t l = (bg - a_t^2)/(b + g)a_t$
$b$ = $h/k$
$C$ = heat capacity of insulating slab
$C_m$ = heat capacity of metal slab
$g$ = $\rho C/\rho_m C_m l_m$
$h$ = coefficient of heat transfer between heating or cooling fluid (hot gases) and surface of insulating slab
$k$ = thermal conductivity of insulating slab
$l$ = thickness of insulating slab
$l_m$ = thickness of metal slab
$m$ = $k/hl$ = dimensionless resistance ratio
$n$ = $\rho_m C_m l_m/\rho C l$ dimensionless heat capacity ratio
$T'$ = temperature at position $x$ at time $\theta$
$T_s$ = temperature of hot surface of insulation at time $\theta$
$T''$ = temperature of heating or cooling fluid (hot gases)
$T_0$ = initial temperature of insulating slab
$X$ = $\alpha\theta/l^2$ = dimensionless time parameter
$x$ = normal distance from surface to point
$Y_s$ = $(T' - T_s)/(T' - T_0)$ dimensionless temperature difference ratio
$Y'$ = $[\mu/m(1 + n)]Y_s$
$\alpha$ = $k/\rho C$ = thermal diffusivity of slab (insulation)
$\beta_t$ = $a_t l$
$\theta$ = time from start of heating or cooling
$\rho$ = density of insulating slab
$\rho_m$ = density of metal slab
$\mu$ = $m + n + mn$ = dimensionless empirical parameter

### References

1 Grover, J. H. and Holter, W. H., "Solution of the Transient Heat-Conduction Equation for an Insulated Infinite Metal Slab," JET PROPULSION, vol. 27, no. 12, Dec. 1957, pp. 1249–1252.
2 McAdams, W. H., "Heat Transmission," McGraw-Hill Book Co., Inc., N. Y., third ed., 1954, p. 37.

---

# Acoustic Instability in Solid Fuel Rockets[1]

**F. T. McCLURE,[2] R. W. HART[3] and J. F. BIRD[4]**

**Applied Physics Laboratory, The Johns Hopkins University, Silver Spring, Md.**

COMBUSTION instability remains the *bête noire* of the rocket motor, despite all the efforts of the past two decades to lay it to rest (1).[5] Recently attention has shifted from devising ad hoc remedies to basic studies of the phenomenon (2). We wish to comment here on certain aspects of oscillatory combustion of solid propellants which have been illuminated by such investigations.

### Source of Oscillation Energy

It is reasonable to hope that a sufficiently basic understanding of the energy sources will allow us one day to alleviate instability effectively. The major source resides undoubtedly in the thin combustion zone at the solid-gas boundary. It is rather generally agreed that it is the response of this combustion zone to acoustic pressure variations that amplifies incipient oscillations. Thus, this amplification is best described in terms of the real part of the acoustic admittance of the burning surface (3, 4). Because it describes the energy source, this response function (real part of boundary admittance vs. frequency of oscillation) is a *vital characteristic* of a propellant. However, little is now known experimentally about the response function, except that it is broad-banded and varies from propellant to propellant (5).

A theoretical calculation of the response function for a (hypothetical) plane combustion zone has been made, under the assumption that all chemical reactions are fast (3). It was shown that the time delays of heat and mass transport across the zone were sufficient to produce acoustic amplification over a broad frequency range for many typical sets of physico-chemical constants of a propellant. The most questionable part of the theory is the treatment of the solid phase reaction. Of course, since the theory is one-dimensional, it cannot be considered even a semiquantitative representation for composite propellants because of the heterogeneity on a scale comparable to the combustion zone thickness. We emphasize, however, that no matter how more complicated and closer to reality a theoretical description of the time dependent combustion becomes, the transport delays are always involved, and it is unlikely that the general broad-bandedness will be destroyed, except in very special cases.

In view of the difficulties facing theory, there is an urgent need for experimental determination of the response curves. There are at present no such data on this characteristic of propellants. It appears that the role of theory in this area

Received Aug. 3, 1960.
[1] This research was supported by the Bureau of Naval Weapons, Department of the Navy, under Contract NOrd 7386.
[2] Chairman, Research Center.
[3] Supervisor, Theoretical Study Group, Research Center.
[4] Physicist, Theoretical Study Group, Research Center.
[5] Numbers in parentheses indicate References at end of paper.

is to be guide to the interpretation of the experimental measurements.

### Viscoelastic Motion of the Solid

Until recently, the wave motion in the propellant during oscillatory combustion has been ignored. That the solid participates in the vibrations is evident from the observation of stress waves in it (6). This participation is also manifested by the fact that brittle propellants are known to shatter during severe oscillatory combustion. Furthermore, it is reasonable to attribute the changes in propellant properties that occur after a period of intense oscillation to the acoustic "working" of the material.

Theoretical studies (4,7) of the oscillation modes of a rocket engine verify that the solid must be considered as sharing in the oscillations. These studies show that for typical propellants the common assumption that the acoustic velocity is null at the solid-gas interface is completely invalid; on the contrary, the acoustic pressure at the surface can be anything between a node or a loop depending on the web thickness of the grain. Since the amplifying property of the surface is a response to pressure, it follows that the various modes of the cavity can be amplified only at certain times during the course of burning. Viscous damping in the solid and in the gas also varies as the web burns away. As a result, the theory leads to the remarkable and important result that a rocket motor will exhibit sporadic periods of oscillatory combustion, sometimes in one mode, sometimes in another, as burning time progresses. Thus it emerges that the viscoelastic motion of the solid is a major reason for the intermittent "ringing" that has been so puzzling in the past.

This theory also predicts that, because of the motion of the solid, the regions of instability will depend markedly on the conditions at the grain-case boundary (i.e., whether loose-fit, slip-fit or case-bonded). This is confirmed by the careful experiments of Angelus (5) and similar observations of Ryan (8). Incidentally, in view of the importance of the boundary conditions at the case as well as of the physical properties of the solid (especially viscosities), it is not hard to understand the observed irreproducibility of the phenomena in terms of variations in mixing, curing and loading operations.

### Influences of Erosion

Although it is recognized that fluctuations in pressure (in contrast to velocity) are the prime factor in converting combustion energy into sound, one may well inquire how important a role gas velocity plays for a propellant that exhibits erosive burning (burning rate dependent on tangential gas velocity at burning surface). It has been observed (6) that very highly erosive propellants seem to burn more stably than others. Aside from a limited analysis by Cheng (9), theoretical work has been directed toward the question of *inherent* rather than acoustic instability (10).

Recently, however, the influence of erosion on acoustic instability has been examined in some detail (11). This theory confirms the stabilizing influence of high *steady* erosion for propellants having positive erosion constants (mean burning rate increasing with increasing erosive velocity), and predicts the contrary for negative erosion constants. Since a mesa propellant when operating on or below the mesa exhibits negative erosion for velocities less than a certain value and positive for higher velocities, it follows from this prediction that such a fuel could differ greatly in stability under different erosive conditions (e.g., in rocket engines of different port area-burning area ratios), other things being equal. The analysis also treated the effect of *acoustic* fluctuations in the erosive velocity in terms of an (unknown) frequency dependent erosion constant. The results were found to depend markedly on the symmetry of the flow field in the rocket. For the usual end-nozzle case it seems that acoustic erosion should have little effect on stability. However, for a side-nozzle rocket as used in some experiments (12), it could affect stability materially, in manner and amount depending on the value of the a-c erosion constant.

An interesting observation of the theory is that acoustic erosion might have a predominant effect on stability for geometries in which two modes of the system are degenerate in frequency. This is reminiscent of Price's observation (13) of catastrophic interaction between degenerate modes. These results cannot be compared directly to the theory (11), however, since the interacting modes are axials and tangentials, which are not coupled in the acoustic (linear) analysis. The orthogonality between axial and tangential modes will, however, be removed for finite amplitude oscillations, and the possibility of large degeneracy effects in such circumstances is now under investigation by the present authors.

With respect to erosive effects for high amplitude fluctuations, it appears that the major factor responsible for the mean pressure level changes observed during severe oscillatory combustion has been uncovered. For it has been shown (4,7) that the rectification of tangential velocity involved in erosive burning (the burning rate depends only on the size of the erosive velocity, not its direction) yields a d-c term which leads, for positive erosion constants, to an increase in mean burning rate, and hence mean pressure, which is of the observed magnitude. We may note that some experiments by Price indicate that the pressure oscillations at high amplitude lead to a *decrease*, but that the positive erosion effect generally overcomes this.

This concept of erosive rectification also accounts for the negative d-c shifts in pressure observed with mesa propellants under moderate oscillations. As noted in the foregoing, for such powders burning on or below the mesa, the erosion constant changes from negative to positive values as erosive velocity increases. Since negative erosion gives a negative d-c shift, we expect either increased or decreased mean pressure level in various degrees depending on operating conditions and on the amplitude of the oscillations. In particular, one can understand in these terms why mesa propellants exhibit a dip in operating pressure at the onset or end of oscillatory combustion, but the usual "top-hat" for well-developed oscillations.

Finally, erosive rectification at finite amplitude has two further consequences. First of all, pressure fluctuations at frequencies harmonic with that of an unstable mode will appear, even though the system is actually *stable* to perturbations at such frequencies (7). This has been confirmed by experiment (5). Secondly, this generation of harmonics will distort the wave form of the acoustic field, quite considerably in the case of pure axial modes. This phenomenon will be treated in detail by the present authors in a paper now in preparation.

### References


1 Price, E. W., "Combustion Instability in Solid Propellant Rocket Motors," *Astronautica Acta*, vol. V, 1959, pp. 63–72.

2 "Progress in Astronautics and Rocketry. Volume 1: Solid Propellant Rocket Research," Academic Press, Inc., N. Y., in press.

3 Hart, R. W. and McClure, F. T., "Combustion Instability: Acoustic Interaction with a Burning Propellant Surface," *J. Chem. Phys.*, vol. 30,1959, pp. 1501–1514; *see also* Bird, J. F., Haar, L., Hart, R. W. and McClure, F. T., "Effect of Solid Propellant Compressibility on Combustion Instability," *J. Chem. Phys.*, vol. 32, 1960, pp. 1423–1429.

4 McClure, F. T., Hart, R. W. and Bird, J. F., "Solid Propellant Rocket Motors as Acoustic Oscillators," in "Progress in Astronautics and Rocketry. Volume 1: Solid Propellant Rocket Research," Academic Press, Inc., N. Y., in press. *Also* ARS preprint 1049-60.

5 Angelus, T. A., "Unstable Burning Phenomenon in Double-Base Propellants," in "Progress in Astronautics and Rocketry. Volume 1: Solid Propellant Rocket Research," Academic Press, Inc., N. Y., in press. *Also* ARS preprint 1066–60.

6 Shuey, H. M., private communication.

7 McClure, F. T., Hart, R. W. and Bird, J. F., "Acoustic Resonance in Solid Propellant Rockets," *J. Appl. Phys.*, vol. 31, 1960, pp. 884–896.

8 Ryan, N. W., private communication.

9 Cheng, S. I., "High Frequency Combustion Instability in Solid Propellant Rockets. Part 2" (particularly Appendix II). JET PROPULSION, vol. 24, 1954, pp. 102–109

10 Nachbar, W. and Green, L., Jr., "Analysis of a Simplified Model of Solid Propellant Resonant Burning," *J. Aero/Space Sci.*, vol. 26, 1959, pp. 518–526.

11 Hart, R. W., Bird, J. F. and McClure, F. T., "The Influence of Erosive Burning on Acoustic Instability in Solid Propellant Rocket Motors," in "Progress in Astronautics and Rocketry. Volume 1: Solid Propellant Rocket Research," Academic Press, Inc., N. Y., in press.
12 Price, E. W. and Sofferis, J. W., "Combustion Instability in Solid Propellant Rocket Motors," JET PROPULSION, vol. 28, 1958, pp. 190–192.
13 Price, E. W., "Analysis of Results of Combustion Instability Research on Solid Propellants," in "Progress in Astronautics and Rocketry. Volume 1: Solid Propellant Rocket Research," Academic Press, Inc., N. Y., in press; *see also* Crump, J. E. and Price, E. W., " 'Catastrophic' Changes in Burning Rate of Solid Propellants During Combustion Instability," ARS JOURNAL, vol. 30, no. 7, July 1960, pp. 705–707.

# Technical Comments

## Comment on "Minimum Time Flight Paths"

ROBERT T. STANCIL[1]

Convair Div., General Dynamics Corp., Fort Worth, Texas

IN HIS recent article (1),[2] Schindler apparently achieved a much simpler solution of the minimum time problem than had been attained previously. However, his results are invalidated by an error in the variational analysis. In carrying out the partial differentiation indicated in Equations [13 and 33], he states that $\alpha$ only occurs explicitly in the quantities $A$ and $B$. Actually, $v_1'$ and $v_2'$ are also explicit functions of $\alpha$. Had the dependence of $v_1'$ and $v_2'$ on $\alpha$ been considered, the partial derivative obtained would have been identically zero. Thus no information would be provided as to the optimum angle of attack.

It should be apparent from a practical point of view that the optimum angle of attack cannot be determined as a function only of the instantaneous values of the position, velocity and applied forces without consideration of the desired end conditions of the trajectory. The function served by Lagrangian multipliers is to correlate the instantaneous and final values of the dependent variables. An all too common lack of understanding of this function exists; e.g., see the recent erroneous paper by Dommasch and Barron (3) as well as Dommasch's incorrect answer to the comments by Miele, Leitmann, Kelley and Edelbaum (2). Through their derivative property, as noted by Breakwell (4), the multipliers indicate at any instant the relative gains to be obtained in the quantity being extremized by variations in the associated dependent variables. The result of eliminating one or more of the required multipliers is not the freeing of a constraint, but rather the omission of part or all of the information regarding the effects of variations in the dependent variables.

An inconsistency appears also in the inclusion of the $(v\ \dot{m})$ terms in the equations of motion [3, 4 and 25] in addition to the thrust term.

Received May 6, 1960.

[1] Senior Aerodynamics Engineer, Aerospace Technology Section.

[2] Numbers in parentheses indicate References at end of paper.

### References

1 Schindler, G. M., "Minimum Time Flight Paths," ARS JOURNAL, vol. 30, no. 4, April 1960, pp. 352–355.
2 Letters to the Editor, *Aero/Space Engng.*, vol. 19, nos. 3, 4, 5, March, April and May 1960.
3 Dommasch, D. O. and Barron, R. L., "Optimum Rocket Trajectories. Parts I and II," *Aero/Space Engng.*, vol. 19, nos. 1 and 2, Jan. and Feb. 1960.
4 Breakwell, J. V., "The Optimization of Trajectories," *J. Soc. Ind. Appl. Math.*, vol. 7, no. 2, June 1959.

## Expansion of Liquid-Oxygen RP-1 Combustion Products in a Rocket Nozzle

S. L. BRAGG[1]

Rolls-Royce Ltd., Derby, England

IN A RECENT Technical Note (1)[2] two points were made which do not seem to the writer to be entirely logical. The first point is really a non sequitur which may be paraphrased thus:

"The theoretical calculation for shifting equilibrium expansion gives one value for the temperature at the nozzle exhaust, whereas calculations based on frozen composition give another. Measurements of the mean temperature give a value near that calculated for frozen expansion. Therefore the expansion is nearly frozen."

Now we already know that in all practical systems the specific impulse is less than would be expected on the grounds of an equilibrium expansion. Thus we would expect the mean temperature to be below the value predicted by calculations based on equilibrium. Measurement of this temperature merely confirms a fact we already know. This fact does *not*, however, necessarily imply that shifting equilibrium is not

Received May 16, 1960.

[1] Chief Performance Engineer, Rocket Division. Member ARS.

[2] Numbers in parentheses indicate References at end of paper.

maintained in the nozzle. An alternative explanation is that the oxidant/fuel mixture ratio varies across the nozzle cross section, or from time to time at a particular section. Since the overall mixture ratio is usually chosen to give the maximum specific impulse, *any* local inhomogeneity *must* result in a deterioration of performance, and could explain theoretically a loss in specific impulse. Since any temperature measurement gives a value that is always a time mean, and often a space mean as well, the theory of inhomogeneity should be quite adequate to account for the observed mean temperature being lower than that for shifting equilibrium. Thus the fact that measured values of mean specific impulse and mean temperature are below the values that would be calculated for equilibrium expansion is no proof that equilibrium does not occur locally, unless it can also be proved that the flow is homogeneous.

The second point is the author's suggestion that the expansion process consists of "a frozen composition expansion with some additional burning." It is extremely hard to picture the physical state of affairs which would correspond to this suggestion.

If we exclude the water-gas reaction $CO_2 + H_2 \rightleftharpoons CO + H_2O$, which is known to be slow but which absorbs only small quantities of energy, the principal difference between equilibrium and frozen composition expansions is the reassociation of oxygen and hydrogen atoms and hydroxyl radicals. But all current theories of combustion assume that it is by the reactions of these very same species that combustion proceeds. They act as chain carriers in a series of steps such as the sequence

$$\begin{aligned} &H + O_2 \rightarrow OH + O \\ &O + H_2 \rightarrow OH + H \\ &OH + H_2 \rightarrow H_2O + H \qquad \text{(twice)} \\ &H + H + M \rightarrow H_2 + M \end{aligned}$$

which, in effect produces $H_2O$ out of $H_2$ and $O_2$. Exactly similar reactions must be involved in maintaining equilibrium. Surely, therefore, it is completely inconsistent to maintain that combustion takes place during expansion but that none of the reactions leading to equilibrium can take place.

Furthermore, calculations by Lemon (2) have shown that the heat release rates required to maintain near equilibrium composition in nozzle flow are no more than those measured, with similar reactants and under similar temperature conditions, in the combustors of aero gas turbines. This correspondence provides another strong argument for supporting shifting equilibrium.

Now the results plotted by Simmons in his Figs. 1 and 2 show two very important points.

First, the measured value of the characteristic velocity varies with mixture ratio in just the same way as the theoretical values calculated on either a shifting or a frozen basis (the latter two curves being parallel) but is below them both. The fact that the $c^*$ value is nearer that predicted on a frozen basis cannot be used as an argument favoring frozen composition expansion. For whatever phenomenon causes the difference between measured and frozen values can also, in a slightly higher degree, cause the observed difference between measured and equilibrium values. The hypothesis of inhomogenity would, in fact, be quite adequate to account for the discrepancy on either basis, since the theoretical $c^*$ is significantly reduced when quite small variations in mixture ratio across the chamber are assumed.

On the other hand, Fig. 1 of Simmons' note shows that as the mixture ratio varies, the exit temperature tends to follow the flat "frozen" line instead of rising at more oxygen-rich mixtures, as would be predicted on the basis of equilibrium expansion. This observation is in line with the present writer's own findings on large engines, where the measured thrust coefficient tends to follow the frozen rather than the shifting line. These facts cannot be explained on the hypothesis of inhomogeneous shifting equilibrium, and they do suggest that the composition is effectively frozen, at least downstream of the throat, since it is the recombination in the expanding portion of the nozzle that really causes the difference between the variations of the values of $C_F$, specific impulse and outlet temperature, with equilibrium flow as opposed to frozen flow.

In the opinion of the writer, therefore, Simmons' results support the suggestion of Bray (3) that shifting equilibrium is maintained up to some point in the nozzle, after which point the flow is effectively frozen. The practical results can in fact be adequately explained by the assumptions that:

1 There is equilibrium flow up to the throat.

2 There is frozen flow downstream of the throat.

3 The residual difference between theoretical and practical results is accounted for by inhomogeneity of the flow.

The magnitude of this effect could be checked by tests at a mixture ratio where the theoretical difference between equilibrium and frozen performance is small. It is submitted that these hypotheses are more reasonable and more consistent than those advanced in the Technical Note cited.

### References


1 Simmons, F. S., "Expansion of Liquid-Oxygen RP-1 Combustion Products in a Rocket Nozzle," ARS JOURNAL, vol. 30, no. 2, Feb. 1960, pp. 193–194.

2 Lemon, M., "Heat Release Rates due to Reassociation in the Rocket Motor Nozzle," Paper to Royal Aeron. Soc. (Derby Branch), Jan. 1960.

3 Bray, K. N. C., "Atomic Recombination in a Hypersonic Wind Tunnel Nozzle," Aeron. Res. Council Rep. 20,562, 1958.

# Book Reviews

**Ali Bulent Cambel**, Northwestern University, *Associate Editor*

**Principles of Optics,** by Max Born and Emil Wolf, Pergamon Press, 1959, xxvi + 803 pp. $17.50.

Reviewed by A. M. ZAREM and HORACE R. MOORE
Electro-Optical Systems, Inc.

It was in Germany in 1933 that Professor Max Born published two books, one of which, "Atomic Physics," appeared in an English translation in 1935. The notable success of this English edition during the subsequent years has only served to emphasize the regret, often expressed, that the other German work, "Optik," a book on optics, was never translated into English.

The book presently under review, "Principles of Optics," by Professors Max Born and Emil Wolf, although certainly the inspirational offspring of the many requests made to Dr. Born for an English version of his "Optik" is no mere translation of that earlier work. Instead, a substantially new book, restricted to those optical phenomena whose interpretation is possible within the framework of Maxwell's electromagnetic theory, has been presented. Even a brief perusal of this work indicates an unusual rapport between the collaborating authors; the elder, Born, needs no introduction to the scientific reader; and the younger, Wolf, is well known both in this country and abroad for his many contributions to optical field theory. The quality of the presentation, both in regard to clarity and uniformity of expression, is unusual for a co authored book and is especially noteworthy in the present case where several specific chapters have been prepared by the following contributing authors: A. B. Bhatia, P. C. Clemmow, D. Gabor, A. R. Stokes, A. M. Taylor, P. A. Wayman and W. L. Wilcock. Professor Wolf, who was responsible for most of the compiling, writing and checking of the text is here commended for a notable job of assimilation and integration.

Following a historical introduction, the book is presented under these main chapter headings: Basic Properties of the Electromagnetic Field; Electromagnetic Potentials and Polarization; Foundations of Geometrical Optics; Geometrical Theory of Optical Imaging; Geometrical Theory of Aberrations; Image-Forming Instruments; Elements of the Theory of Interference and Interferometers; Elements of the Theory of Diffraction; The Diffraction Theory of Aberations; Interference and Diffraction with Partially Coherent Light; Rigorous Diffraction Theory; Diffraction Theory by Ultrasonic Waves; Optics of Metals; Optics of Crystals. Then come nine Appendixes on such relevant mathematical techniques as the calculus of variations.

The foregoing list of chapter headings indicates the presentational logic as well as the content of "Principles of Optics." Limited to the electromagnetic theory of propagation, interference and diffraction of light, the book deals with those optical phenomena whose explanation can be conceived in terms of a continuous distribution of matter and which can be described deductively on the basis of Maxwell's

ENGINEERS • SCIENTISTS

OPPORTUNITIES

ON

SPACE POWER PROGRAMS

RANGING FROM AIR-BREATHING BOOST VEHICLES TO ION ENGINES

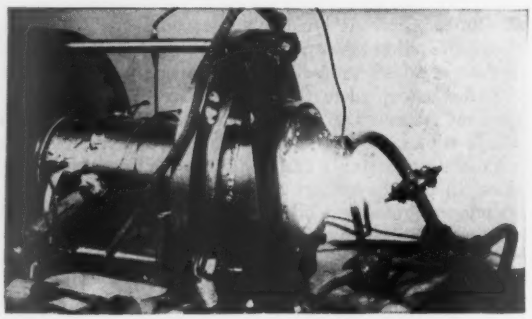

Scientists and engineers at G.E.'s Flight Propulsion Division are working with theoretical performance envelopes extending from earth orbits to intergalactic travel.

We are specifically seeking physical science and research oriented EE's and ME's from related fields—men who can contribute to *development and design* in areas where for the most part only the physical principles have been well established.

*At least 2 years of experience required in any of these areas:*

| | |
|---|---|
| Magnetohydrodynamics | Ion Acceleration |
| Plasma Acceleration | Space Charge |
| Gaseous Discharge | Electric Arcs |
| Electron-Ion Optics | Heat Transfer |
| Ion Generation | Rarefied Gas Dynamics |

Write informally, or forward your resume in confidence to Mr. Mark Peters, Dept. 35-MI, Bldg. 100.

FLIGHT PROPULSION DIVISION

GENERAL ELECTRIC

Cincinnati 15, Ohio

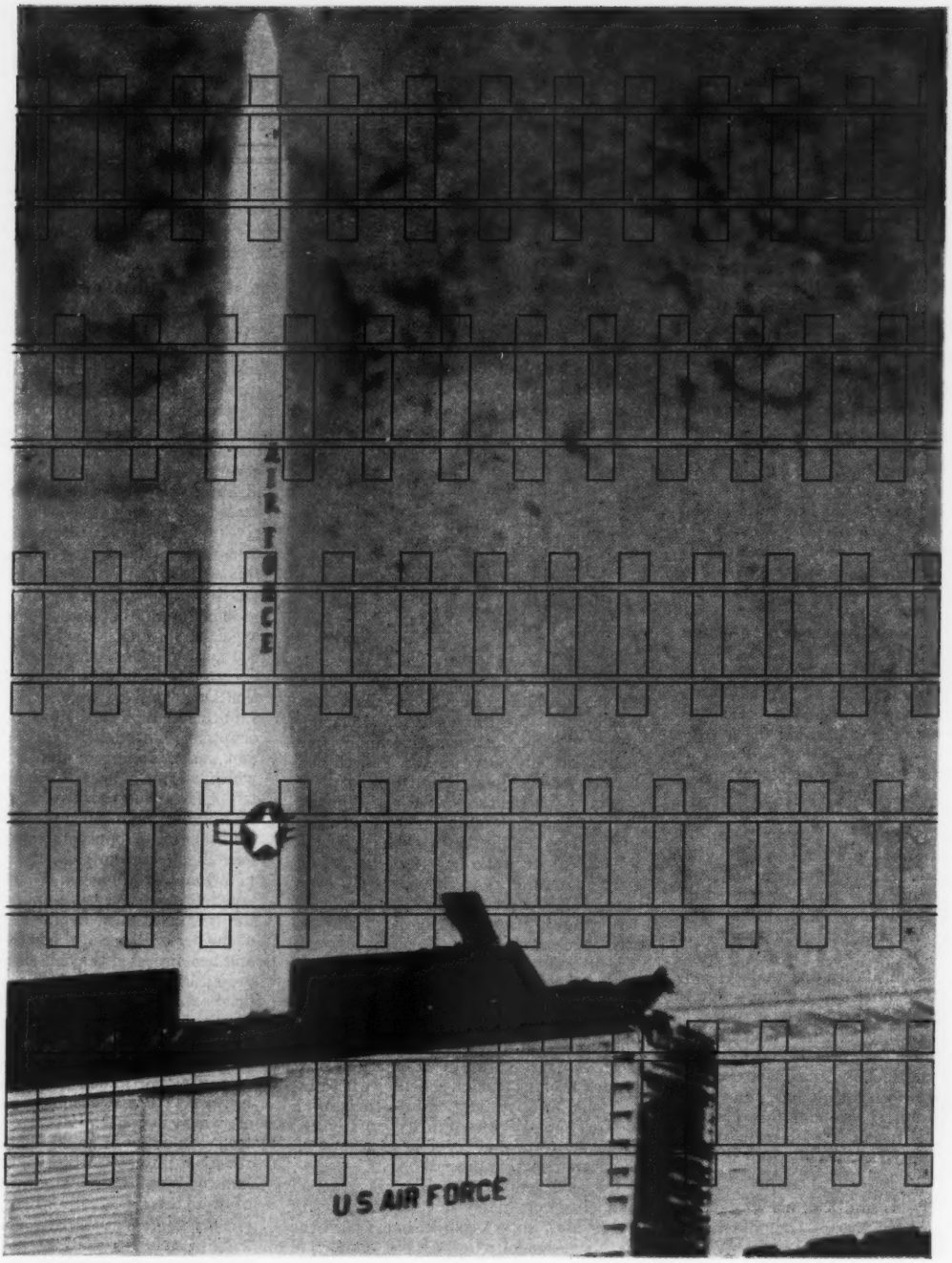


***24-hour commuter with an intercontinental job.*** Air Force Minuteman is a solid-fuel ICBM capable of instant action. It can be fired from a fixed base, railroad car or truck to a target 6,000 miles away. Its launching sites will be as flexible and widely dispersed as the country's transportation network can make them. Its important re-entry vehicle, the "business end" of the ICBM, is developed and produced by Avco—also producer of warhead-carrying nose cones for the Titan and Atlas ICBM's.

UNUSUAL CAREER OPPORTUNITIES FOR QUALIFIED SCIENTISTS AND ENGINEERS . . . WRITE AVCO TODAY.

Avco

AVCO CORPORATION, 750 THIRD AVENUE, NEW YORK 17, NEW YORK

equations alone. Such a treatment necessarily excludes consideration of physiological optics, x-ray and $\gamma$-ray optics, electron optics, the optics of moving media, the theory of spectra and other connecting links between atomic physics and optics. Anyone conversant with the diversity of these various fields both in concept and formalism and the degree to which they are now developed will recognize the wisdom of the authors in thus limiting the scope of "Principles of Optics." This has allowed both a logical and complete treatment of classical optics as it is presently known. The result is a noteworthy contribution to the reference literature in an important field.

A discursive reading of this text indicates that there will be few faults found by the informed reader. Some criticism may arise at points where the need to limit the discussion to the chosen subject matter has resulted in a summary treatment of certain aspects which might be of special interest to particular readers. However, the judicious use of clearly written reference footnotes relieves any tendency to discontinuity in such cases.

Despite the exclusion of the several fields of optics earlier noted, this book is not small, running to some eight hundred pages. Unfortunately, the quality of the binding may not match the weight of so many pages; at least, in the case of the copy received by the reviewers the covers have become detached during the normal handling of a few weeks. Moreover, the paper used is not sufficiently white to provide the contrast necessary for easy reading. This is unfortunate in view of an excellent typographical performance by the printers on a predominantly mathematical text. The figures are adequate with the exception of some of the photographic reproductions which do not compare favorably with their counterparts in other texts.

In conclusion, it is noted that typesetting for a book of this nature must dictate a large part of its formidable price of $17.50. Probably the technical reading world is sufficiently conditioned to this situation to dispel any qualms a reviewer might have in strongly recommending the acquisition of this book by all individuals or institutions who have a serious concern with the science of optics.

**Plasma Physics and Thermonuclear Research,** edited by C. Longmire, J. L. Tuck and W. B. Thompson, Pergamon Press, New York, 1959, 612 pp. $15.

Reviewed by ROBERT A. GROSS
Columbia University

This is an edited and reduced-size version of Volumes 31 and 32 of the "Proceedings of the International Conference on the Peaceful Uses of Atomic Energy" that took place in Geneva, 1958. The majority of the papers on plasma and thermonuclear research are reproduced here with some of the particular subjects somewhat condensed. This single volume is of more reasonable physical size and costs less than the Geneva volumes, and therefore more easily obtainable for the specialist's private library.

The volume is in four parts and includes the contributions of experts throughout the world. Survey papers are given by leaders in fusion research. The major devices used in attempting to attain fusion and to gain understanding of plasmas are described, and some of the important theoretical papers are contained in this volume.

Because the second Geneva Conference permitted for the first time a free exchange of information on fusion research, this volume contains a wealthy backlog of important information. This book is for the specialist working in the field, and only a few papers, such as the introductory survey papers, would be of interest to the general technical reader. Most technical libraries contain the official Geneva books, and therefore this reviewer assumes that the publisher has made this single volume available because the private demand is sufficient to warrant another printing of these important contributions.

**Formation and Trapping of Free Radicals,** edited by Arnold M. Bass and H. P. Broida, Academic Press, New York, 1960, 538 pp. $16.

Reviewed by GEORGE C. SZEGO
Space Technology Laboratories, Inc.

The entire science of free radicals, in the modern sense of the words, dates back 60 years, to the discovery by Professor Gomberg, at the University of Michigan, of the existence of aromatic organic free radicals. Only 30 years ago, Paneth and his co-workers at the University of Berlin discovered the existence of aliphatic free radicals and actually measured their lifetimes. Yet in this very new field a great deal of work has been done. Of particular interest is the relatively even more recent work done on the storing of free radicals after initiation has been carried out. This volume describes work which resulted from a rather unusual research program at the National Bureau of Standards, with which the writer was fortunate in having a direct connection for more than a year. The project itself began under the auspices of the United States Department of Defense, whose interest in an investigation into the storing of free radicals was primarily motivated by a desire to find possible super-propellants for reaction propulsion.

Nevertheless the project was carried out on a completely unclassified security basis, and, in fact, gained much from the participation of a substantial number of foreign scientists. The program itself was staffed partly by employees of the Bureau of Standards and partly by employees of private industry from both here and abroad who were given leaves of absence from their regular full-time duties and took up residence in Washington, actually carrying out their work in the laboratories of the National Bureau of Standards. At that time the writer was with the General Electric Co. in Cincinnati, which not only had a full-time employee with the Free Radical Project, but also was engaged in generating for the Bureau of Standards, the basic thermodynamic tabular and graphical data for the purpose of evaluating free radicals, from the theoretical point of view, as high energy rocket propellants. From this work, a very substantial volume was published by GE which consisted of well over 1000 pages of thermodynamic data.

The volume "Formation and Trapping of Free Radicals" now brings together in one useful book all the work which took place in the laboratories of the Bureau of Standards on the entire problem of the formation and the trapping of free radicals of a number of varieties. For the scientist who wants to be brought up to date on the accumulative work which has been done in this field, this volume is an extremely valuable working tool. The volume itself, written by some 17 principal authors, brings together an invaluable chronology and analysis of the basic reference literature in the entire field. Most of the chapters have extremely satisfactory bibliographic material to which reference has been made through the text. Material generated outside of the National Bureau of Standards project is naturally also included. A glance at the chapter headings gives one an insight into the truly interdisciplinary nature of a sound attack on this extremely broad and particularly difficult problem.

In addition to topics which would be expected in such a volume, there are a couple of bonus chapters, specifically, Chapter 14, "Trapped Radicals in Radiation Damage" and Chapter 15, "Trapped Radicals in Biological Processes." These chapters point directly at the rationale and understanding of the processes with which we must learn to cope as we attempt to penetrate space, particularly with living cargo. Chapter 13 "Trapped Radicals in Propulsion" which was of most immediate interest to the writer is unfortunately somewhat cursory, inasmuch as its author has employed less than the best and latest available information of the performance of the various systems, and has discussed the field of nonchemical propulsion in a relatively brief and superficial way. Particularly unsatisfactory were the sections on alternative methods of nonchemical propulsion systems and the complete omission of the possibilities of using free radicals found trapped in Earth's upper atmosphere and possibly elsewhere in space. However, this chapter is somewhat of an adjunct to the main topics of interest of the volume and perhaps no more than a very brief treatment of propulsion is called for here.

This volume is an extremely valuable starting tool for the laboratory scientist who desires to be brought up to date on the theoretical and experimental work and the results thereof which have been realized in the field of creating and stabilizing free radicals. Details about the equipment for generating and analyzing free radicals are given, as well as details of the techniques of handling, trapping and measuring many aspects of the physical properties characteristic of the unpaired electron and other properties of free radicals. A great deal of material is provided on spectroscopy, cryogenics, electron spin resonance and many other theoretical and experimental aspects of this extremely broad and difficult field. The volume is absolutely essential to those undertaking experimental research in this field.

**Engineering Thermodynamics,** by James B. Jones and George A. Hawkins, John Wiley and Sons, Inc., New York, 1960, 724 pp. $8.50.

Reviewed by WILLIAM T. SNYDER
North Carolina State College

The task of selecting a suitable introductory thermodynamics book for teaching or self-study purposes is becoming more difficult because of the large number of books that must be examined. It is, of course, not sufficient to scan the preface with the expectation of determining the level or maturity of the presentation. It is necessary to do considerable reading in the text with certain broad criteria of evaluation well in mind.

An introductory textbook in thermodynamics should possess at least the following characteristics:

1 A preciseness in the language and definitions used.

2 An emphasis on the scientific basis of thermodynamics which clearly delineates the basic laws from the deductively derived results.

3 The mathematics of thermodynamics should be treated as an integral, necessary, part of the development rather than as a special topic which may be arbitrarily included or omitted.

The authors have done a very good job of incorporating these characteristics into their writing. A considerable effort has been devoted to elaboration on definitions and concepts in the early part of the book. The first 11 chapters of 390 pages are used to develop the basic aspects of classical thermodynamics through the second law and mathematics of property relationships. The remaining 10 chapters, or approximately 40 per cent of the book, are devoted to applications, such as mixtures, chemically reactive systems, chemical equilibrium, thermodynamics of fluid flow, cycles and refrigeration. A brief chapter on heat transfer concludes the book, but this inclusion is not necessary because of the full status now accorded heat transfer in modern engineering curricula.

The developments for a closed system are very carefully made, but certain aspects of the open system treatment could be improved. For example, the system is defined as both a definite quantity of matter and a region in space. Except for the treatment of electromagnetic phenomena (which are not covered in the present book), a dual definition of the system is not necessary. The control volume concept is, of course, essential for flow situations, but a separate statement of the first law for the control volume is not necessary. This can be a derived result from the closed system formulation. It is the reviewer's opinion that a more consistent introductory treatment results by using the system definition of a definite quantity of matter. It is then a straightforward matter to apply the first law formulation for a closed system to a definite quantity of matter which is instantaneously contained within the control volume.

The book has numerous illustrative examples throughout which effectively demonstrate new concepts as they are introduced. Each chapter concludes with

Archimedes and the
**iron birds of prey**

The ancient city of Syracuse seemed doomed. Marcellus, the Roman conqueror, had arrived before the walls of Syracuse with "a fleet of sixty vessels filled with all sorts of men and missiles."

But Marcellus had reckoned without the engineering ability of Archimedes (287-212 B.C.) and his amazing new invention: the pulley. Attaching enormous iron grappling hooks to the new invention, Archimedes swung the enemy galleys high over the cliffs of Syracuse and dashed them upon the jagged rocks below.

Here at CEA, our scientists and engineers analyze advanced systems. For example, we supply missile and ground support equipment manufacturers with detail data on the response of their structures to thermal and aero-elastic environments. In our studies, we use an invention that would have amazed Archimedes: our Direct Analog Computer.

COMPUTER ENGINEERING ASSOCIATES, INC.
350 North Halstead Pasadena, California
Elgin 5-7121

Creative Engineers
for unusual
assignments in
AEROJET-GENERAL'S
Advanced
Development
Division

*Analysis and Evaluation Manager*
*Operations Analyst*
*Vehicle Performance Analyst*
*Propulsion Systems Analyst*
*Thermodynamics and Fluid Dynamics Analyst*
*Structural Analyst*
*Chemist*

Aerojet-General's operations near Sacramento, California, are expanding in new fields of rocketry and propulsion, leading toward man's most advanced assault on the frontier of space.

We're looking for mature, experienced and universally capable individuals, preferably over 35 years of age. These men must be trained in engineering or be engineering-minded physicists or chemists. Either the Master's or Ph.D. degree is preferred, although a strong B.S. is acceptable. The men we need must possess imaginative and creative insight in the advanced development of liquid rocket, propulsion systeems.

These top engineers will be given the responsibility and freedom to work on a broad spectrum of problems. Excellent salaries are offered, commensurate with proven ablity and experience. Our location near Sacramento, between Lake Tahoe and San Francisco, offers the finest living conditions.

*We invite you to send your resume and any detailed questions to*

MR. E. P. JAMES
SUPERVISOR, TECHNICAL AND SCIENTIFIC PERSONNEL
BOX 1947D
**AEROJET-GENERAL CORPORATION**
SACRAMENTO, CALIFORNIA

a significant summary which gives the basic concepts of the chapter rather than a tabulation of derived formulas. Because of the clear style of writing and the complete elaboration of new concepts as they are introduced, the book can be highly recommended both as an introductory text and as a review source for those persons faced with the necessity of self-study of thermodynamics.

# Technical Literature Digest

**M. H. Smith, *Associate Editor***
The James Forrestal Research Center, Princeton University

## Propulsion and Power (Combustion Systems)

**The Uses of Chemical Power Systems in the Construction, Servicing, and Operation of Manned Space Stations,** by H. F. Howard and R. M. Laughlin, *Aero/Space Engng.*, vol. 19, May 1960, pp. 62–63.

**On the Design of Nozzles,** by I. M. Yur'ev, ARS JOURNAL, vol. 30, no. 4, April 1960, *Russian Suppl.*, pp. 374–375.

**Analysis of Operation of Simplest Ramjet Combustion Chamber Under Flying Conditions,** by A. V. Talantov, ARS JOURNAL, vol. 30, no. 4, April 1960, *Russian Suppl.*, pp. 379–385.

**Aerodynamic Instability of Supersonic Inlet Diffusers,** by Chieh-Chien Chang and Cheng-Ting Hsu, ARS JOURNAL, vol. 30, no. 5, May 1960, pp. 468–475.

**Ballistic Effect of Pyrolyzed Liner in Solid Propellant Motor Firings,** by L. J. Gordon, ARS JOURNAL, vol. 30, no. 5, May 1960, pp. 502–503.

**Problems and Possibilities in the Development of Rocket Fuel and Propulsion Systems,** by A. Dadieu, *Raketentechnik und Raumfahrtforschung*, vol. 4, no. 2, June 1960, pp. 41–45. (In German.)

**More on the Energy Requirements of Rockets,** by G. Leitmann, *Raketentechnik und Raumfahrtforschung*, vol. 4, no. 2, June 1960, p. 58. (In German.)

**Current Trends in Large Booster Developments,** by Eldon W. Hall and Francis C. Schwenk, *Aero/Space Engng.*, vol. 19, May 1960, pp. 20, 21.

**Design of Axisymmetric Exhaust Nozzles by Method of Characteristics Incorporating a Variable Isentropic Exponent,** by Eleanor Costilow Guentert and Harvy E. Neumann, *NASA Tech. Rep.* R-33, 1959.

**Application of Boundary Theory in Turbomachinery,** by H. H. Schlichting, *Belgium, Training Center for Exptl. Aerodyn., Tech. Mem.* 5, March 1959, 33 pp.

**Reliability Aspects of Solid Propellant Rocket Engines,** by B. R. Adelman and A. C. Keathley, *ARS Preprint* 1043-60, 1960, 18 pp.

**Solid Propellant Rocket Motors as Acoustic Oscillators,** by F. T. McClure, R. W. Hart and J. F. Bird, *ARS Preprint* 1049-60, Jan. 1960, 36 pp.

EDITOR'S NOTE: Contributions from Professors E. R. G. Eckert, J. P. Hartnett, T. F. Irvine Jr. and P. J. Schneider of the Heat Transfer Laboratory, University of Minnesota, are gratefully acknowledged.

**Detonation Wave Hypersonic Ramjet,** by W. H. Sargent and R. A. Gross, ARS JOURNAL, vol. 30, no. 6, June 1960, pp. 543–549.

**Determination of Diffusion Coefficients from Asymmetric Concentration Profiles,** by A. W. Blackman, ARS JOURNAL, vol. 30, no. 6, June 1960, p. 557.

**Approximation of Optimum Thrust Nozzle Contour,** by G. V. R. Rao, ARS JOURNAL, vol. 30, no. 6, June 1960, p. 561.

**Combustion Instability in Solid Propellant Rocket Motors,** by E. W. Price, ARS JOURNAL, vol. 30, no. 6, June 1960, pp. 574–576.

**Isothermal Nozzle Flows,** by V. Stingelin, *Astronautica Acta*, vol. 6, no. 1, 1960, pp. 61–74. (In German.)

**Cheaper and Lighter Rockets with Filament Winding,** by Richard Gorcey, *Space/Aeronautics*, vol. 33, May 1960, pp. 117–132.

## Propulsion and Power (Non-Combustion)

**Astronautics Information: Advanced Propulsion,** by Edda Barber, *Calif. Inst. Tech., Jet Prop. Lab., Literature Search* 207, April 1960, 40 pp.

**A Comparison of Nuclear and Solar Power Systems for Manned Space Stations,** by William C. Cooley, *Aero/Space Engng.*, vol. 19, May 1960, pp. 54–55, 100.

**Integrated Thermodynamic Systems for Manned Space Stations,** by Michael G. DeiDuca, Andrew Babinsky and Floro D. Miraldi, *Aero/Space Engng.*, vol. 19, May 1960, pp. 56–57, 104.

**Utilization of Plasma-cell Energy Conversion in Nuclear Reactors,** by William A. Ranken and Thurman G. Frank, *Aero/Space Engng.*, vol. 19, May 1960, pp. 58–59.

**A Circulating Dust-fueled, Radiation-cooled Space Power Reactor,** by W. R. Corliss, *Aero/Space Engng.*, vol. 19, May 1960, pp. 60–61.

**On Detonation Wave Pressures in Hot Water-fission Rockets,** by E. Sänger, *Raketentechnik und Raumfahrtforschung*, vol. 4, no. 2, June 1960, pp. 46–57. (In German.)

**Electrode Boundary Layers in Direct Current Plasma Accelerators,** by Jack L. Kerrebrock, *Calif. Inst. Tech., Daniel & Florence Guggenheim Jet Prop. Center, TN* 1, Jan. 1960, 35 pp.

**Analytical Wave Function III; the Spin-orbit, Spin-other Orbit and Spin-spin**

**Interactions,** by R. G. Breene Jr., *General Electric Co., Missile & Space Vehicle Dept., TIS* R59SD414 (revised), 1960, 16 pp.

**Pinch Dynamics with Nonuniform Initial Conditions,** by William J. Guman and Irving Granet, *Republic Aviation Corp., Plasma Prop. Lab.*, PPL-TR-60-6, Jan. 1960, 22 pp.

**Solar Batteries,** by V. S. Vavilov, A. P. Landsman and V. K. Subashiev, *Artificial Earth Satellites,* vol. 2, ed. by I. V. Kurnosova, translated from Russian, Plenum Press, N. Y., 1960, pp. 96–104.

**On the Focussing Problem of Photon Rocket Propulsion and Weapon Radiation,** by Eugene Sänger, *Forschungsinstitut für Physik der Strahlantriebe,* e.v., Stüttgart, *Mitteilungen* 21, Dec. 1959, 145 pp. (In German.)

**STX—A Proposed Thermonuclear Device,** by Richard W. Hales, *Space Tech. Labs., Inc., Phys. Res. Lab.*, STL/TR-60-0000-09085, April 1960, 13 pp.

**Isentropic One Dimensional MHD Channel Flow,** by Boris Popolsky and A. Sherman, *General Electric Co., Flight Propulsion Lab. Dept., Cincinnati, TIS* R60FPD193, May 1960, 12 pp.

**Induced Magnetic Fields in MHD Channel Flows,** by A. Sherman, *General Electric Co., Flight Propulsion Lab. Dept., Cincinnati, TIS* R60FPD301, April 1960, 9 pp.

**Direct Conversion of Heat to Electricity,** Kaye, Joseph and Welsh, John A., eds., John Wiley & Sons, N.Y., 1960, 1 vol.

**Analysis and Experimental Results of a Diode Configuration of a Novel Thermoelectron Engine,** by G. N. Hatsopoulos and J. Kaye, pp. 1–14.

**The Thermionic Diode as a Heat-to-electrical Power Transducer,** by W. B. Nottingham, pp. 2-1-16.

**Thermodynamics of Thermionic Engines,** by G. N. Hatsopoulos pp. 3-1-12.

**Prediction of Optimum Performance of Vacuum-diode Configuration of Thermionic Engines,** by G. N. Hatsopoulos, J. Kaye and E. Langberg, pp. 4-1-15.

**Theoretical Analysis of a Magnetic Triode as a Thermionic Engine,** by J. A. Welsh, G. N. Hatsopoulos and J. Kaye, pp. 5-1-18.

**Thermionic Energy Converter,** by K. G. Hernqvist, M. Kanefsky and F. M. Norman, pp. 6-1-14.

**The Gas-filled Thermionic Converter,** by V. C. Wilson, pp. 7-1-12.

**Cesium Plasma Diode as a Heat-to electrical-power Transducer,** by W. B. Nottingham, pp.1-37.

**Thermionic Power Conversion and Its Possibilities in the Nuclear Field,** by K. G. Hernqvist, pp. 9-1-11.

**Characteristics of a Plasma Thermocouple,** by R. W. Pidd, G. M. Grover, E. W. Salmi, D. J. Roekling and G. F. Erickson, pp. 10-1-12.

**Energy Converter Using Low Pressure Cesium,** by H. Steele, pp. 11-1-9.

**Magnetohydrodynamic Energy Conversion Techniques,** by R. J. Rosa and A. Kantrowitz, pp. 12-1-13.

**The Plasma Heat Engine,** by E. N. Carabaieas, pp. 13-1-12.

**Review of Thermoelectric Effects,** by F. E. Jaumot Jr., pp. 14-1-37.

**Thermodynamics of Thermoelectric Generators,** by G. N. Hatsopoulos and J. H. Keenan, pp. 15-1-19.

**An Elementary Design Discussion of Thermoelectric Generation,** by E. W. Ballmeir, pp. 16-1-17.

**Design Parameters for Optimizing the**


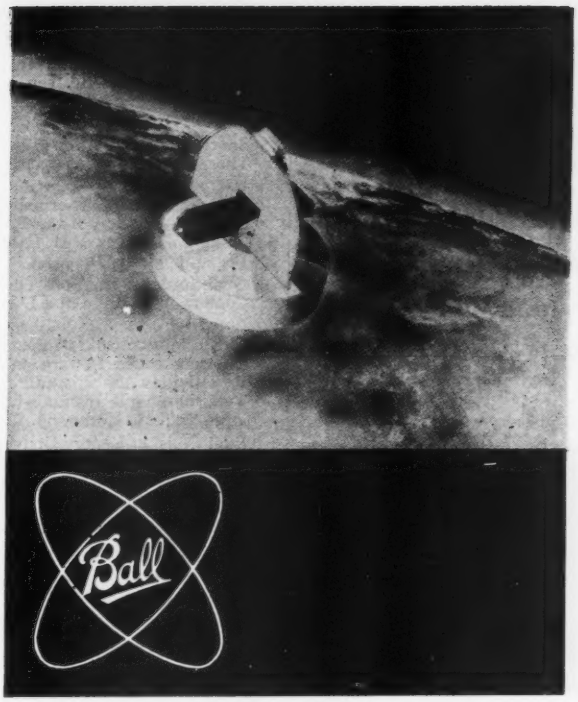


# CONTRACT RESEARCH, DEVELOPMENT, FABRICATION

*Specializing in the fields of*

- **Rocket and Satellite Instrumentation**
- **Payload Systems**
- **Solar and Stellar Pointing Systems**
- **Guidance and Control Systems**

***WRITE FOR BROCHURE***

*Prime Contractors to the NASA, Air Force, Navy*

Employment Opportunities Available for Scientists and Engineers with Above Average Abilities

**BALL BROTHERS RESEARCH CORP.**

INDUSTRIAL PARK BOULDER, COLORADO

Hillcrest 2-2966

example...

FIBERITE

Compression molded high temperature insulation materials at work...

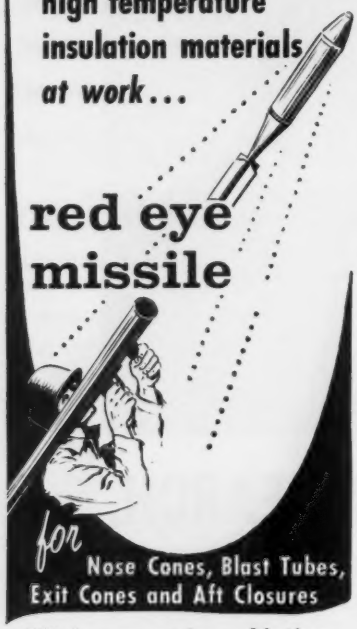


Minimum erosion, ablation combined with dimensional stability and shock resistance over 5000°F.

Fiberite compression molded high temperature insulation materials designed for MIL-M-19536 applications; chopped fiber impregnated phenolic with special reinforcement materials as fiberglass, graphite cloth, ceramic, and quartz. Fiberite insulation is specified in the LAR, Bull-Pup, Polaris, Minuteman, Nike Zeus and many others.

EXPLORE FIBERITE

Missile engineers will find our research helpful in solving problems requiring materials for special performance. Write factory for bulletin on high temperature insulation materials.

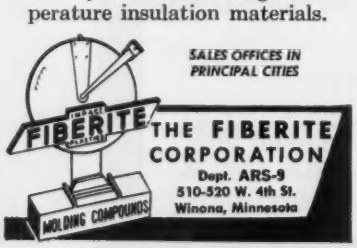


SALES OFFICES IN PRINCIPAL CITIES

THE FIBERITE CORPORATION
Dept. ARS-9
510-520 W. 4th St.
Winona, Minnesota

**Efficiency of Thermoelectric Generators Utilizing P-type and N-type Lead Telluride,** by R. W. Fritts, pp. 17-1-13.

**Optimisation of a Conventional Fuel-fired Thermoelectric Generator,** by E. V. Semers and B. W. Swanson, pp. 18-1-8.

**Special Techniques for Measurement of Thermoelectric Properties,** by T. C. Harman, pp. 19-1-2.

**Measurement of Thermal Conductivities by Utilization of the Peltier Effect,** by T. C. Harman, J. H. Cahn and M. J. Legan, pp. 20-1-20.

**Quantitative Design of a Thermoelectric Cooler,** by J. Kaye and I. T. Saldi, pp. 21-1-14.

**The Effect of Oxide Impurities on the Thermoelectric Powers and Electrical Resistivities of Bismuth, Antimony, Tellurium, and Bismuth-tellurium Alloys,** by T. A. Horne, pp. 22-1-13.

**Fuel Cells as Energy Converters,** by J. F. Yeager, pp. 23-1-15.

**Refractory Materials, Part I —Technology and Low-temperature Behavior,** by Robert I. Jaffee and Daniel J. Maykuth, *Aero/Space Engng.*, vol. 19, June 1960, pp. 22–27, 48.

**Calculation of Electrical Conductivity of Ionized Gases,** by A. Sherman, ARS JOURNAL, vol. 30, June 1960, pp. 559–560.

**Non-propulsive Power for Advanced Vehicles—III,** by Robert W. Curran, *Space/Aeron.*, vol. 33, May 1960, pp. 52–54.

**Instrumentation for Plasma Propulsion, Measuring Performance of Space Engines,** by J. H. Pearson, *Electronics*, vol. 33, June 10, 1960, pp. 66–69.

**Atomic Rockets for Space Flight,** by E. Sänger, *Astronautica Acta*, vol. 6, no. 1, 1960, pp. 3–15. (In German.)

## Propellants and Combustion

**Temperature and Composition of a Plasma Obtained by Seeding a Cyanogen-oxygen Flame with Cesium,** by Richard A. Hord and J. Byron Pennington, *NASA TN* D-380, May 1950, 18 pp.

**Study of Additive Effects in Solid Propellant Burning,** by H. Burwasser, H. F. Calcote and H. Silla, *AeroChem Res. Labs., Inc., 3d Quart. Progr. Rep., Tech. Mem.* 20, Feb. 1960, 11 pp.

**Studies on Deflagration to Detonation in Propellants and Explosives,** *Bureau of Mines, Explosives Res. Lab., Quart. Rep.*, Jan. 1, 1960–March 31, 1960, 6 pp.

**Propellant Evaluation Tests with the 250-pound Motor,** by Dean H. Couch and Donald G. Nyberg, *U. S. Naval Ord. Test Station, NavOrd Rep.* 7012, *NOTS TP* 2369, March 1960, 15 pp.

**The Chain Transfer of Nitro Compounds in Polymerization Reactions,** by T. R. Fukuto and J. P. Kispersky, *Aerojet Gen. Corp., Rep.* 700, May 1953, 39 pp. (Declassified from Confidential by authority OIVR:426:RLH:bg-NR 093-224a, dated 20 April 1960.)

**Effect of Transverse Acoustic Oscillations on the Vaporization of a Liquid-fuel Droplet,** by Paul R. Wieber and William R. Mickelson, *NASA TN* D-287, May 1960, 25 pp.

**Fluorescent Technique for Determining the Cross-sectional Drop Size Distributions of Liquid Sprays,** by G. M. Benson, M. M. El-Wakil, P. S. Meyers and O. A. Uyehara, ARS JOURNAL, vol. 30, no. 5, May 1960, pp. 447–454.

**Specific Impulse Nomograph,** by William L. Senn Jr. and Ronald V. Repetti,

Another of a series of files on precision products by ALINCO

LOAD CELLS

Model 344
Tension
Compression
Load Cells

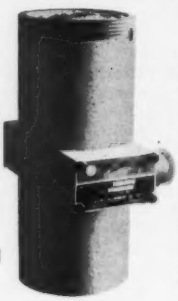

Accuracy, Linearity, Low Hysteresis—ALINCO

- ACCURACIES OF ±0.1%
- HIGH LINEARITY
- LOW HYSTERESIS

ALINCO is now producing a new tension compression load cell, thoroughly tested and use-proven for reliability and accuracy.

Designed by ALINCO to meet the latest and most stringent requirements in rocket and missile testing, Model 344 and 344LS (Linear Standard Series) tension compression load cells are reliable, rugged and accurate force transducers. Reliability is assured by using two and more bridges. In ranges of 10,000 lbs. and above, termination boxes are recessed to prevent accidental damage to the connectors due to rough usage. For greater accuracy, a standard bridge resistance of 350 ohms is used with split modules and factor resistors. ALINCO unique electrical circuitry and mechanical layout minimize the effects of non-axial loads. Ranges to 3,000,000 lbs. are available, permitting use of a single load cell for obtaining measurements where previously several parallel units were necessary.

For additional information on the Model 344 Load Cells or for the answer to a specific load cell requirement, write:

ALINCO

ALLEGANY INSTRUMENT CO.
A Division of
Textron Electronics, Inc.
Dept. A , 1091 Wills Mountain
Cumberland, Maryland
Regional Sales Offices:
Palo Alto, Calif. • Washington, D. C.

ARS JOURNAL, vol. 30, no. 5, May 1960, pp. 489–491.

**Specific Impulse Measurements by the Vented Closed Bomb Method,** by W. H. Groetzinger III, *Rohm & Haas Co., Redstone Arsenal Div., Rep.* P-60-5, May 10, 1960.

**Quarterly Progress Report on Engineering Research,** Rep. P-60-5, *Rohm & Haas Co., Huntsville, Ala.,* May 1960, 40 pp.

**Resonant Burning of Solid Propellants: Review of Causes, Cures, and Effects,** by R. H. Wall, *ARS Preprint* 1065-60, Jan. 1960, 20 pp., 15 refs.

**A One-dimensional Theory of Liquid-fuel Rocket Combustion, III: The Effect on Non-uniform Droplet Radii, Injection Velocities and Physical Properties,** by J. Adler, *Gt. Brit., Aeron. Res. Council, Current Paper* 469 (Feb. 1959), 1960, 9 pp.

**Thermal Stresses in Spherical Case-bonded Propellant Grains,** by Irvin Krause and Gerhard W. Shaffer, *New York Univ., Coll. of Engng., Res. Div., Tech. Rep.* 4, April 1960, 20 pp.

**The Conformal Transformation of a Solid-propellant Grain with a Star-shaped Internal Perforation onto an Annulus,** by H. B. Wilson, *Rohm & Haas Co., Redstone Arsenal Div., Rep.* P-60-5, May 10, 1960, pp. 1–7.

**Thermal Decomposition of Organic Nitrogen and Sulfur Compounds; a Survey of *Chemical Abstracts,* 1930–1956,** by Irven C. Jacobson Jr., *Bureau of Mines, Info. Circ.* 7947, 1960, 99 pp., Bibliography: pp. 86–99, 147 refs.

**Solid State Chemical Reactions (with Special Reference to the Kinetics of the Reaction of Potassium Perchlorate with Polydivinylbenzene),** by Saul Patai, Harold Cross and Michael Albeck, *Hebrew Univ., Jerusalem, TN* 1, Feb. 1960, 24 pp.

**Cryogenic Propellant Storage for Round Trips to Mars and Venus,** by George R. Smolak and Richard H. Knoll, *Aero/Space Engng.,* vol. 19, June 1960, pp. 42–46.

**The Kinetics of the Homogeneous Gas Phase Thermal Decomposition of Ozone,** by J. A. Zaslowsky, H. B. Urbach, F. Leighton, R. J. Wnuk and J. Wojtowicz, *J. Amer. Chem. Soc.,* vol. 82, June 5, 1960, pp. 2682–2686.

**Pressure - density - temperature Relationship of Liquid $O_2$,** by Eugene A. Tkachenko, ARS JOURNAL, vol. 30, no. 6, June 1960, pp. 566–568.

**Vibration Phenomena in Detonation Waves in Hydrogen-oxygen Mixtures,** by D. H. Edwards and T. G. Jones, *Brit. J. Appl. Phys.,* vol. 11, May 1960, pp. 190-194.

**The Liquid-vapour Equilibrium of the System Nitrogen+Oxygen at Pressures up to 10 Atm,** by F. Din, *Trans. Faraday Soc.,* vol. 56, May 1960, pp. 668–681.

**The Slow Reactions Between Hydrogen and Oxygen in Boric-acid-coated Vessels,** by R. R. Baldwin and L. Mayor, *Trans. Faraday Soc.,* vol. 56, Jan. 1960, pp. 80–92.

**The Mechanism of the Hydrogen+Oxygen Reaction in Aged Boric Acid Coated Vessels,** by R. R. Baldwin, *Trans. Faraday Soc.,* vol. 56, Jan. 1960, pp. 103–114.

**Measurement of Heats of Vaporization by the Method of Gas-liquid Chromatography,** by H. Mackle, R. G. Maytrick and J. J. Rooney, *Trans. Faraday Soc.,* vol. 56, Jan. 1960, pp. 115–117.

**The Equilibrium Bond Lengths in Acetylene and HCN,** by C. Overend, *Trans. Faraday Soc.,* vol. 56, March 1960, pp. 310–314.

**The Origin of the Blue Continuum in the Hydrogen Flame,** by P. J. Padley, *Trans. Faraday Soc.,* vol. 56, April 1960, p. 449–454.

**The Gas-liquid Critical Temperatures of Binary Mixtures, Part I,** by E. J. Partington, J. S. Robinson and J. F. Weston, *Trans. Faraday Soc.,* vol. 56, April 1960, pp. 479–485.

**The Thermal Decomposition of Ammonium Perchlorate in the Presence of Carbon,** by A. K. Galwey and P. W. M. Jacobs, *Trans. Faraday Soc.,* vol. 56, April 1960, pp. 581–590.

**Computation of the Equilibrium Composition of Burnt Gases,** by Robert L. Potter and Wouter Vanderkulk, *J. Chem. Phys.,* vol. 32, May 1960, pp. 1304–1310.

**Effect of Solid Propellant Compressibility on Combustion Instability,** by J. F. Bird, L. Haar, R. W. Hart and F. T. McClure, *J. Chem. Phys.,* vol. 32, May 1960, pp. 1425–1431.

**Thermal Conductivity of Helium and Hydrogen at High Temperatures,** by Normand C. Blais and Joseph B. Mann, *J. Chem. Phys.,* vol. 32, May 1960, pp. 1459–1464.

**Boron: Impressive Properties, Impressive Problems,** by D. N. Williams, *Space/Aeron.,* vol. 33, May 1960, pp. 101-102, 104, 112.

## Materials and Structures

**Small Oscillations of Thin Resilient Conical Shells,** by E. I. Grigolyuk, *NASA Tech. Transl.* F-25, May 1960, 12 pp.

**Analysis of Frame-reinforced Cylindrical Shells, Part I—Basic Theory,** by Richard H. MacNeal and John A. Bailie, *NASA TN* D-400, May 1960, 57 pp.

**Analysis of Frame-reinforced Cylindrical Shells, Part II—Discontinuities of Circumferential-bending Stiffness in the Axial Direction,** by Richard H. MacNeal and John A. Bailie, *NASA TN* D-401, May 1960, 48 pp.

**Analysis of Frame-reinforced Cylindrical Shells, Part III—Applications,** by Richard H. MacNeal and John A. Bailie, *NASA TN* D-402, May 1960, 136 pp.

**Development and Evaluation of Materials for High Temperature Applications,** by Charles E. Shulze, Frank A. Saulino, William T. Adams, Gustave E. Mangsen, James C. Andersen and Howard W. Emmons, *Wright Air Dev. Center, Tech. Rep.* 59-10, Part I, May 1959, 52 pp.

**Meteoroids—Implications for the Design of Space Structures,** by Lloyd E. Kaechele and Arnold E. Olshaker, *Aero/Space Engng.,* vol. 19, May 1960, pp. 44–45, 98.

**The Ionizing Radiation in Space—Structural Implications,** by Norris F. Dow, *Aero/Space Engng.,* vol. 19, May 1960, pp. 46–47, 98.

**Inflatable Manned Orbital Vehicles,** by J. W. Carter and B. L. Bogema, *Aero/Space Engng.,* vol. 19, May 1960, pp. 48–49, 99.

**The Role of Damping in Space Structures,** by Charles W. Coale, *Aero/Space Engng.,* vol. 19, May 1960, pp. 50–51.

**Thermal Control of Space Vehicles—Structural Approach,** by Peter E. Glaser, *Aero/Space Engng.,* vol. 19, May 1960, pp. 52–53, 99–100.


SOUTHWEST
"Monoball"
SELF-ALIGNING BEARINGS

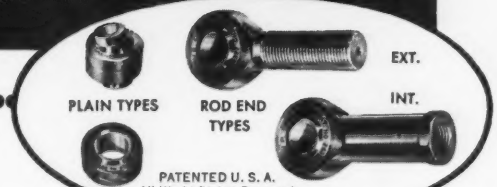


PATENTED U. S. A.
All World Rights Reserved

CHARACTERISTICS

| | ANALYSIS | RECOMMENDED USE |
|---|---|---|
| 1 | Stainless Steel Ball and Race | For types operating under high temperature (800-1200 degrees F.). |
| 2 | Chrome Alloy Steel Ball and Race | For types operating under high radial ultimate loads (3000-893,000 lbs.). |
| 3 | Bronze Race and Chrome Steel Ball | For types operating under normal loads with minimum friction requirements. |
| 4 | "Dyflon"® Plastic Alloy Inserts. CRES Ball and Race. Chrome Alloy Steels. | For types operating under rotational, high radial loads and long cycle life where lubrication is impossible. |

Thousands in use. Backed by years of service life. Wide variety of Plain Types in bore sizes 3/16" to 6" Dia. Our engineers welcome an opportunity of studying individual requirements and prescribing a type or types which will serve under your demanding conditions. Southwest can design special types to fit individual specifications. Write for Engineering Manual No. 551. Address Dept. ARS60.

SOUTHWEST PRODUCTS CO.
1705 SO. MOUNTAIN AVE., MONROVIA, CALIFORNIA

STRETCH, the world's fastest and most versatile computer, will soon be added to the array of research tools at Los Alamos Scientific Laboratory. This multi-million dollar machine, built by IBM, is 50 to 75 times faster than the IBM 704.

STRETCH can complete more than 75 billion arithmetic operations a day. The system can execute as many as 2 million instructions per second.

A "look ahead" device anticipates instructions and data requirements, thus increasing the effective memory speed to make use of the enormous speed of the arithmetic units.

*For employment information write:*
*Personnel Director Division 60-81*

los alamos
scientific laboratory
OF THE UNIVERSITY OF CALIFORNIA
LOS ALAMOS, NEW MEXICO

# Index to Advertisers

AEROJET-GENERAL CORP. ..... Back cover, 916
*D'Arcy Advertising, Co., Los Angeles, Calif.*

AEROSPACE CORP. ..... 796–797

ALLEGANY INSTRUMENT CO., INC. ..... 918
*S. Gunnar Myrbeck & Co., Quincy, Mass.*

AVCO CORP. ..... 798
*Benton & Bowles, Inc., New York, N. Y.*

AVCO-EVERETT RESEARCH LAB. ..... 913
*Benton & Bowles, Inc., New York, N. Y.*

BALL BROTHERS RESEARCH CORP. ..... 917
*Walter L. Schump Advertising, Denver, Colo.*

COMPUTER ENGINEERING ASSOCIATES ..... 915
*Guerin, Johnstone, Jeffries, Inc., Los Angeles, Calif.*

FIBERITE CORP. ..... 918
*Harold C. Walker, Advertising, Minneapolis, Minn.*

FOOD MACHINERY & CHEMICAL CORP., CHLOR-ALKALI DIV. ..... Second cover
*James J. McMahon, Inc., New York, N. Y.*

GENERAL ELECTRIC CO.

FLIGHT PROPULSION DIV. ... 912

MISSILE & SPACE VEHICLE DEPT. ..... Third cover
*Deutsch & Shea, Inc., New York, N. Y.*

LOS ALAMOS SCIENTIFIC LABORATORY ..... 920
*Ward Hicks Advertising, Albuquerque, N. Mex.*

RADIO CORP. OF AMERICA, DEFENSE ELECTRONIC PRODUCTS ..... 793
*Al Paul Lefton Co., Inc., Philadelphia, Pa.*

SOUTHWEST PRODUCTS CO. ... 919
*O. K. Fagan Advertising Agency, Los Angeles, Calif.*

SPACE TECHNOLOGY LABORATORIES, INC. ..... 795
*Gaynor & Ducas, Inc., Beverly Hills, Calif.*